EFFECTS OF VARIOUS HEAT TREATMENTS ON THE CREEP/STRESS-RUPTURE BEHAVIOR OF 2 1/4CR - 1MO PIPING MATERIAL

Jeffrey William Carter
B. S. Massachusetts Institute of Technology, 1962
M. S. E. University of Michigan, 1963

A dissertation submitted to the faculty of the
Oregon Graduate Institute of Science & Technology
in partial fulfillment of the
requirements for the degree
Doctor of Philosophy
in
Materials Science and Engineering

April 1996

The dissertation "Effects of Various Heat Treatments on the Creep/Stress Rupture Behavior of 2 1/4Cr-1Mo Piping Material" by Jeffrey W. Carter has been examined and approved by the following Examination Committee:

David G. Atteridge, Thesis Advisor
Professor

William E. Wood
Professor and Department Head

Jack H. Devletian
Professor

Milt Scholl
Assistant Professor

ACKNOWLEDGEMENTS

The author gratefully acknowledges the support from Dave Atteridge's programs. His guidance and assistance as my thesis advisor are especially appreciated. Additional support for the laboratory testing involved in this project by Portland General Electric is also appreciated.

I thank the members of my thesis committee for their efforts on my behalf. They and the rest of the Materials Science and Engineering Department faculty have provided a high level of intellectual challenge and personal interest. This has combined with the good will and good wishes of the department staff and my fellow students to make this entire experience a highly positive one.

This thesis is dedicated to my wife Dee Ann, who encouraged me to proceed, and has cheerfully assumed more responsibilities so that I could do so.

TABLE OF CONTENTS

FIGURES

TABLES

ABSTRACT

Effects of Various Heat Treatments on the Creep/Stress-Rupture Behavior of 2 1/4Cr - 1Mo Piping Material

Jeffrey W. Carter

Supervising Professor: David G. Atteridge

The long term high temperature creep/stress-rupture behavior of 2 1/4Cr - 1Mo low alloy steel is known to depend on prior thermal exposure. Understanding and predicting this behavior is important in service life assessment of pressurized piping, vessels, and other load bearing components. The effects of field hot fabrication and heat treatment on the service life are also important. A model has recently been developed to predict the effect of service exposures. Its applicability to the other type of thermal exposure is not known.

Typical commercial ASME SA335 P22 piping material was utilized. Heat treatments ranged from normal service exposure at 1005°F, to exposures typical of field hot bending processes, and extended exposures above and below the Ac_1 temperature. Both weld containing and base metal samples were included. Stress-rupture performance was quantified and correlated with such life prediction parameters as hardness, and carbide morphology. Comparison with the model was made, and the applicability of the laboratory data to field installed piping was evaluated by field hardness testing and metallographic replication.

It was found that the normal service exposed material obeyed the model closely, while the additionally heat treated materials deviated in the nonconservative direction. All additional heat treatments were found to be deleterious, and welded samples had poorer properties than their base metal counterparts. Field characterization methods were found to be limited by anomalous surface conditions.

1.0 INTRODUCTION

1.1 Overview

A recently developed model[56] for the prediction of the effects of prior thermal exposure on the creep/stress-rupture properties of 2 1/4Cr-1Mo piping used for high temperature service was investigated by means of laboratory specimens, and compared with actual field piping. Thermal regimes evaluated included normal service, exposures used in hot bending of field piping, and extended treatment above and below the Ac_1 temperature.

The model to be investigated is one of several used in life prediction for Cr-Mo superheater tubes. In this instance, only the effects of thermal exposure (in-service degradation) on the material mechanical strength were evaluated. An oxidation corrected rupture database was used to generate a predictive equation relating initial tensile strength to the Larson-Miller Parameter for rupture (LMP). This permits the prediction of rupture life if the original tensile strength is known.

If the initial tensile strength is not known, as was the case here, another predictive equation calculates a Larson-Miller Parameter for ageing (LMP_{age}) if the time and temperature are known. This LMP_{age} is then used to calculate a K_{age}, which relates the present tensile strength to the original tensile strength. The original rupture life can then be determined. Present tensile strength can be determined by testing removed samples (not desirable), or estimated from hardness tests.

If the initial and present tensile strengths are known, it is possible to use the model to assess the effective metal temperature. This is sometimes in question in the case of boiler tubes, but is not generally an issue with steam piping.

Life prediction parameters such as carbide morphology, hardness, and grain boundary cavity formation were assessed for both laboratory samples and field installed piping. The possibility of anomalous surface conditions rendering some or all of these parameters suspect was evaluated.

Typical commercial ASME SA335 P22 material was available to evaluate both base metal and weld region performance. There was little information published on the creep/stress-rupture properties of weld heat affected zones, although it has often been qualitatively accepted that they will be inferior to the adjacent base metal. It was decided to conduct identical tests on the weld containing material to quantitatively determine the degradation in properties relative to the base metal, and to examine the microstructural differences.

The field installed material used for comparison was 40" diameter, 2" thick 2 1/4Cr-1Mo hot reheat steam line. Some field piping sections had been previously hot bent at 1450°F to establish proper alignment. Several sections of the service exposed material were used to fabricate the laboratory specimens after varied heat treatments.

The hot bending process was carried out at a temperature (1450°F) stated by the ASME B31.1 Piping Code to be 30°F below the lower critical temperature (Ac_1) for 2 1/4Cr-1Mo. This does not appear to be true under many circumstances. One extensive investigation found that for commercial 2 1/4Cr-1Mo steels the actual Ac_1 temperature is variable and somewhat below 1450°F (1382°F to 1436°F), depending on the chemistry of

the material and its prior heat treatment.

An evaluation of the Ac_1 temperature for the base material used in this program was conducted using a Gleeble apparatus. The value of 1472°F was determined, which is in agreement with the ASME B31.1 Piping Code statement. However, longer thermal exposure at 1450°F clearly produced austenization in the same material.

The hot bending thermal treatment used was thus not a simple tempering type exposure or sub-critical thermal aging. It actually involved partial austenization of the material. The end result of such a thermal exposure will depend on the prior history of the material, the chemical composition, the time at temperature, and the cooling rate. The ability of the model to predict subsequent stress-rupture properties was investigated.

These complicating factors required additional work beyond that required to evaluate a simple extended tempering treatment. This included additional heat treatments, as well as characterization of frequently used life prediction parameters for both the laboratory samples and field piping.

Additional thermal treatments included extended exposures at 1450°F to assess trends in properties and microstructure. Exposures at a temperature just below Ac_1 were conducted to determine the comparative consequences of thermal exposures in this region, which would be typical of piping adjacent to that exposed above Ac_1.

1.2 Objectives

The specific objectives of this project were the following.

1. Determine the validity of a recently proposed life prediction technique for 2 1/4Cr-1Mo piping material that has

been thermally exposed to different temperature regimes.

2. Quantitatively assess the results of the hot bending heat treatment on the creep/stress-rupture properties of sample material in order to predict the long term performance of the field installed piping.

3. Quantitatively assess the effects of a weld heat affected zone thermo-mechanical history on the creep/stress-rupture properties of commercial 2 1/4Cr-1Mo piping material.

4. Quantitatively assess the effects of other high temperature heat treatments on the creep/stress-rupture properties of commercial 2 1/4Cr-1Mo piping material.

5. Assess the validity of determining life prediction parameters by field characterization of commercial 2 1/4Cr-1Mo piping.

2.0 BACKGROUND

2.1 Creep of Metals

Creep is a mode of deformation in which plastic strain increases as a function of time at a constant stress. It occurs in a particular stress/temperature regime for a given metal. Creep deformation may be fully ductile or almost completely brittle, with a continuous spectrum of behavior between these two extremes. Creep is one of a number of modes of deformation that a metallic material may exhibit in response to the application of stress.

The relationship of creep in its different forms to other modes of deformation can be appreciated most readily by reference to deformation mechanism maps (Figures 1 & 2). These maps were first proposed by M. F. Ashby, and the concept has been greatly expanded by Ashby and others.[1-6] For the purposes of this discussion, a generalized map from Dieter[7], and a map for pure iron from Ashby[1] are used.

These maps can be plotted in a variety of ways in order to highlight the particular quantity of interest. This map plots normalized shear stress vs homologous temperature. Normalized tensile stress is sometimes used in place of shear stress. Other presentations use strain-rate vs temperature, strain-rate vs stress, strain-rate vs reciprocal temperature (Tm/T), and stress vs failure time. For simple tension, the shear stress $\sigma_s=\sigma_1/(3)^{1/2}$, and the shear strain rate $\dot{\gamma}=(3)^{1/2}\dot{\epsilon}_1$, where σ_1 and $\dot{\epsilon}_1$ are the principal stress and the principal strain rate respectively.[1]

The fields of the generalized map (Figure 1) schematically indicate the basic modes of deformation observed

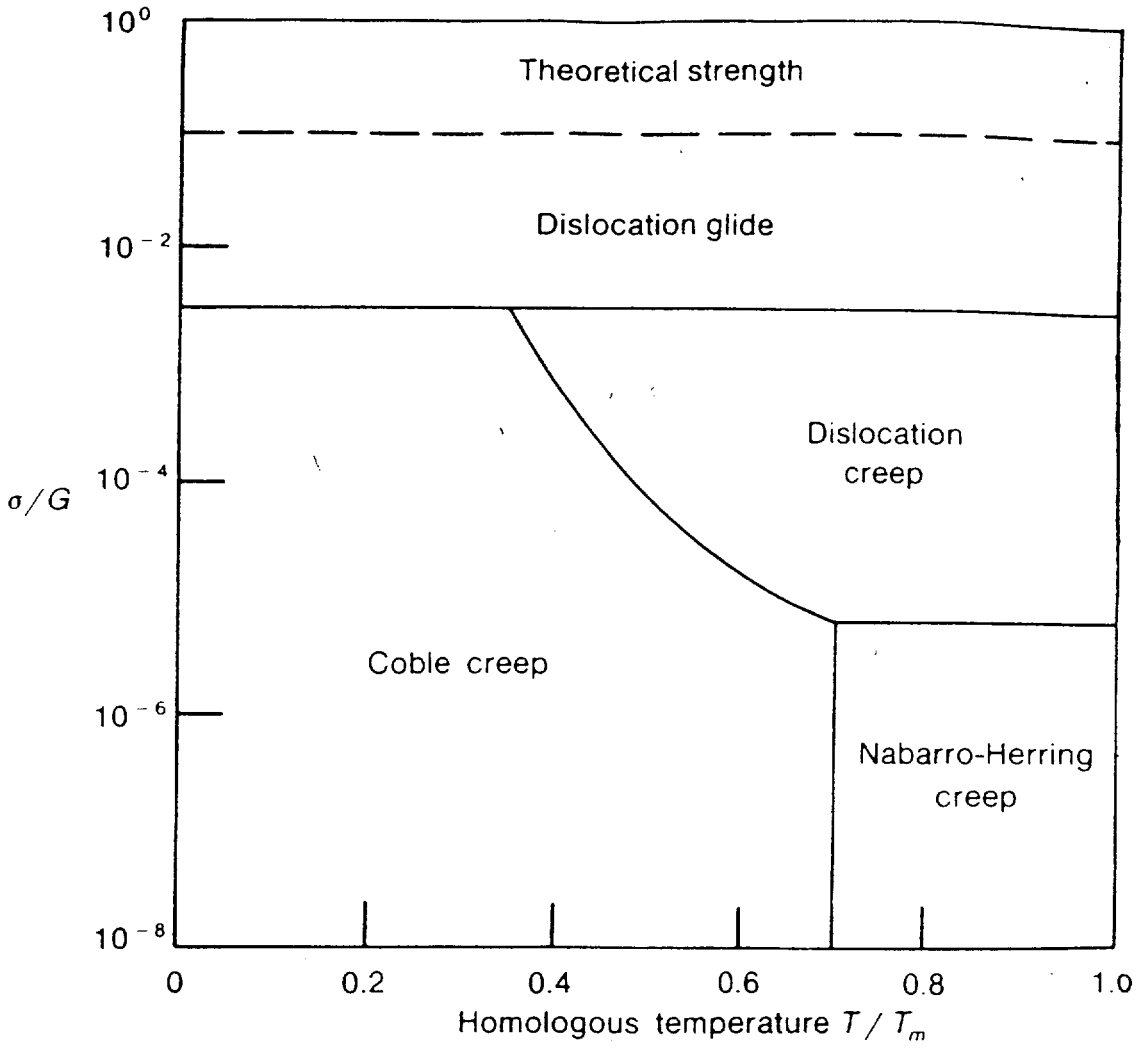

Figure 1

Generalized Ashby Deformation Mechanism Map[7]

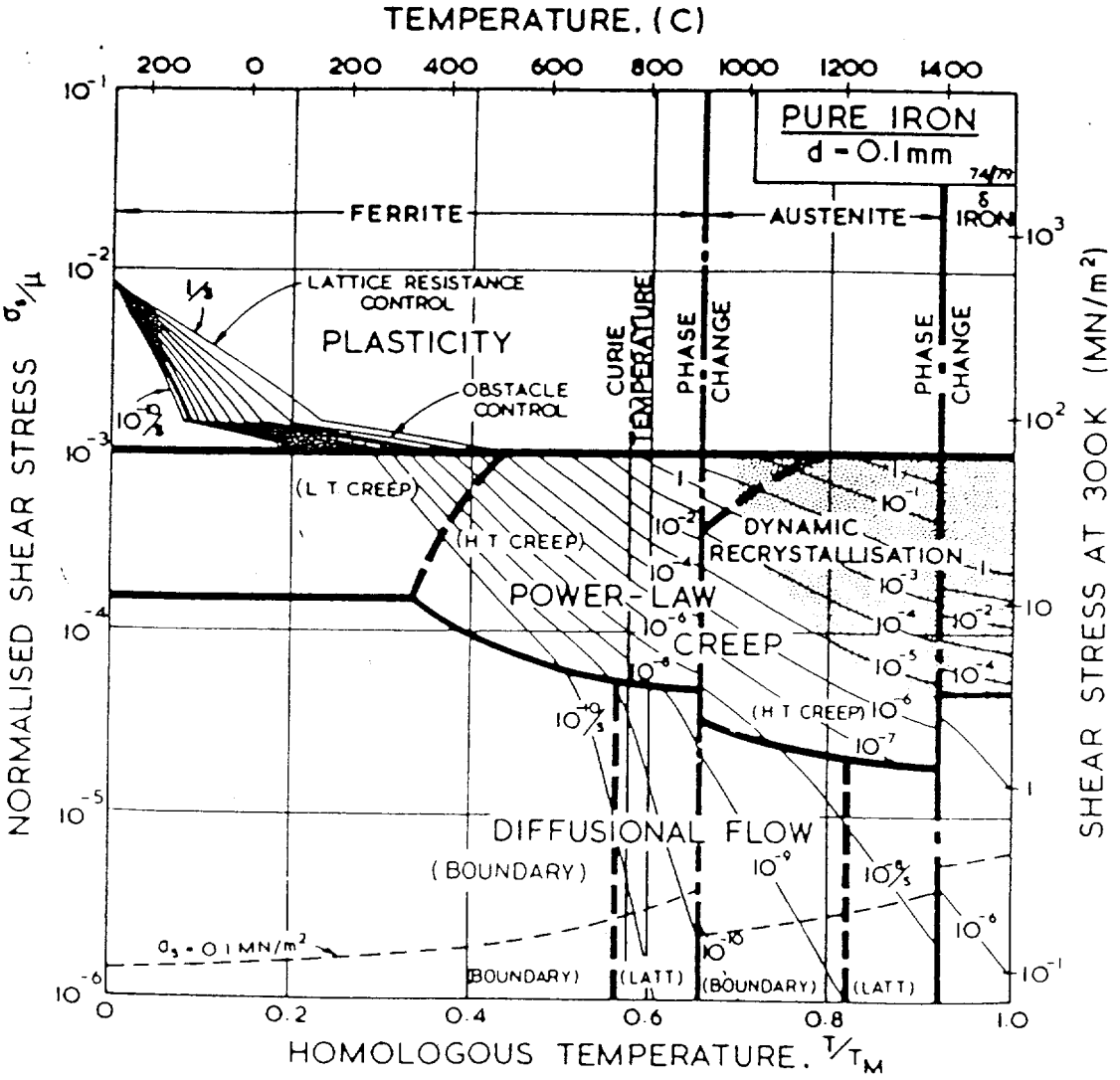

Figure 2
Ashby Deformation Map for Iron[1]

for a generalized metal. Figure 2 is a detailed portrayal of the fields for α-iron. Other body centered cubic metals would be similar. Metals and alloys with different crystal structures or extensive second phases will not have maps with the same proportions. The mechanisms commonly observed are described below.

Elastic collapse due to the theoretical strength being exceeded is at the highest stress level in Figure 1. This defines a shear stress level where a perfect crystal, or one without mobile defects will collapse. It will theoretically occur when $\sigma_s > \alpha G$. The quantity α has been calculated to be between 0.05 and 0.1, depending partly upon the crystal structure. For fcc metals the value of 0.06 is reasonable, while for the bcc metals a value of 0.1 is more appropriate.

If the shear stress is lower but still relatively high, the region of interest is the one labeled dislocation glide in Figure 1, or plasticity in Figure 2. Dislocation glide is the mechanism most often observed in room temperature plastic deformation of a material with an adequate number of operative slip systems. It may be the major mechanism operative up to 0.5 Tm as well.

At low temperatures relative to the melting point of the metal, deformation due to dislocation glide is limited by discrete obstacles or by lattice resistance. In the first case, the strain rate is dependent upon the nature of the obstacles, which may range from strong precipitates to the weak effects of minor solid solution hardening. In the latter case, the Peierls force, which is derived from the interaction of the dislocations with the periodicity of the lattice, sets up a barrier to dislocation motion. This Peierls force exists even in the absence of precipitates or solid solution effects.

Both of these resistances decrease as temperature increases. At lower temperatures the phenomena of work

hardening increases the energy required for dislocation movement to the point where the strain rate becomes zero. As the temperature increases past 0.3 Tm, thermally activated dislocation glide can lead to creep. According to Ashby, this type of creep is not well understood.

At lower stresses deformation by diffusional flow becomes the operative mechanism. This is termed Coble creep at lower temperatures, where grain boundary diffusion is limiting, and Nabarro-Herring creep at higher temperatures where lattice diffusion is most important. In either case, this diffusional flux will lead to plastic strain if coupled with grain boundary sliding, which is necessary to maintain continuity in the structure. In fact, these two phenomena are not independent, and the overall deformation may be described either as "diffusional creep" or as "grain boundary sliding with diffusional accommodation".[8] Others prefer to assign two additional separate fields in deformation maps to grain boundary sliding, placing a grain boundary diffusion controlled mechanism just above the Coble creep field, and a lattice diffusion controlled mechanism just above the Nabarro-Herring creep field.[5]

The stress and temperature dependence of these two fields turn out to be the same as for Coble and Nabarro-Herring creep. The strain rate in these latter cases may be expressed as:

Nabarro-Herring $$\dot{\gamma} = A_{NH} D_{lattice} b^3 \sigma_s / d^2 kT$$

Coble $$\dot{\gamma} = A_{Co} D_{gb} b^4 \sigma_s / d^3 kT$$

Here, A_{NH} and A_{Co} are dimensionless constants, while $D_{lattice}$ and D_{gb} are the diffusion coefficients for lattice and grain boundary diffusion respectively. The quantities b and d are

the Burger's vector and the grain diameter. T and k are the absolute temperature and Boltzmann's constant.

It is interesting to note that in pure iron (Figure 2) the higher creep resistance of the fcc lattice relative to the bcc lattice causes a re-establishment of Coble creep just above the transformation temperature. It is not clear whether this is due to the lower lattice diffusion in the fcc structure, or to differences in deformation characteristics. The strain rate in either mode of diffusional creep is highly temperature dependent, and becomes negligible at lower temperatures.

The other observed major mechanism of creep deformation is called dislocation creep or power law creep. Its general shear stress/temperature regime is indicated in Figure 1, and delineated for pure iron in Figure 2. The specific mechanism of deformation appears to be dislocation glide with thermally activated climb over obstacles. The climb step is rate limiting, but produces little plastic deformation.

Climb is facilitated by diffusion of ions and vacancies that act to raise the dislocation above obstacles. At higher temperatures lattice diffusion is most important, while at lower temperatures diffusion via the dislocation cores is controlling. The overall strain rate can be expressed as a function of the total diffusion rate and the normalized shear stress to some power. This power can be as low as three for the power law creep by glide only mentioned earlier. For dislocation creep by glide and climb, the power may be as high as ten. The higher the temperature the lower the stress dependence. The two regimes of high temperature and low temperature creep are indicated in Figure 2.

The rate equation for power law creep may be expressed as:[1,4]

$$\dot{\gamma} = A_1 D_{eff} \mu b (\sigma_s/\mu)^n / kT$$

where A_1 is a dimensionless constant, and μ is the shear modulus. The quantities b and σ_s have been previously defined. D_{eff} is the effective diffusion coefficient, and is equal to $D_{lattice}f_{lattice} + D_{core}f_{core}$, where f is the fraction of atom sites associated with each process. For all practical purposes, $f_{lattice}=1$, and $f_{core}= a\rho$, where a is the cross sectional area of the dislocation core, and ρ is the dislocation density. At lower temperatures, the increased influence of the core diffusion coefficient (which is a function of σ_s^2) causes the overall stress dependence to become a function of σ_s^{n+2}.

As the stress is increased in this region, the climb step is no longer limiting, and the "power law" correlation breaks down. Flow appears to become glide controlled and the strain rate is increased.

As temperature is increased dynamic recrystallization may occur in some metals, as shown for pure iron in Figure 2. This unbalances the strain hardening - recovery relationship by reducing the dislocation network. The uniform strain rate that resulted from this balance changes to a variable and higher rate.

Harper-Dorn creep is a form of dislocation creep that is observed in some metals (e.g., pure aluminum) at high temperatures and low stresses. It was discovered by J. G. Harper and J. E. Dorn, who noted that the creep rates they were observing experimentally were two orders of magnitude greater than expected for the anticipated Nabarro-Herring creep.

Harper-Dorn creep occurs in large grained pure metals above a certain critical grain size. It is also necessary that the preexisting dislocation density be very low. Plastic deformation appears to take place because of dislocation multiplication by cross-slip.[9] The constitutive equation for

Harper-Dorn creep is:

$$\dot{\gamma} = A_{HD} D_{lattice} b\sigma_s / kT$$

Wu and Sherby have proposed a unified theory for Harper-Dorn creep, power law creep, and power law creep breakdown utilizing the idea of an internal stress.[10] This internal stress is visualized as aiding the movement of half the moving dislocations and retarding the movement of the other half. The resulting constitutive equation uses a constant normalized internal stress to adjust the stress dependence of the strain rate for several pure metals.

This use of an internal stress differs from that proposed by Ahlquist et al in Reference 11. Here, the internal stress is viewed as a measure of the relative effects of strain hardening and recovery on the resistance of the lattice to dislocation movement. It opposes the applied stress and diminishes the effective stress for creep. At lower temperatures, where recovery is minimal, the internal stress rises to approximate the applied stress, and plastic deformation ceases. At higher temperatures, a balance is struck, and a steady state creep rate is observed.

Two frequent observations in high temperature creep are wedge cracking at grain boundary triple points, or the nucleation and growth of cavities at the material grain boundaries. These phenomena tend to occur at relatively long times and lower stresses, and result in intergranular fracture. This is invariably the mode of fracture of ferrous alloys in long term power plant service. However, it is not the typical outcome of a short term accelerated test, where failure is usually of a ductile transgranular nature.

Wedge cracks are thought to be nucleated and grown by grain boundary sliding.[12] They are observed at intermediate stress levels. Most intergranular cracking in field service

is due to the grain boundary cavitation mechanism, which has received a considerable amount of research and analysis. References 12 through 24 are a modest but representative fraction of published papers dealing with the subject. Treatments range from concrete empirically based analyses to somewhat abstract formulations. While the methodology may vary, there is universal agreement that the process is a complex one.

In either theoretical or empirical analyses, it is important to separate the distinct processes of cavity nucleation and cavity growth. Cavity nucleation mechanisms vary from material to material, as do cavity growth mechanisms. Lumping the two processes together makes it very difficult to form a coherent picture of the overall process.

Cavity nucleation was originally hypothesized to occur due to stress driven vacancy condensation. This was found to be unrealistic because of the very high level of vacancies/stress required. It is now felt that cavity nucleation will tend to occur where there is non-uniform deformation under an applied stress. Grain boundaries and their intersections with each other, with slip bands, and with particles are prime locations for cavity nucleation.

It is generally accepted that cavities nucleate continuously throughout most of the creep deformation process. Figure 3 shows that the rate of cavity nucleation as a function of strain varies widely.[23] Pure iron has a relatively low nucleation rate, while Type 347 austenitic stainless steel and 2 1/4Cr - 1 Mo ferritic steel have very high rates. Both of these latter alloys have a much higher grain boundary particle density than does pure iron.

One of the difficulties in correlating creep behavior to cavity nucleation rate is that cavities must grow to a size of 0.2 μm to be detected by SEM, and to 1.0 μm to be detected by

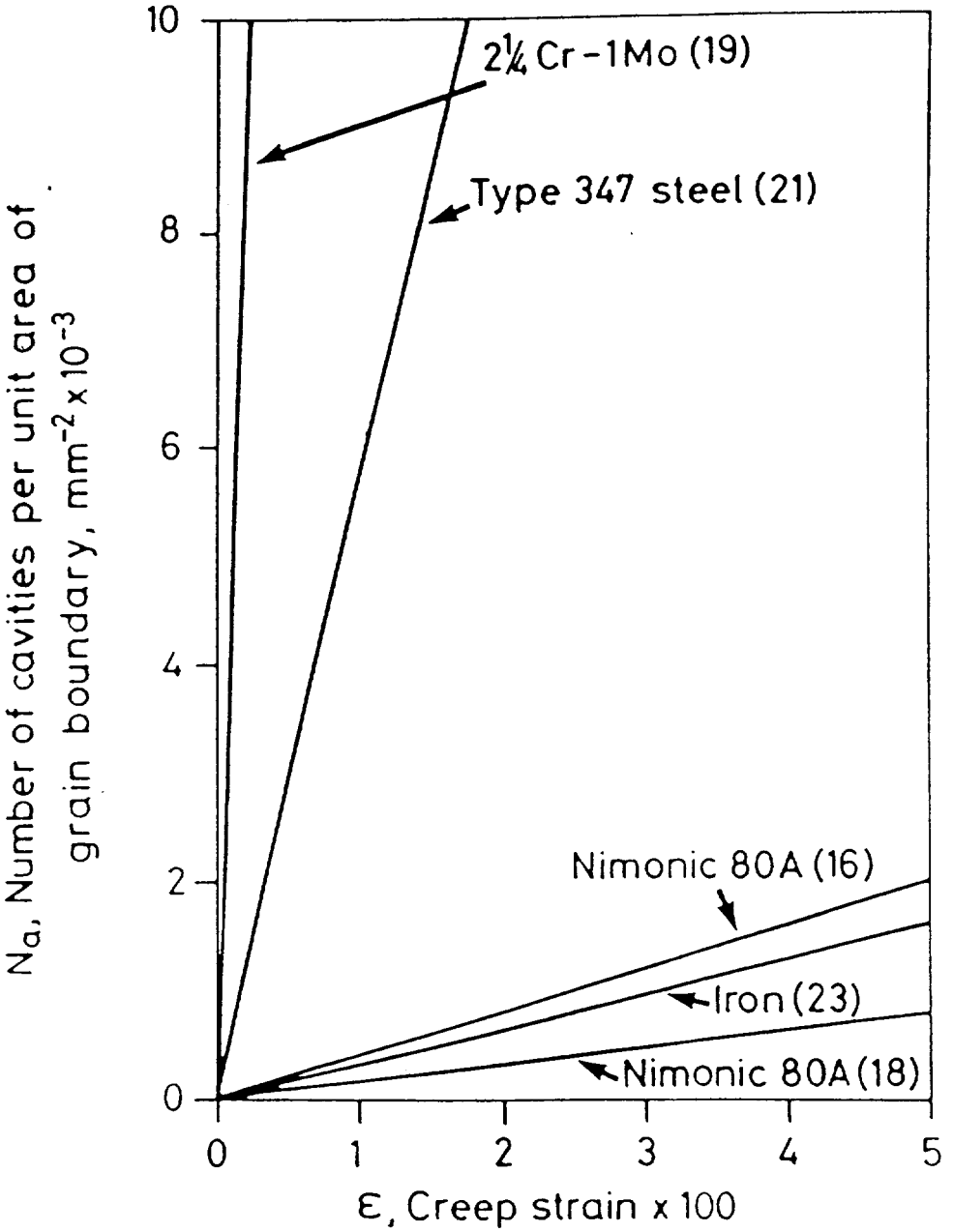

Figure 3
Cavity Nucleation Rate[23]

optical microscopy. Questions regarding such things as the sintering rate of freshly nucleated cavities are more or less beyond convenient investigation.

Some insight into the importance of the cavity nucleation mechanism may be found by considering the familiar and empirical Monkman-Grant relationship.[25] This relationship states that the product of the minimum creep rate and the rupture time is a constant for many engineering alloys over a considerable range of stress and temperature.

$$\dot{\epsilon}\, t_r = C$$

It has been observed that if the nucleation step is circumvented by the implantation of grain boundary cavities in a material, the Monkman-Grant relationship no longer describes the creep behavior. This implies that cavity nucleation controls the overall fracture process.[22]

Cavity growth is thought to be controlled by one of several mechanisms depending on the applied stress and temperature.[20] Grain boundary diffusion and plastic growth are the two primary growth mechanisms. The resulting deformation is accommodated by either diffusional creep or dislocation (power law) creep within the grain.[19] The predicted stress dependency for the different mechanisms is shown for silver in Figure 4.[20] The dashed line represents the effective growth rate at a given stress. The effective cavity growth rate is dominated by the accommodation mechanism, which especially limits the grain boundary diffusion growth mechanism usually seen.

Cavity growth may be either unconstrained, or constrained. Unconstrained growth is associated with relatively uniformly cavitated grain boundaries, with each

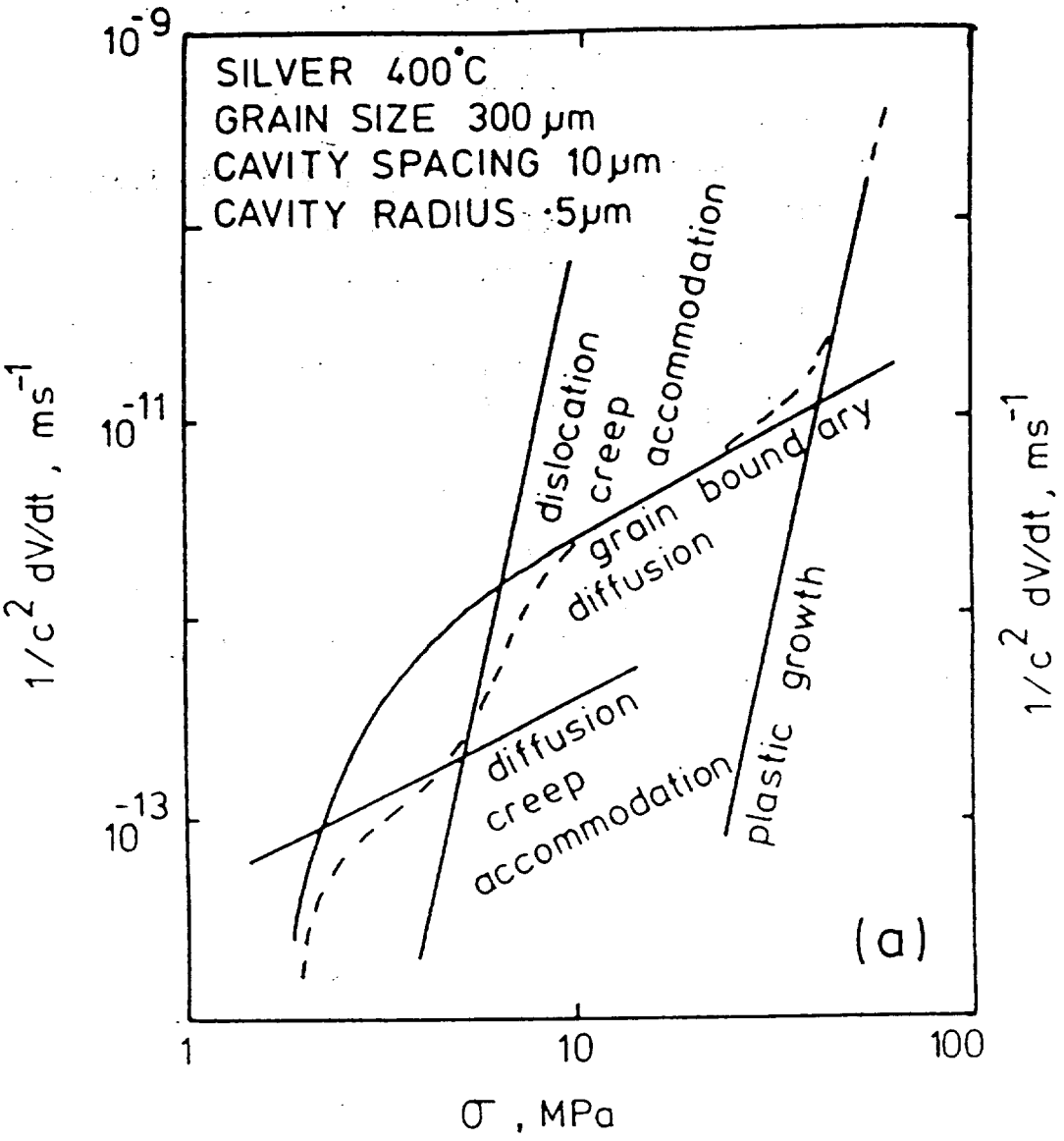

Figure 4
Cavity Growth Rate Mechanisms[20]

grain cavitating by diffusion and accommodating by the mechanism appropriate for the particular temperature and stress. Constrained growth occurs when the distribution of grain boundary cavities is inhomogeneous, and deformation in a highly cavitated grain is constrained by resistance from an adjacent less cavitated grain.[15,23]. This leads to load shedding from the cavitated grains to the uncavitated ones. Dyson points out that the dislocation creep rate in the limiting uncavitated grain is a function of the octahedral shear stress to some nth power. In unconstrained growth the stress dependence is theoretically linear.

Argon observed that while the theoretical studies of cavity formation and growth have shed much light, complete models using these results tend to be substantially in error when predicting times to failure.[19]

2.2 Creep of 2 1/4Cr-1Mo Ferritic Steel

The creep behavior of 2 1/4Cr-1Mo steel follows the same general pattern as outlined above. The fracture mechanism map for an annealed material is seen in Figure 5.[26]. The fracture mechanisms are similar to those in pure iron, although the extent and position of the various fields differ somewhat because of the alloying effects. It was noted that creep fracture is ductile and transgranular for test times of up to $1X10^7$ secs. While this does not mean that cavitation is not occurring, it is not the limiting fracture mechanism.

For perspective, both the field service and the laboratory stress/rupture tests to be discussed later are at a nominal stress of 41 MN/m^2 (6,000 psi) and range in temperature from 0.45Tm (field service - 1005°F) to 0.55Tm (highest test temperature - 1350°F). Field service has already exceeded $1X10^8$ seconds, and the laboratory tests did

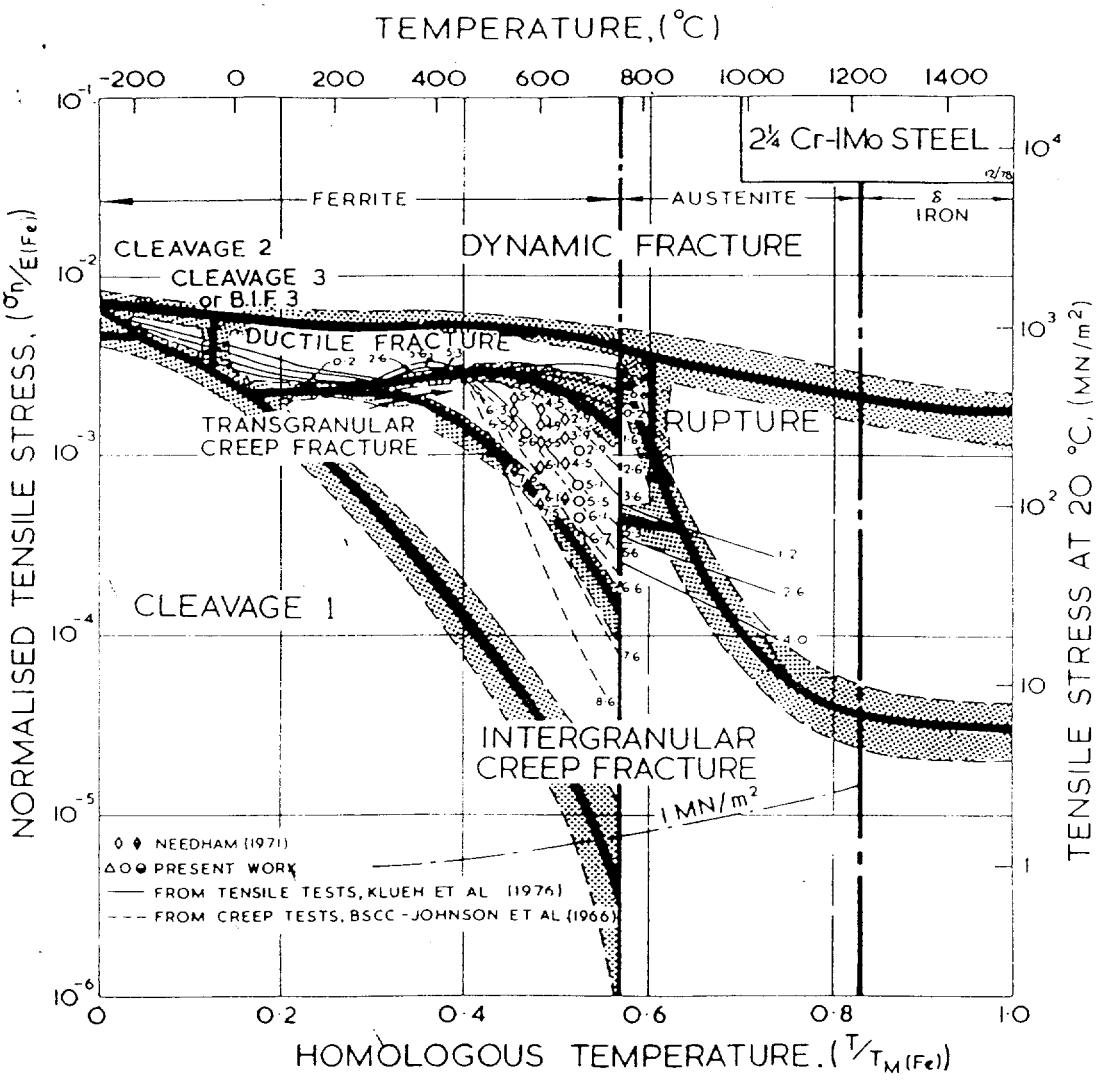

Figure 5
Ashby Deformation Map for 2 1/4Cr-1Mo[26]

not extend beyond about $2X10^6$ seconds. Therefore, it was not expected that the as-removed base metal would exhibit intergranular failure by cavity formation. However, this was not always the case with the weld heat affected zones as modified by the simulated field heat treatment.

The chromium-molybdenum steels exhibit a variety of carbide types depending on their state of heat treatment. These carbides confer a greater or lesser degree of creep resistance and hot tensile strength. The extent of this varies with the specific carbide, and also upon the amount of molybdenum remaining in solid solution. This latter effect is also not a simple one.

Investigations into the effects of interstitial and substitutional solid solutions of alloying elements in iron, such as C, N, Cr, Mo, and Mn, have shown synergistic interactions between the two classes of additives[27-30]. If one type or the other were added, the improvement in strength was modest. However, if both an interstitial and a substitutional alloying element were added the increase in creep and elevated temperature tensile strength could be substantial, even though no precipitation was observed.

This effect was especially strong when N was added to an Fe-Mn alloy, or when C or N was added to Fe-Cr or Fe-Mo alloys. It was noted that greatest strengthening occurred in the latter alloys. In all of these, the observed improvement has been ascribed to what is termed interaction solid solution strengthening by clusters of associated interstitial and solid solution atoms.

These clusters interact with the three dimensional dislocation networks to impede plastic deformation. The amount of molybdenum required to produce effective strengthening is not high. It is felt that the dislocation networks are saturated with Mo at about 1 w/o in solid solution.[31]

This type of solution hardening is not stable at elevated temperatures because of the chemical affinity of the various elements present. Precipitates form which include atoms from the iron matrix and the interstitial and solid solution atoms. These precipitates, which vary in their strengthening abilities, assume the role of impeding dislocation movement as the alloying elements are depleted from the matrix.

The nature, size, and spacing of the precipitates relative to the structure and spacing of the dislocation network have important effects on the creep strength. When exposed to elevated temperatures, it is usual for a precipitate system to change. Earlier metastable types either transform to or provide material for later more stable precipitates, which typically are larger, more rounded, and more widely spaced. This reduces the interaction with the dislocation network, leading to lower creep strength.

The precipitates present depend upon the overall chemistry of the steel, the thermal exposure, and the degree of creep deformation experienced. Plain carbon steels always have the orthorhombic M_3C present, where M is almost completely Fe. In steels containing molybdenum only, there is also a hexagonal close packed molybdenum rich M_2C. This phase transforms to the complex cubic M_6C containing iron and molybdenum in a 2:1 or 1:1 ratio.[32-34] In chromium steels, the trigonal Cr_7C_3 is present, as is the $M_{23}C_6$ complex fcc precipitate.[33] In Cr-Mo steels, all of these precipitates may be present, with substitution of one metal atom for another being the rule rather than the exception.

In the absence of creep deformation, transformations are driven by chemical and structural free energy considerations. If creep deformation is occurring, it may retard or accelerate the transformation.[35-36] The Mo_2C to M_6C transformation is accelerated by plastic strain, while the Cr_7C_3 to $Cr_{23}C_6$

transformation is slightly retarded.

The heat treatment and microstructure of the steel are also important. Carbide stability and creep strength are influenced by whether the microstructure is martensite, bainite, or ferrite.

The classic study of carbide development in a 2 1/4Cr-1Mo steel was performed by Baker and Nutting in 1959.[37] They tempered both quenched (martensite) and normalized (ferrite + bainite) material over a temperature range of 400°C to 750°C for times up to 1,000 hours. The transformation kinetics for the normalized material are shown in Figure 6 (after Ref. 12). Note that ϵ-carbide is an early transformation product with a hexagonal close packed structure and a general formula of $Fe_{2-3}C$.

In fact, the ferrite and bainite structures go through different transformation sequences. The bainite transforms as shown below, in a manner similar to martensite, while the ferrite exhibits different behavior.[37]

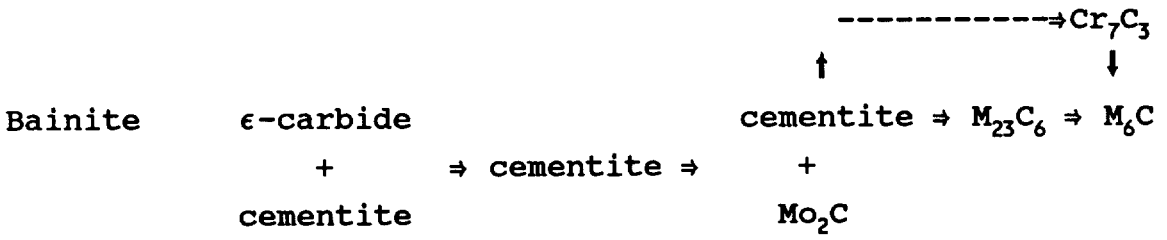

Ferrite $Mo_2C \Rightarrow M_6C$

It is generally accepted that Mo_2C is the primary strengthening phase in this steel. It is the only carbide other than the ϵ-carbide that nucleates as a dispersion in the matrix. It persists for a considerable time in the ferrite phase, and it has been observed that ferritic structures have

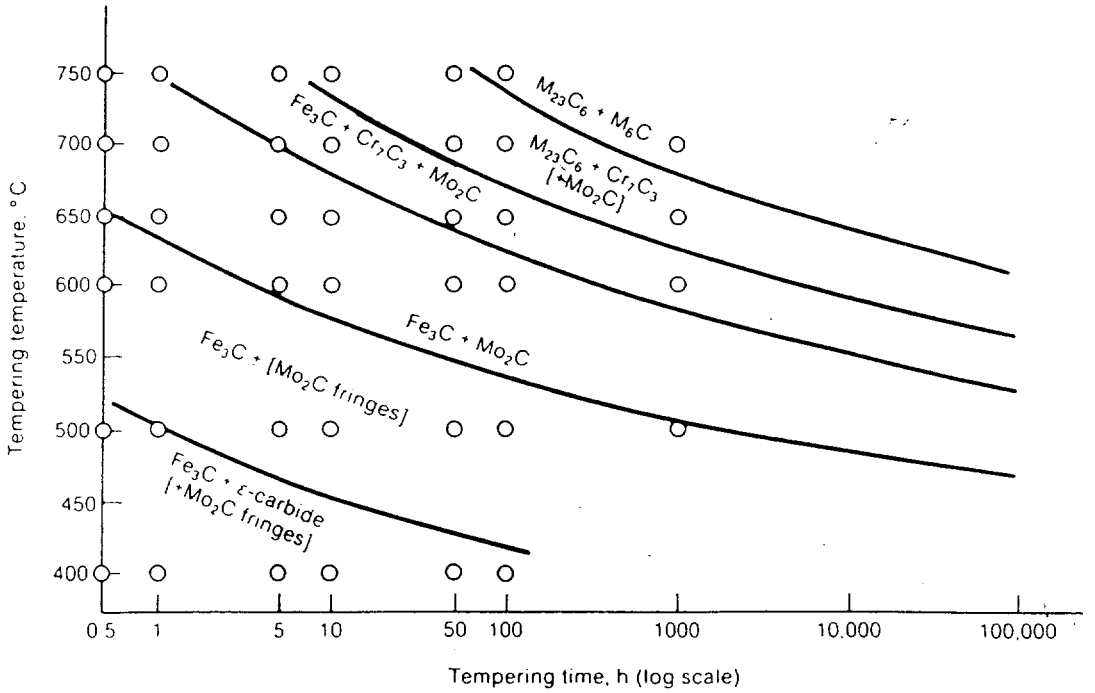

Figure 6
Carbide Development in 2 1/4Cr-1Mo[37]

better long term creep strength than tempered martensite or bainite. These latter structures are initially harder and stronger, and the early appearance of Mo_2C gives them higher short term creep resistance. This early advantage eventually dissipates as the ultimate transformation to the coarse M_6C continues. This terminal phase, and the intermediates $M_{23}C_6$ and Cr_7C_3, nucleate, for the most part on earlier carbides, or at the carbide/matrix interfaces.

The Baker & Nutting paper has a large amount of information and insights which are of considerable assistance in stress/rupture test data evaluation. Supplementary studies conducted by others have also proven of value.[38] In addition to the optical and electron microscope examinations of the various structures and carbide morphologies other analytical techniques have been utilized. These include anodic dissolution to recover the carbides, and differential dissolution/x-ray methods to quantify and analyze them.[39-40] Such techniques can be used to rationalize the information derived from creep rupture testing.

Evaluation of creep experiments on the chromium - molybdenum steels has taken many forms.[41-46] The treatments range from detailed models of a limited data set[42-44,46], to more general models of large data sets[41,45]. These latter treatments are related to the mathematical extrapolation methods to be described shortly.

These references point out the caution necessary in any extrapolation or modelling of creep behavior in these materials. Most extrapolative testing is done in the creep ductile range where intragranular failure occurs, while long term service behavior is more often low ductility creep with intergranular failure and profuse cavity formation. The most literature accessible constant for the Monkman-Grant relationship described earlier was, for 2 1/4Cr-1Mo, derived

for test times of up to 10,000 hours.[45] This constant is known to change as a function of stress, and is an integral part of some extrapolative schemes. In addition, many experiments have been conducted using quenched and tempered material, which has better short term creep properties than structures that are largely ferrite. A Monkman-Grant constant derived from short term tests of the former material would not necessarily reflect the long term service behavior of the latter.

In addition to the above factors, the variation in impurity levels is likely to change the creep/stress-rupture properties of 2 1/4Cr-1Mo. The effect of impurities on cavity formation and growth has been the subject of some study. It is generally acknowledged that impurities such as sulfur, phosphorus, tin, antimony, and copper are deleterious. The specific mechanism of property degradation for a given element is not always clear.

Cane and Middleton reported that cavities prefer to nucleate on grain boundary sulfides[43] at much lower stress levels than are required for nucleation on carbides. A general reduction in impurity levels relative to commercial steels was shown to sharply reduce cavity formation in Cr - Mo steels[68]. More detailed work revealed that P acted both to produce embrittlement as well as reducing the critical size for stable cavity nucleation[69,70]. Sn, Sb, Cu, and S were found by the same experimenters to migrate to cavities and increase the cavity growth rate. This is not completely consistent with Ref. 43 in the case of sulfur.

Stevens and Flewitt found that the most important decrease in creep/stress-rupture properties due to phosphorous was not related to its effect on cavity nucleation or growth[71]. Instead, they observed a strong propensity for phosphorous to enhance the formation and stability of the non

strengthening M_6C phase. Later work has shown sulfur to be the most important impurity for causing low ductility intergranular crack initiation and propagation[72,73]. Dissolved sulfur was thought to be the most important source.

These observations suggest that reduction of impurity levels in 2 1/4Cr-1Mo steel by improved steel making processes would increase the creep/stress-rupture properties and improve the high temperature creep ductility of the material. If this were accompanied by an appropriate increase in the room temperature tensile properties there might be no change in the validity of the oxidation corrected industry database to be discussed shortly. If the room temperature tensile strength were unaffected, the relationship derived from the database would be excessively conservative.

It should be recognized that the database, and the steel used for testing in this project, are typical of older material produced, in the latter case, prior to 1980.

2.3 Extrapolation Methods

A variety of methods have been developed for extrapolating observed creep rates or rupture lives to longer times and different temperatures.[47-55]. Some methods involved nothing more complicated than simple graphical extrapolation.[47-48] Most involve a defined parameter and are derived from very general descriptions of the creep rupture process.[12,49-55] A selection of the latter are shown in Figure 7.[12] The terms used are defined as follows: P = parameter value, t_r = time to rupture, t_a = intercept on the time axis, T_a = intercept on the absolute temperature axis, K_1, B, and B_2 = constants.

There is an additional method called the MCM or minimum commitment method, which imposes few constraints on the

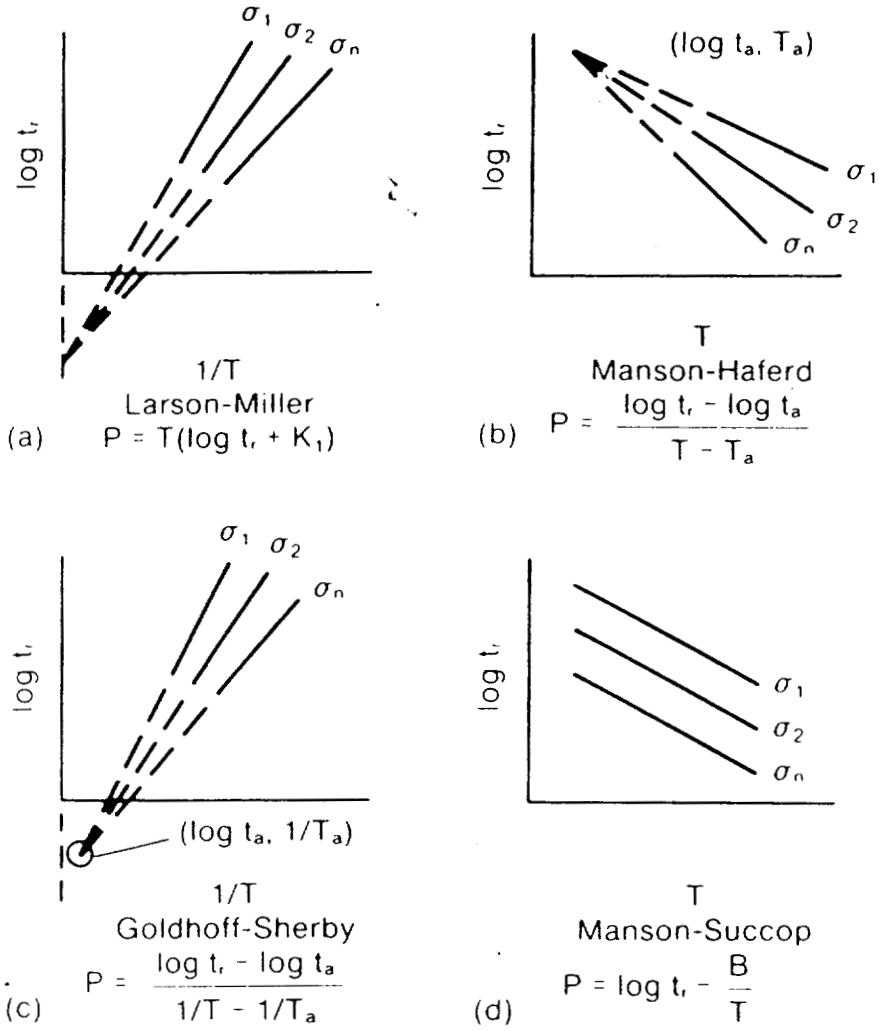

(a) Larson-Miller
$P = T(\log t_r + K_1)$

(b) Manson-Haferd
$$P = \frac{\log t_r - \log t_a}{T - T_a}$$

(c) Goldhoff-Sherby
$$P = \frac{\log t_r - \log t_a}{1/T - 1/T_a}$$

(d) Manson-Succop
$$P = \log t_r - \frac{B}{T}$$

(e) Orr-Sherby-Dorn
$$P = \log t_r - \frac{B_2}{2.3T}$$

Figure 7
Parametric Stress/Rupture Expressions[12]

parametric description.[12] It is calculated by a computer program, whereas the other methods shown may be derived graphically given adequate data.

The Larson-Miller parameter (LMP) is probably the most used method, and is usually as accurate as any.[52] This parameter can be derived from the generalized stress and temperature dependence of the creep rate or rupture time.[12]

$$t_r = A \exp(B/T)$$

$$\log t_r = \log A + B/2.3T$$

If A is assumed to be a constant and only B varies with stress:

$$B/2.3 = T(\log t_r - \log A)$$

$$B/2.3 = LMP = T(\log t_r + C)$$

It has been observed that the constant C varies for different materials and for heats within a material. Strictly speaking, it should be evaluated as locally as possible. However, a value of 20 is reasonably accurate for many metals, and is quite close for 2 1/4Cr-1Mo steel in particular.[54]

In any case, the stress-rupture testing in this program was all conducted at one stress, which makes it impossible to derive heat specific values of C, or to derive the constants for any of the other extrapolative expressions. Also, using the Larson-Miller parameter expression, $LMP = T(\log t_r + 20)$, allows direct comparison with an oxidation corrected industry standard database (Figure 8).[56] This database also relates the material behavior to the pretest tensile strength.

2.4 Other Considerations

The strong probability that the hot bending process

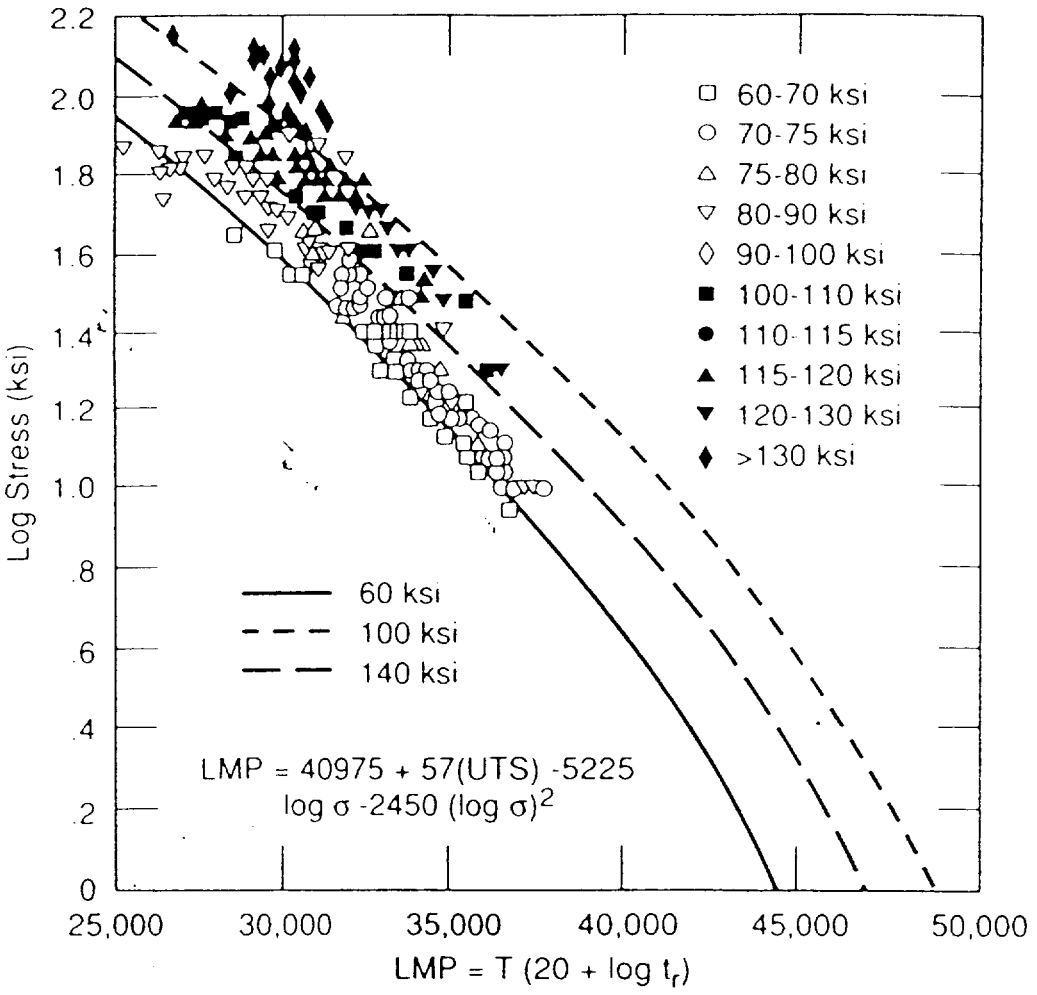

Figure 8
Stress vs LMP for 2 1/4Cr-1Mo[56]
Oxidation Corrected

raised the material above the Ac_1 temperature complicates this assessment. If the process truly amounted to only a long term temper, it would be expected that stress-rupture properties would decrease with increasing time at temperature. This might be modified by movement of Mo from ineffective strengthening precipitates to solid solution. It would be of concern if the loss of stress-rupture properties were as bad as has been observed for 1Cr-0.5Mo material, where the effect of a similar temper reduced time to rupture from 2800 hours to 290 hours.[57] Lesser effects could be accepted, since the use of the material is conservative, and the normal stress-rupture life is so long.

It is not known what effect raising the material into the partially austenitic range might have on the stress-rupture properties. Anything that either resets the precipitation clock, or releases Mo from a non-strengthening precipitate back to the matrix, should reduce the deleterious effects of over-tempering. However, the heat treatments used tested this issue directly.

If exposure at 1450°F does produce better results than anticipated from tempering below Ac_1, then primary concern would be shifted to adjacent areas that saw an extended tempering just below Ac_1. This required testing of additional samples that had been appropriately heat treated.

An item of interest was the relative performance of the weld containing samples. The geometry of the material/stress system means that the 6,000 psi stress for these tests is much higher than the coarse grained bainitic weld heat affected zones actually see in service. They are not a primary concern unless their properties are extremely poor. However, in headers and other complex weldments this is not necessarily true, and these tests permit comparative evaluations.

3.0 EXPERIMENTAL PROCEDURE

3.1 Purpose of the Laboratory Testing

The purpose of the laboratory testing was to generate a database that would allow quantitative comparison with both industry standard data and field observations. This included duplication of field material by heat treating material removed from the field at the time of the repairs to match the thermal exposure experienced by the field material. The appropriately heat treated material was then stress-rupture tested, hardness tested by a variety of instruments, and examined metallographically. This series of examinations produced some apparent anomalies, and additional heat treatments were also tested.

3.2 Laboratory Heat Treatments

Based on field heat treatment records, the following time-temperature histories were applied to two main sets of samples that were compared to the as-removed material.

Heat Treat Schedule 1

1. Heat to 600 °F at unrestricted degrees F per hour.
2. Heat from 600 °F to 1100 °F at 250 °F per hour maximum.
3. Heat from 1100 °F to 1460 °F (+/- 10 °F) at 100 °F per hour maximum.
4. Hold at 1460 °F (+/- 10 °F) for 5 hours.
5. Cool to 1100 °F at 100 °F per hour maximum.
6. Cool from 1100 °F to 600 °F at 250 °F per hour maximum.
7. Cool from 600 °F to room temperature at unrestricted °F per hour.

Heat Treat Schedule 2 was the same as Schedule 1 except that

the holding time at 1460°F was 10 hours.

Two series of samples were used. The first was from a pipe section designated A, and consisted entirely of base metal samples tested in the hoop direction. The second was from a second pipe section designated B, and consisted of longitudinal samples which included a circumferential girth weld in the gage section. In this way, the effects of the weld and weld heat affected zone on the creep properties were evaluated.

In order to investigate the effects of the hot bending process on the weldments a group of samples were prestrained to 2% plastic strain at 1460°F after the schedule 2 heat treatment and prior to stress-rupture testing. This was intended to approximate the most severe field procedure. Since the plastic strain was applied to both the weld and the base metal, both conditions were tested at the same time.

3.3 Stress-Rupture Testing

3.3.1 General

Both pipe sections were characterized prior to testing to insure that they represented acceptable material under the ASME Code. The requirements of ASME A335 Gr P22 were applicable.

Stress-rupture testing was conducted at a stress of 6,000 psi and a variety of temperatures. Temperatures were chosen so that times to rupture fell in the range of 50 to 1,000 hours. This required temperatures in the 1200°F to 1350°F range. The increased temperature method of test acceleration has been shown to be acceptable for the chromium-molybdenum steels. It has been found to be accurate for test times as low as 432 hours.[57] In contrast, the increased stress method of test acceleration was observed to produce extremely

pessimistic results, especially for shorter term tests.[57]

The stress chosen for the stress-rupture testing was calculated by the maximum Lame hoop stress formula. This has been shown to be a conservative choice by an evaluation reported in Reference 56. When uniaxial tests were compared to burst tests the use of the maximum Lame hoop stress led to an 1130 psi overage in the uniaxial test. This shifted the uniaxial curve to lower rupture times than for the burst tests. The use of this stress for test purposes is admittedly conservative. However, it is a known conservatism, and is intended to allow for possible below minimum wall pipe. Also, the evaluation being performed here is a comparative one, with the treated and untreated material each being exposed at the conservative stress level.

The effects of oxidation on stress-rupture test results must also be considered. This is especially true when increased temperature is used to accelerate the test. The actual pipe will not experience meaningful oxidation during its life. However, small samples tested at increased temperatures suffer loss of load bearing area due to oxidation. This effect was corrected for so that accurate comparisons may be made with the oxidation corrected industry database. The equations used are reported in Reference 56, and were originally due to work by Moles, Westwood, and Pinder in two earlier papers. The equations are shown in Figure 9.

Reference 56 also reports on an ageing curve developed for 2 1/4Cr-1Mo by Chopra. This curve, shown in Figure 10, relates the reduction in tensile strength to the thermal exposure. It will be used in later data analysis.

In all of these correlations there appears to be an implicit assumption that the material remains below its lower critical temperature, Ac_1. A continuous cooling transformation diagram on page 203 of Reference 12 implies

$$t_{r(o)} = \frac{[(1 - Zt_{r(act)})^{(1-2N)} - 1]}{Z(2N-1)}$$

$$Z = \frac{x}{Rt_{r(act)}} \text{ where } x^2 = Kt_{r(act)}\ 3600$$

$$K = {}_{10}{}^{[-70.2 + 1.36 \times 10^5 (1/T) - 7.4 \times 10^7 (1/T)^2]} \text{at } T < 888^\circ K$$

$$K = {}_{10}{}^{[-3.505 - 6552(1/T)]} \text{at } T > 888^\circ K$$

T = temperature, °K

K = temperature effect parameter

$t_{r(act)}$ = actual rupture time, hrs.

R = specimen radius in cm.

N = creep constant (8)

$t_{r(o)}$ = oxidation corrected rupture time

Figure 9
Oxidation Correction Equations[56]

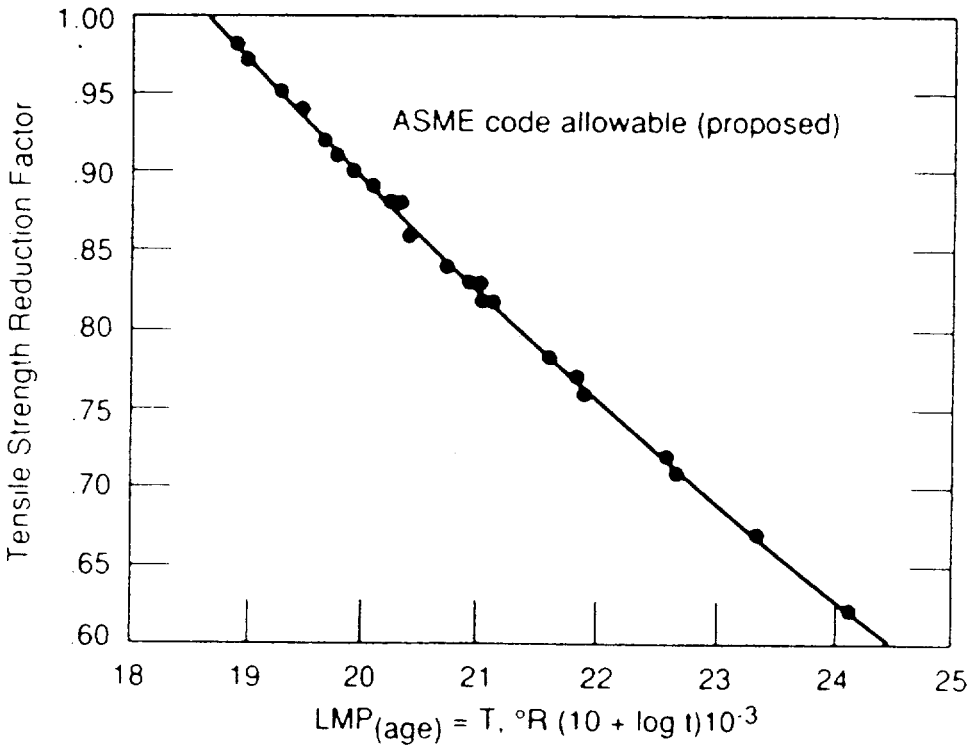

Figure 10
Ageing Curve for 2 1/4Cr-1Mo[56]

that Ac_1 is about 1470°F. The ASME B31.1 Power Piping Code gives it as 1480°F in Table 129.3.2. However, Wada and Eldis measured Ac_1 for three standard 2 1/4Cr-1Mo steels and found it to be in the range of 750-780°C (1382-1436°F).[58] In addition, they discovered that it varied within this range for a specific steel depending on heat treatment. Most other researchers data fell within this 1382-1436°F range. A Gleeble evaluation of the starting material used here yielded a value of 1472°F, yet partial austenization has clearly taken place in many of the samples.

There is probable that in many instances the 1450°F hot bending process did not act only as a tempering heat treatment, but also caused austenization of the alloy to some extent. This extent would depend on the exact chemistry of the steel, as well as the prior partitioning of alloying elements between the matrix and the alloy carbides. The section being heat treated might end up in a more creep resistant condition than the material immediately adjacent to it.

In addition to the possible effects of heating the material above Ac_1, long term service exposed 2 1/4Cr-1Mo has been observed to regain elevated temperature strength when tempered for a short time at 730°C (1346°F).[59] This has been explained by the hypothesis that the additional exposure had caused the dissolution of a molybdenum containing precipitate, releasing Mo to act as a matrix strengthener. Analysis did, in fact, show that Mo in the matrix increased from 0.28 w/o to 0.44 w/o during tempering.

All of the above considerations may affect the behavior of the hot bent field material. For this reason, the sample material must experience the same thermal exposure prior to testing.

3.3.2 Laboratory Sample Description

Standard 0.500" diameter, 2" gage length samples were used for both tensile testing, and stress-rupture testing. Samples were removed from the appropriately heat treated block. The basic sample designation reflects the block that it came from. Additional heat treatment may have been performed. This is indicated by additional nomenclature, which will be explained as encountered.

The use of the various blocks is as follows:

1. A1. As-removed material with no additional heat treatment. Always tested in the transverse (hoop) direction. Base metal only.
2. A2. As-removed material with several heat treatments discussed later. Always tested in the transverse direction. Base metal only.
3. A3. Equivalent to A1 plus heat treatment schedule 1 (five hours at 1460°F). Always tested in the transverse direction. Base metal only.
4. A4. Equivalent to A1 with several heat treatments discussed later. Always tested in the transverse direction. Base metal only.
5. A5. Equivalent to A1 plus heat treatment schedule 2 (ten hours at 1460°F). Always tested in the transverse direction. Base metal only.
6. B1. As-removed material with circumferential butt weld. No additional heat treatment. Always tested in the axial direction with the weld/base metal interface in the gage section.
7. B3. Equivalent to B1 plus heat treatment schedule 1. Always tested in the axial direction with the weld/base metal interface in the gage section.
8. B5. Equivalent to B1 plus heat treatment schedule 2. Always tested in the axial direction with the weld/base metal

interface in the gage section.

9. B6. Same as B5, except strained to 2% plastic strain at 1450°F prior to testing. Always tested in the axial direction with the weld/base metal interface in the gage section.

The room temperature tensile properties of the main test series samples are shown in Table I. The B1T sample was a transverse sample from the base metal of one of the pipes comprising the B series weldment. All as-removed material met the chemical and physical property requirements of ASME SA 335, P22. The weld metal in the B series samples was also analyzed. The relevant chemistries are found in Table II.

The main test series samples were intended to evaluate the effects of the simulated field hot bending thermal exposures. In addition, it was decided to evaluate the effects of longer term exposures at 1450°F and 1375°F. The former was intended to test the hypothesis that the material was in fact above its Ac_1 temperature. After 2, 25, 50, and 100 hours at 1450°F, the samples were air cooled, rather than slowly cooled as in the simulated field exposure.

The 1375°F exposures were intended to provide some insight into the behavior of material adjacent to the heated regions. Three samples were chosen to provide trend information. The exposure times of 8, 13.7, and 28.2 hours were calculated, using the aging formula in Reference 56, to be nominally equivalent to 1450°F exposures of 3, 5, and 10 hours.

3.4 Laboratory Hardness Testing

In addition to the stress-rupture samples, sections were machined from each heat treated block, and surface ground for hardness measurements. In the case of the B series samples, this involved a hardness traverse across each longitudinal

TABLE I
Tensile Properties

	YS, psi	UTS, psi	%El in 2"	%RA
A1T	30,200	68,800	31.0	62.0
A3T	26,800	63,700	32.5	65.5
A5T	29,400	68,000	31.6	66.0
B1T	30,200	72,000	29.0	64.0
B1L	37,400	74,700	22.5	67.2
B3L	29,800	66,900	29.5	71.2
B5L	34,200	70,300	26.0	70.2

Notes: T = transverse sample from base metal. L = longitudinal sample including weld/basemetal interface in gage section.

A1, B1 As-removed
A3, B3 As-removed + 5 hrs 1460°F + Furnace Cool
A5, B5 As-removed + 10 hrs 1460°F + Furnace Cool

Table II
Chemical Analyses

Element	A Samples	B Samples	B Weld Metal
C	0.10 w/o	0.12 w/o	0.052 w/o
P	0.011 w/o	0.012 w/o	0.019 w/o
S	0.011 w/o	0.008 w/o	0.015 w/o
Mn	0.55 w/o	0.52 w/o	0.78 w/o
Cr	2.14 w/o	2.06 w/o	2.03 w/o
Mo	1.03 w/o	0.96 w/o	1.23 w/o
Si	0.41 w/o	0.47 w/o	0.61 w/o

sample from base metal to base metal. For all A series samples a sufficient number of hardness readings were taken to characterize each condition.

Hardness tests were conducted using a Rockwell hardness tester and an Equotip hardness tester. The latter device works by comparing the velocity of an incoming impact body with the velocity after striking the test surface. It has proven to be very accurate and reliable in both the laboratory and field settings. It was used exclusively for the field measurements described later.

In addition to the conversion tables provided by the device manufacturer, equivalences were developed between the Equotip tester and standard macrohardness test methods using the laboratory samples. This provided a check on the accuracy of the Equotip general conversion tables as applied to 2 1/4Cr-1Mo material.

Hardness changes have been investigated as a method of evaluating in-service microstructural degradation.[62] For maximum utility, the beginning hardness of the material should be known. While this is not known for the field material here, a relationship was developed for the laboratory samples. Also, the use of hardness to estimate tensile strength should permit analyses similar to those employed in superheater tube evaluation in Reference 56. If the exposure parameters of the material are known, this methodology allows recovery of the initial tensile strength (and hardness) for comparison to a large database for 2 1/4Cr-1Mo material. The recent publication of this paper opens up a number of previously unexplored evaluation paths.

3.5 Metallography on Laboratory Samples

Metallography was conducted on a broad spectrum of pre

and post test samples. Standard metallographic procedures were used. Etchants were 1 - 4 % Nital, or Picral, depending on the aspect of the structure being investigated. All photomicrographs are of Nital etched samples.

3.6 Anodic Dissolution of Matrix

In order to investigate the effect of matrix or solid solution alloy content on stress-rupture behavior a limited number of anodic dissolutions of the matrix were performed. The technique may also be used to collect carbides for differential dissolution or X-ray diffraction, and has been shown to reliably dissolve the matrix without attacking the carbides[39,40]. The dissolution was accomplished by making the sample the anode vs a platinum cathode in a 10% HCl in methanol solution, which was subsequently analyzed by the inductively coupled plasma (ICP) method.

3.7 Purpose of the Field Evaluations

The field evaluations were intended to establish an equivalence between specific sections of installed piping and similarly treated laboratory samples. If this were not always possible, it was necessary, at a minimum, to detect if there was any evidence of serious degradation. The methodology for this was similar to that used in determining remaining life for high temperature systems.

The primary tools available for such evaluations are metallographic replication and field hardness measurements. If serious degradation is found by these methods, removal of mechanical test samples from the piping is possible.

3.8 Metallographic Replication

3.8.1 General

Metallographic replication may be used to detect the nature of the alloy carbides present and their degree of coarsening. The progress of this coarsening can be related to expected service life.[60-61] However, the number of different precipitates in service exposed 2 1/4Cr-1Mo is rather large[37], and there is a range of shapes present, depending on whether the mode of inquiry is optical or electron microscopy.

In the present instance, an already complex material has been subjected to some atypical heat treatments. Tracking quantitative changes in precipitate morphology is not likely to be profitable. However, metallographic replication may be used to establish a nominal equivalence between field and laboratory material.

The most important use of replication is to determine if serious damage has occurred by detecting cavities about 1 μm or larger in diameter. The presence and number of these cavities can be related to the creep life fraction consumed, as shown in Figures 11 & 12 (reported in Reference 12). Note that one of these figures is quantitative in nature, while the other describes a qualitative trend. The presence of cavities in the field material at this time would be of considerable concern.

In a long term examination scheme, it is not clear that material with the unusual thermal exposure imposed on these pipe sections would respond as expected. Since the pattern of precipitation has been altered, it is possible that the quantitative manifestation of detectable cavities will be altered. If it were altered to be more like that of a carbon steel, the fraction of cavitated grain boundaries might be much lower even when fracture was imminent.

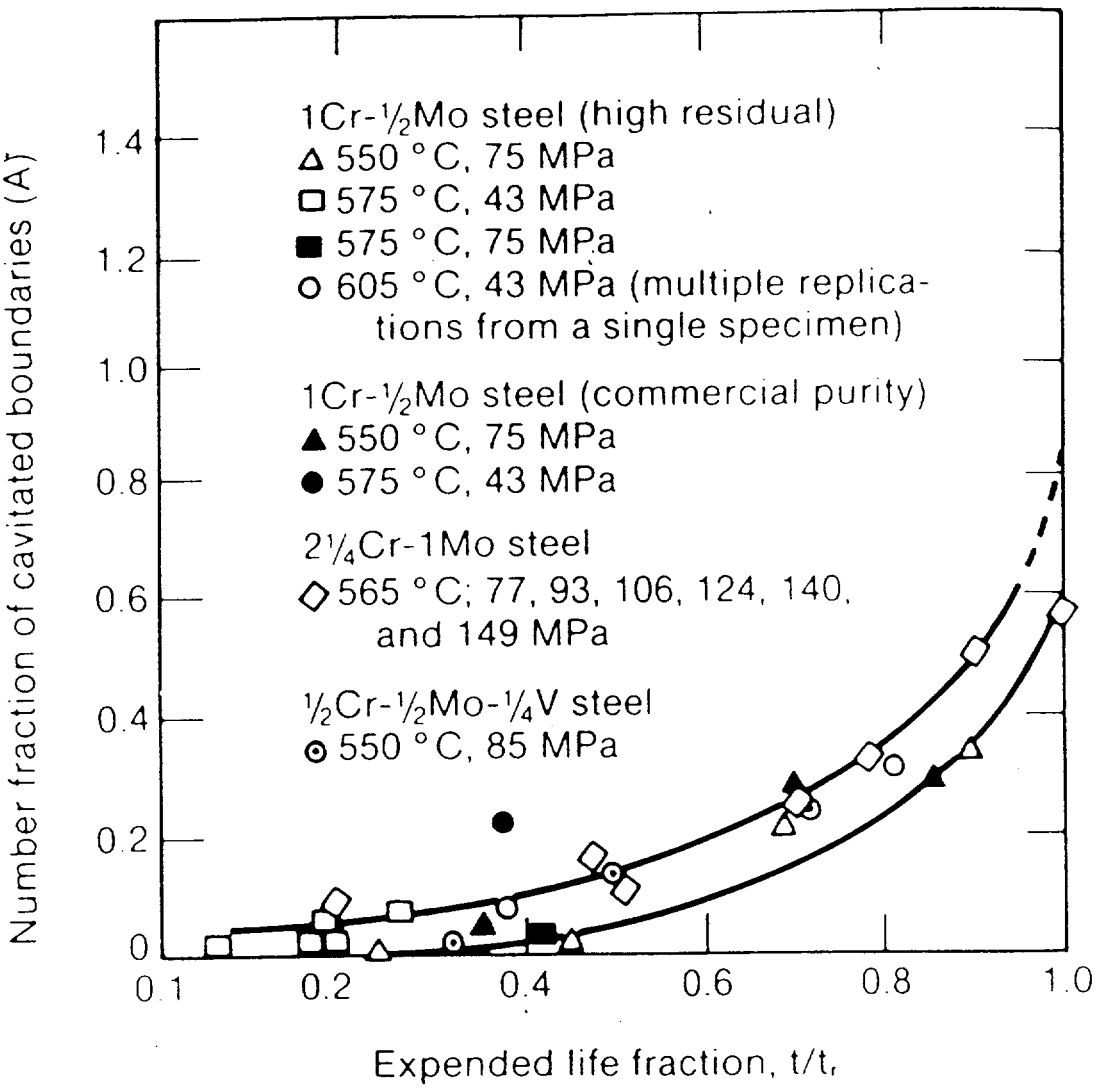

Figure 11
Quantitative Cavity Formation vs Life Fraction
for Cr-Mo Steels[12]

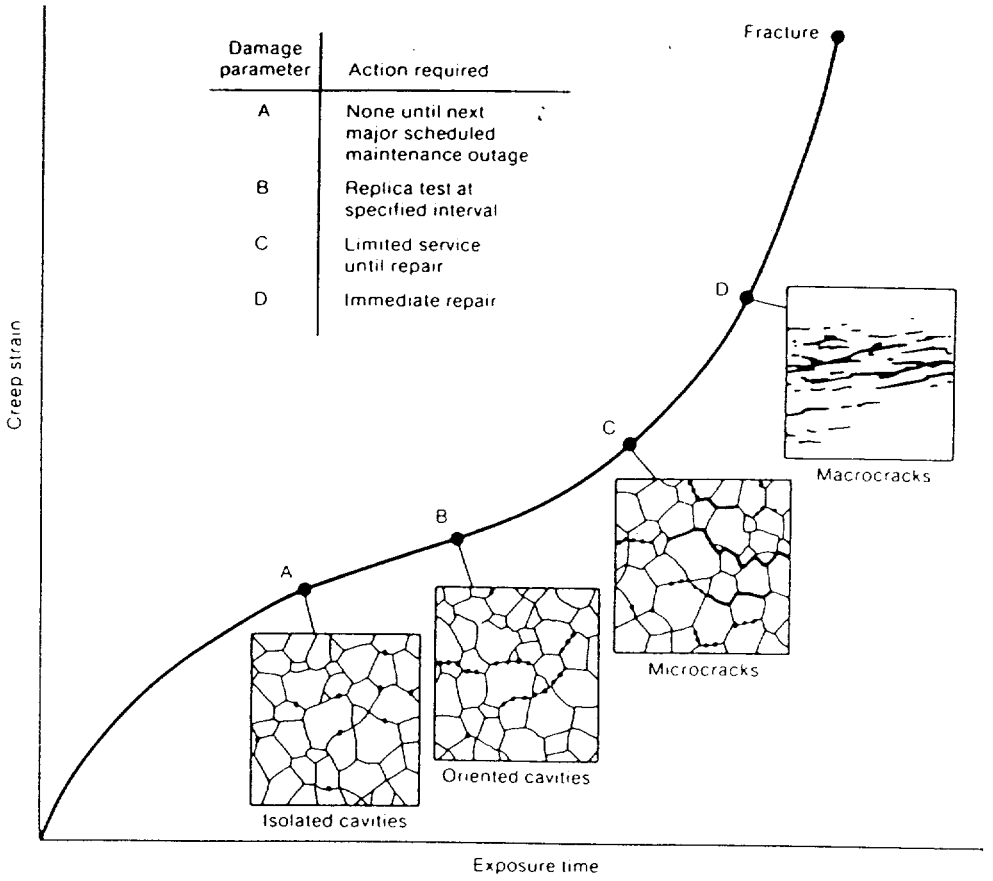

Figure 12
Creep Life Assessment vs Cavity Classification[12]

For example, Figures 13 & 14 show the microstructure near the stress-rupture failure location of a carbon steel tube that was exposed at 1005°F for 26,500 hours. It was inadvertently installed in a superheater bundle in place of a 2 1/4Cr-1Mo tube. If one refers back to Figure 3[23], it appears that this may well be the expected level of cavitation for a carbon steel tube. A normally heat treated and service exposed 2 1/4Cr-1Mo pipe with this level of cavitation would not be expected to be near failure, although it would warrant further investigation.

Another drawback to field replication is the concern that the structure being replicated is the real structure through the nominal 2" wall thickness of the pipe. These pipes may have decarburized surfaces, which will remove all clues to pipe condition other than the presence or absence of cavities. Sections removed from the inside diameter of this line in 1986 exhibited an anomalous microstructure with substantial surface decarburization of from 0.035" to 0.137". The cause of this anomalous surface microstructure is not known. Several examples will be presented in conjunction with the field replication results later.

If this decarburized microstructure also exists on the outside surface, metallographic preparation and replication will reveal a structure with very few carbides. This will remove key correlation parameters with the laboratory samples, which are examined throughout their cross section. The pipe sections in this hot reheat line unfortunately tend to run near their minimum wall of 1.869". There is a real reluctance on the part of plant operators to risk encroachment on this minimum. Therefore, some of the replicas may not yield any more information than the presence or absence of grain boundary cavitation.

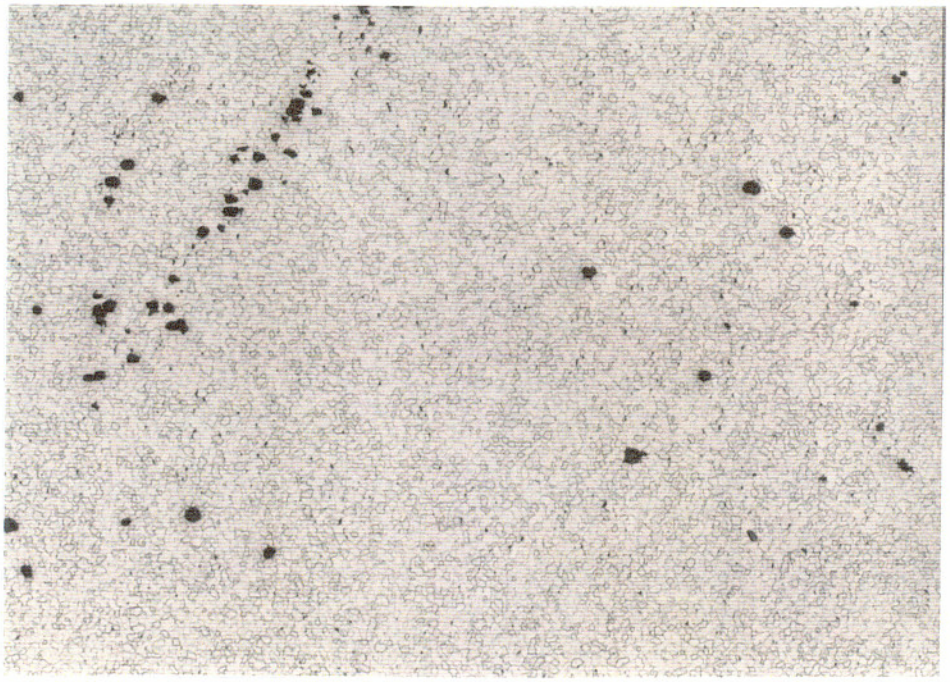

Figure 13
Ruptured Carbon Steel Boiler Tube - Cavity Formation
50X Nital Etchant

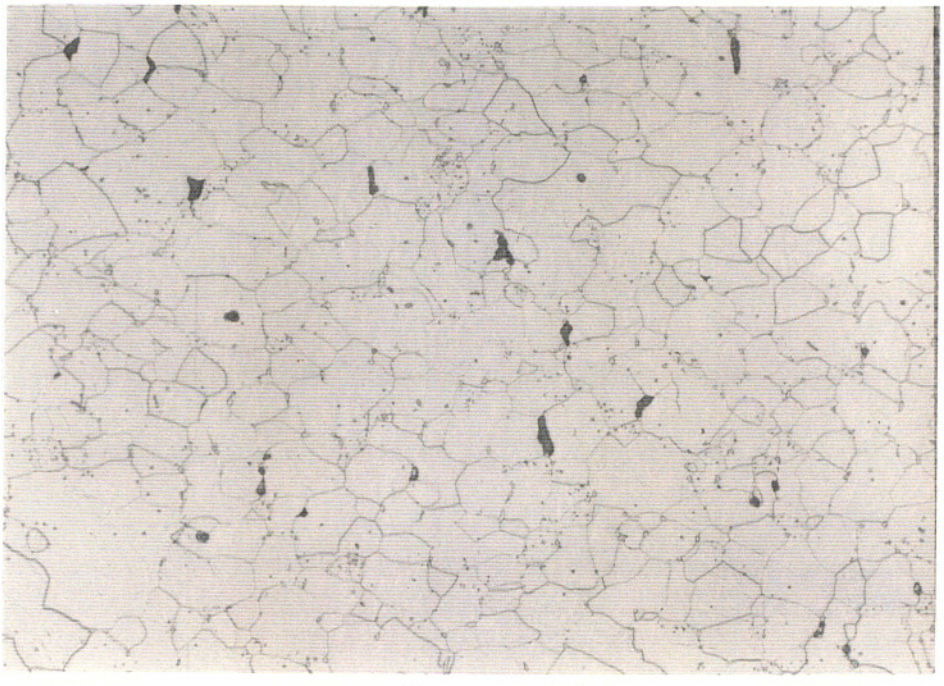

Figure 14
Ruptured Carbon Steel Boiler Tube - Cavity Formation
400X Nital Etchant

3.8.2 Replication Procedure

The replication process consists of the following steps.

1. Grind flat surface on pipe in area of interest using commercial abrasive wheels up to 240 grit (e.g., 3M Scotchbrite).
2. Prepare surface using metallographic abrasive papers ranging from 80 grit to 600 grit.
3. Continue metallographic polish of surface using 9, 6, 3, and 1μm diamond pastes.
4. Final polish with 0.05μm alumina powder.
5. Etch with 4% Nital.
6. Repeat steps 4 & 5 two more times.
7. Replicate using acetate tape and acetate containing solution. Spray back of replica with flat black enamel and mount on glass slide with double sided carpet tape.
8. Repeat steps 4 & 5 with progressively longer etching periods to obtain a satisfactory range of replica definition for examination at different magnifications.
9. Examine using light microscope.

The surface preparation process seeks to produce the same quality of surface as is achieved in laboratory metallography. The replication step is intended to reproduce the microstructure and preserve it for examination. These goals are not always attained because of the difficult working conditions in a power plant during an outage. For instance, the large pipe had a very thin oxide scale, which was popping off in tiny pieces as the pipe slowly cooled to ambient temperature. If introduced into the work area, one of these small abrasive pieces of magnetite could spoil a prepared surface at almost any point in the process. The technique is laborious in the extreme, and one is never completely satisfied with the results.

3.9 Field Hardness Testing

Hardness tests were also employed for comparison of field conditions with laboratory samples. Field hardness testing was conducted exclusively with the Equotip hardness tester. Tests were conducted in the areas prepared for replication.

It should be noted that the presence of decarburization on the outside diameter of the field piping will sharply reduce the accuracy of the hardness measurements. In such a case, the hardness based evaluation will predict lower strength and shorter projected life than the interior properties of the pipe would justify.

4.0 RESULTS

4.1 Stress-Rupture Testing

The stress-rupture test results for the main series samples are given in Table III. Test temperature, actual time to rupture, oxidation corrected time to rupture, and the calculated Larson-Miller parameter are tabulated. The average Larson-Miller parameter (LMP) for each group of samples is also given, along with the standard deviation for that group. Equivalent data are reported in Table IV for the supplementary stress-rupture tests of the A2 and A4 sample groups. Note that the rupture times used from now on will be the oxidation corrected rupture times.

The main series stress-rupture test results are plotted in Figures 15-17. Examination of these figures reveals that where duplicate tests were run, there is some scatter. However, as will be seen shortly, there are definite average trends and predicted differences in outcome among the heat treatment conditions.

A wider spread in properties is reflected in the supplementary A2 and A4 samples (Figure 18). Finally, from a practical standpoint, the heat treatment conditions reflected in Figure 19 are the ones of most importance in evaluating the expected performance of the real piping. These represent the thermal history of the piping and the adjacent piping.

The differences in the various heat treatment conditions may be more easily be seen in terms of the experimentally determined mean Larson-Miller parameters. The situation for the main series of samples is seen in Figure 20. This shows a similar pattern of variation for both A and B series

Table III
Main Series Stress-Rupture Test Results

	°F	°R	tact, hr.	tcorr, hr.	LMPcorr	
A1	(As-removed)					
	1350	1810	57.2	60.5	39.42	
	1350	1810	97.1	104.5	39.85	
	1306	1766	307.6	342.9	39.80	
	1330	1790	183.6	201.5	39.92	
	1287	1747	475.6	538.8	39.71	
	1275	1735	569.0	647.6	39.58	
					39.71	0.18
A3	(As-removed + 5 hrs 1460°F + Furnace Cool)					
	1287	1747	306.1	338.1	39.36	
	1287	1747	235.7	257.2	39.15	
	1304	1764	145.8	156.9	39.10	
	1338	1798	67.6	71.6	39.30	
	1270	1730	534.1	603.6	39.41	
					39.26	0.13
A5	(As-removed + 5 hrs 1460°F + Furnace Cool)					
	1270	1730	569.2	645.9	39.46	
	1330	1790	91.4	97.5	39.36	
	1287	1747	368.9	411.6	39.51	
	1306	1766	201.6	220.1	39.46	
					39.45	0.06
B1	(As-removed)					
	1279	1739	326.0	360.0	39.23	
	1295	1755	255.5	280.7	39.40	
	1313	1773	177.1	192.7	39.51	
	1330	1790	135.3	146.5	39.68	
	1350	1810	43.2	45.3	39.20	
					39.40	0.20
B3	(As-removed + 5 hrs 1460°F + Furnace Cool)					
	1252	1712	581.2	653.6	39.06	
	1252	1712	448.1	496.6	38.86	
	1316	1776	93.0	98.9	39.06	
	1287	1747	193.8	209.7	39.00	
	1264	1724	463.3	517.5	39.16	
					39.03	0.11
B5	(As-removed + 5 hrs 1460°F + Furnace Cool)					
	1287	1747	270.6	297.1	39.26	
	1270	1730	371.0	410.7	39.12	
	1330	1790	48.8	51.2	38.86	
	1306	1766	139.1	149.6	39.16	
					39.10	0.17
B6	(As-removed + 5 hrs 1460°F + Furnace Cool + Strained 1460°F+ Air Cool)					
	1287	1747	241.7	264.0	39.17	
	1306	1766	144.6	155.7	39.19	
	1325	1785	213.1	235.0	39.93	
	1260	1720	632.4	718.3	39.31	
					39.40	0.36

Table IV
A2 & A4 Stress-Rupture Test Results

T°F	T°R	tact, hr.	tcorr, hr.	LMPcorr	
A2-2 (As-removed + 2 hrs 1450°F + Air Cool)					
1330	1790	126.9	137.0	39.62	
1290	1750	316.6	350.8	39.45	
				39.54	0.12
A2-25 (As-removed + 25 hrs 1450°F + Air Cool)					
1330	1790	45.9	48.1	38.82	
1290	1750	199.2	216.0	39.09	
				38.96	0.19
A2-50 (As-removed + 50 hrs 1450°F + Air Cool)					
1330	1790	49.5	51.9	38.87	
1290	1750	202.4	219.6	39.10	
				38.98	0.16
A2-100 (As-removed + 100 hrs 1450°F + Air Cool)					
1330	1790	52.2	54.8	38.91	
1290	1750	168.1	181.1	38.95	
				38.93	0.03
A4-8 (As-removed + 8 hrs 1375°F + Air Cool)					
1330	1790	82.9	88.2	39.28	
1290	1750	301.0	332.7	39.41	
				39.34	0.09
A4-13.7 (As-removed + 13.8 hrs 1375°F + Air Cool)					
1330	1790	80.8	85.9	39.26	
1290	1750	418.7	471.3	39.68	
				39.47	0.30
A4-28.2 (As-removed + 28.2 hrs 1375°F + Air Cool)					
1330	1790	56.9	59.9	38.98	
1290	1750	272.0	299.1	39.33	
				39.16	0.25

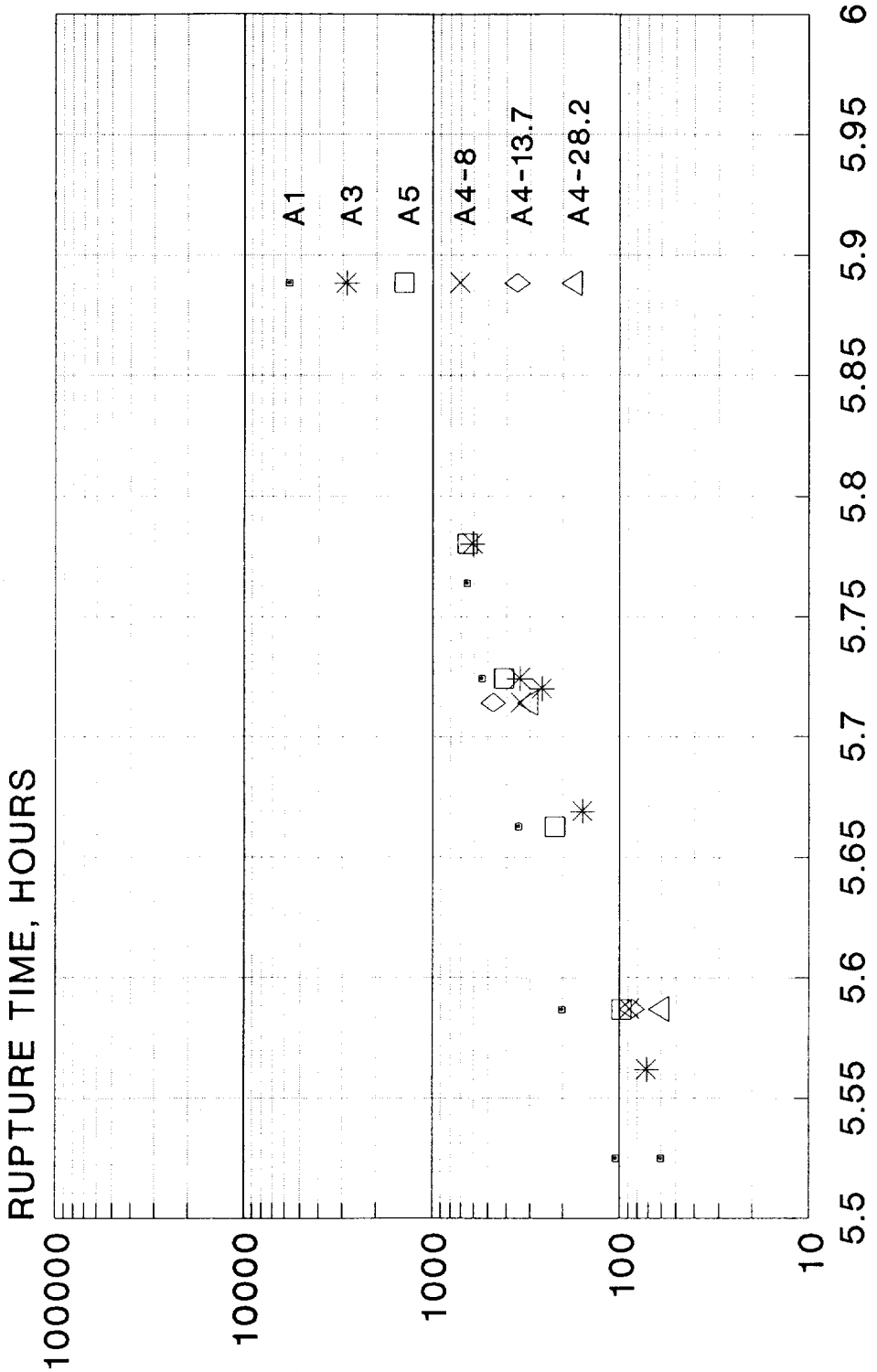

Figure 15 A Samples Rupture Time vs 1/T

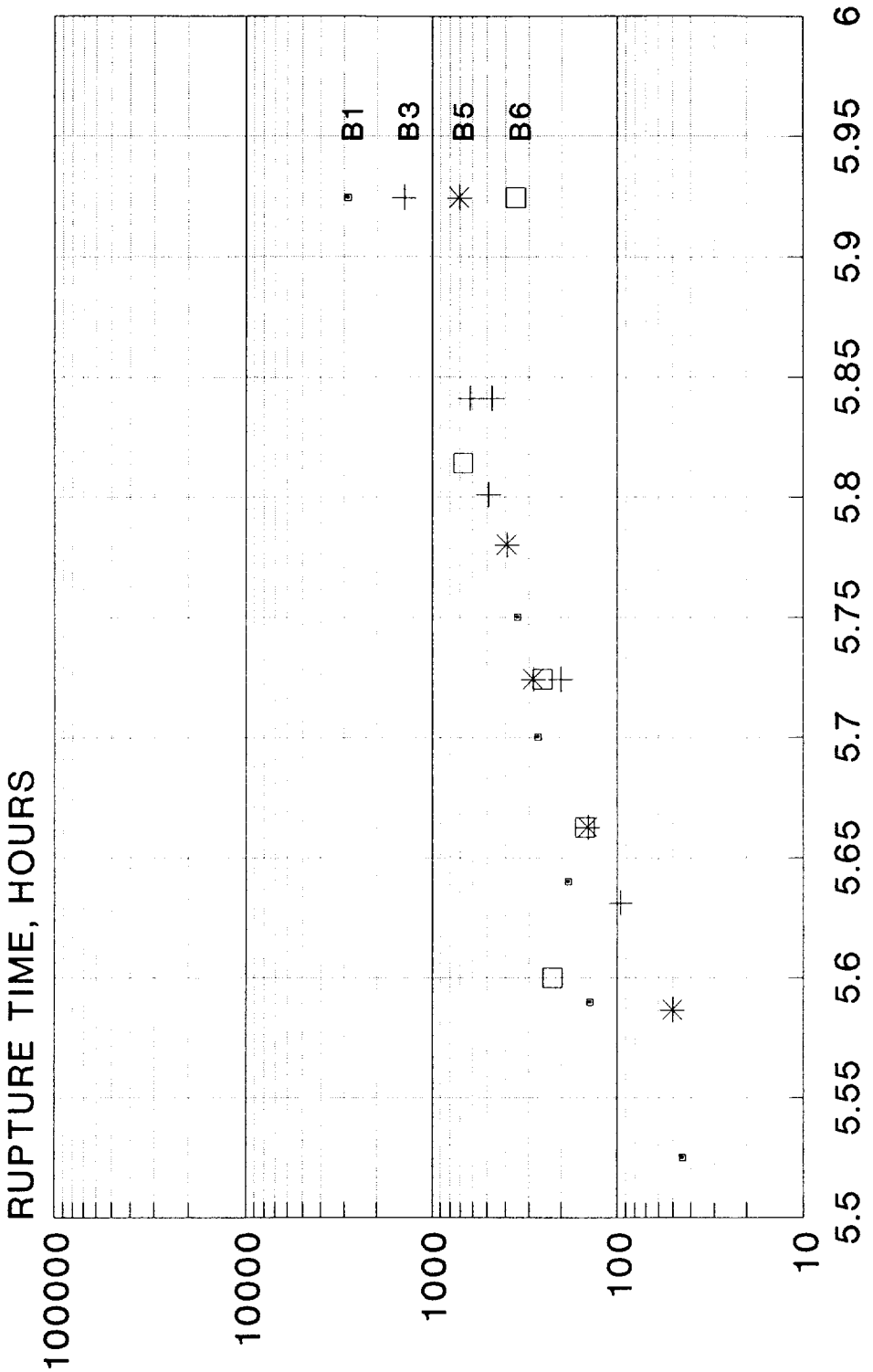

Figure 16 B Samples Rupture Time vs 1/T

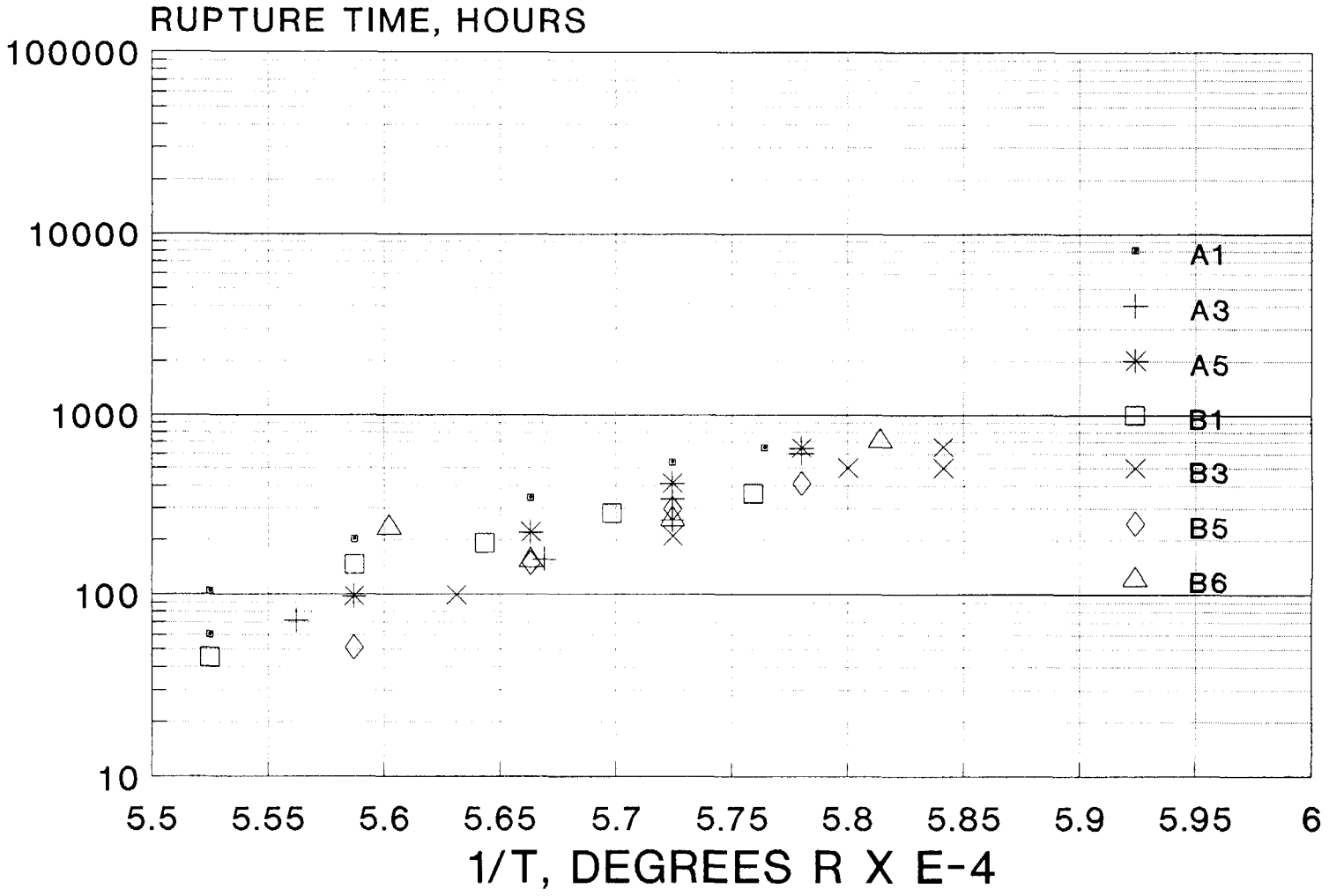

Figure 17 A & B Samples Rupture Time vs 1/T

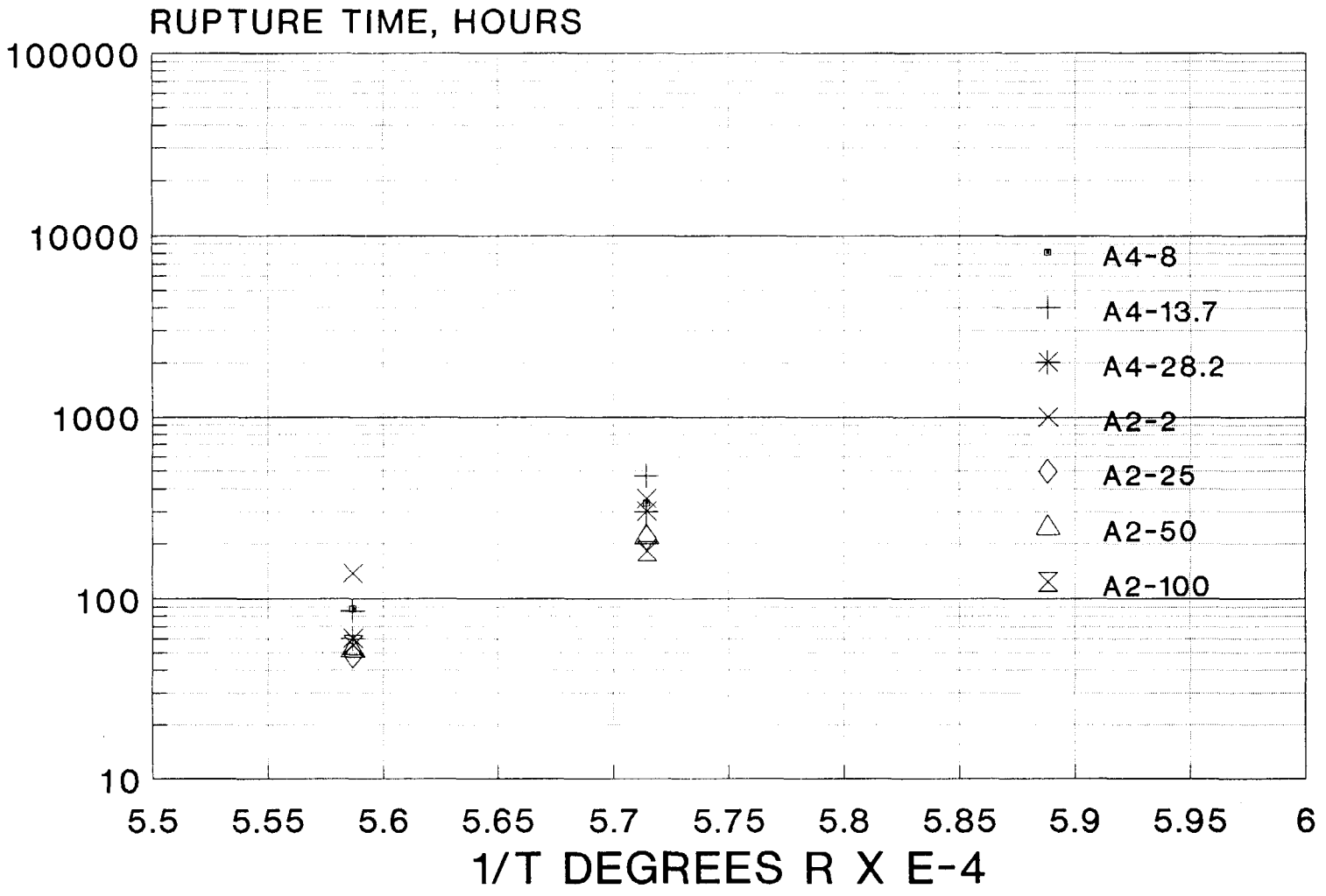

Figure 18 Supplementary A Samples Rupture Time vs 1/T

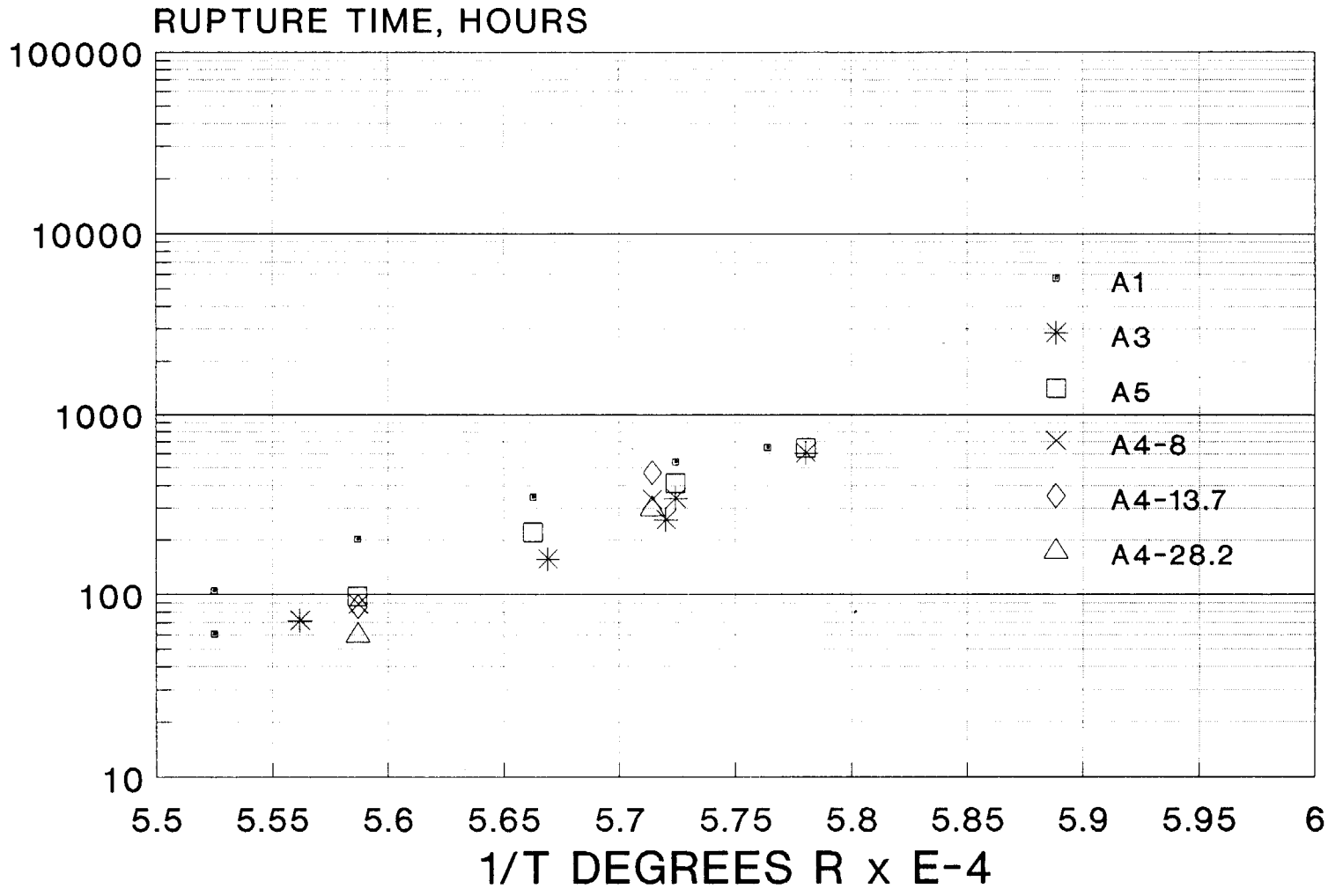

Figure 19 Selected A Samples Rupture Time vs 1/T

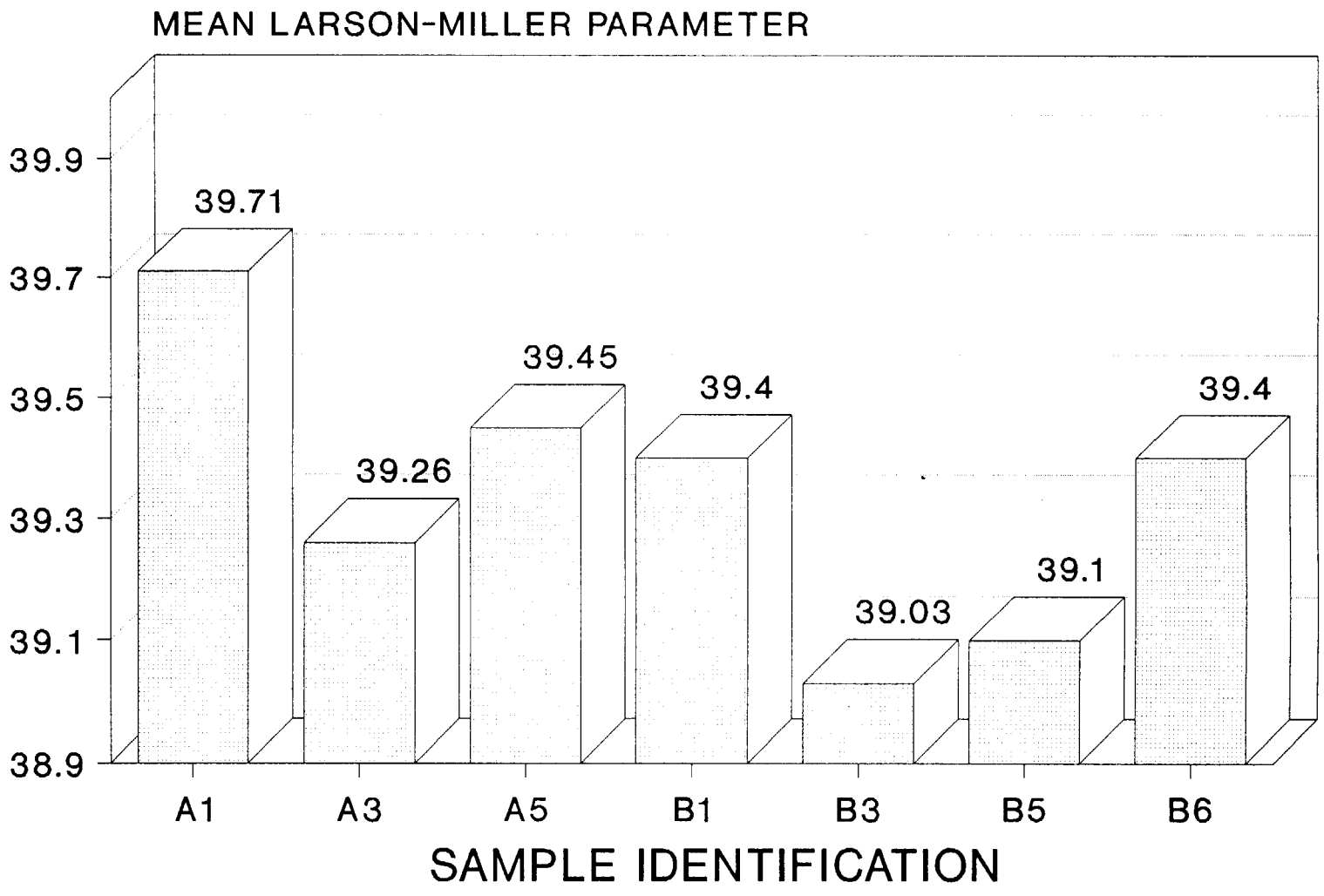

Figure 20 Larson-Miller Parameter Main Series

samples, and also demonstrates the effect of the weld heat affected zone in the B series. As mentioned earlier, this WHAZ is oriented so that it does not see the maximum hoop stress in the field heat treated piping.

Figure 21 presents similar information for all the A samples, both from the main and supplementary series heat treatments. It is apparent that 1460°F exposure for increasing time followed by a slow cool as per heat treatments 1 or 2 does not lead to continually decreasing properties, as would be expected from extended subcritical tempering. It is also apparent from the longer term A2 sample results that extended exposure at 1450°F followed by air cooling is more deleterious to stress-rupture properties.

The extended exposure of the A4 samples below the expected Ac_1 temperature does lead to slowly decreasing properties, except for the 13.7 hour exposure results. These results are based on only two samples, one of which was substantially higher that the other. If the higher data point were excluded and only the other one used (see Table IV), the LMP value of 39.26 would be appropriate relative to the other exposure time results.

If the LMP values in these figures are used to calculate the predicted rupture times at the operating temperature of 1005°F, the results are as shown in Figures 22 & 23. It is apparent that the predicted loss of stress-rupture properties is not as severe as the factor of ten observed for the overtempered 1Cr-1/2Mo steel described in Reference 57. In fact, at the longer test times observed here the actual variation in rupture time from the worst sample (A2-100) to the best sample (A1) was slightly under a factor of 3.5.

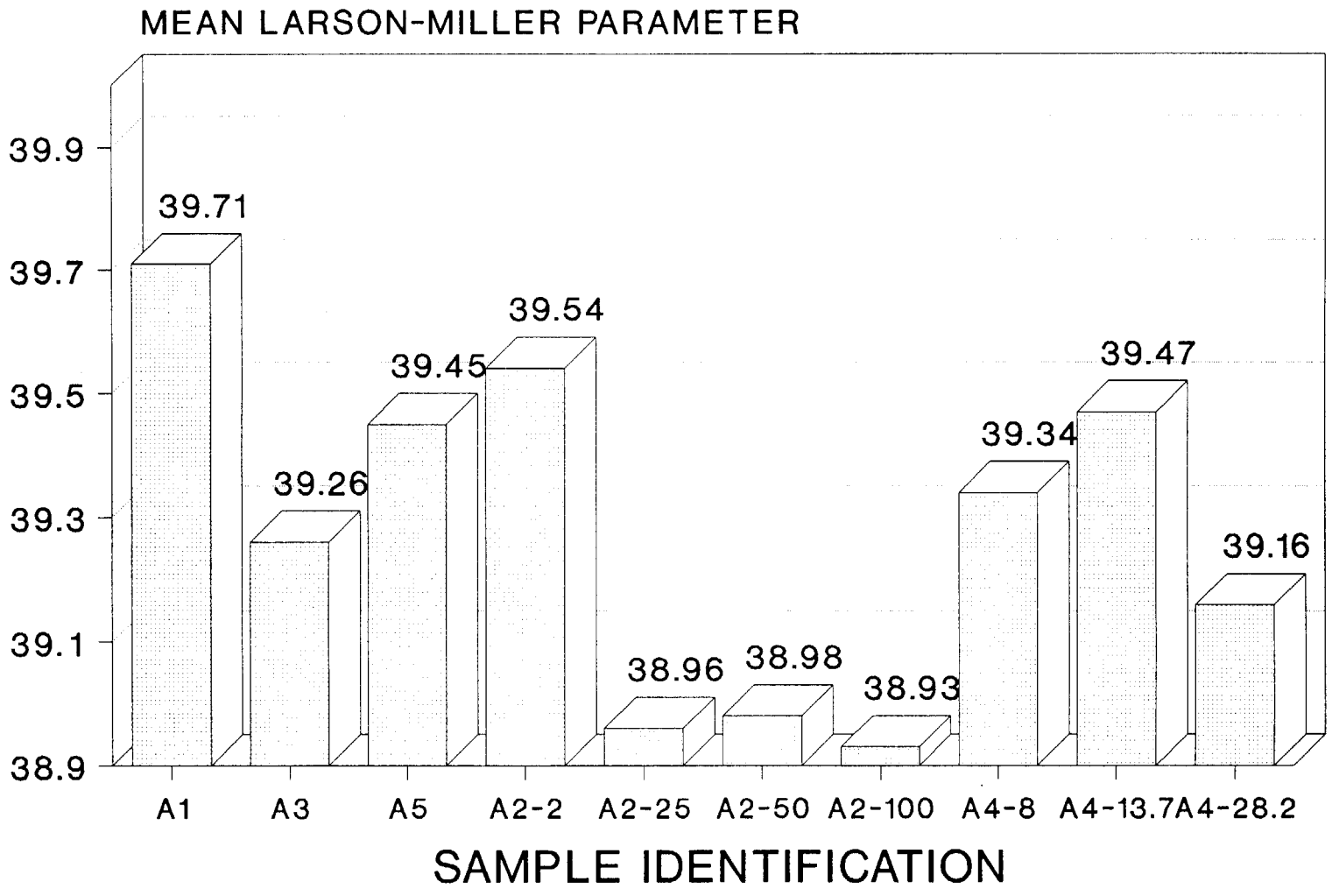

Figure 21 Larson-Miller Parameter All A Samples

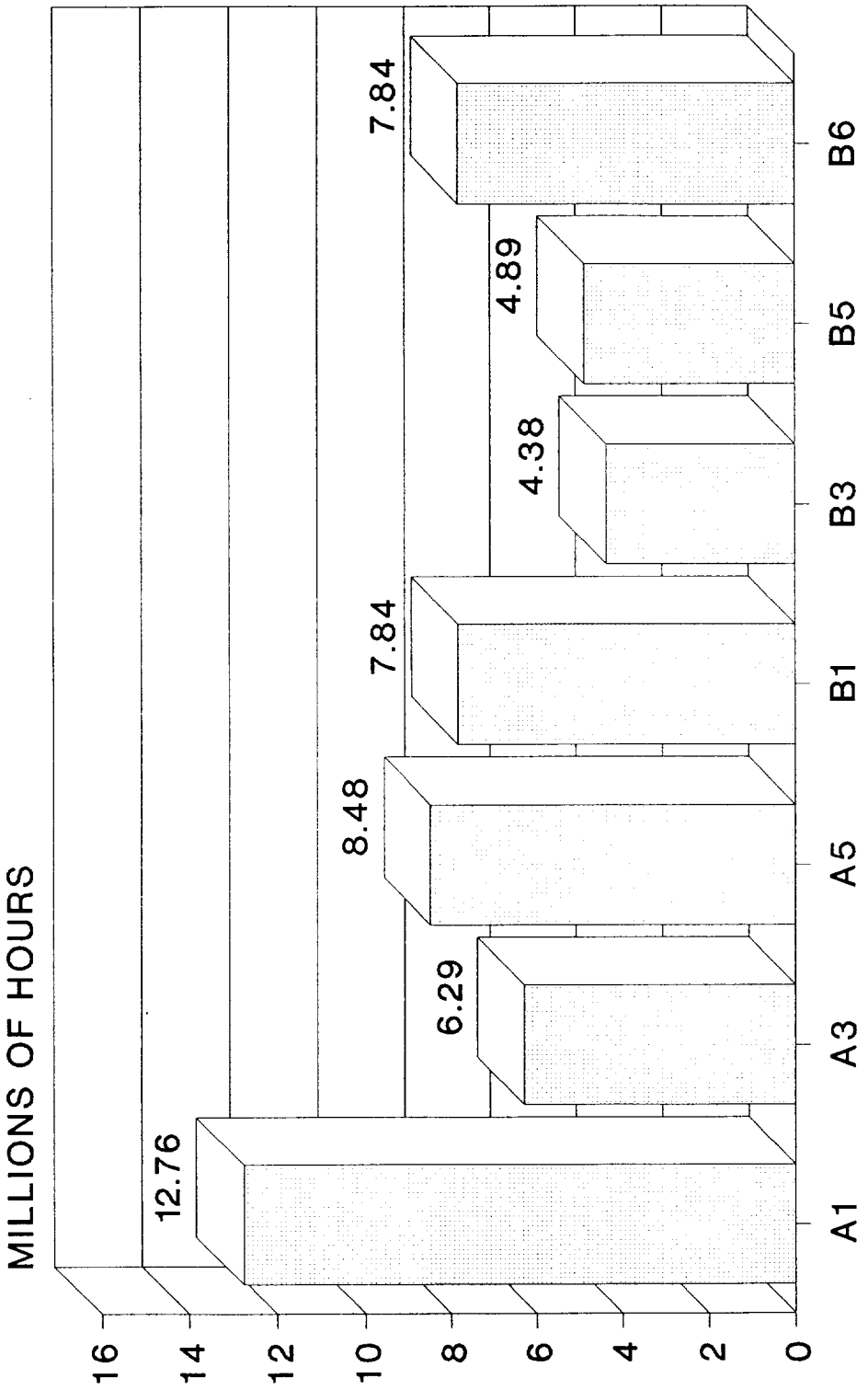

Figure 22 LMP Rupture Time Prediction at 1005F

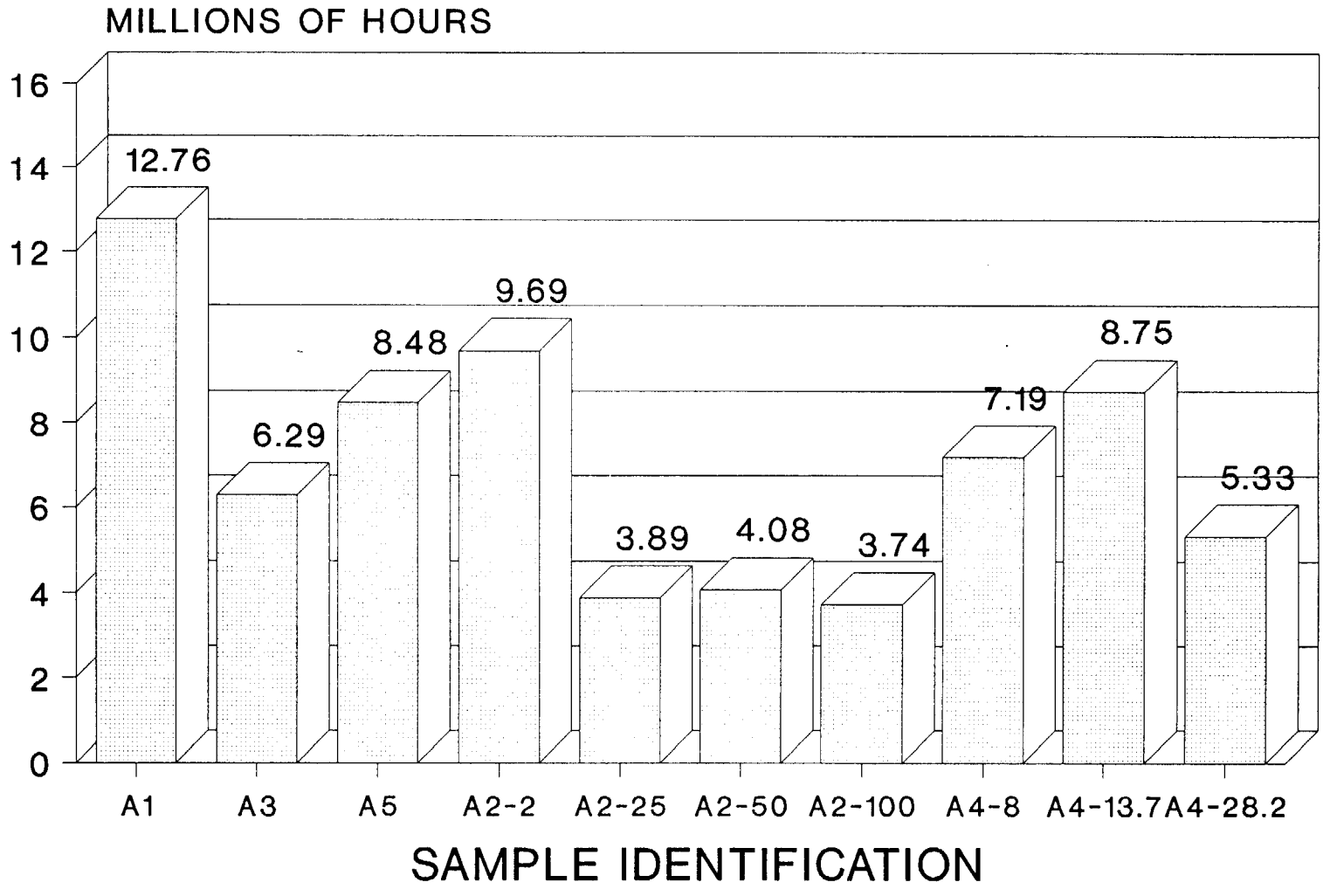

Figure 23 LMP Rupture Time Prediction at 1005F

4.2 Laboratory Sample Hardness Testing

Hardness testing using the portable Equotip hardness tester is one of the field useable investigative methods. In order to have a basis for comparison, the laboratory samples were fully characterized by this method. In addition, hardness tests of the same samples were made using the Rockwell hardness tester on the Rockwell B scale. The results are found in Table V. The purpose of performing the Rockwell B hardness tests (which cannot be done in the field) was to check the accuracy of the conversion tables provided with the Equotip tester.

The measured Rb hardness is compared to converted Rb hardness in Figure 24. It is apparent that the conversion tables tend to slightly under call the hardness compared to the measured values. The average deviation is 1.3 units on the Rb scale. This is only slightly more than the calibration tolerance of 1.0 units commonly observed in this range. Since a substantial fraction of the deviation may have originated from the Rockwell tester, no correction will be made in later use of the conversion tables.

As noted in Table V, the B series plate samples contained two different heats of base metal. The value for each base metal is reported for each condition. The results of hardness traverses across each plate are shown in Figures 25-27. In addition to the Equotip hardness, an estimated tensile strength corresponding to each hardness is also plotted. The tensile strength was estimated using the Equotip conversion tables and accepted empirical correlations.

The weld hardness drops sharply during the first five hours exposure at 1460°F, but is little affected by the second five hours.

If the base metal hardness variations of the main series

TABLE V

SAMPLE HARDNESSES

A1 (As-removed)
Rb 73.5 Sd 1.1 Ld 384.3 Sd 4.9 Rb_c = 71.8

A3 (As-removed + 5 hrs 1460°F + Furnace Cool)
Rb 71.0 Sd 0.6 Ld 380.4 Sd 2.8 Rb_c = 70.6

A5 (As-removed + 10 hrs 1460°F + Furnace Cool)
Rb 72.3 Sd 0.8 Ld 380.3 Sd 6.3 Rb_c = 70.6

A4-8 (As-removed + 8 hrs 1375°F + Air Cool)
Rb 75.7 Sd 0.7 Ld 394.0 Sd 3.6 Rb_c = 74.7

A4-13.7 (As-removed + 13.7 hrs 1375°F + Air Cool)
Rb 74.5 Sd 0.4 Ld 388.0 Sd 1.8 Rb_c = 72.9

A4-13.7 (As-removed + 13.7 hrs 1375°F + Air Cool)
Rb 73.3 Sd 0.4 Ld 383.0 Sd 2.0 Rb^c = 71.4

A2-2 (As-removed + 2 hrs 1450°F + Air Cool)
Rb 82.3 Sd 1.0 Ld 425.9 Sd 8.1 Rb_c = 82.9

A2-25 (As-removed + 25 hrs 1450°F + Air Cool)
Rb 79.7 Sd 0.5 Ld 408.7 Sd 5.8 Rb_c = 78.7

A2-50 (As-removed + 50 hrs 1450°F + Air Cool)
Rb 84.6 Sd 0.4 Ld 427.4 Sd 3.1 Rb_c = 83.2

A2-100 (As-removed + 100 hrs 1450°F + Air Cool)
Rb 84.6 Sd 0.6 Ld 429.1 Sd 3.8 Rb_c = 83.6

B1A (As-removed)
Rb 75.6 Ld 394.0 Rb_c = 74.7

B1B (As-removed)
Rb 74.7 Ld 386.0 Rb_c = 72.3

B3A (As-removed + 5 hrs 1460°F + Furnace Cool)
Rb 72.6 Ld 382.0 Rb_c = 71.1

B3B (As-removed + 5 hrs 1460°F + Furnace Cool)
Rb 69.7 Ld 379.0 Rb_c = 70.2

B5A (As-removed + 10 hrs 1460°F + Furnace Cool)
Rb 74.5 Ld 386.0 Rb_c = 72.3

B5B (As-removed + 10 hrs 1460°F + Furnace Cool)
Rb 71.5 Ld 376.0 Rb_c = 69.2

Notes: B samples have two different base metal sections, A & B.
Rb = Rockwell B Hardness
Ld = Equotip Hardness
Rb_c= Rockwell B hardness by conversion using Equotip table.
Sd = Standard Deviation

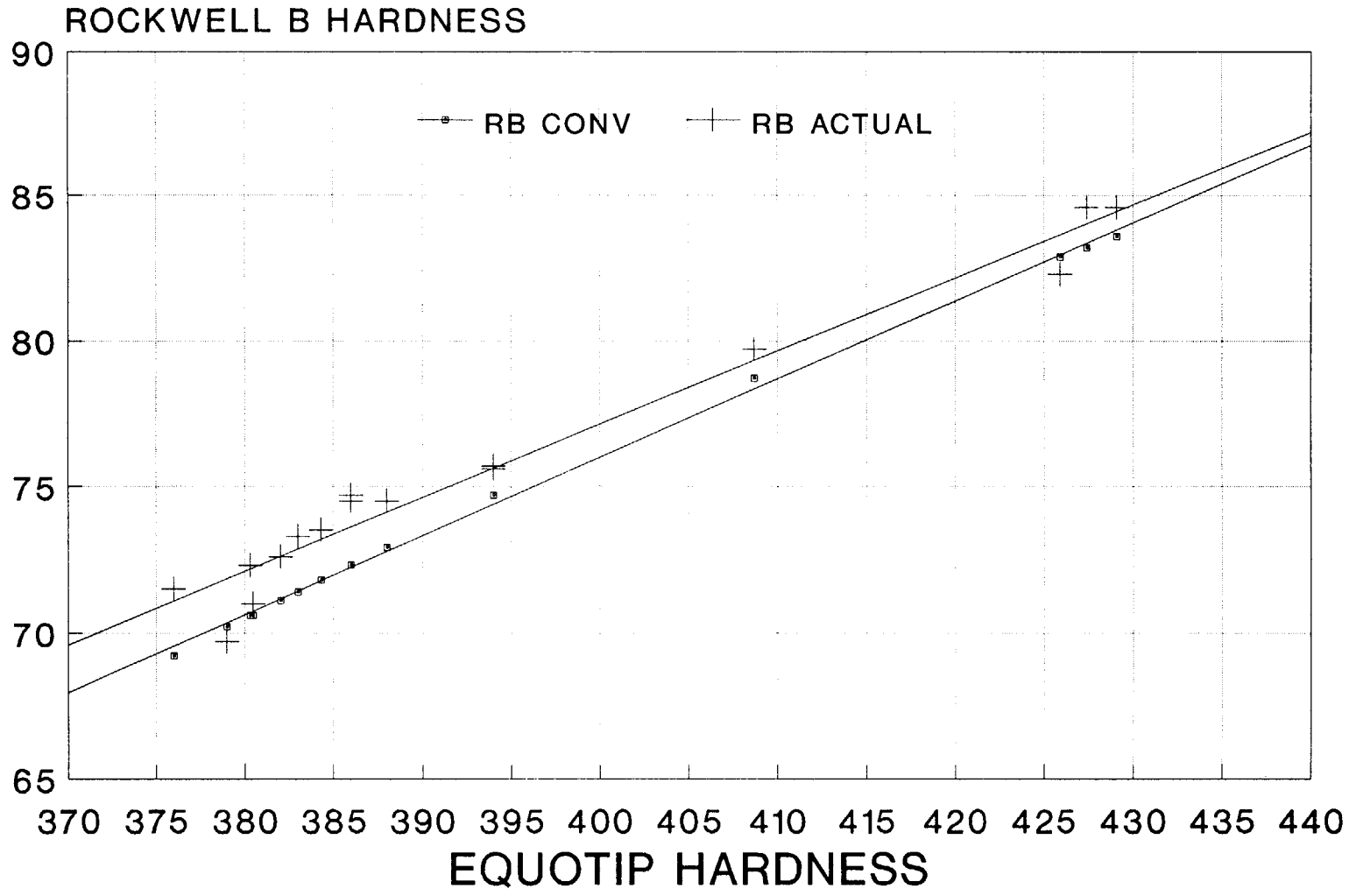

Figure 24 Hardness Conversion for Program Materials

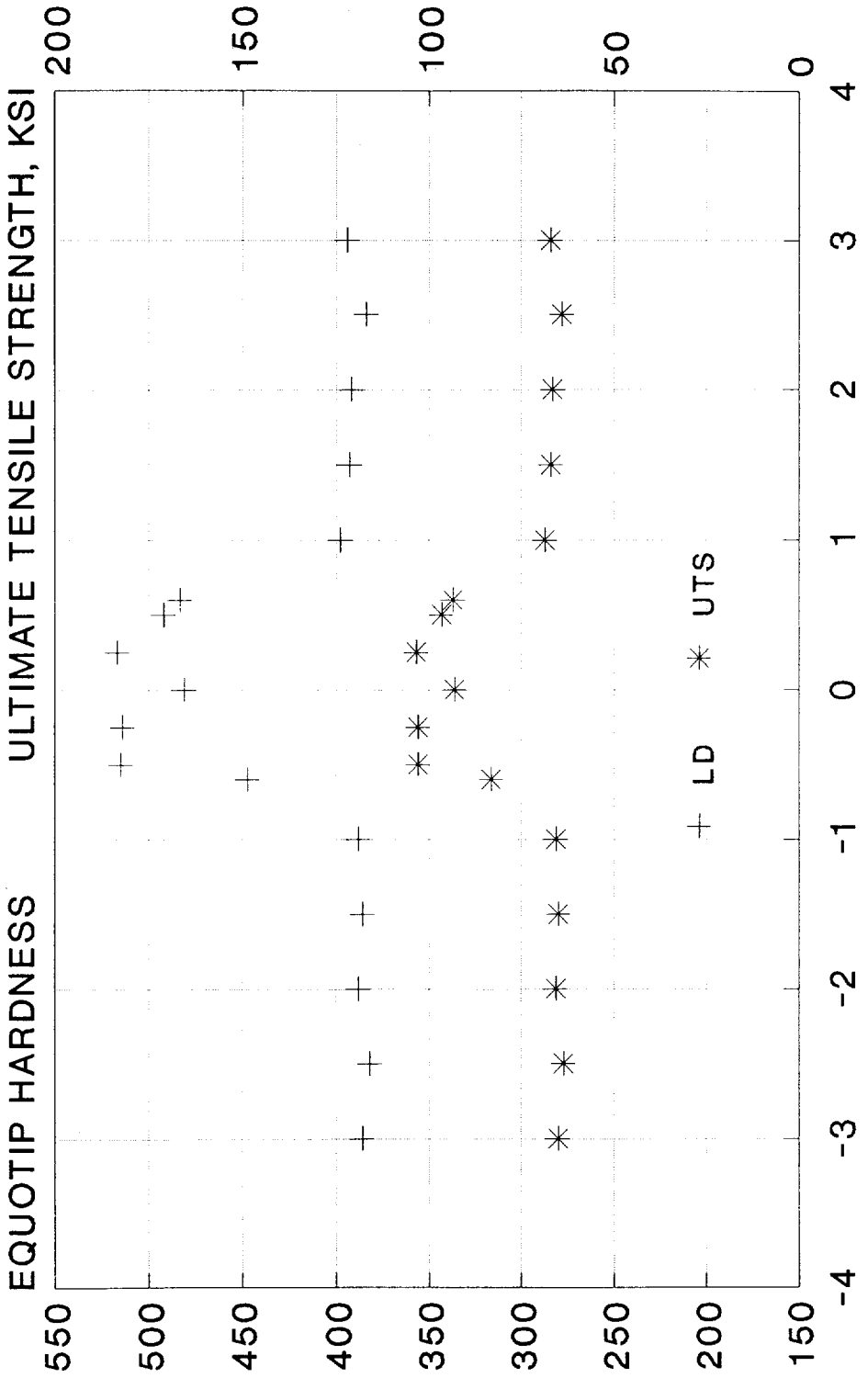

Figure 25 Hardness and UTS Traverse - B1 Plate

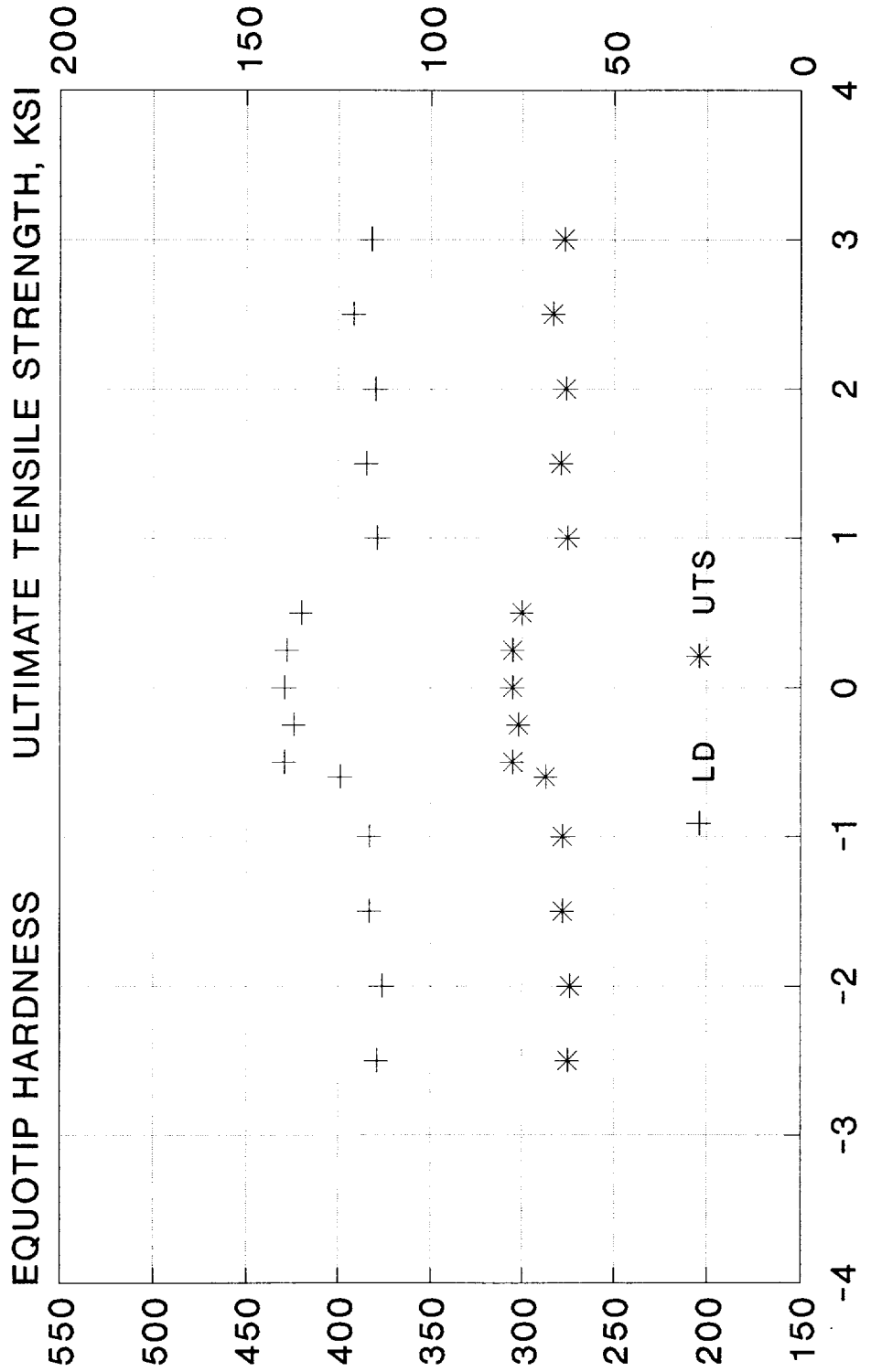

Figure 26 Hardness and UTS Traverse - B3 Plate

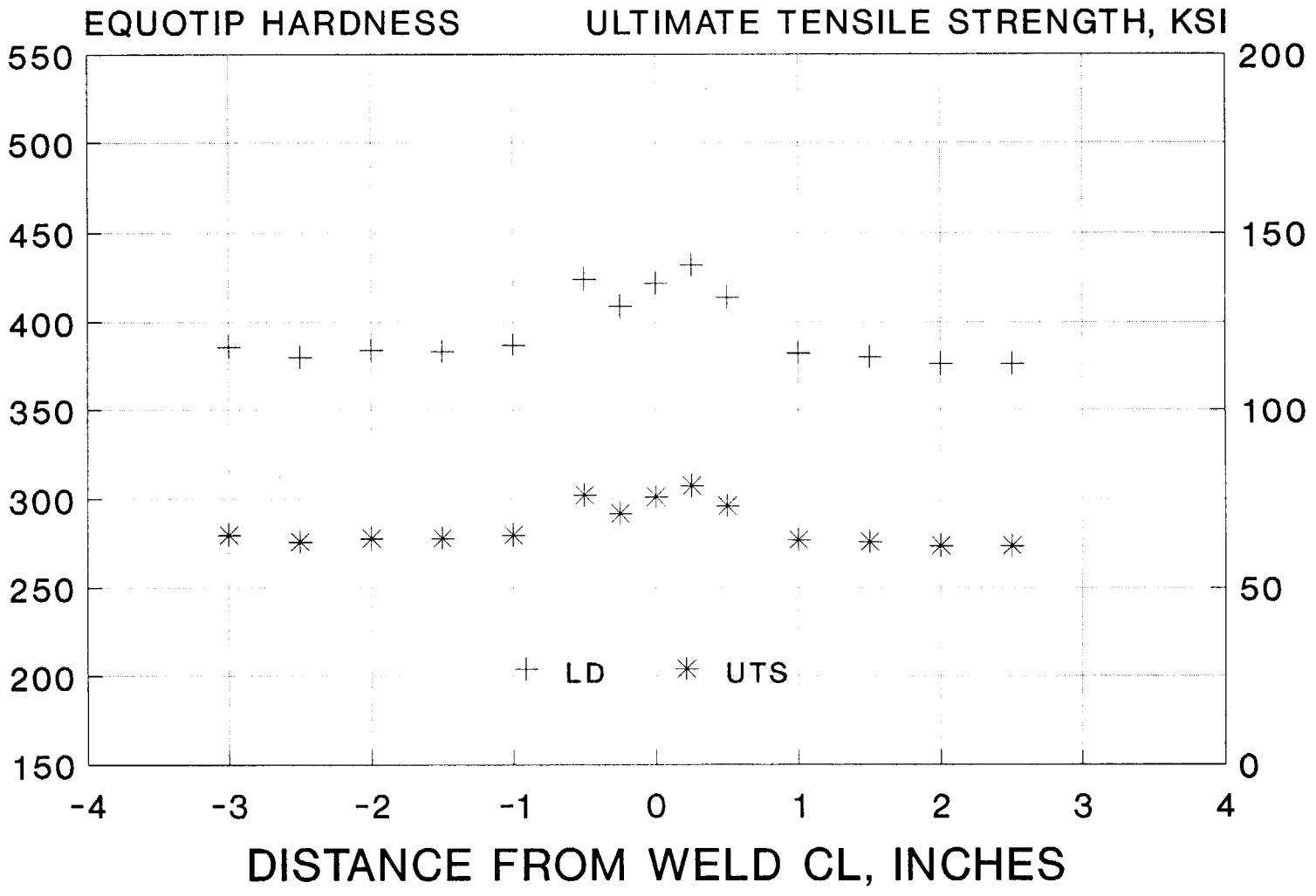

Figure 27 Hardness and UTS Traverse - B5 Plate

samples (A1, A3, A5, B1, B3, & B5) are examined, it appears that there is a decrease in hardness after the first five hours of exposure. This is followed by a subsequent increase (or no change) in the hardness after ten hours. The same pattern has been observed in the Larson-Miller Parameter variation for these samples.

4.3 Metallographic Examination of Laboratory Samples

4.3.1 Pretest Examination

Optical metallography was conducted on all heat treatment conditions using a range of etchants and magnifications. This permits a general appreciation of the microstructure as a function of heat treatment. However, detailed identification of precipitates is not reliable using optical metallography. This can only be accomplished by a combination of electron microscopy and selected area electron diffraction[33].

Fortunately, a general characterization of the precipitation sequence has been performed by others[32-38]. The most useful aids in interpreting changes in the microstructure are the tempering charts developed by Baker and Nutting[37]. The chart for a normalized and tempered 2 1/4Cr-1Mo steel has been previously presented as Figure 6.

The CCT diagram presented by Wada and Eldis[58] is also of considerable assistance. This CCT diagram is shown in Figure 28. Cooling rates for the A3, A5, B3, and B5 heat treatments are around 1°C/minute, while the rates for A2, A4, and B6 are somewhat more rapid. These latter specimens were air cooled from their final thermal exposure prior to testing.

The CCT diagram was developed for a completely austenitized steel cooled from 900°C (1652°F). The exposure temperature of 1450°F (788°C) would lead to only partial austenitization prior to cooling. The degree of austenization

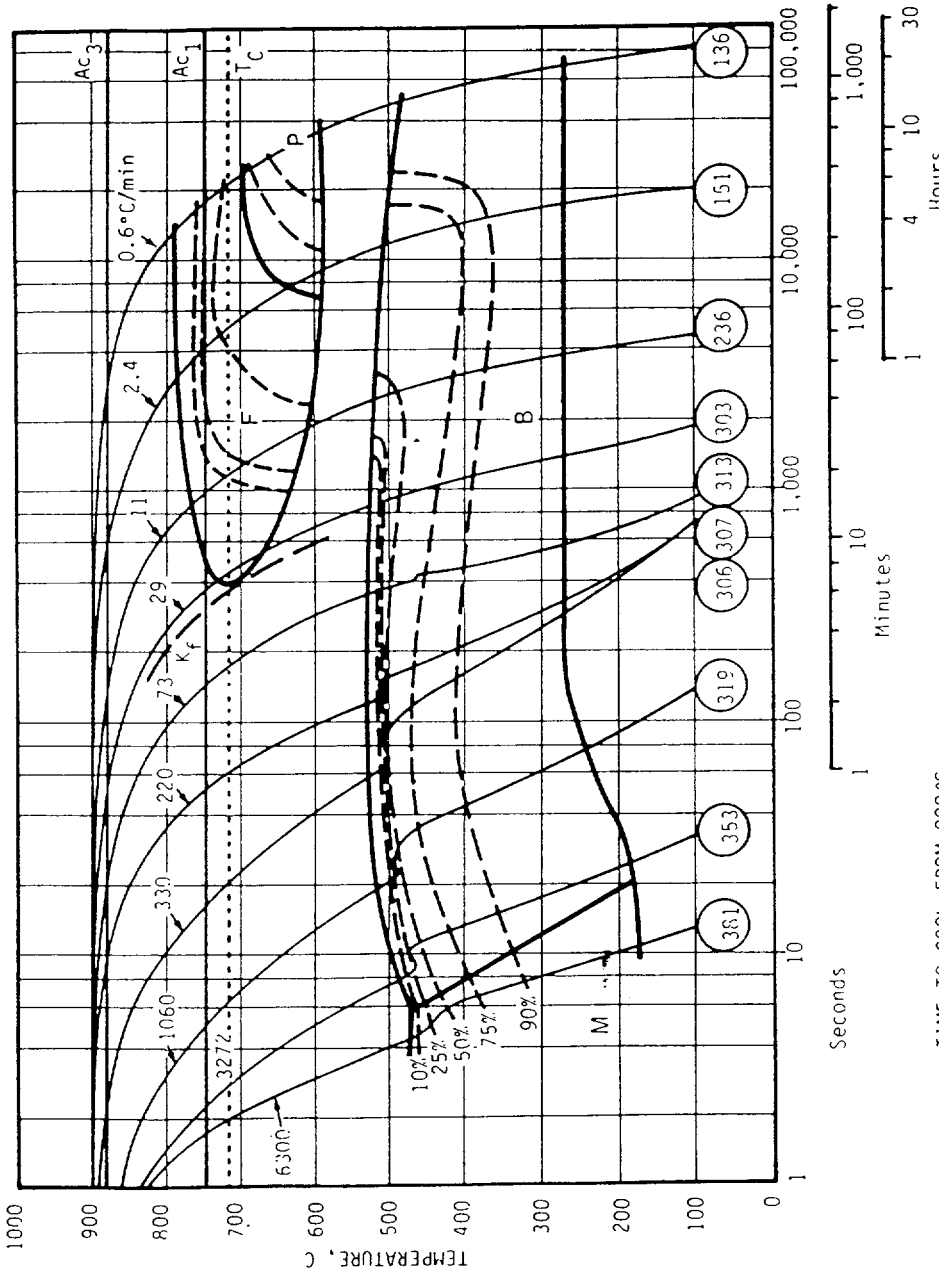

Figure 28 CCT diagram for 0.1 percent carbon 2¼Cr-1Mo steel (Steel A); ASTM grain size No. 7. F = polygonal ferrite; P = pearlite; B = bainite; M = martensite.

and the nature of the remaining ferritic structure would depend on the following factors.

1. The original heat treatment and microstructure of the material.
2. The inservice thermal and mechanical exposure of the material.
3. The time of exposure at 1450°F.

The first two considerations would determine the identity of the carbide phases present, their relative abundance, and their alloy content. All of the carbide phases will incorporate multiple elements, thus depleting the matrix, and each other, of these elements. Stabilities of the carbide phases vary as a function of temperature, and may be roughly predicted by examining the respective free energies of formation. The transitions in the tempering sequence determined by Baker and Nutting[37] reflect this.

The progress of austenization would also be affected by the diffusion of austenite forming elements such as carbon and manganese and the ferrite forming elements such as chromium and molybdenum. These elements are incorporated in the carbides, as mentioned above, and must go somewhere when the carbides dissolve. Thus the degree of austenization at any particular time would depend strongly on prior history. This effect has been noted for a 2 1/4Cr-1Mo steel of known composition which showed a 54°F variation in Ac_1 temperature depending on the prior heat treatments[58].

Because of the complexity of the factors involved, it is difficult to predict the exact outcome of a given thermal exposure. The microstructures resulting from the basic heat treatments used in this investigation are shown in Figures 29 - 36. They are described below.

1. Figures 29 & 30. Material A1. As removed from the plant at 13,000 hours. The structure appears to consist of ferrite,

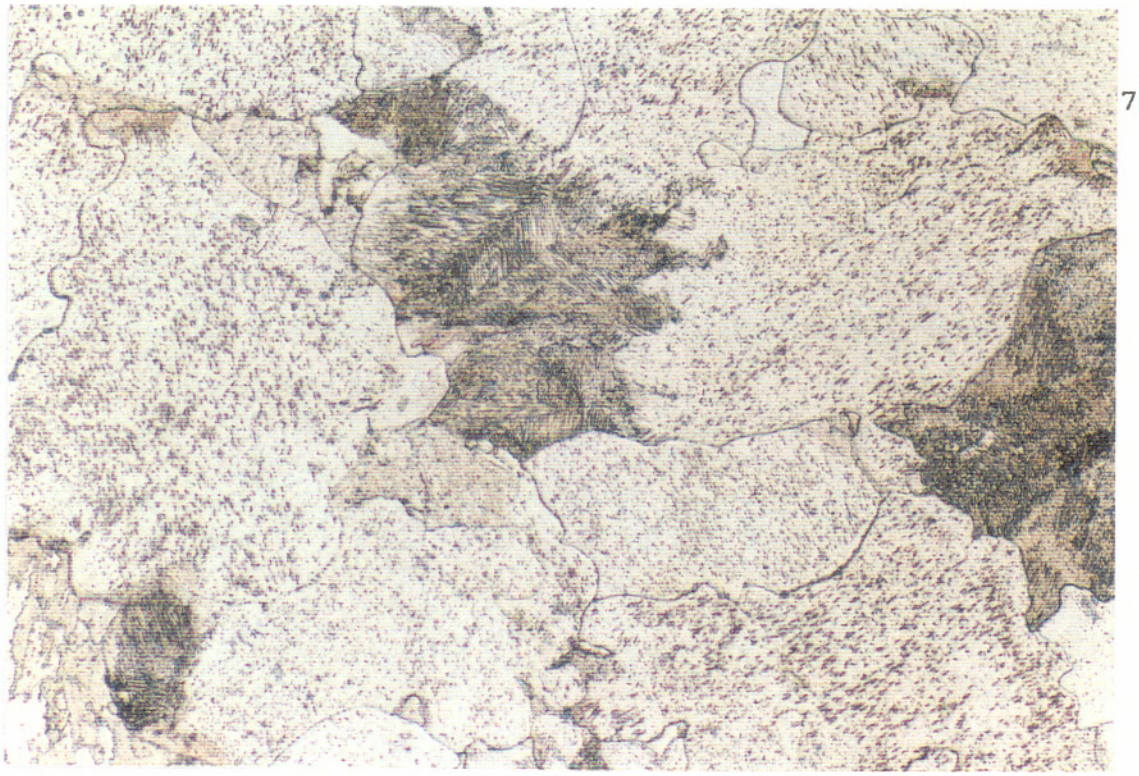

Figure 29
Sample A1 (As-removed) 440X Nital

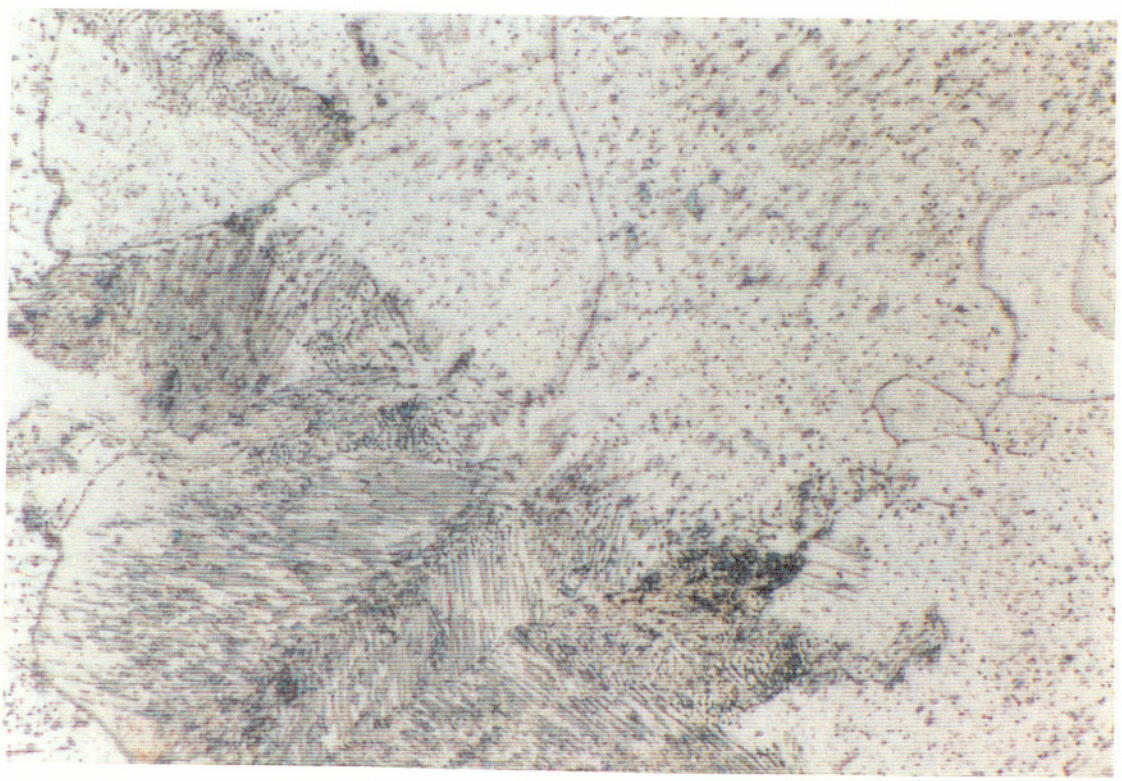

Figure 30
Sample A1 (As-removed) 1100X Nital

pearlite (Fe_3C and ferrite), and Mo_2C, which is the profuse elongated intragranular precipitate. Some of the rounded minor grain boundary precipitate may also be Mo_2C. Baker & Nutting suggest that $M_{23}C_6$ may also be present. Others have suggested that the carbide in the pearlite is at least partly $M_{23}C_6$[65].

2. Figures 31 & 32. Material A3. As removed after 13,000 hours plus Heat Treatment Schedule 1 (5 hours at 1450°F plus controlled cool). The structure appears to consist of ferrite, degraded pearlite, and a high level of blocky grain boundary precipitate. The profuse elongated Mo_2C precipitation has been replaced by a few smaller and more rounded precipitates. The grain boundary precipitate could be Cr_7C_3.

3. Figures 33 & 34. Material A5. As removed after 13,000 hours plus Heat Treatment Schedule 2 (10 hours at 1460°F plus controlled cool). The structure appears to consist of ferrite, pearlite remnants, and a light tan phase that is probably bainite. There is a fine intragranular precipitate that appears to be in an ordered array.

4. Figure 35. Material A4-28.2. As removed after 13,000 hours plus 28.2 hours at 1375°F, air cool. This heat treatment was intended to be just below the Ac_1 temperature. The most notable features of the microstructure are the remnants of pearlite, the grain boundary precipitate, and the readily visible fine intergranular precipitate.

5. Figure 36. Material A2-100. As removed after 13,000 hours plus 100 hours at 1450°F, air cool. After this long exposure in the austenite plus ferrite range about 25% of the structure became austenite which transformed to bainite upon air cooling. There is only the faintest trace of the original pearlite, with almost no visible intragranular precipitates. The bainite is quite apparent.

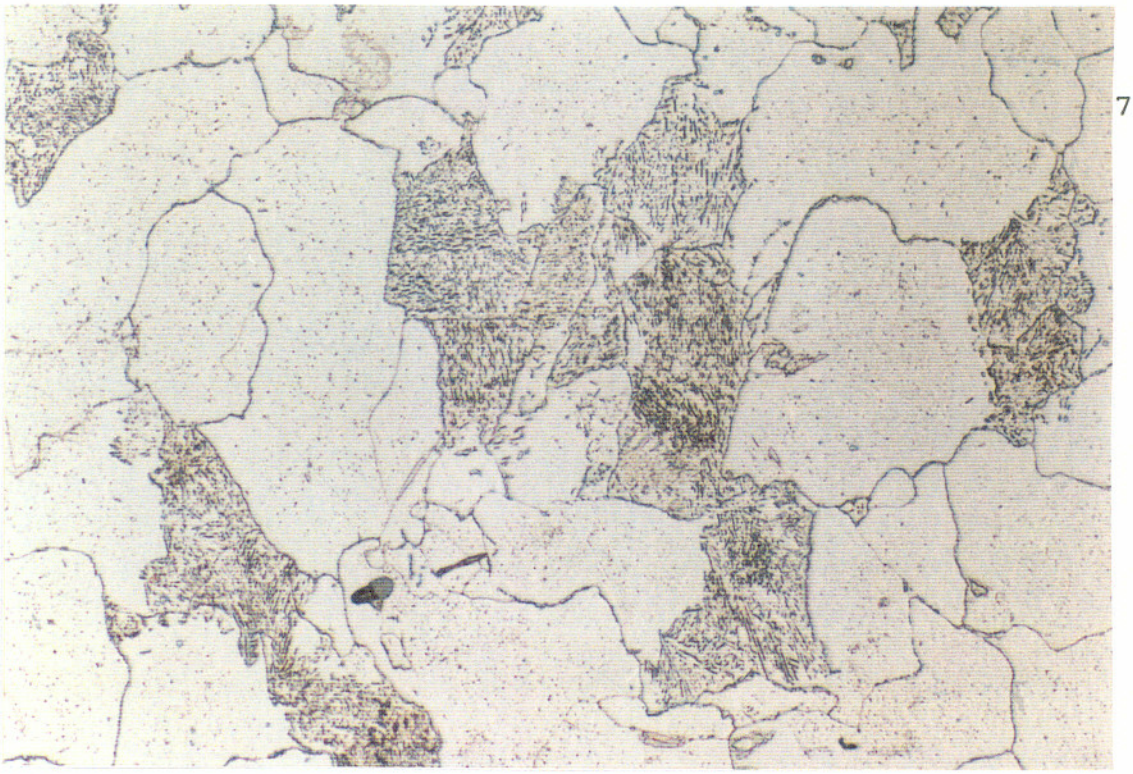

Figure 31
Sample A3 (As-removed + 5 hrs 1460°F + Furnace Cool)
440X Nital

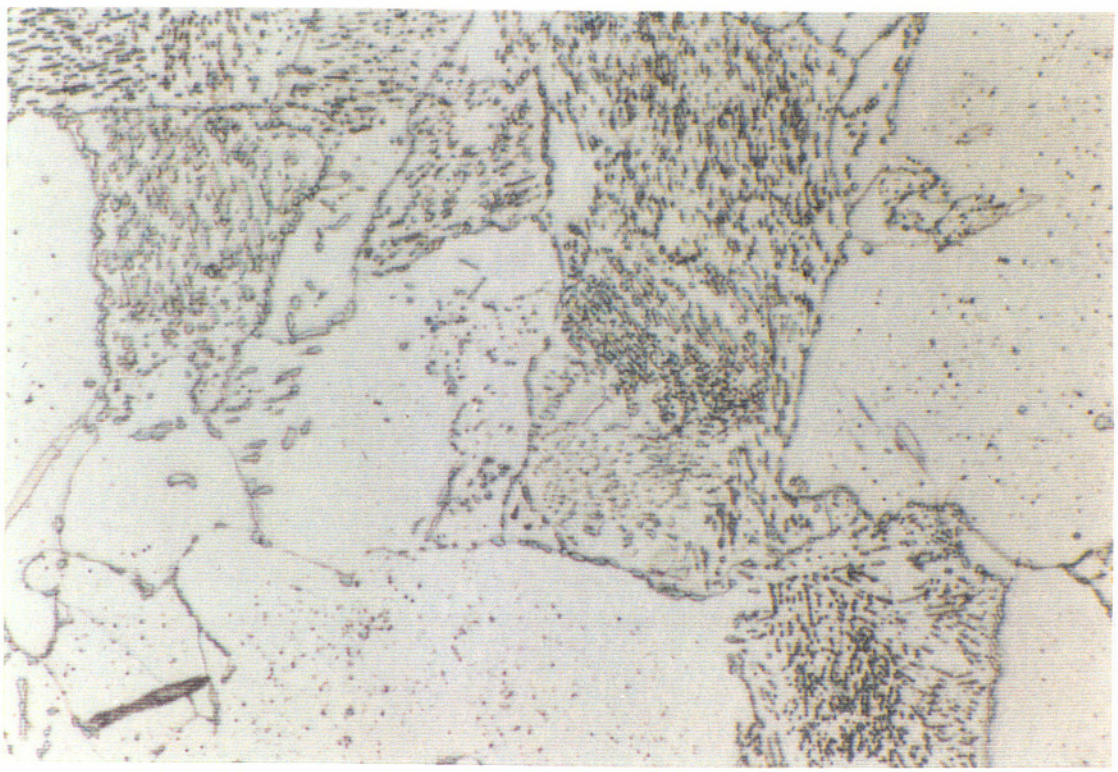

Figure 32
Sample A3 (As-removed + 5 hrs 1460°F + Furnace Cool)
1100X Nital

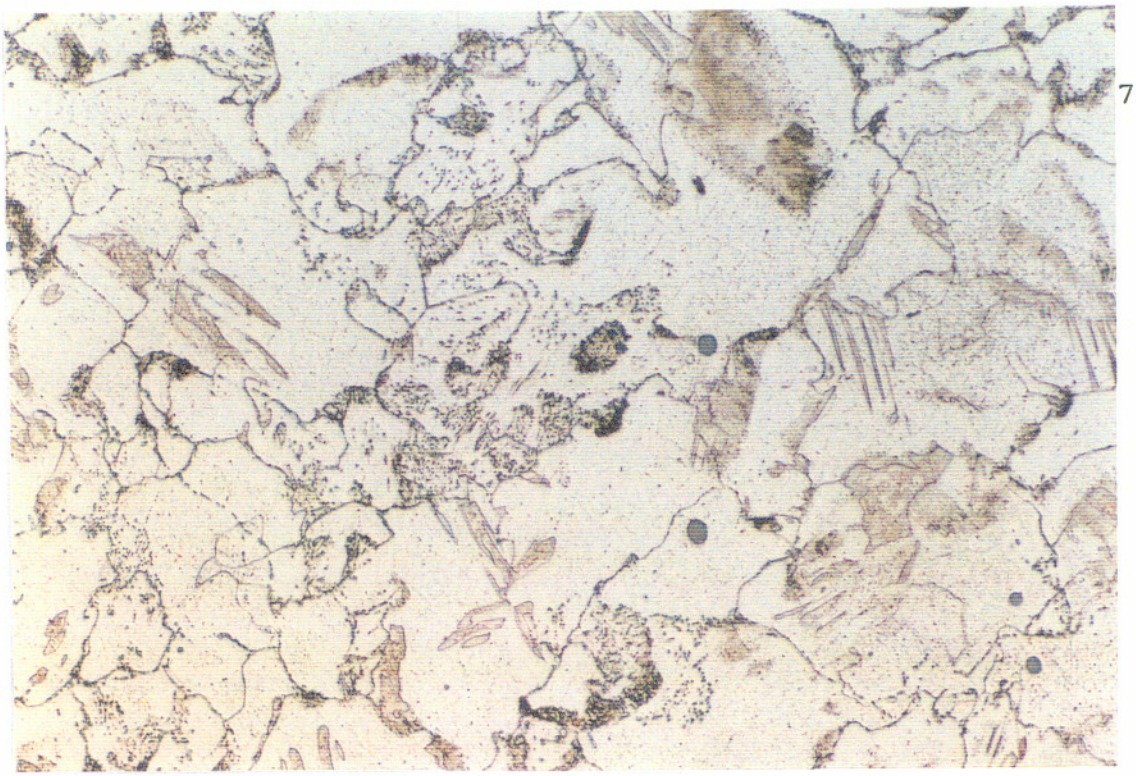

Figure 33
Sample A5 (As-removed + 10 hrs 1460°F + Furnace Cool)
440X Nital

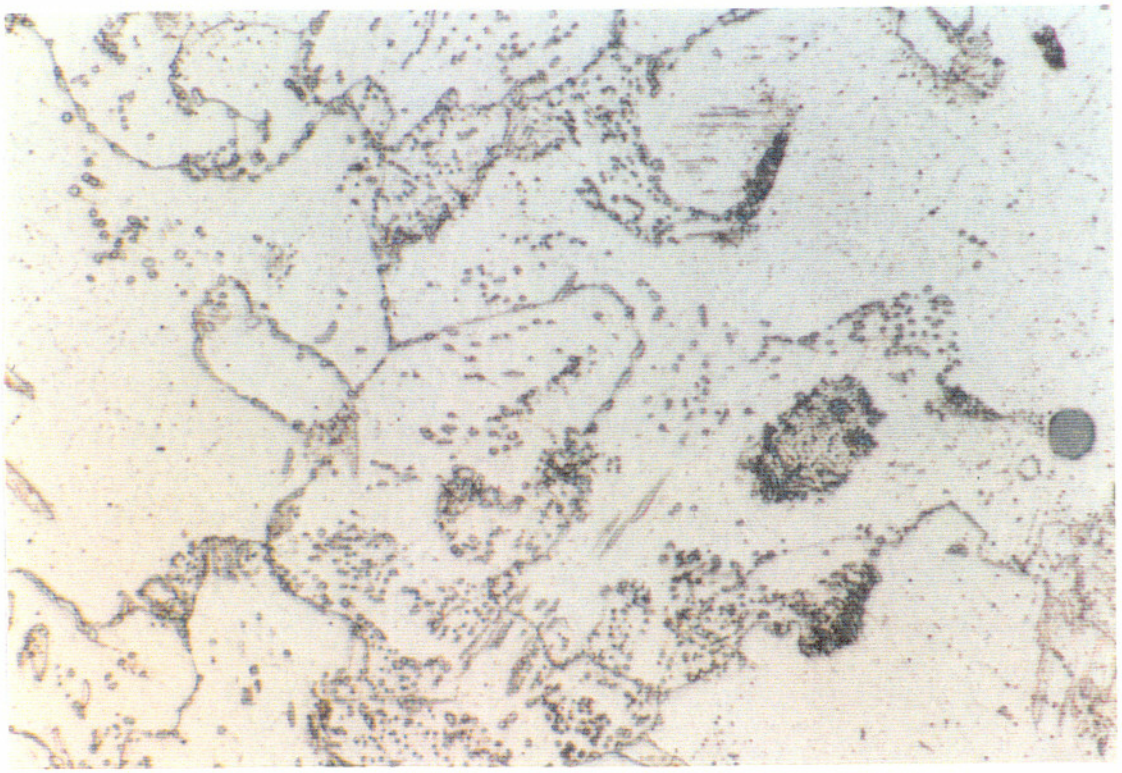

Figure 34
Sample A5 (As-removed + 10 hrs 1460°F + Furnace Cool)
1100X Nital

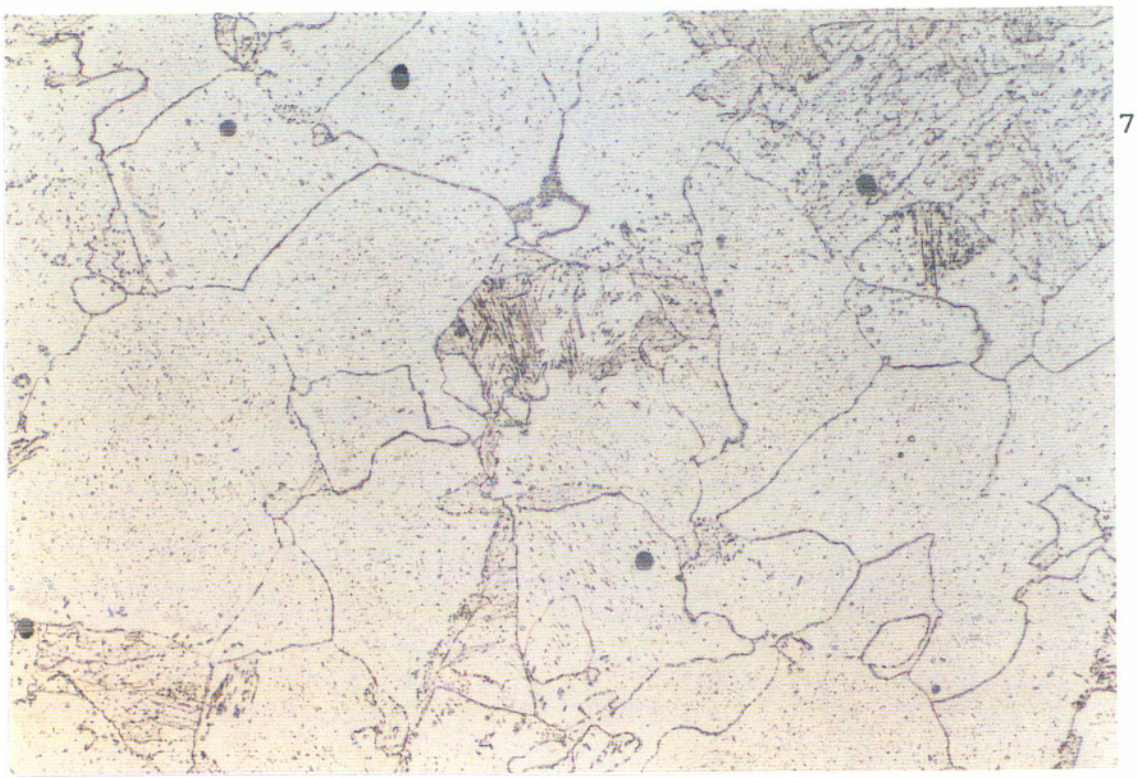

Figure 35
Sample A4-28.2 (As-removed + 28.2 hrs 1375°F + Air Cool)
440X Nital

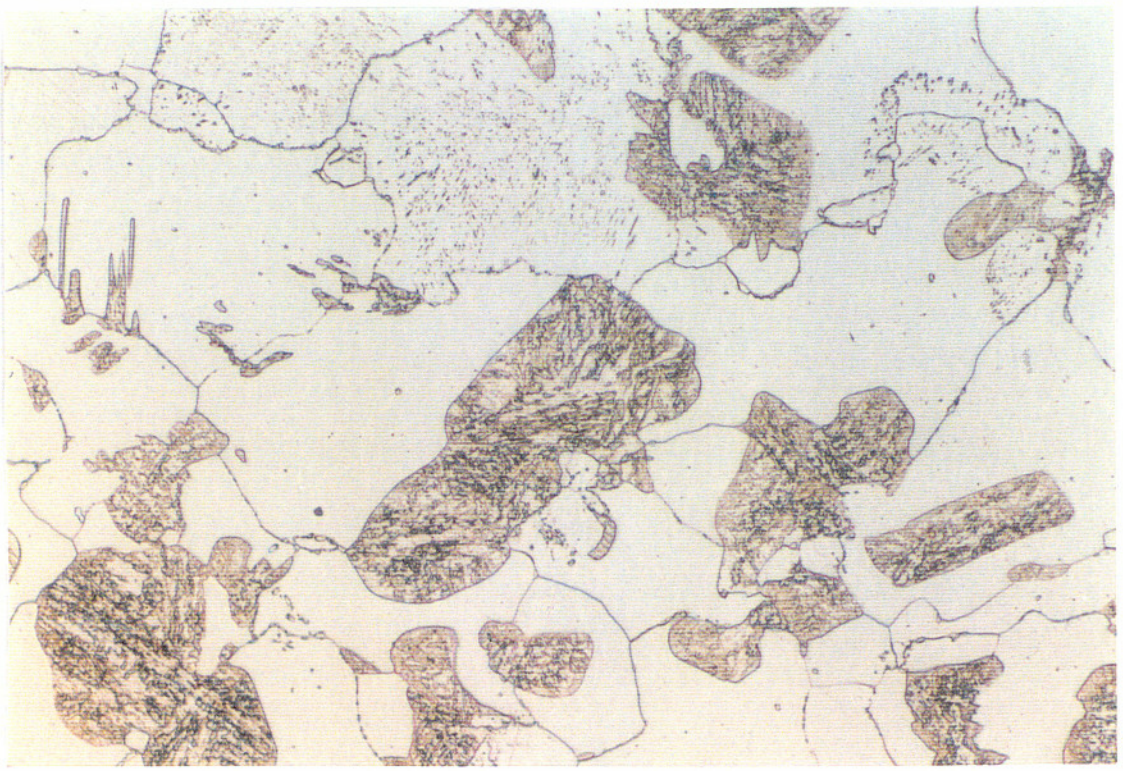

Figure 36
Sample A2-100 (As-removed + 100 hrs 1450°F + Air Cool)
440X Nital

The complete set of pretest metallographic micrographs is found in Appendix 1. Captions with each micrograph include the pertinent data. Note that in the A2 series there was some variability of etching of the bainite. The B series micrographs are similar to the A series in their base metal views. Several micrographs of the coarse grained (bainitic) heat affected zone are included. In subsequent stress-rupture testing this was the fracture location in all the samples examined.

4.3.2 Post Test Examination

Metallographic examination was conducted on representative samples after stress-rupture testing. Failure was ductile in all cases, although the all base metal samples showed higher levels of ductility. In the weld containing B series sample, fracture took place at the location of the coarse grained weld heat affected zone.

Most of the metallographic sections may be found in Appendix 2. For purposes of illustration, one A and one B series sample will be discussed in detail here. The typical appearance for an A series sample is seen in Figures 37 - 39. The sample here is an A1 sample which was tested at 6 ksi and 1275°F. Failure occurred at 648 hours (oxidation corrected), and was ductile in nature.

Figure 37 shows the fracture surface in profile. Note the high level of plastic deformation and the voids due to inclusion drop out. These are not intergranular cavitation voids. The decohesion of an inclusion may also be seen in Figure 38. The combination of thermal aging and plastic deformation have substantially degraded the microstructure. Only rounded carbides remain. Carbide degradation is substantially advanced in a section of the specimen further away from the fracture surface (Figure 39).

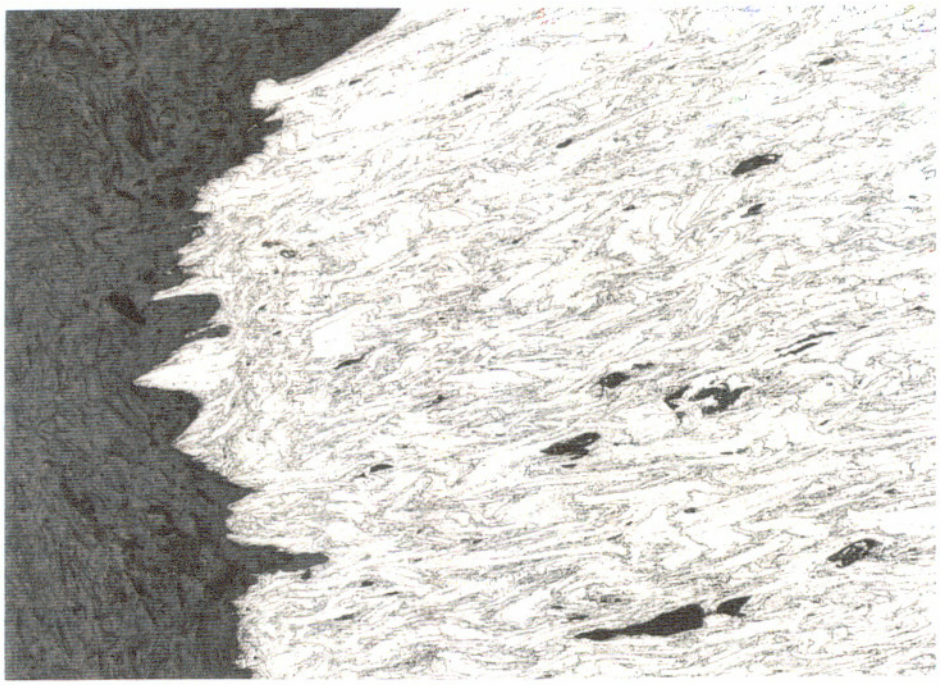

Figure 37
Sample A1-5 100X
Tested at 1275°F Ruptured at 648 hours

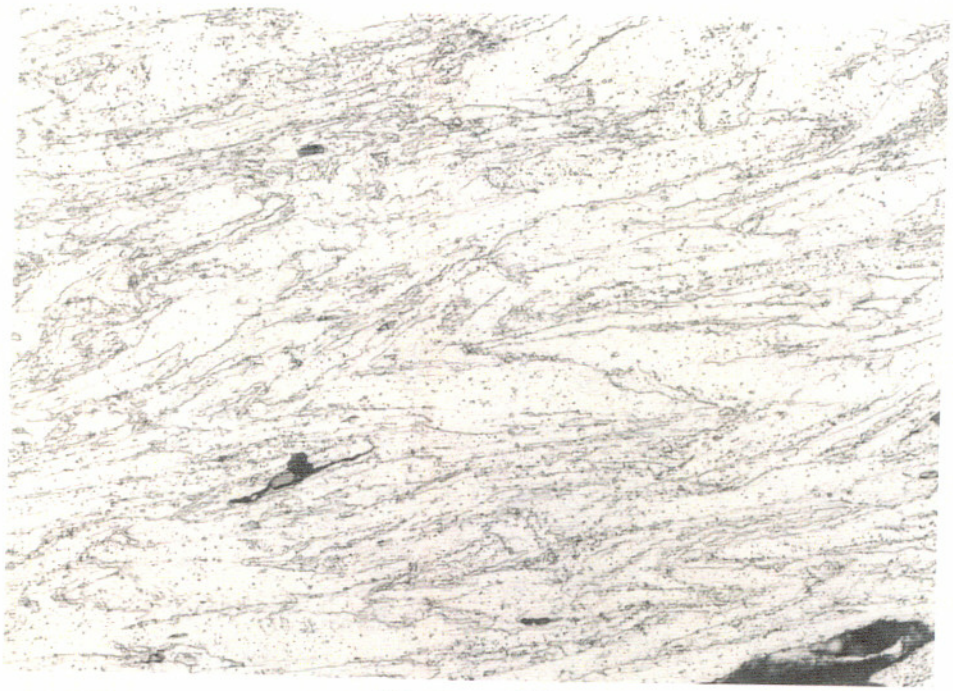

Figure 38
Sample A1-5 400X
Tested at 1275°F Ruptured at 648 hours

Figure 39
Sample A1-5 400X
Tested at 1275°F Ruptured at 648 hours

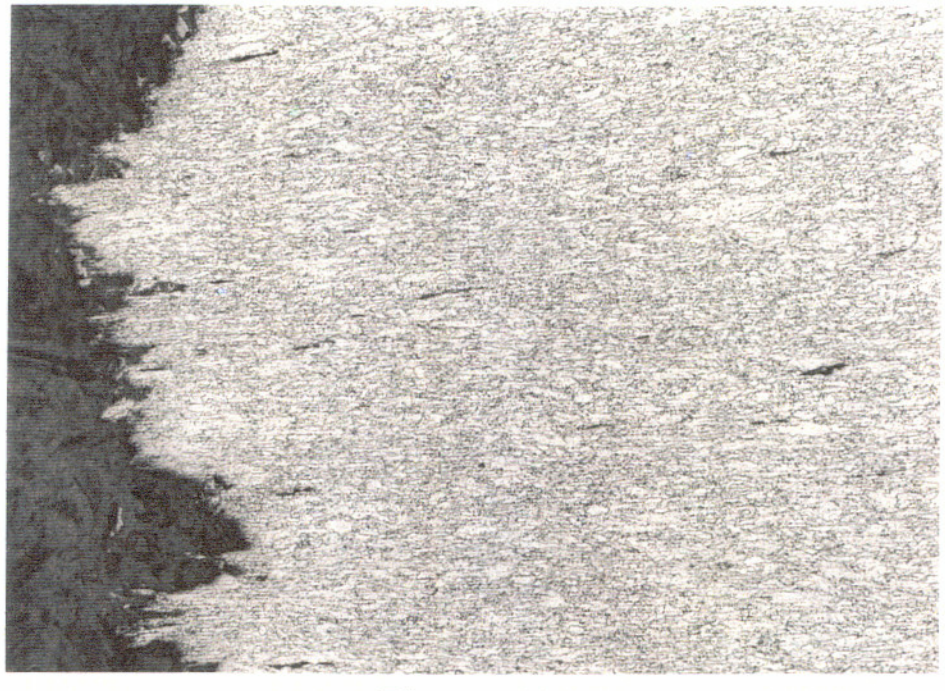

Figure 40
Sample B6 (As-removed + 10 hrs 1460°F +
Strained 1460°F + Air Cool) 100X Nital

A B6 sample (hot strained prior to stress-rupture testing) that had a relatively long time to failure showed somewhat less evidence of ductility (Figure 40). The undeformed base metal showed no evidence of void formation (Figure 41), but voids were noted in the nearby weld region (Figures 42 & 43). The B6 samples in general exhibited lower ductility than any other sample group, although their stress-rupture failure times were among the best.

In Appendix 2, the low magnification (50X & 100X) views are of the highly deformed region near the fracture. Photomicrographs at 400X magnification are usually of relatively undeformed material away from the fracture. Exceptions to this are Figures 2-2 and 2-5 which show deformed regions with no evidence of void formation, and Figures 2-26 and 2-29 which are of deformed areas with possible cavity formation at grain boundaries.

4.4 Matrix vs Total Alloy Content

Samples of A1, A3, A5, A2-100, and A4-28.2 were evaluated by the anodic dissolution technique. Because of the small size and fluid volume of the cell used, only a small amount of material (3 - 4 mg) was dissolved from each sample. This led to some difficulties in determining the weight dissolved accurately. In order to rationalize the results, the data for each sample were normalized to yield an additive total content of 100%. These normalized results for the matrix alloy content are compared to the total alloy content (a constant for all A samples) in Table VI.

The solution of 10% HCl in methanol was analyzed by the inductively coupled plasma (ICP) method. Analysts should be aware that the methanol base may cause problems with the ICP method. Adequate material must be dissolved to allow for

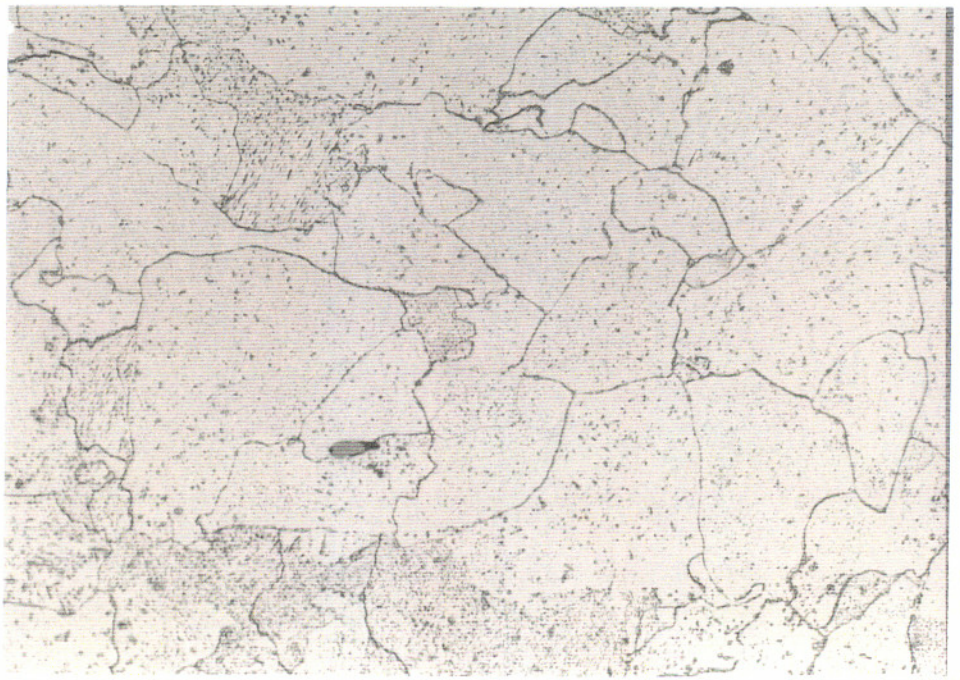

Figure 41
Sample B6 (As-removed + 10 hrs 1460°F +
Strained 1460°F + Air Cool) 400X Nital

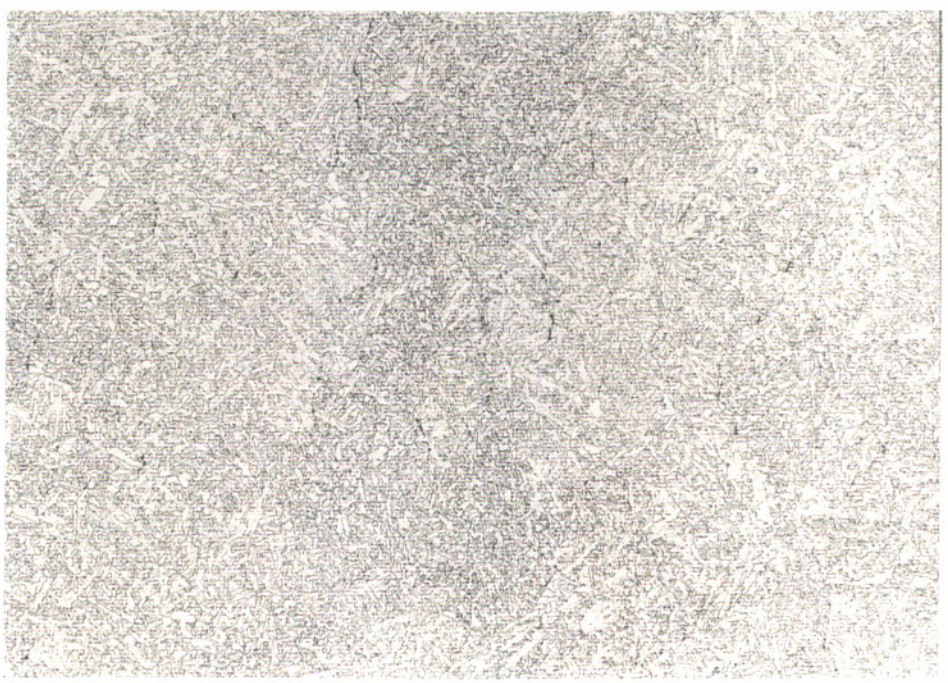

Figure 42
Sample B6 (As-removed + 10 hrs 1460°F +
Strained 1460°F + Air Cool) 100X Nital

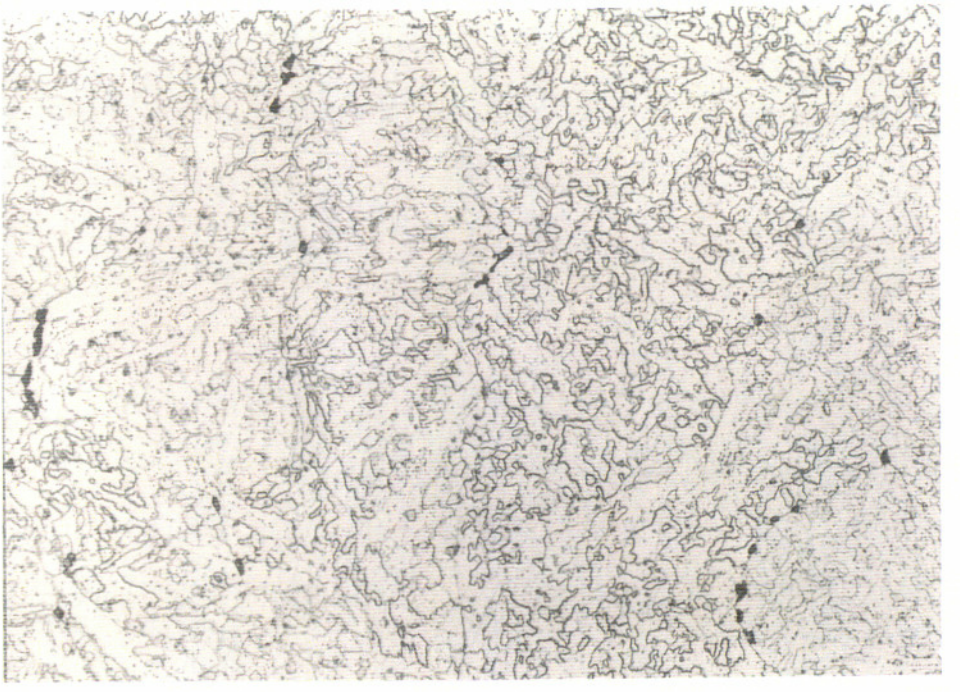

Figure 43
Sample B6 (As-removed + 10 hrs 1460°F +
Strained 1460°F + Air Cool) 400X Nital

Table VI
Total and Matrix Alloy Contents, W/O

Sample	Cr_M	Mo_M	Mn_M
A1	1.65	0.44	0.59
A3	1.85	0.76	0.56
A5	1.87	0.70	0.57
A2-100	2.14	0.83	0.50
A4-28.2	1.90	0.72	0.56
	Cr_T	Mo_T	Mn_T
A11	2.14	1.03	0.55

Notes: A1 (As-removed)
A3 (As-removed + 5 hrs 1460°F + Furnace Cool)
A5 (As-removed + 10 hrs 1460°F + Furnace Cool)
A2-100 (As-removed + 100 hrs 1460°F + Air Cool)
A4-28.2 (As-removed + 28.2 hrs 1375°F + Air Cool)

considerable dilution with water.

4.5 Field Hardness Testing

Field hardness testing was performed on potential replica areas that had been prepared through the 240 grit abrasive level. These areas were designated Field Areas 1 - 6, and are shown schematically in Figure 44. The history of these areas is summarized below.

1. Field Area 1 had been exposed to 10 hours at 1450°F nominal (heat treatment schedule 2).
2. Field Area 2 had the same nominal exposure as FA1, except that the end of the thermal blanket was supposed to be located 12 inches to the right of the weld. The left side of FA2 is a 45° elbow.
3. Field Area 3 was on the side of the pipe. It included a field weld, and had been exposed to 4-6 hours at 1450°F nominal (heat treatment schedule 1).
4. Field Area 4 was at the same location as FA3 except that it was 90° above on top of the pipe. The pipe on the left side of the weld in these areas was the other end of the of pipe in Field Areas 5 & 6.
5. Field Areas 5 & 6 were on the side and top respectively of a pipe to tee weld that had seen 4 - 6 hours at 1450°F.

The hardness traverses across the field areas are shown in Figures 45-49. Note that the data for Field Area 1 is shown on the right hand side of the Field Area 2 graph. The Equotip hardness has been corrected for position where appropriate. The estimated tensile strength is also plotted. It was calculated in the same manner as was done for the laboratory samples.

These data show the field installed piping to be equal to or lower than the laboratory samples in hardness and estimated

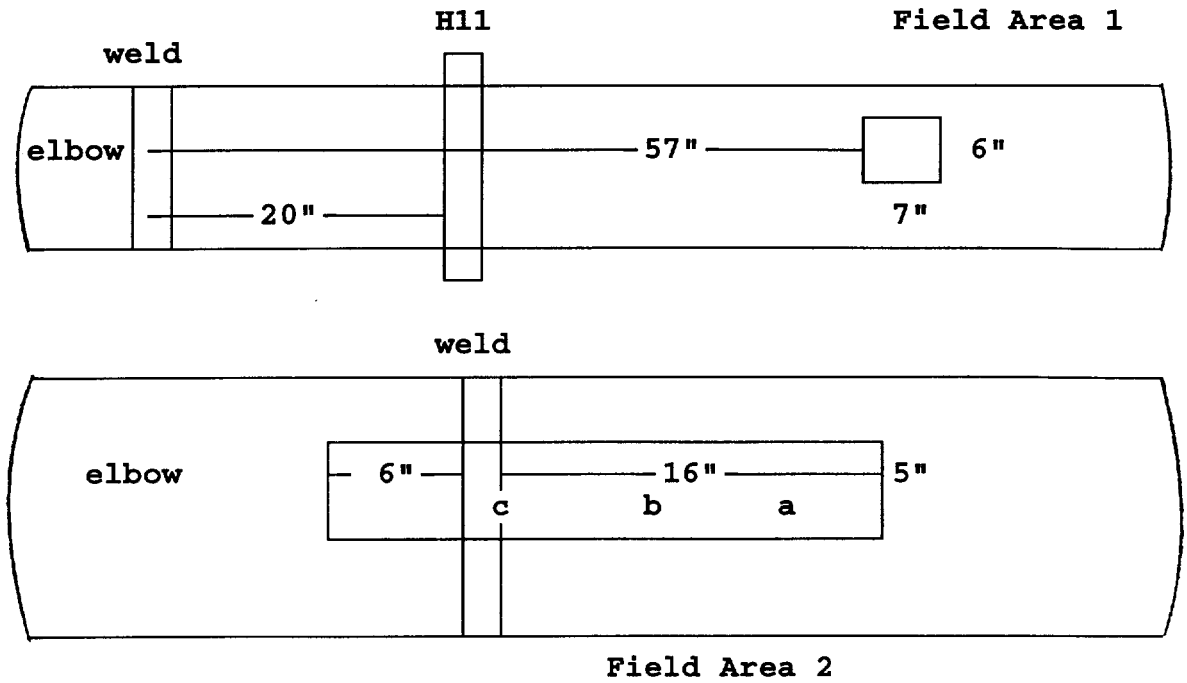

Field Area 2

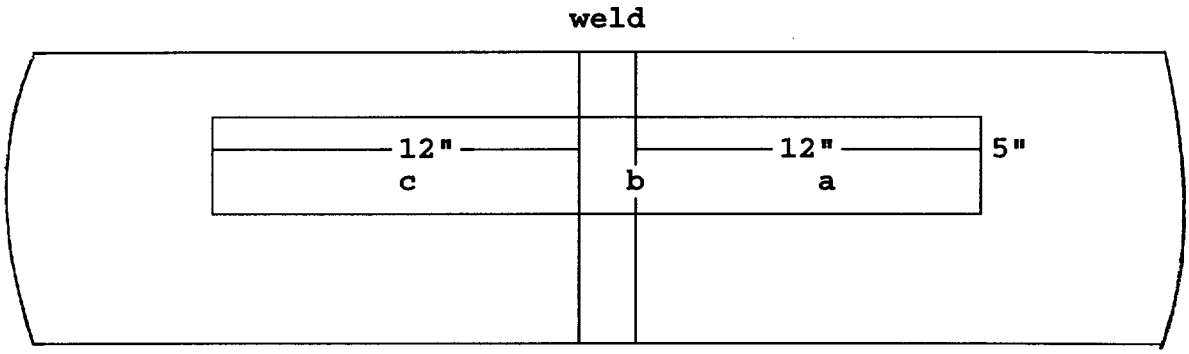

Field Area 3

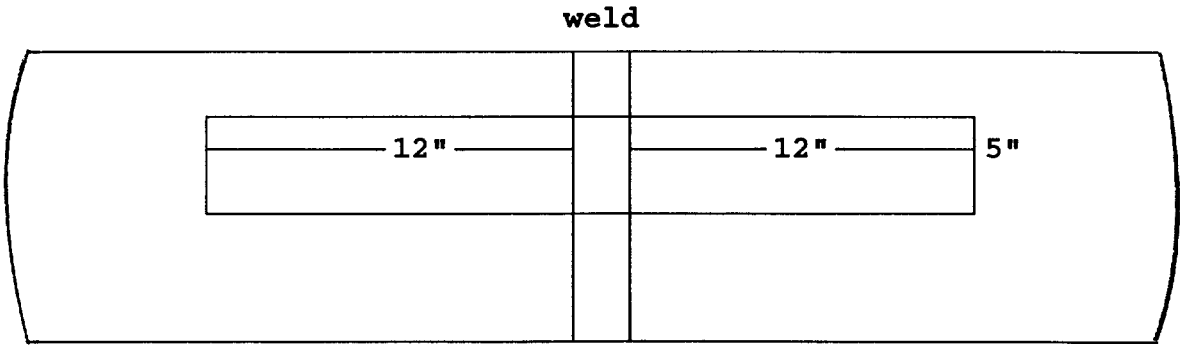

Field Areas 4, 5, & 6

Figure 44
Schematic Arrangement of Field Areas

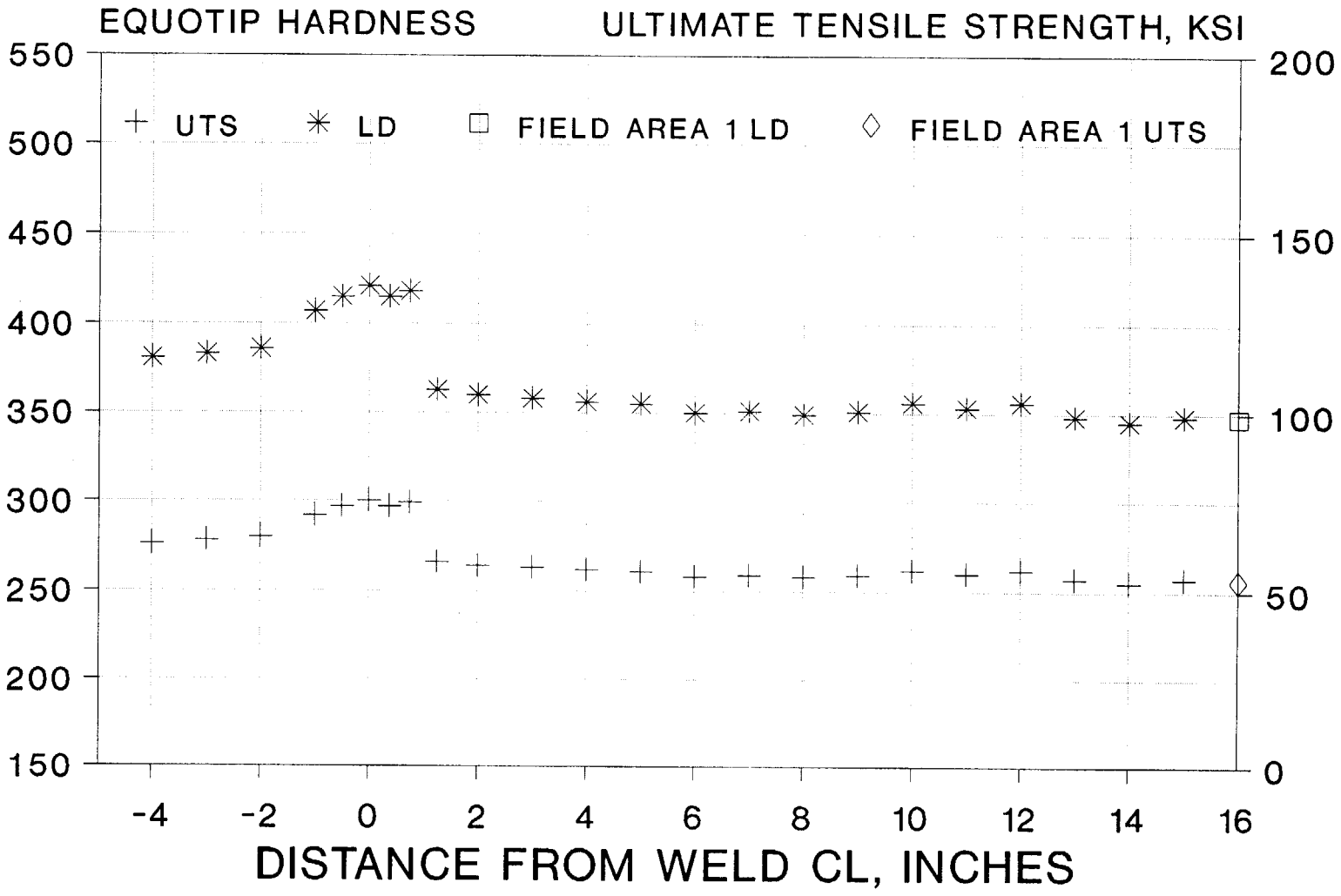

Figure 45 Hardness and UTS Traverse - Field Area 2

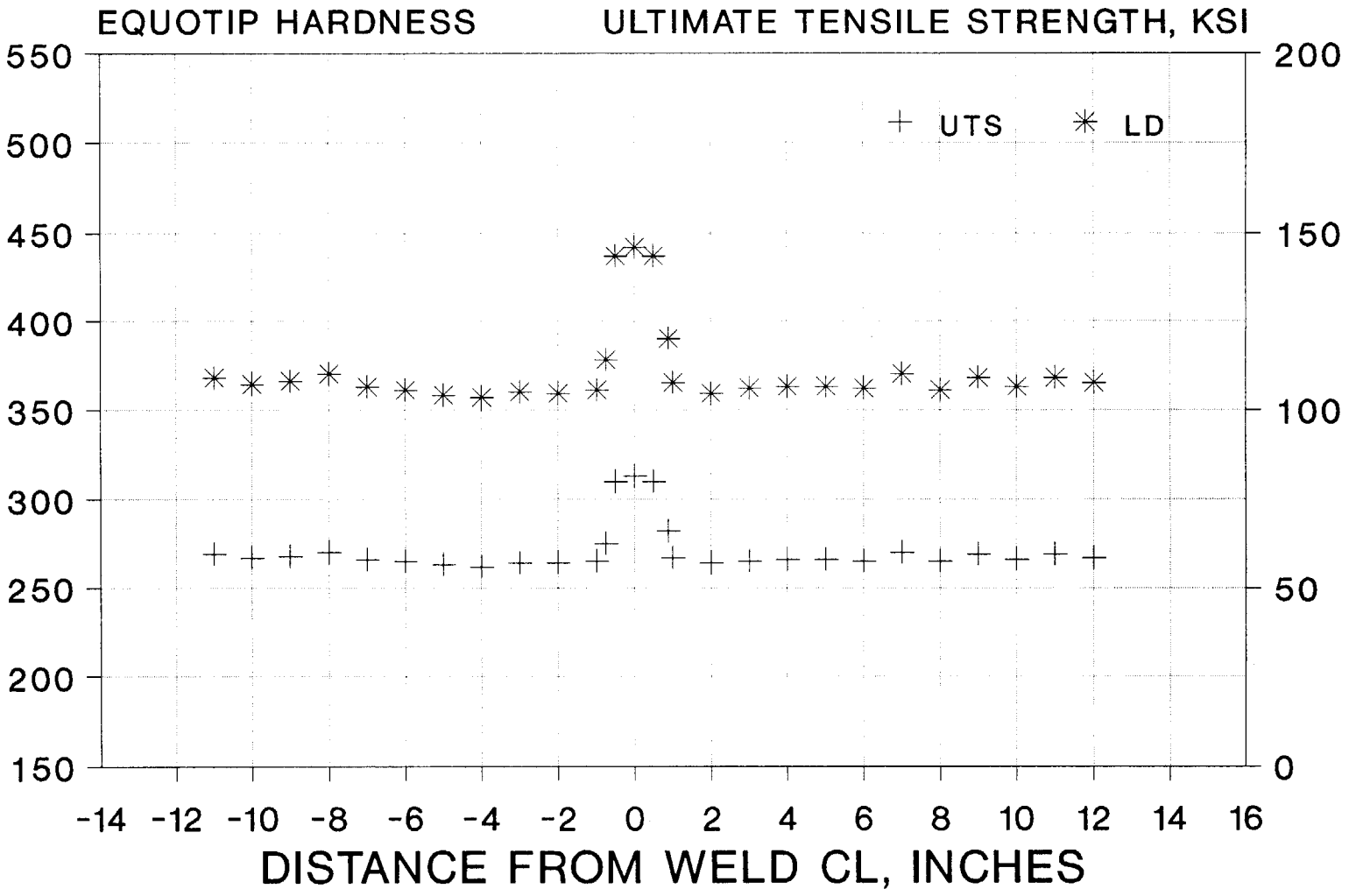

Figure 46 Hardness and UTS Traverse - Field Area 3

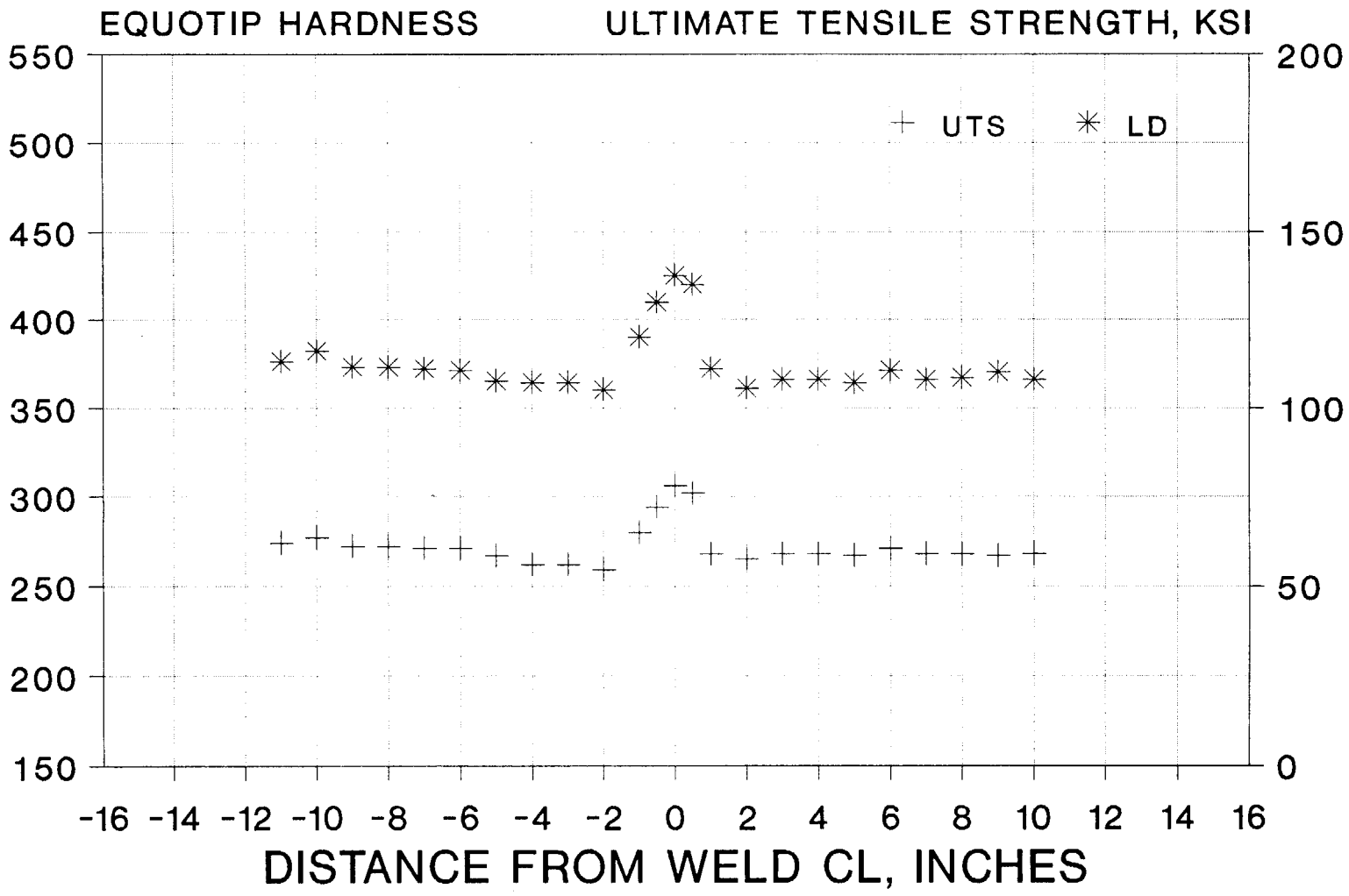

Figure 47 Hardness and UTS Traverse - Field Area 4

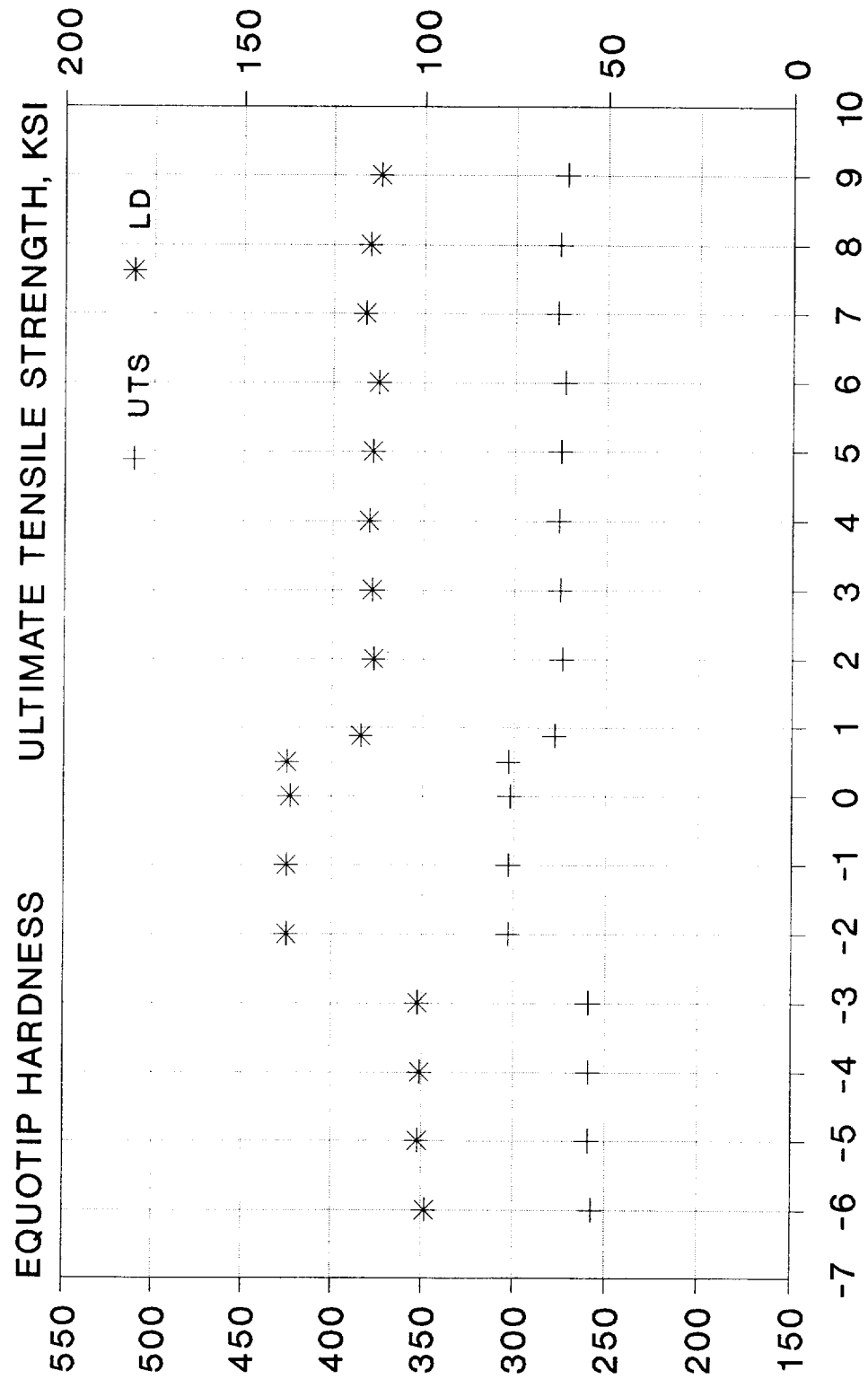

Figure 48 Hardness and UTS Traverse - Field Area 5

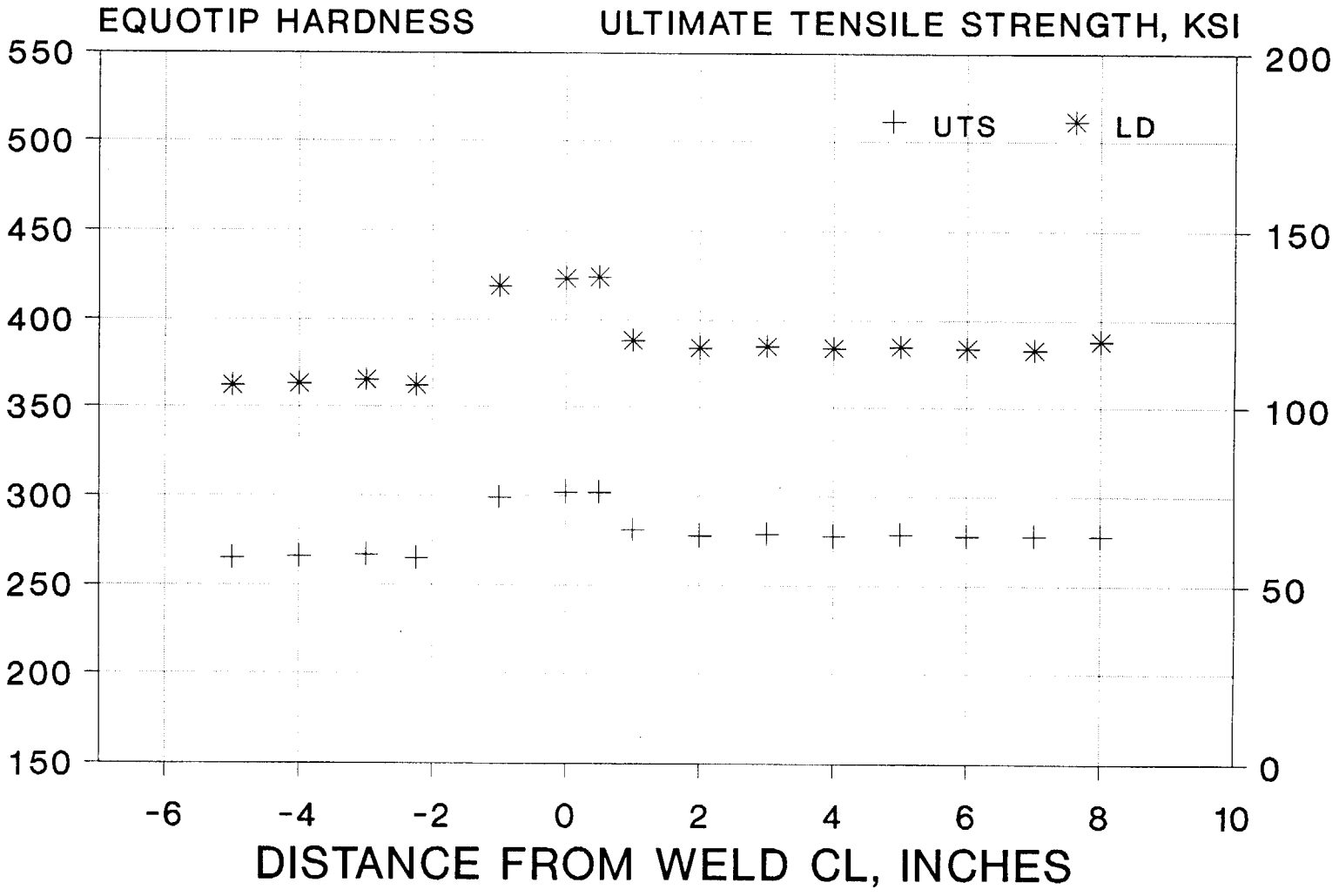

Figure 49 Hardness and UTS Traverse - Field Area 6

tensile strength. There are several possible reasons for this, which will be discussed later.

4.6 Field Replication and Metallographic Examination

Field replication was conducted on Field Areas 1-3. Replica locations for Field Areas 2 & 3 are indicated by the letters a, b, and c in Figure 44. Surface preparation was as described in 4.4.2 above. Replicas were made after multiple polish and etch procedures. The replicas were then examined using an optical microscope under bright field illumination. The replicas presented below are a small fraction of those actually made. Careful study of the complete set of replicas at a variety of magnifications revealed no trace of grain boundary cavities or voids. As mentioned, cavity formation at this short time in service would be of serious concern.

The quality and resolution of the replicas is obviously a concern when microstructural condition assessments are made. Poor resolution may result at different stages of the process. Some problems are:

1. Inadequate preparation of the surface and etching. The causes here are basically the same as for conventional metallography. Painstaking adherence to procedure and maintenance of cleanliness are of paramount importance. This is made difficult by the generally poor working conditions, and the usual requirement to conform to plant schedules. Errors at this stage cannot be recovered.
2. Use of the wrong replicating material or improper use of the correct replicating material. One replicating system sold by a major metallographic supply house was not easy to use and produced poor replicas even under the best of circumstances. It was not very good even when used on a mounted sample under laboratory conditions. The regular acetate tape softened by

acetone gives good detail but is difficult to handle in the field. A kit consisting of a dissolved acetate material and an acetate tape proved easiest to use.

3. Even the best replica firmly affixed to a glass slide with double back tape has a tendency to curl. This degrades image quality in the optical microscope. Fortunately, most of this minor curling can be compensated for by the human eye. The camera is not so tolerant , however, and some replicas with inherently high resolution are difficult to document. It was noted that the overall quality obtained from a given replica decreased with storage time. Replicas should be examined and photographed as soon as possible after they are taken.

When everything works out, the clarity of an optical photomicrograph made from a replica is distinguishable from its direct counterpart only by the reversed relief. It will look different because of this, and of course will have no color. Figure 63 (weld metal), Figure 70 (base metal), and Figure 72 (base metal-WHAZ), are comparable in resolution and clarity to most of the black and white photomicrographs in this report.

Prior to discussing typical field replicas, some photomicrographs of the anomalous decarburized surface condition mentioned earlier will be presented for the purpose of comparison. These views have been rephotographed from the 1986 work, and are found in Figures 50 - 52. The metallographic sections were taken in the transverse or longitudinal through thickness direction rather than the radial direction used in taking the replicas.

The interesting feature of the microstructures is the transition from an interior pearlite containing region of normally oriented equiaxed grains to a decarburized subsurface region containing oriented nonequiaxed grains. The thermomechanical process responsible for the formation of this

Figure 50
1986 Sample Near Surface
67X Nital

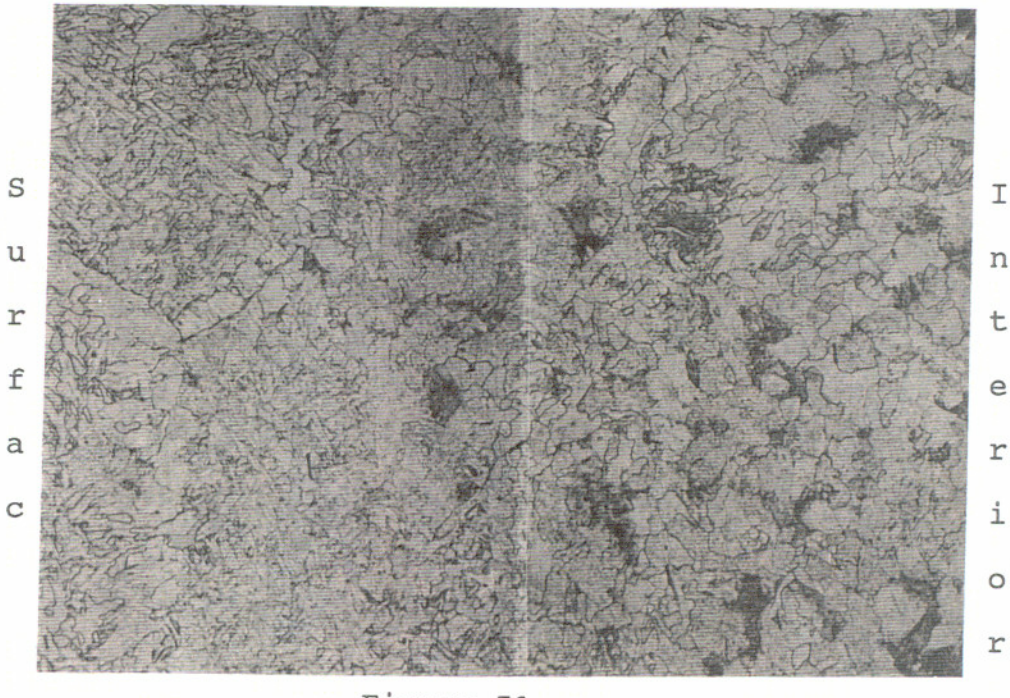

Figure 51
1986 Sample Near Surface
67X Nital

Figure 52
1986 Sample Near Surface
67X Nital

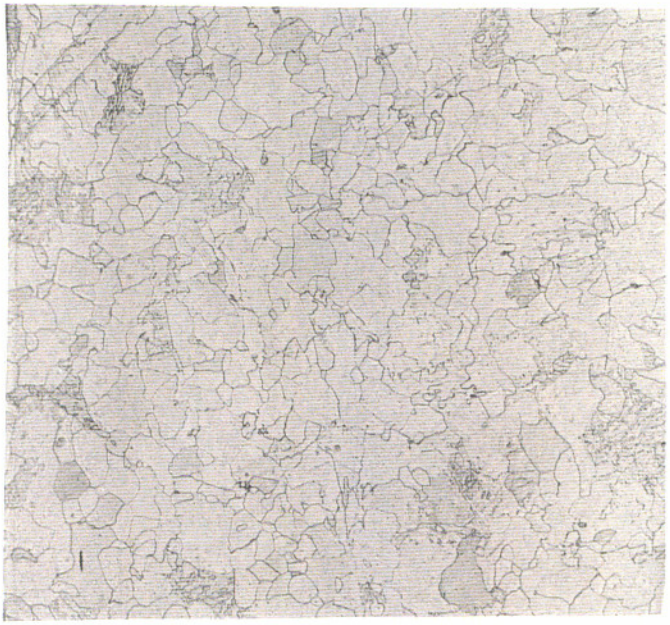

Figure 53
Field Area 1 (10 hrs 1450°F+ Furnace Cool) Base Metal
100X Nital

microstructure is not known. The apparent lower carbon and carbide level suggest that its mechanical properties would be substandard compared to the interior of the pipe.

Figures 53 - 58 are typical of the microstructure in Field Area 1. While some carbides are visible, the amount is small compared to those seen in Samples A5 and B5 (Figures 33, 1-5, 1-6, and 1-25). Field Area 2a was much like Field Area 1 in appearance (Figures 59 - 62), although there is more evidence of carbides in Figure 62. Field Area 2c (the weld) is seen in Figures 63 & 64. These micrographs demonstrate that the technique used clearly delineates both the basic microstructure and the presence of carbides (rounded in this case).

Field Area 3a exhibits microstructures comparable to the nominally equivalent laboratory samples A3 & B3 in Figures 31 and 1-23. It should be noted that the field replicas in Figures 65 - 68 are of a structure with an additional exposure of about 27,000 hours at 1005°F. With this in mind, the appearance of the carbides and the degree of degradation of the pearlite is quite reasonable.

Field Area 3b contains both base metal and a weld, with the intermediate weld heat affected zone. The base metal is shown in Figures 69 & 70. The appearance is similar to that of Field Area 3a. The base metal-WHAZ interface is seen in Figures 71 & 72, while the weld-WHAZ region is found in Figure 73. A rather fine textured area of the weld (Figures 74 & 75) is contrasted to a coarser area (Figures 76 & 77). Weld microstructure in a given area depends on a number of factors. These include the initial field welding parameters, the nearness of a subsequent weld bead, the stress relief heat treatment employed during construction, the hot bending heat treatment experienced later, and the accumulated service thermal exposure. Predicting the cumulative effects of

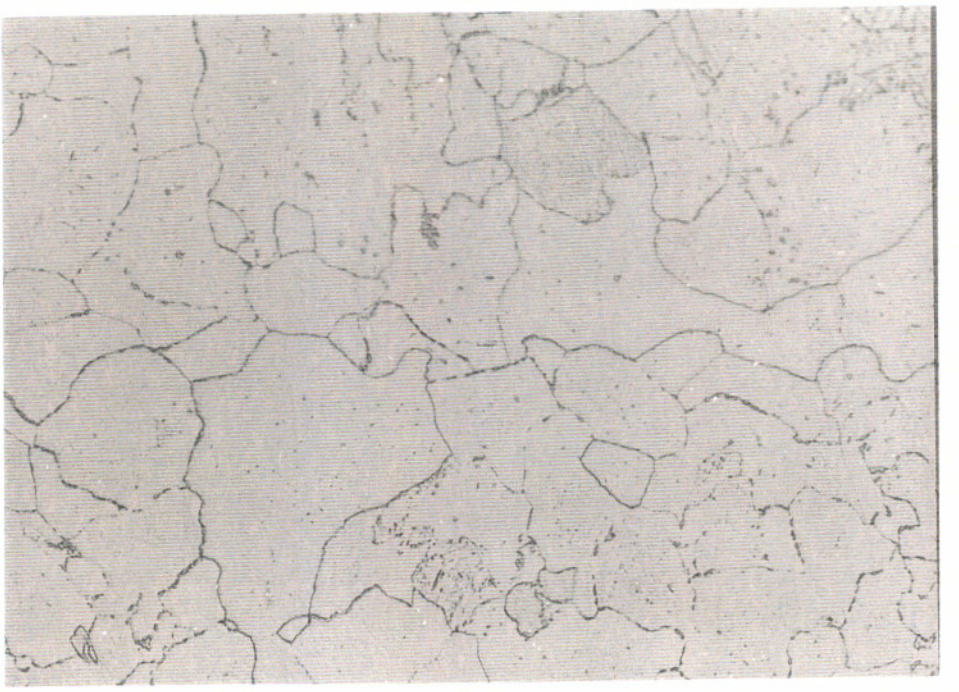

Figure 54
Field Area 1 (10 hrs 1450°F+ Furnace Cool) Base Metal
400X Nital

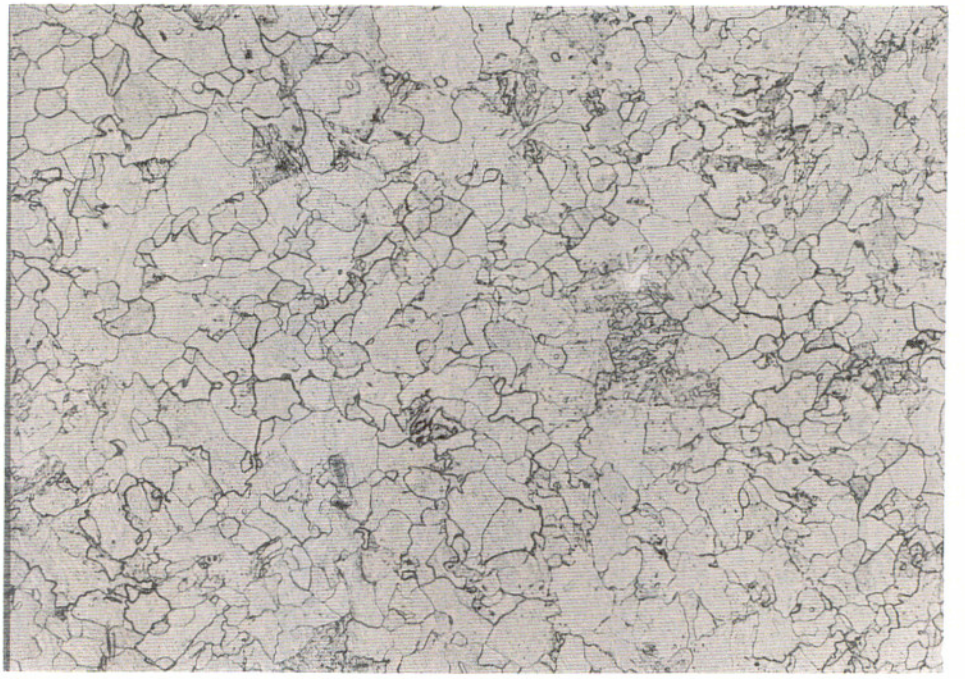

Figure 55
Field Area 1 (10 hrs 1450°F+ Furnace Cool) Base Metal
100X Nital

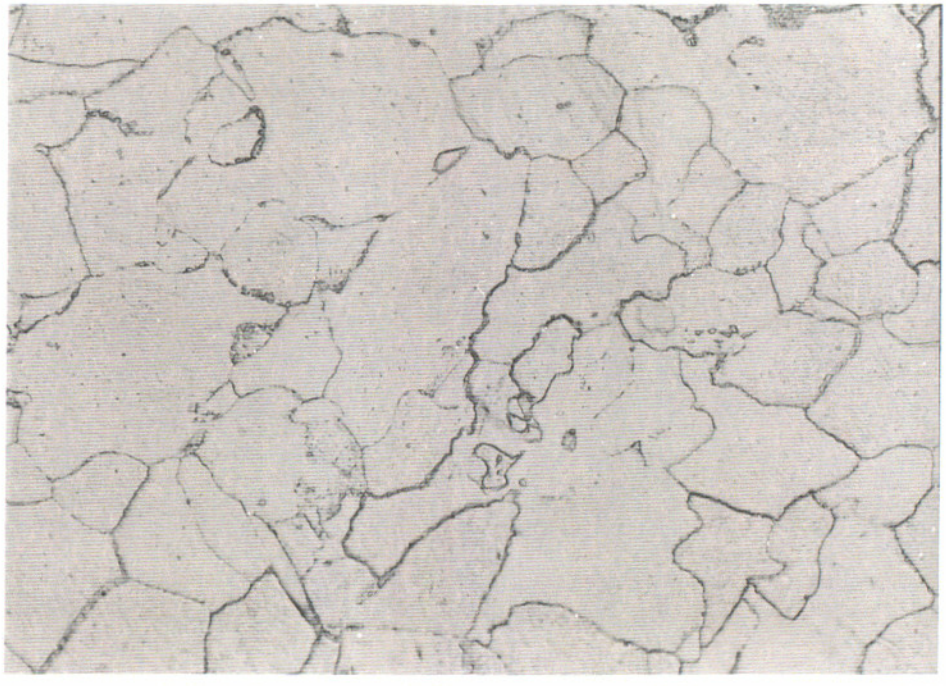

Figure 56
Field Area 1 (10 hrs 1450°F+ Furnace Cool) Base Metal
400X Nital

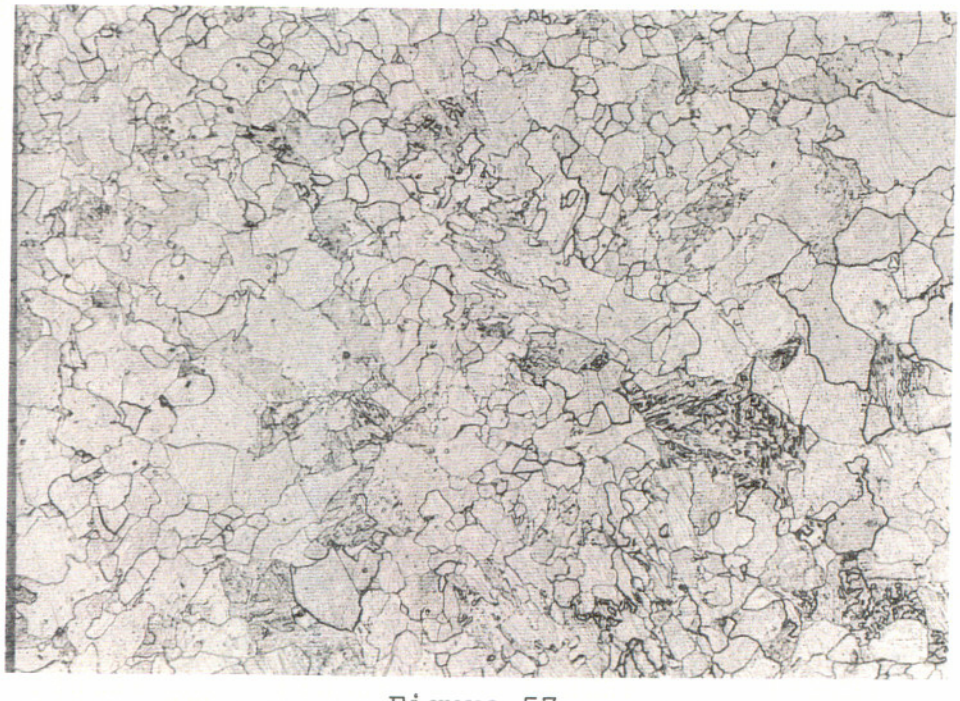

Figure 57
Field Area 1 (10 hrs 1450°F+ Furnace Cool) Base Metal
100X Nital

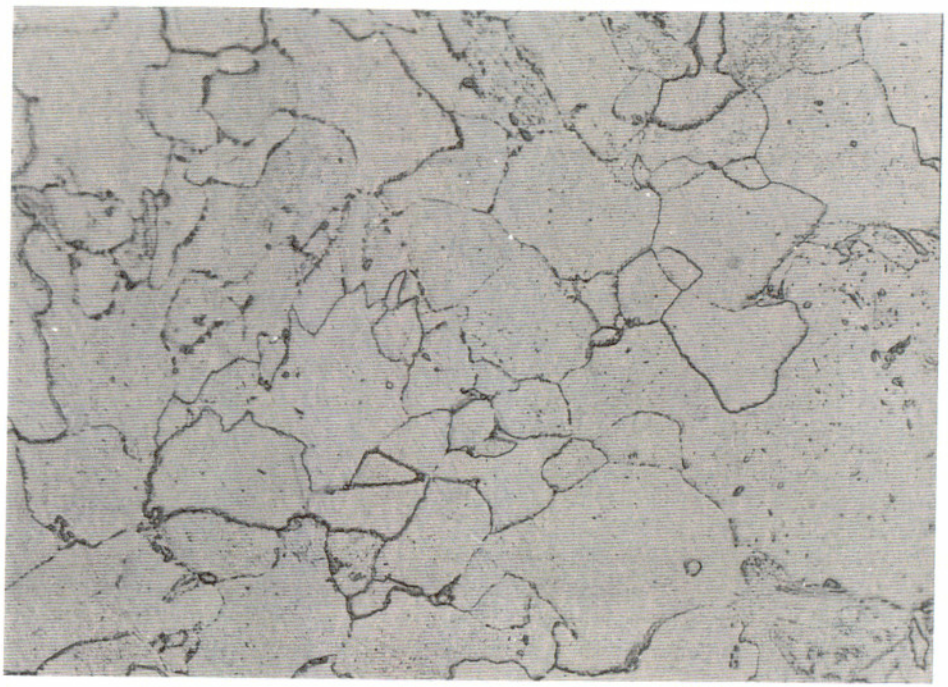

Figure 58
Field Area 1 (10 hrs 1450°F+ Furnace Cool) Base Metal
400X Nital

Figure 59
Field Area 1 (10 hrs 1450°F+ Furnace Cool) Base Metal
100X Nital

Figure 60
Field Area 2a (5 hrs 1450°F+ Furnace Cool) Base Metal
400X Nital

Figure 61
Field Area 2a (5 hrs 1450°F+ Furnace Cool) Base Metal
100X Nital

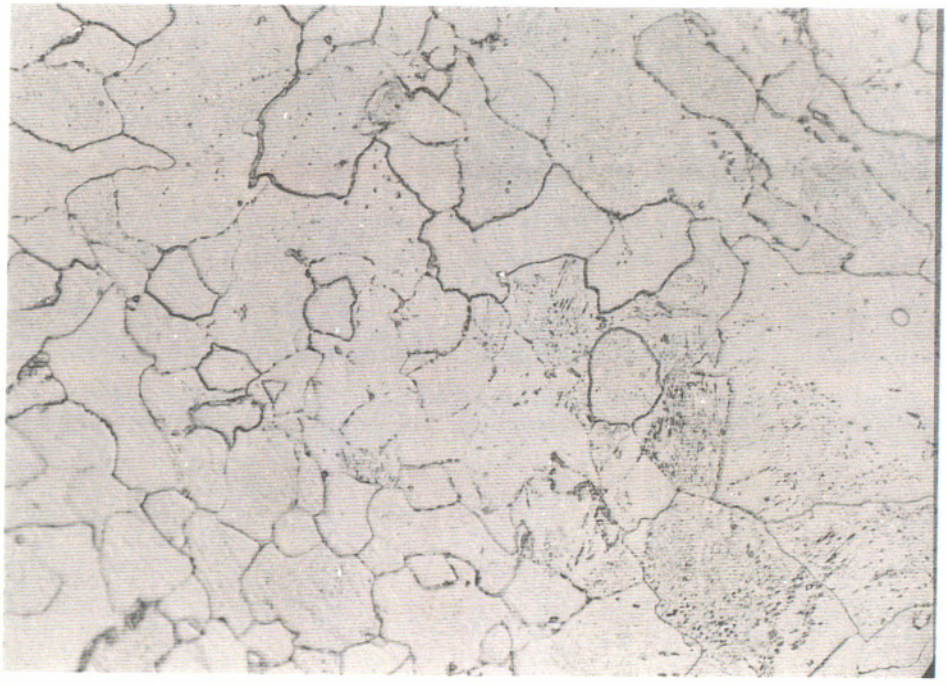

Figure 62
Field Area 2a (5 hrs 1450°F+ Furnace Cool) Base Metal
400X Nital

Figure 63
Field Area 2c (5 hrs 1450°F+ Furnace Cool) Weld Metal
100X Nital

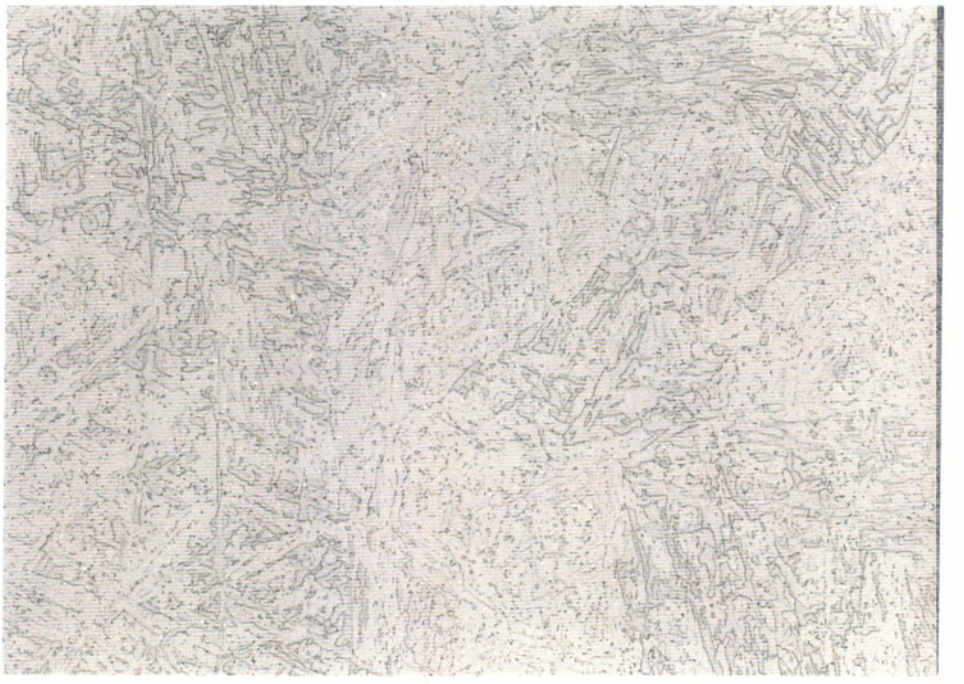

Figure 64
Field Area 2c (5 hrs 1450°F+ Furnace Cool) Weld Metal
400X Nital

Figure 65
Field Area 3a (5 hrs 1450°F+ Furnace Cool) Base Metal
100X Nital

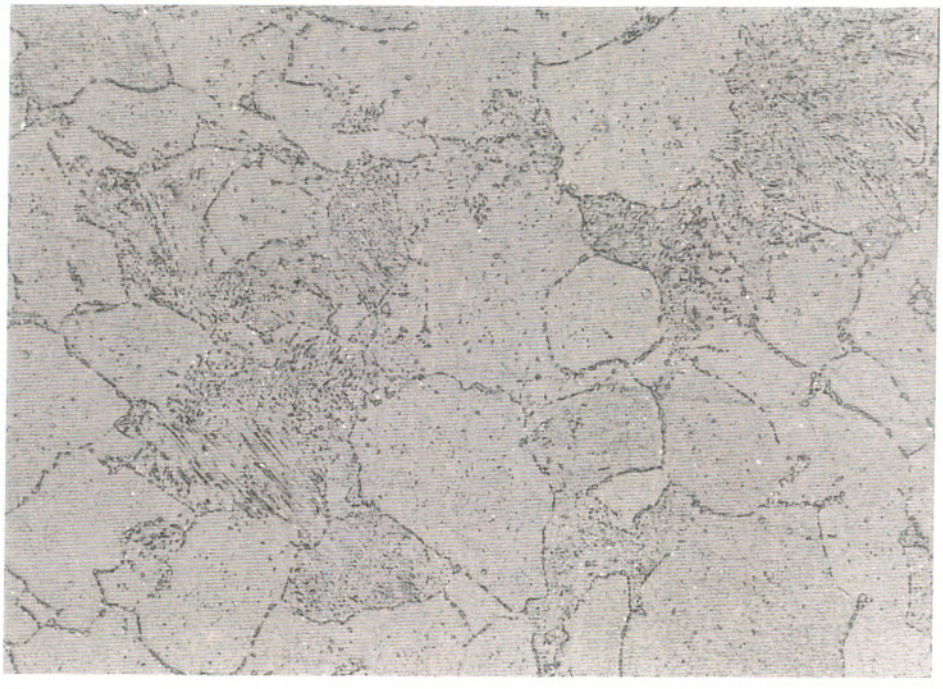

Figure 66
Field Area 3a (5 hrs 1450°F+ Furnace Cool) Base Metal
400X Nital

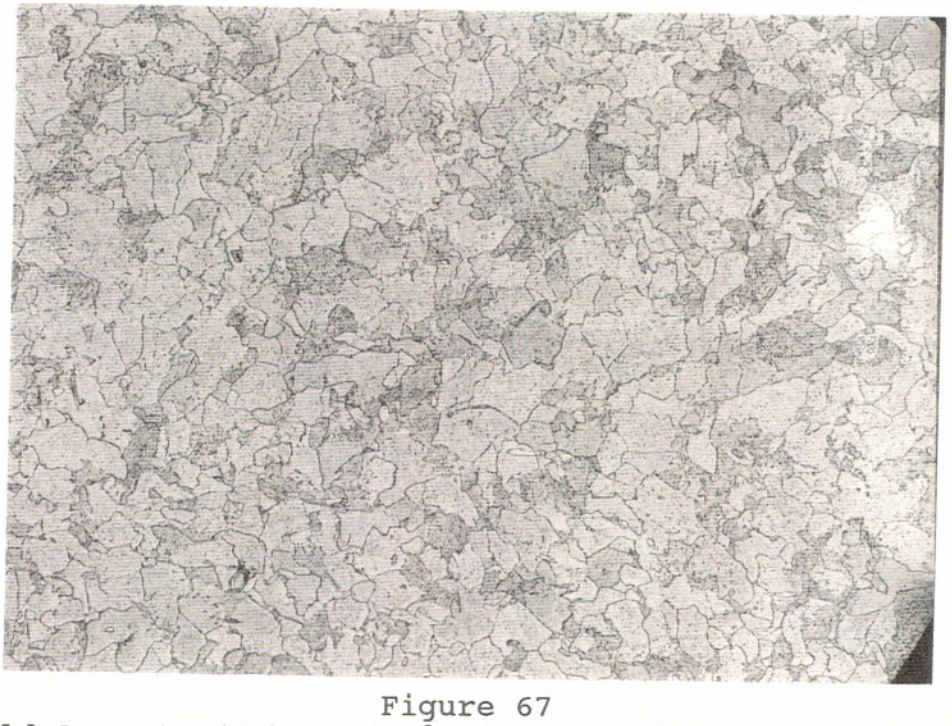

Figure 67
Field Area 3a (5 hrs 1450°F+ Furnace Cool) Base Metal
100X Nital

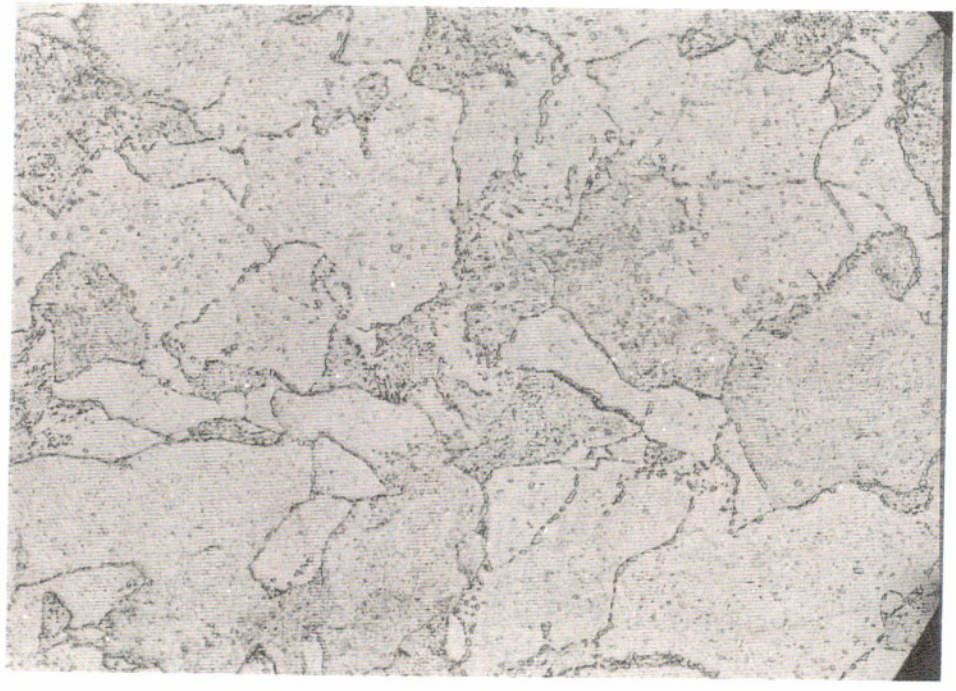

Figure 68
Field Area 3a (5 hrs 1450°F+ Furnace Cool) Base Metal
400X Nital

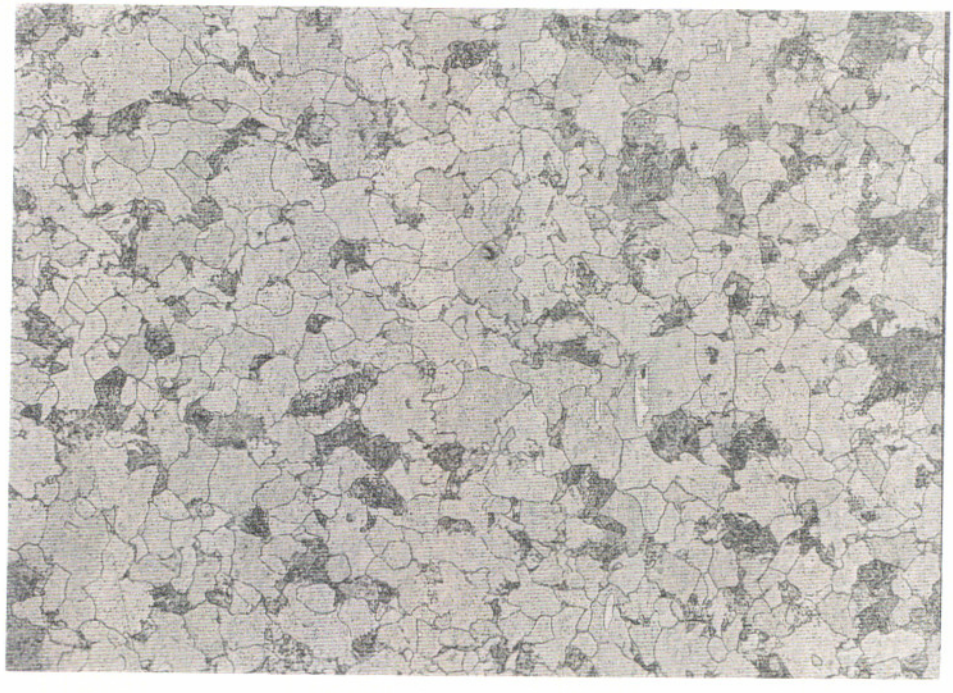

Figure 69
Field Area 3b (5 hrs 1450°F+ Furnace Cool) Base Metal
100X Nital

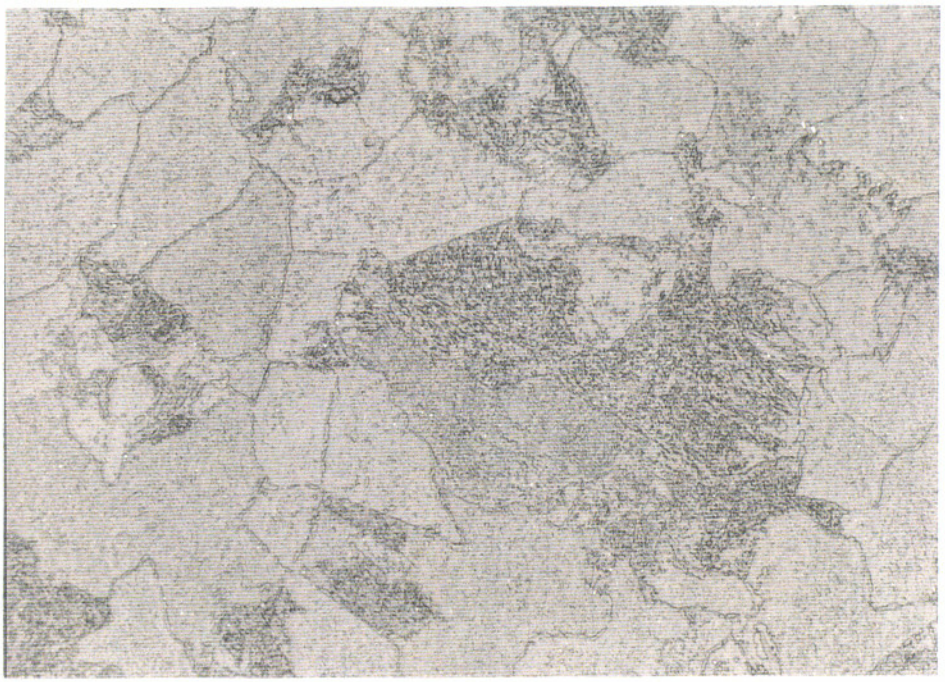

Figure 70
Field Area 3b (5 hrs 1450°F+ Furnace Cool) Base Metal
400X Nital

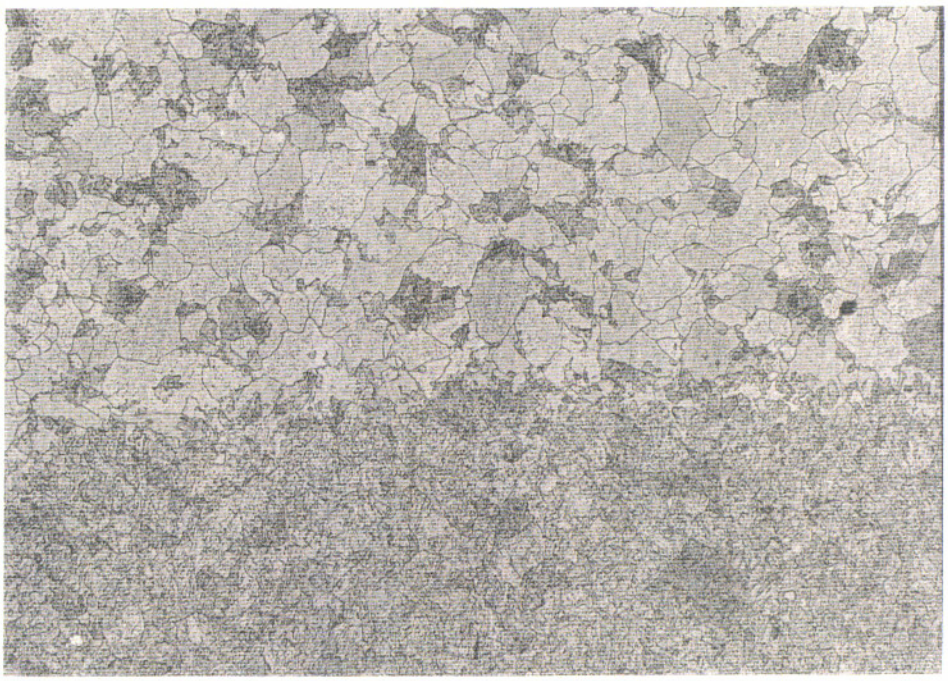

Figure 71
Field Area 3b (5 hrs 1450°F+ Furnace Cool) Base-WHAZ
100X Nital

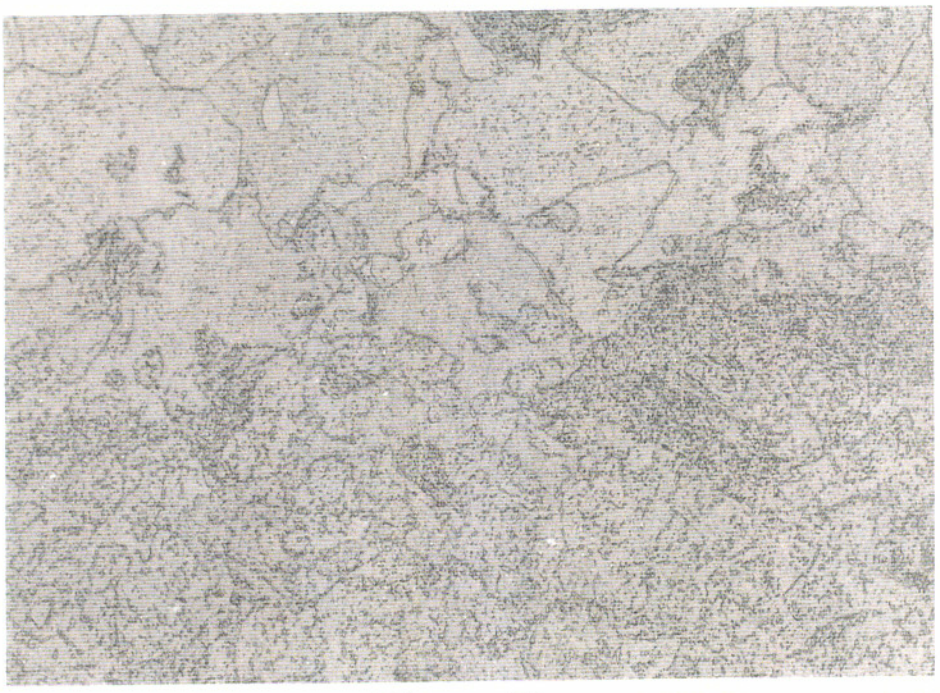

Figure 72
Field Area 3b (5 hrs 1450°F+ Furnace Cool) Base-WHAZ
400X Nital

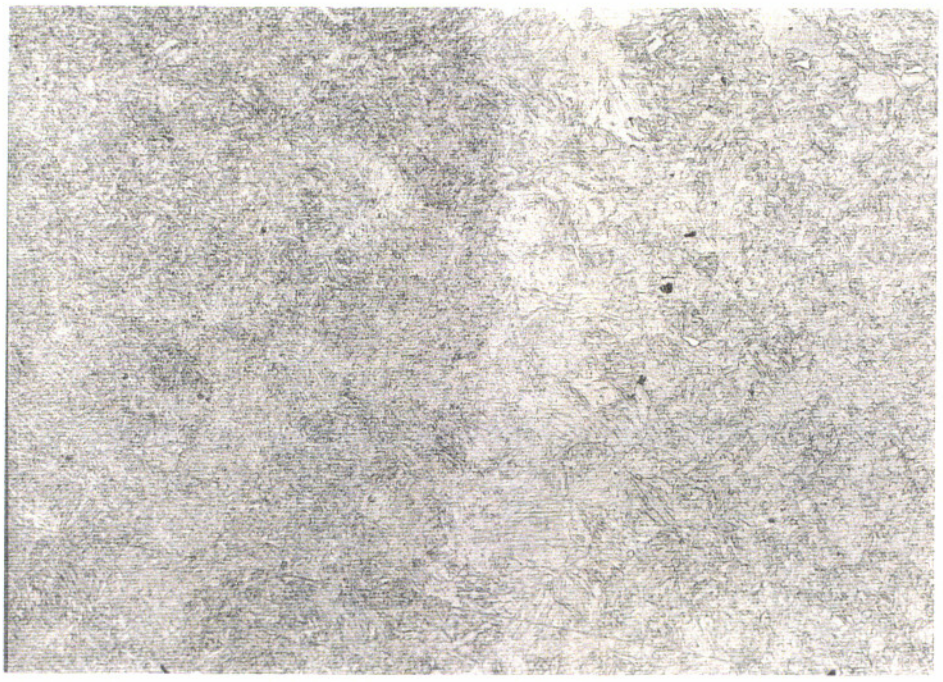

Figure 73
Field Area 3b (5 hrs 1450°F+ Furnace Cool) Weld-WHAZ
100X Nital

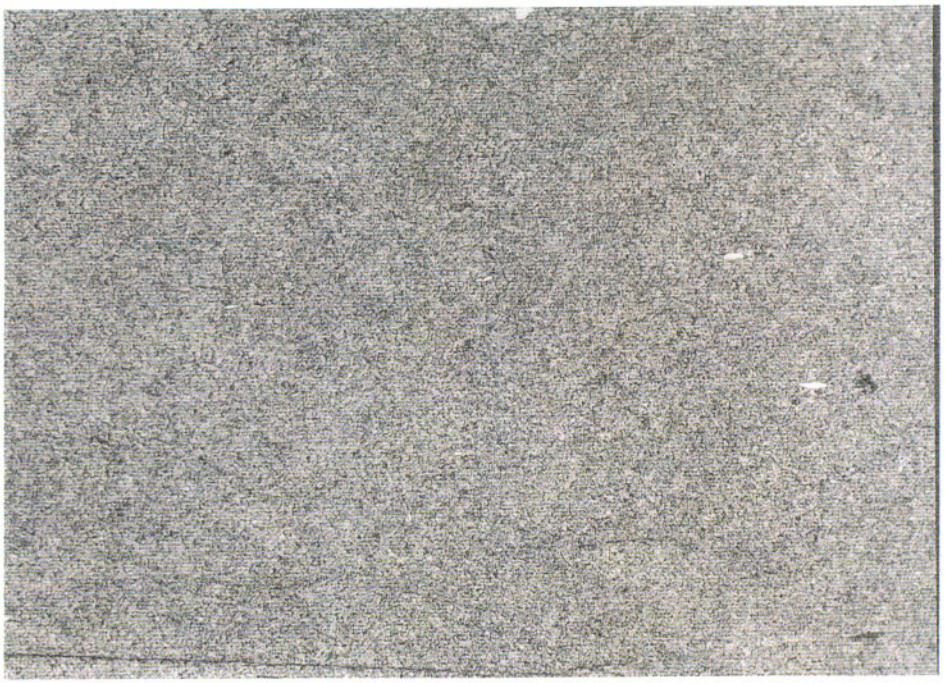

Figure 74
Field Area 3b (5 hrs 1450°F+ Furnace Cool) Weld
100X Nital

Figure 75
Field Area 3b (5 hrs 1450°F+ Furnace Cool) Weld
400X Nital

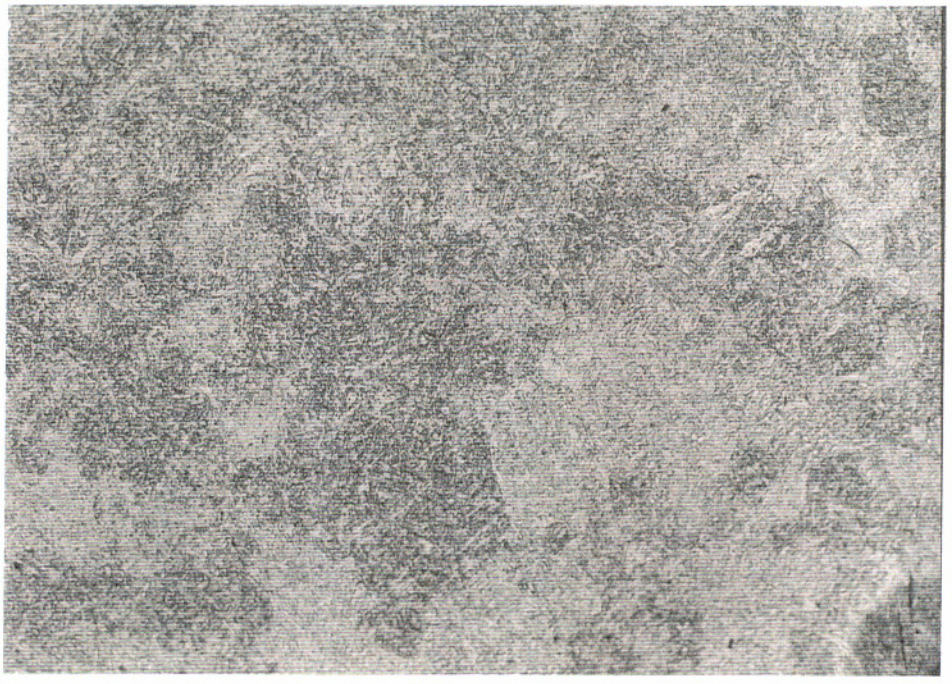

Figure 76
Field Area 3b (5 hrs 1450°F+ Furnace Cool) Weld
100X Nital

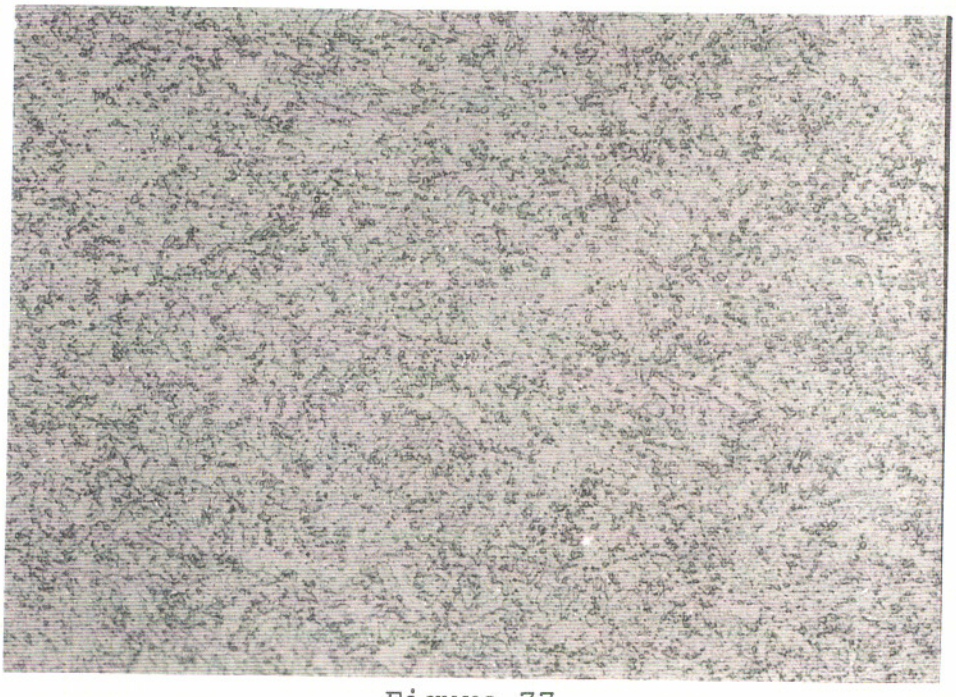

Figure 77
Field Area 3b (5 hrs 1450°F+ Furnace Cool) Weld
400X Nital

these factors analytically seems quite difficult. Fortunately, everything but the additional 27,000 hours of service exposure has been encompassed by the stress-rupture testing.

The replicas from Field Area 3c (Figures 78 - 81) show an area with somewhat fewer carbides or pearlite remnants than the equivalent areas 3a & 3b. The appearance is similar to the replicas from Field Areas 1 and 2. In addition, several regions of grain growth were found (Figure 82). These regions appear to correspond to what were originally bands of cold deformation caused by a surface finishing process that leaves grooves of constant width but of varying depth. Subsequent recrystallization has also resulted in grain growth.

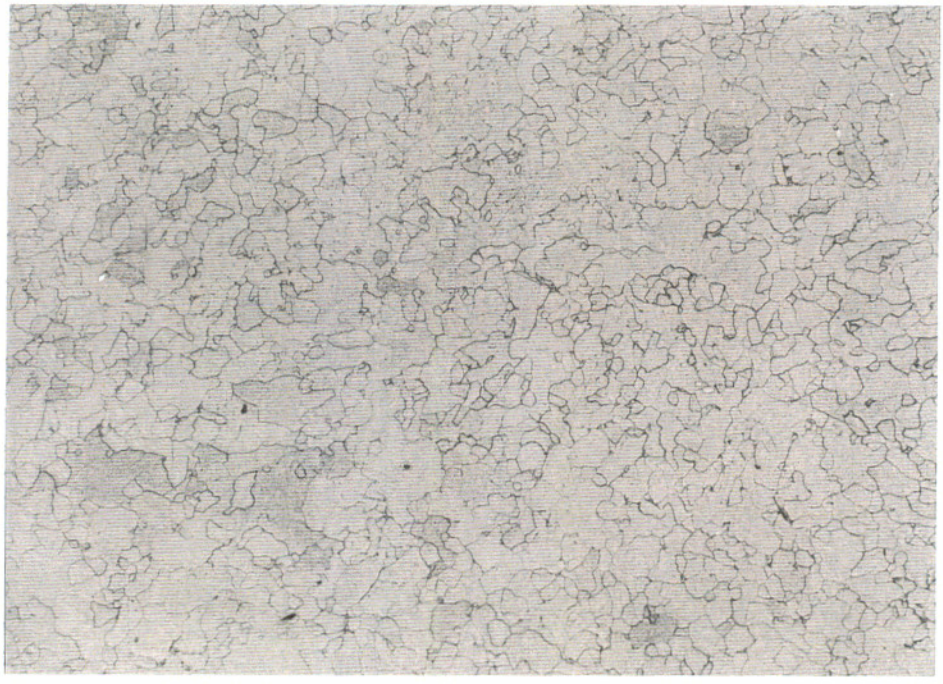

Figure 78
Field Area 3c (5 hrs 1450°F+ Furnace Cool) Base Metal
100X Nital

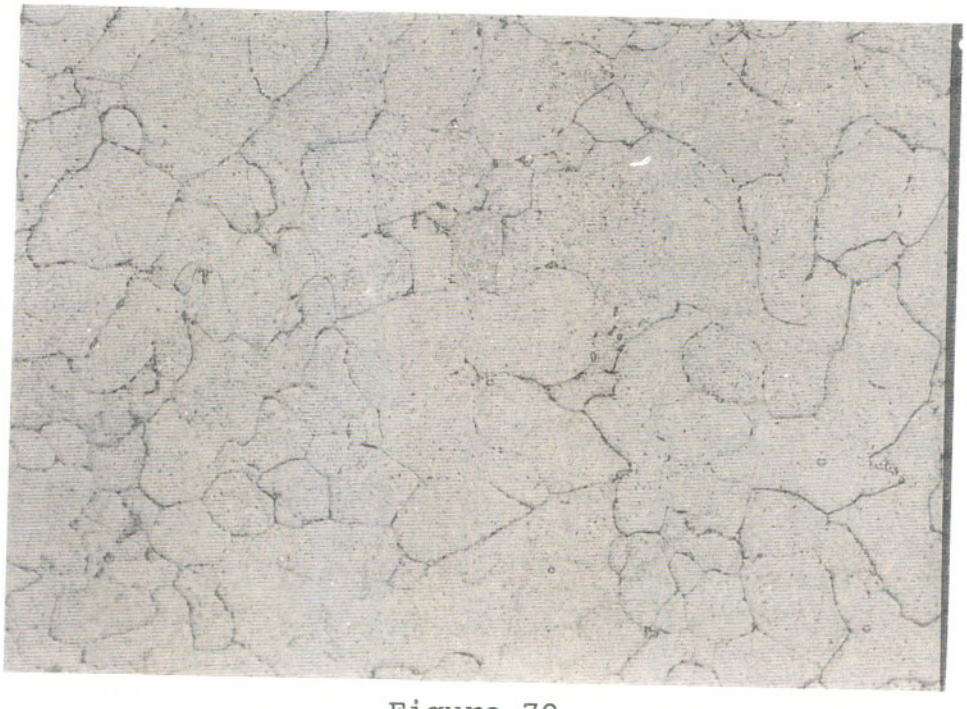

Figure 79
Field Area 3c (5 hrs 1450°F+ Furnace Cool) Base Metal
400X Nital

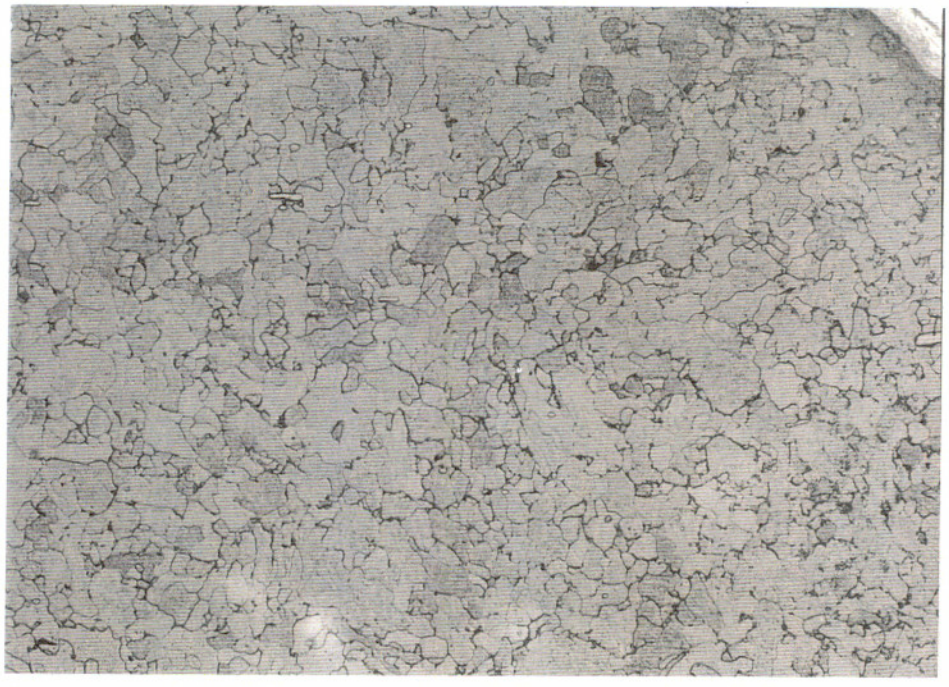

Figure 80
Field Area 3c (5 hrs 1450°F+ Furnace Cool) Base Metal
100X Nital

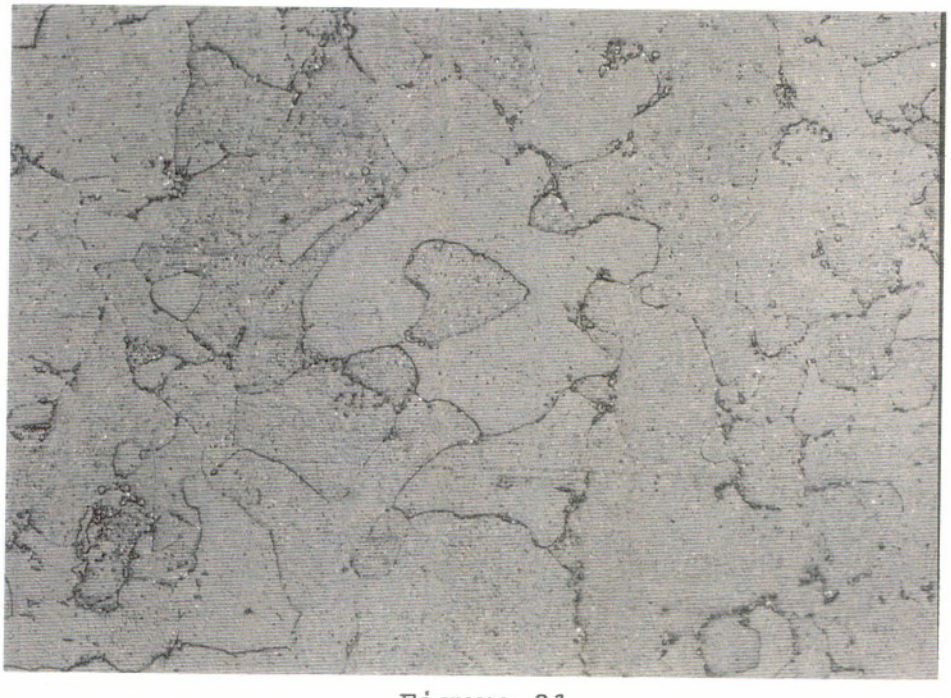

Figure 81
Field Area 3c (5 hrs 1450°F+ Furnace Cool) Base Metal
400X Nital

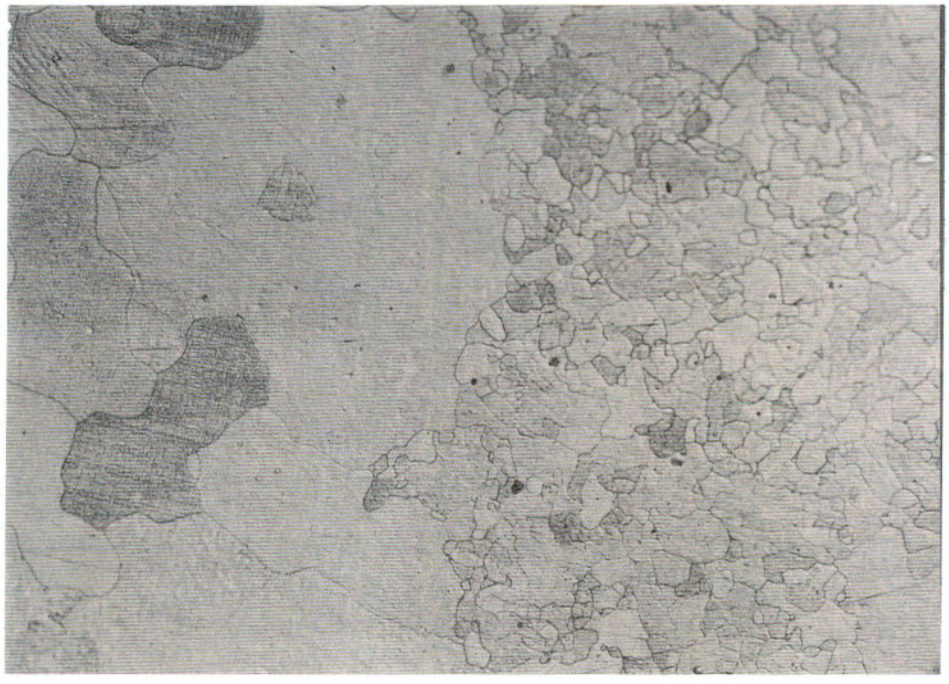

Figure 82
Field Area 3c (5 hrs 1450°F+ Furnace Cool) Grain Growth
100X Nital

5.0 DISCUSSION

5.1 General Considerations

Prior to discussing the results of these investigations in comparison to each other and the industry database some consideration must be given to the validity of the conceptual framework constructed earlier. While the theories and correlations are thought to be valid, none of them are fundamental in nature, since they are based primarily on empirical observations.

5.1.1 Extrapolative Methods

For instance, while the much used Larson Miller parameter is derived from one model of the creep process, this model is not necessarily valid for any real material over any significant range of temperatures and stresses. In this respect it is no different from many proposed models that have been based on the behavior of relatively pure metals and simple alloys.

The primary virtue of the Larson Miller parameter is that it works for a number of materials over some range of variables. It has been found to be reasonably accurate for 2 1/4Cr-1Mo steel, and is the basis of the predictive approach outlined in Ref 56 by Viswanathan et al. The oxidation corrected database for this material, shown earlier in Figure 8, can actually be analyzed to predict LMP at rupture based on the preservice tensile strength.

It has been shown, however, that 100,000 hour rupture properties for carbon steel based on such projections only become reasonably accurate when test times approach 30,000

hours[63]. Because 2 1/4Cr-1Mo is a much more stable material, time to rupture may not show the downward trend seen for carbon steel data over a similar time period. That this stability will continue for the millions of hours of life predicted for field material here is questionable.

The use of increased temperature as an accelerant in stress-rupture testing is inherently acceptable in the Larson Miller parameter. Using the database charted in Figure 5, there is no reason to suspect that stress could not be equally well accounted for, although the correlation is not inherent in the Larson Miller parameter itself. However, Hart has shown that life prediction via the life fraction rule ($\Sigma t/t_r=1$ at failure) is only accurate for data collected via temperature acceleration, and that stress acceleration leads to grossly conservative results[57].

5.1.2 Fracture Mode Disparity

Another issue in regard to the accelerated testing of 2 1/4Cr-1Mo material is the disparity in fracture mode between the test material and the field material. It was pointed out in Section 2.2 that intergranular failure was not observed to occur below $1X10^7$ seconds, while the test times in this investigation do not exceed $2X10^6$ seconds. The effect of this on the validity of the long term projections is not known. Intergranular cavity nucleation and formation occurs at a high rate in this alloy, and may still strongly influence the stress-rupture behavior even where the failure mode is primarily transgranular.

5.1.3 Microstructural Complexity

The microstructural complexity of the 2 1/4Cr-1Mo steel may make short term test results suspect for comparative evaluations. The work reported in Ref. 56 suggests that this

may not be a real problem where service or thermal exposure is around normal service temperatures. The analysis discussed there leads to a predictably decreasing strength (and presumably hardness) as exposure time increases. At a minimum, the strength at a known time and temperature history may be related back to the original strength and the original rupture life calculated.

Thermal exposure outside of the regime anticipated in the above model may render the model nonconservative. In the case of exposures above the lower critical temperature, Ac_1, the material may be hardened or softened depending on the cooling rate. Since the model is based on a normally heat treated virgin material, it may be very inaccurate in either direction.

Also, strengthening effects have been observed in service exposed material that was tempered briefly at a temperature above the service temperature but well below Ac_1[59]. This is thought to be due to the release of carbon and molybdenum from nonstrengthening precipitates. Once returned to the matrix the carbon and molybdenum can participate in interactive solid solution hardening. It is not known if this effect leads to a rejuvenation of stress-rupture properties as well. It seems apparent that the model will not be able to deal with this type of behavior.

5.1.4 Ambiguities in the Model

The analysis model presented in Ref. 56 appears to have some ambiguities associated with it. The model is based on the oxidation corrected data base and the derived LMP life equation formula ($LMP=40975 + 57(UTS) - 5225\log\sigma - 2450(\log\sigma)^2$) seen in Figure 8. In addition, the $LMP_{(age)}$ factor shown in Figure 10 may be used to predict an aged tensile strength knowing the original tensile strength and the

exposure details, or it may be used to calculate an original tensile strength given the aged tensile strength and the exposure details. This seems reasonable.

However, it is also stated that the LMP life equation uses a real time tensile strength to predict remaining life. This implies that it is the current tensile strength that is used in the calculation and not the original tensile strength. Figure 83 shows that the ultimate tensile strength of the material is predicted to drop relatively rapidly in the early hours of exposure (for illustrative purposes a temperature of 1000°F has been chosen).

In order to update the remaining rupture life one would use this presumably reality based prediction of the tensile strength as a function of exposure as input to the LMP life equation ($LMP=40975 + 57(UTS) - 5225\log\sigma - 2450(\log\sigma)^2$) with a chosen stress (10 ksi for example). If this is done, the predicted time to rupture varies as shown by the lower curve in Figure 84.

The real time update method is not realistic. It predicts that a material under constant and reasonable service conditions will show a precipitate drop in rupture life within the first few thousand hours of service. It further implies that a material can exist for many hundreds of thousands of hours with a predicted time to rupture at any time of only about one hundred thousand hours.

Therefore, in the remainder of this paper, the time to rupture predicted by this model will be calculated using the known exposure regimes and the $LMP^{(age)}$ equation to predict an original UTS from a current UTS. For the hypothetical conditions used earlier, this method leads to the behavior shown by the upper curve in Figure 84. This upper curve is based on a simple subtraction of elapsed time from the originally predicted time to rupture.

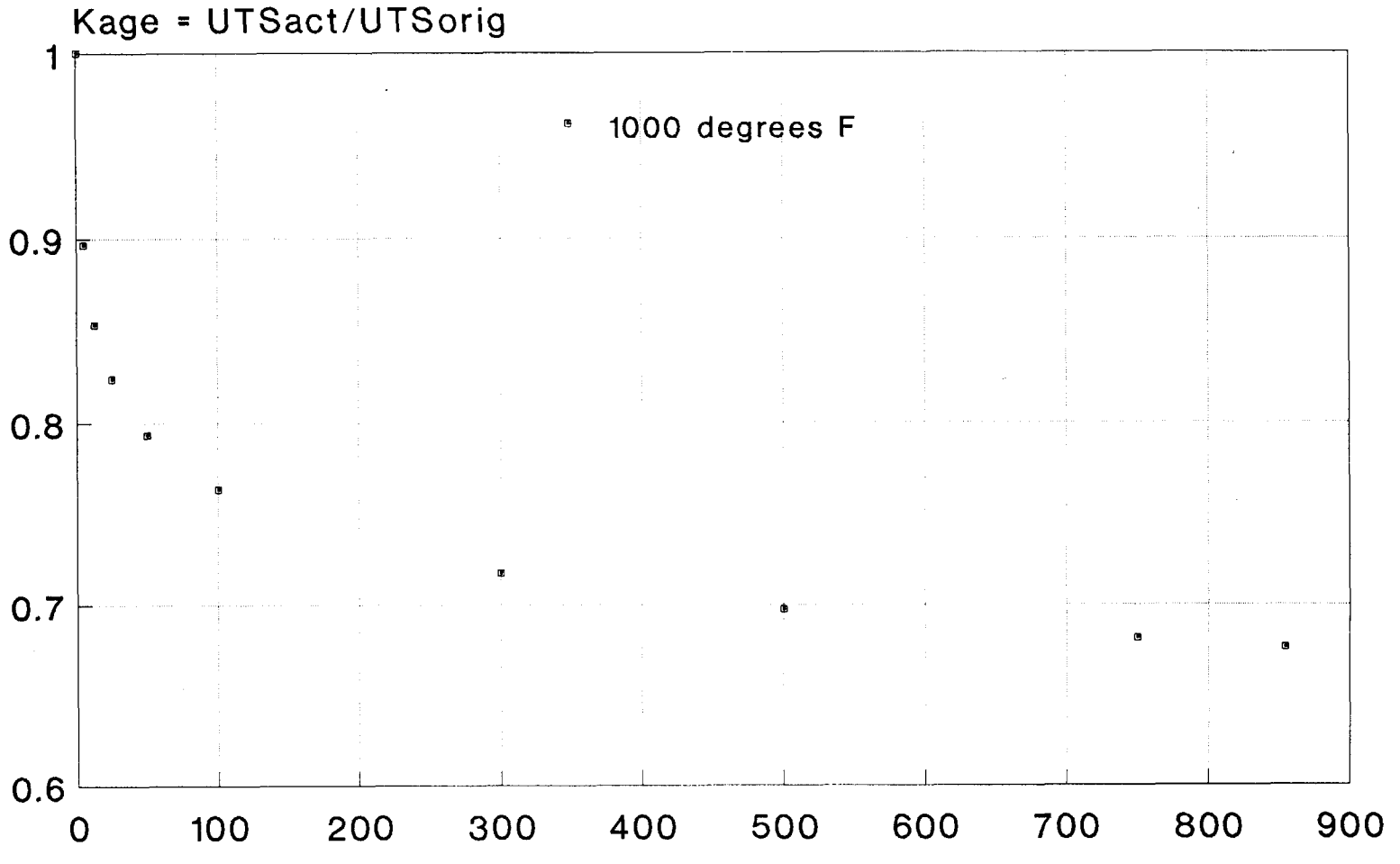

Figure 83 Kage Calculated from Reference 56

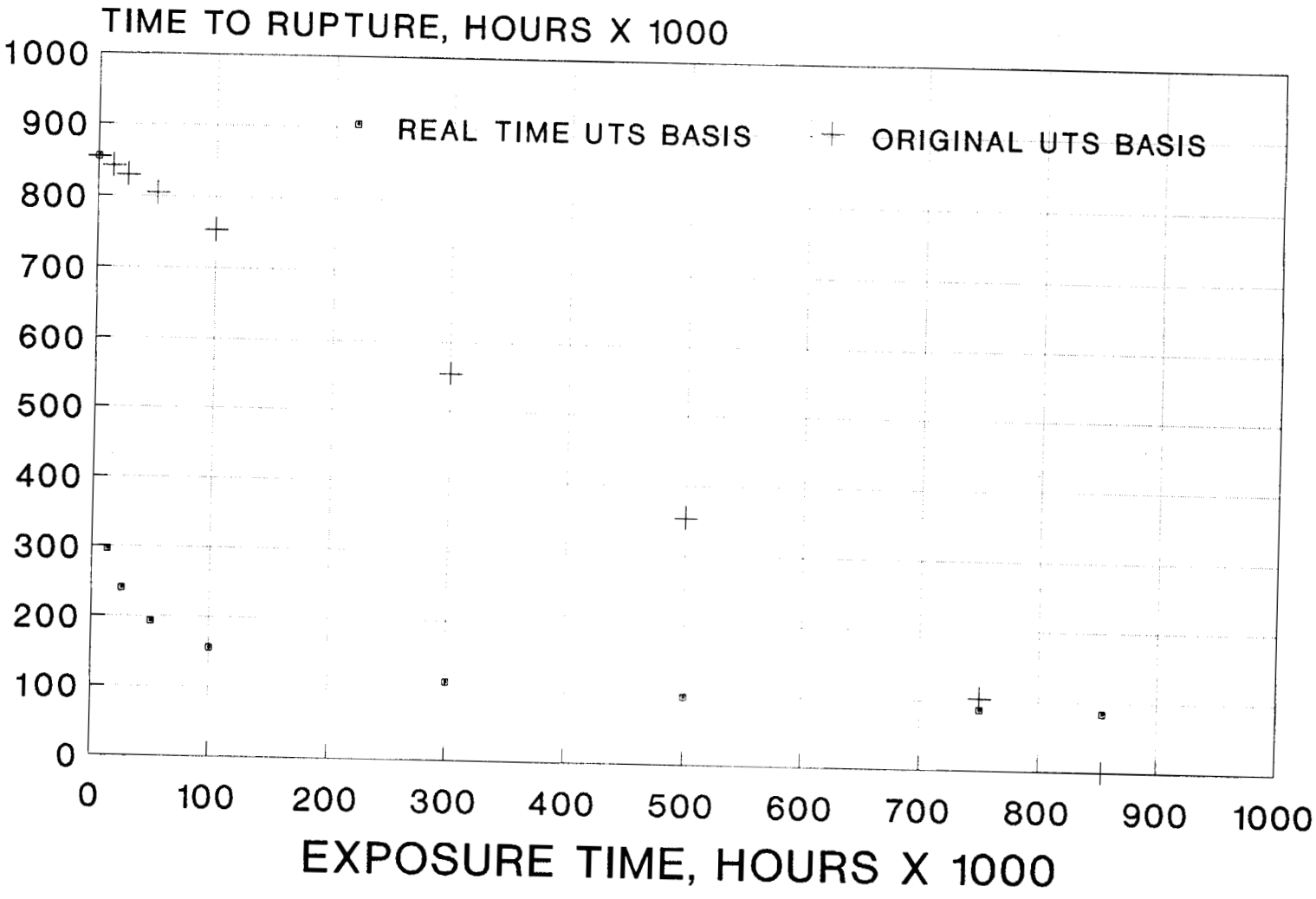

Figure 84 Rupture Time Predictions UTSo = 80 ksi, T=1000F

Tensile strengths were determined for all samples by conversion of Equotip hardnesses. The conversion involves the use of empirical formulas that embody both the relationship between the Equotip hardness and Brinell hardness, and between Brinell hardness and tensile strength. The formulas used were:

1. HB = 0.65 LD - 120.4
2. UTS = 0.2969 LD - 49.8

Where comparisons were possible, the predictions were found to be acceptably accurate.

5.2 Use of the Model

In order to compare the stress-rupture behavior of a given sample or group of samples with the model, two graphs have been constructed using the methodology of Ref. 56 at the service conditions of 6 ksi and 1005°F. These graphs relate the Larson Miller parameter and the time to rupture at 1005°F to the projected original hardness, and are shown in Figure 85. The performance of the tested material will be compared by entering the experimental data on the graphs. Obedience to the model will be indicated by the degree of nearness to the particular curve.

The projected original hardness was calculated by the following method.

1. Present Equotip hardness was converted to present UTS (UTS_p).
2. LMP_{age} was calculated using the relationship $LMP_{age} = T\ ^{\circ}R(10 + \log t)10^{-3}$. This was done for each thermal exposure by converting all time-temperature regimes to an equivalent exposure at 1005°F, and summing the hours.

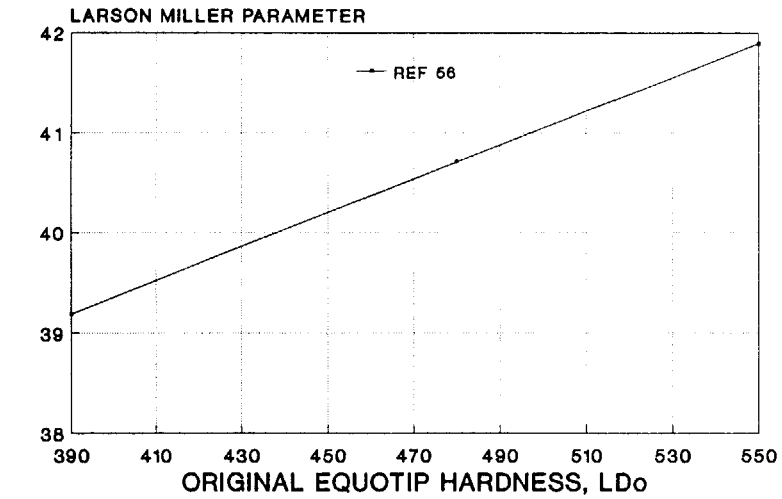

Ref 56 curve is calculated relationship

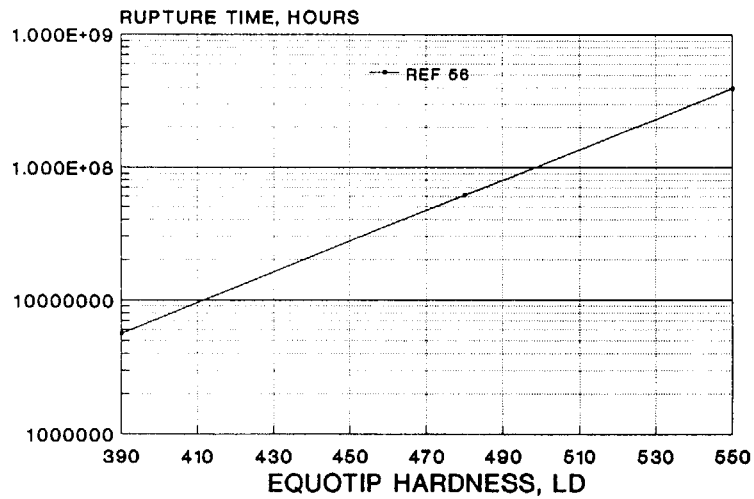

LMP prediction at 1005 degrees F

Figure 85
Larson-Miller Parameter and Rupture Time
Predictions per Reference 56 Model

3. K_{age} was calculated using the formula $K_{age} = 3.033 - 1.404X10^{-4}LMP_{age} + 1.679X10^{-9}(LMP_{age})^2$
4. UTS_o was calculated by dividing UTS_p by K_{age}.
5. UTS_o was converted to projected original Equotip hardness.

5.3 Effects of Hot Bending Heat Treatment on Base Material

5.3.1 Base Metal Heat Treatment

The base metal samples tested in the transverse direction were designated A1, A2, A3, A4, or A5 depending on whether they were in the as-received condition or had received subsequent heat treatment. A1 samples were as removed from service after 13,000 hours of exposure at 6 ksi and 1005°F. A3 samples had received an additional 5 hour exposure at 1460°F followed by a slow cool, while the A5 samples had received an additional 10 hour exposure followed by a slow cool.

The A4 series was intended to represent nearby metal that was below the Ac_1 temperature, but had experienced comparable time/temperature exposure both in terms of real time and thermal aging time. According to the $LMP_{(age)}$ equation, the A4-8, A4-13.7, and A4-28.2 exposures were equivalent to 1.6, 5, and 10 hours at 1450°F.

The A2 series was intended to investigate the effects of long term exposure beyond the Ac_1 temperature. The exposure times were chosen arbitrarily.

5.3.2 A1 Material Behavior

The A1 material is effectively the baseline for this project. The $LMP_{(age)}$ parameter for this material considered only the 13,000 hours at 1005°F. If one plots the average Larson Miller parameter from the stress-rupture tests, and the

predicted time to rupture derived from that LMP, on the model curves, the match is extremely good. This point is shown in Figure 86.

The extrapolation using the model suggests that the original true tensile strength of A1 material was 76 ksi. This value will be compared to the projected values for the other samples derived from the A blocks.

The A1 material appears to have a microstructure that is completely compatible with Baker & Nutting and others. In Figures 29 & 30 the pearlitic carbide structure (probably $M_{23}C_6$ rather than Fe_3C) is still relatively sharp. The ferrite contains a profusion of elongated precipitates (probably Mo_2C), while the grain boundaries are partially decorated with small equiaxed precipitates.

5.3.3 A3 Material Behavior

The A3 samples exhibited a slightly lower actual hardness than the A1 material, and had poorer stress-rupture properties. The predicted rupture life at 1005°F was only 49% of the A1 material.

They were comparable to the A5 material in terms of room temperature strength and hardness. The stress-rupture properties were substantially lower, even though the A5 material had a more extended thermal exposure. The predicted rupture life at 1005°F of the A3 material was about 74% of the A5 material.

The positions of both A3 and A5 relative to the model curve are seen in Figure 87. Both materials exhibit a stress-rupture capability somewhat compatible with their predicted original hardness, assuming a simple tempering exposure. The correlation is not as good as for the A1 material, and is on the nonconservative side.

The microstructure of A3 in Figures 31 & 32 is strikingly

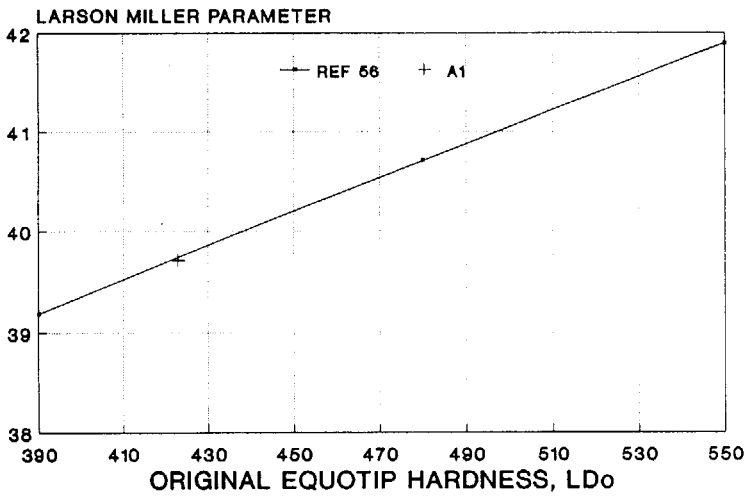

Ref 56 curve is calculated relationship

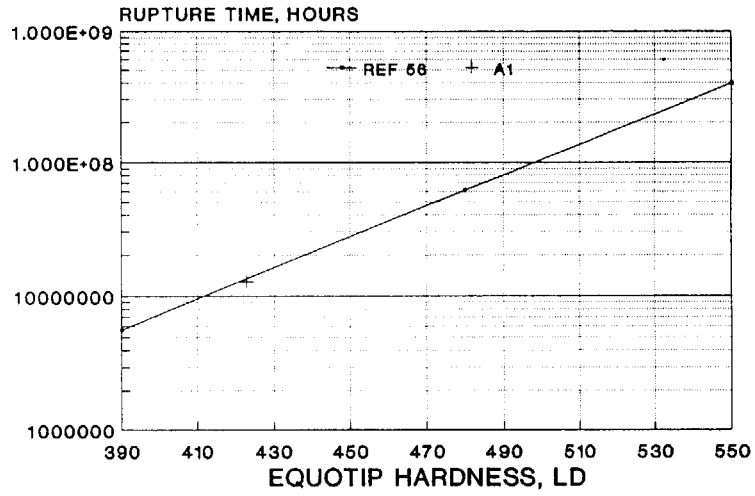

LMP prediction at 1005 degrees F

Figure 86
A1 Larson-Miller Parameter and Rupture Time
Compared to Reference 56 Predictions

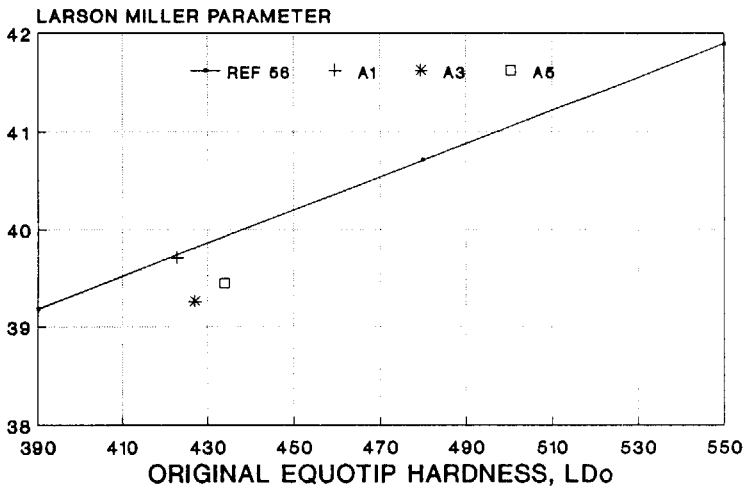

Ref 56 curve is calculated relationship

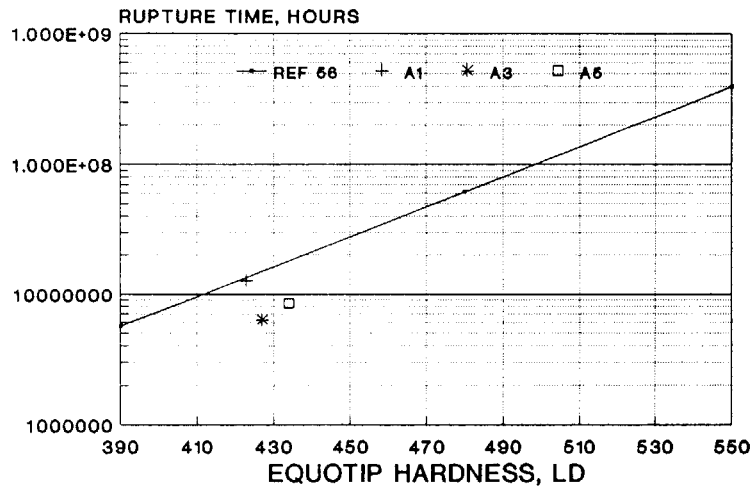

LMP prediction at 1005 degrees F

Figure 87
A1, A3, & A5 Larson-Miller Parameter and Rupture Time Compared to Reference 56 Predictions

different from that of the A1 material. The pearlitic carbides have coarsened considerably, and the elongated intragranular precipitates of Mo_2C have disappeared and been replaced by more rounded ones. In addition, heavy blocky precipitates have formed at the grain boundaries.

Since the really effective high temperature strengthening in 2 1/4Cr-1Mo is derived from either the Mo-C interaction solid solution hardening or the elongated Mo_2C precipitates, the lower properties seen here are not surprising.

5.3.4 A5 Material Behavior

The A5 samples had a slightly lower hardness than the A1 material, with lower stress-rupture properties. The predicted rupture life at 1005°F was about 66% of the A1 material. As in the case of the A3 material, the predicted original hardness is slightly higher than the model would anticipate for the actual stress-rupture properties.

The microstructure of A5 is seen in Figures 33 & 34. It differs noticeably from that of A1 or A3. The pearlitic structure is substantially degraded, and there appear to be scattered platelets/islands of tempered bainite. Grain boundary precipitation is similar to that seen for A3.

Intragranular precipitation is finer than for A3, and there appears to be an ordered pattern present in many grains. This latter possibility is intriguing, but is not further resolvable with the optical microscope. It may be that this ordered precipitate, and/or the presence of tempered bainite has raised the short term stress-rupture properties relative to A3.

5.3.5 A4 Material Behavior

A4 samples were heat treated at 1375°F for 8, 13.7, and 28.2 hours followed by an air cool. They were intended to

represent piping material adjacent to that exposed above the Ac_1 temperature. The ageing model predicts the following properties after tempering this as-removed base metal.

	Hardness	UTS	LMP	rupture time
A4-8	Ld 381	63.2 ks	39.03	$4.37X10^6$
A4-13.7	Ld 378	62.4 ksi	38.98	$4.07X10^6$
A4-28.2	Ld 372	60.8 ksi	38.89	$3.52X10^6$

Reference to Table V and Figures 21 & 23 shows the above values to be too low. Hardnesses, Larson Miller parameters, and estimated times to rupture at 1005°F for the actual samples exceed the model predictions.

Figure 88 shows how the A4 series samples compare to the model predictions based on their measured hardness, and to those simulating the 1460°F heat treatment. They do not achieve the stress-rupture properties the model predicts for their estimated original hardness, but they do exceed that predicted by the aging model for their thermal exposure.

The microstructure of these samples is seen in Figure 35, and Figures 1-7 through 1-12. The general picture relative to sample A1 is one of more degraded pearlite and more grain boundary precipitation. There is no evidence of any transformation to austenite, which would be manifested in the formation of fresh bainite upon air cooling. This suggests that Ac_1 for this steel in the A1 type condition is above 1375°F.

The increased hardness and improved stress-rupture properties may be due to the phenomena noted by Wada and Biss, which was discussed in 5.1.3. This unexpected improvement after a tempering treatment is clearly not reflected in the model.

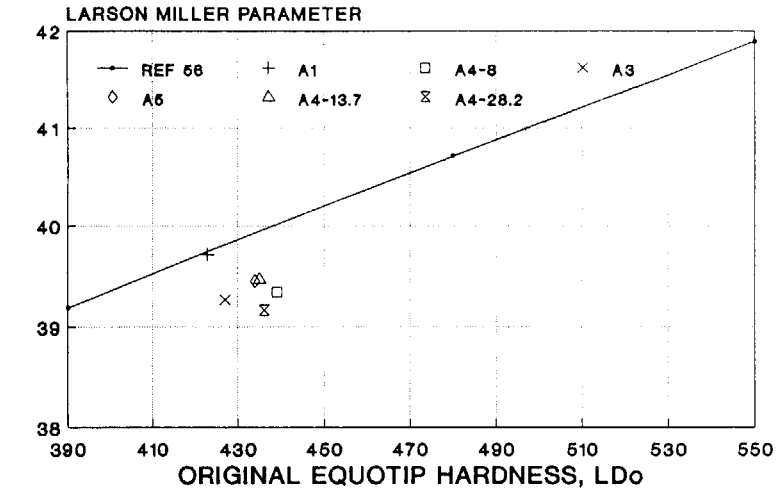

Ref 56 curve is calculated relationship

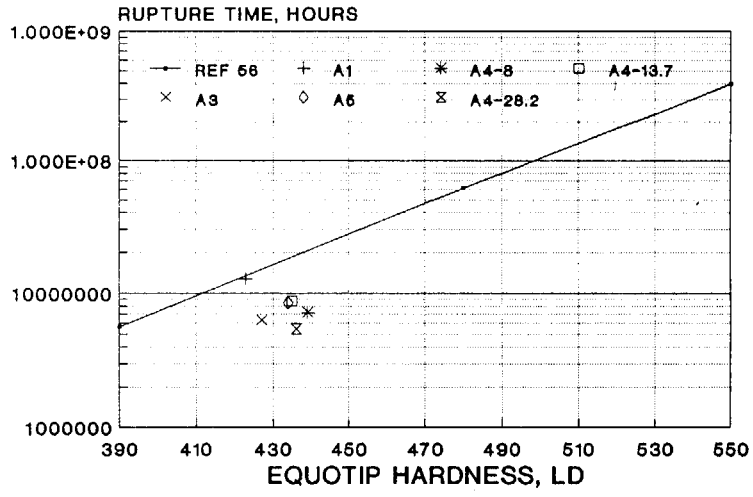

LMP prediction at 1005 degrees F

Figure 88
A1, A3, A4, & A5 Larson-Miller Parameter and Rupture Time Compared to Reference 56 Predictions

5.3.6 A2 Material Behavior

The A2 samples were intended to evaluate the effects of various exposures above the Ac_1 temperature on the microstructure of the material. Samples were exposed at 1450°F for 2, 25, 50, & 100 hours followed by air cooling. The 100 hour sample microstructure in Figure 36 consists of nearly completely degraded pearlite, bainite, and grain boundary precipitates. There is almost no intragranular precipitation visible.

The process of microstructural change as a function of time may be seen in a series of figures found in Appendix 1. At 2 hours (Figures 1-13 & 1-14), the structure consists of pearlite, a modest amount of bainite, and intragranular precipitates. After 25 hours (Figures 1-15 & 1-16), the pearlite has degraded somewhat, the intragranular precipitates have coarsened, and the amount of bainite has increased. For some reason the bainite etched much more strongly in the 2 and 100 hour samples than it did in the 25 and 50 hour samples.

The 50 hour samples (Figures 1-17 & 1-18) and 100 hour samples (Figures 1-19 & 1-18) carry on the above trends. The amount of bainite appears to have saturated at 50 hours, although the pearlite degradation and disappearance of the intragranular precipitates appear to advance over this time period. Whatever the changes, they have no meaningful effect on the measured material hardness (Table V).

Table IV and Figure 89 show that the changes between the 25 and 100 hour exposures have no effect on the stress-rupture properties as measured by the Larson Miller parameter and the extrapolated rupture time at 1005°F. What is affected is the stress-rupture behavior as a function of original hardness as back calculated using the thermal aging model. Since the material has clearly been partially austenitized, the failure of a model that envisages a gradual degradation in properties

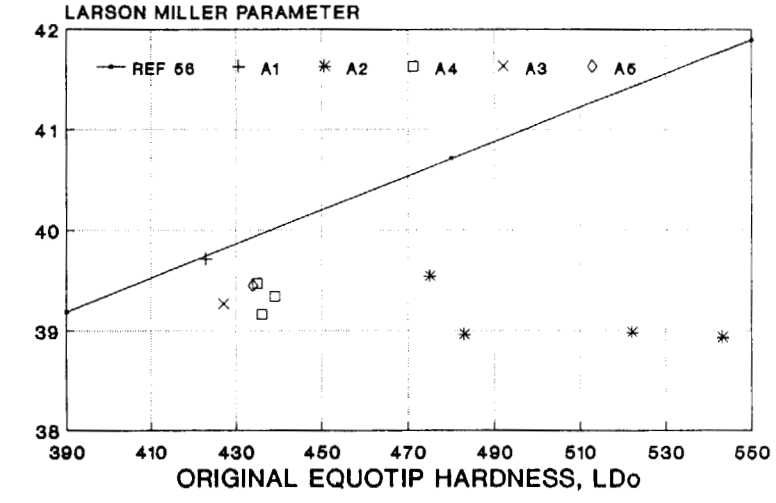

Ref 56 curve is calculated relationship

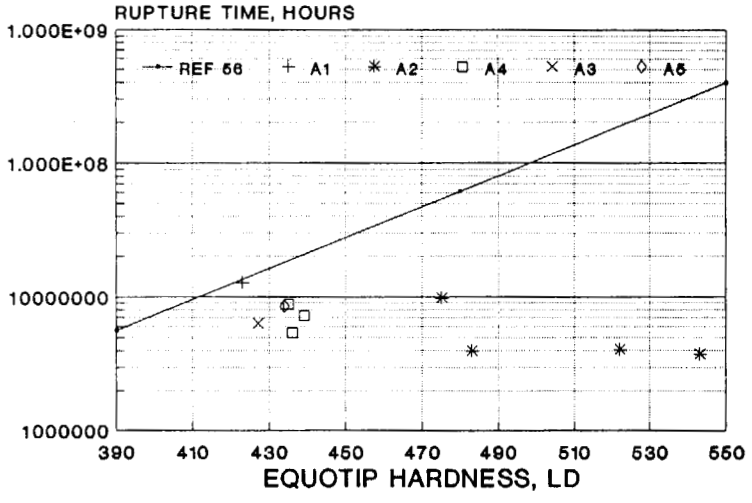

LMP prediction at 1005 degrees F

Figure 89
All A Conditions Larson-Miller Parameter and Rupture Time Compared to Reference 56 Predictions

due to tempering is not surprising.

As a matter of interest, the volume fraction of prior austenite was estimated by using the Leco Analyzer to evaluate a polished and etched sample of the A2-100 material. The average of multiple runs was 25.3 volume percent. This value was used, along with a calculated value for Ac_3, to estimate the Ac_1 temperature for the A1 material. The Ac_3 value was calculated using the following formula from Ref. 66 and the chemistry data from Table II.

$$Ac_3 = 910 - 203\sqrt{C} + 44.7Si + 31.5Mo - 11Cr + 700P - 30Mn$$

$$Ac_3 = 910 - 203\sqrt{0.1} + 44.7(0.41) + 31.5(1.03) - 11(2.14) + 700(0.011) - 30(0.55)$$

$$Ac_3 = 1588^{\circ}F$$

Assuming that the α-ferrite single phase region is small, and that the Ac_3 line is straight, the fraction of austenite, f_γ, is given by:

$$f_\gamma = 1 - [(Ac_3 - T)/(Ac_3 - Ac_1)]$$

$$f_\gamma = 1 - [(1588^{\circ}F - 1450^{\circ}F)/(1588^{\circ}F - Ac_1)] = 0.253$$

$$Ac_1 = 1403^{\circ}F \ (762^{\circ}C)$$

This value is within the range (750°C to 780°C) reported by Wada and Eldis[58].

Since the value of Ac_1 for a specific heat of 2 1/4Cr-1Mo steel depends both on the chemistry and the prior heat treatment, the effects of temperature exposures above about 1400°F are somewhat unpredictable.

5.4 Variation in Matrix Alloy Content

The variation in matrix or solid solution alloy content was presented in Table VI. Because of the amount of sample taken there was some uncertainty in the weight of material dissolved. This required that the data be normalized. This diminishes the level of confidence, but some observations may still be made.

There appear to be only three distinctive conditions here. A1 and A2-100 differ from each other and the other three conditions, A3, A5, and A4-28.2. These latter conditions are effectively the same in terms of matrix alloy content. Some data from Ref. 78 indicates that the A1 material has a normal proportion of Cr and Mo in the carbide phase for material exposed at lower temperatures (maximum exposure for the Ref. 78 material was 1200°F).

Ratio of Cr, Mo, in Carbides to Total Contents

Sample	Cr	Mo	LMP_{age}
A1	0.23	0.57	20.68
Ref. 78 (NT)	0.2	0.63	20.29
Ref. 78 (A)	0.2	0.63	21.32

NT stands for normalized and tempered, while A stands for annealed.

The matrix Mn contents seem to be unaffected by heat treatment and are effectively the same as the total. This must be due to the preferential incorporation of the other alloying elements in the precipitates, since there are equivalent isomorphous manganese carbides to M_3C, M_7C_3, and $M_{23}C_6$. This was also observed in Ref. 78.

The chromium and molybdenum contents of the A1 material matrix are the lowest of all samples. It is apparent from these data and the metallography that there is a very high degree of precipitation present. According to Baker &

Nutting, the anticipated precipitates at this juncture are Fe_3C, Mo_2C, and Cr_7C_3[37]. Many of the latter two precipitates would be expected to be unresolved by the optical microscope.

The A2-100 material appears to have released a great deal of the chromium and molybdenum back to the matrix. On this basis, one would expect more effective interactive solid solution hardening. However, the stress-rupture properties of this sample are the worst of all those tested. This outcome can be rationalized as follows. The prolonged austenization treatment has led to the dissolution of most precipitates (except possibly the very stable but non-strengthening M_6C), and the segregation of much of the carbon into the 25% austenite that was formed. Upon air cooling, the austenitic regions have transformed to bainite, tying up the carbon that would otherwise be in the matrix.

5.5 Effects of Hot Bending Heat Treatment on Welded Material

5.5.1 Welded Material Heat Treatment

The weld containing samples tested in the axial direction were designated B1, B3, B5, and B6 depending on whether they were in the as-received condition or had received subsequent heat treatment. B1, B3, & B5 received the same heat treatments as their A series counterparts. B6 samples were made prior to the realization that the Ac_1 temperature was being significantly exceeded by exposure at 1450°F. These samples consisted of B5 material prestrained 2% at 1450°F, followed by air cooling. This produced specimens which have equivalent stress-rupture properties to the B1 material, but which have no obvious applicability to the hot bent field material, which was slowly cooled after hot bending.

5.5.2 Nature of Weld Region

The base metal of the original A and B materials is identical for all practical purposes. While the B samples do have two different base metals, the weaker of these will determine the mechanical behavior in axial tests. The weaker B material here has almost exactly the same hardness as the A material. Metallographic examination found no apparent differences in any of the base metals after identical heat treatments.

As mentioned earlier, the weakest region in a welded joint is the coarse grained bainitic heat affected zone. This was the observed failure location in the weld containing samples tested here. If the base metal properties of geometrically identical weld containing and non-weld containing samples are the same, differences in mechanical behavior can logically be ascribed to the properties of this weld heat affected zone.

The diminished properties of the coarse grained heat affected zone in a circumferential butt weld will have no effect on the stress-rupture properties of a pressurized pipe in service that is free of additional non-pressure stresses. This zone is not oriented to respond to the hoop stress, which is twice the nominal axial stress. It is oriented to respond to the axial stress, but the stress reduction far outweighs the reduced metal properties, and the pipe will ultimately fail due to the hoop stress in the base metal.

It should be noted that this assessment is not valid where non-pressure stresses are important. These may occur at header welds, and where pipe hangars are not properly adjusted. The former locations are especially troublesome.

5.5.3 Effect of Heat Affected Zone Dimensions

Under many circumstances, it is not expected that the

diminished properties of the coarse grained heat affected zone will be fully reflected in the axial properties of the material. This portion of the heat affected zone is about 0.04" wide at most, and is more typically 0.02" wide.

Since the material is fully contiguous with the adjacent (and stronger) weld and base metals, it is very likely that a reinforcement effect will occur. Such an effect in ductile materials is well documented, and is important over much greater dimensions than that of a weld heat affected zone[67]. This reinforcement effect should be more important for short term tests where specimen plasticity is high. As test times increase and plasticity tends toward lower values load transfer should decrease and the effect of adjacent material should diminish.

5.5.4 Measured Effect of Weld Heat Affected Zone

The effect of this weld heat affected zone is seen in Figure 90, where the diminished properties of the B samples relative to the A samples are shown in terms of rupture times during the stress-rupture tests. The Larson Miller parameter variations and the calculated times to rupture at 1005°F were shown in Figures 20 and 22.

The comparative effects on the 1005°F rupture times for the three different heat treatments are: $t_{B1}/t_{A1} = 0.61$, $t_{B3}/t_{A3} = 0.70$, and $t_{B5}/t_{A5} = 0.58$. When the scatter in the Larson Miller parameters from which these rupture times were calculated is considered, one could argue that these ratios may actually be the same.

This variation between welded and non-welded material is comparable to that for the various heat treatments in these two series. These data were presented earlier, the time to rupture ratios being: $t_{A3}/t_{A1} = 0.49$, $t_{A5}/t_{A1} = 0.66$, $t_{B3}/t_{B1} = 0.56$, and $t_{B5}/t_{B1} = .62$.

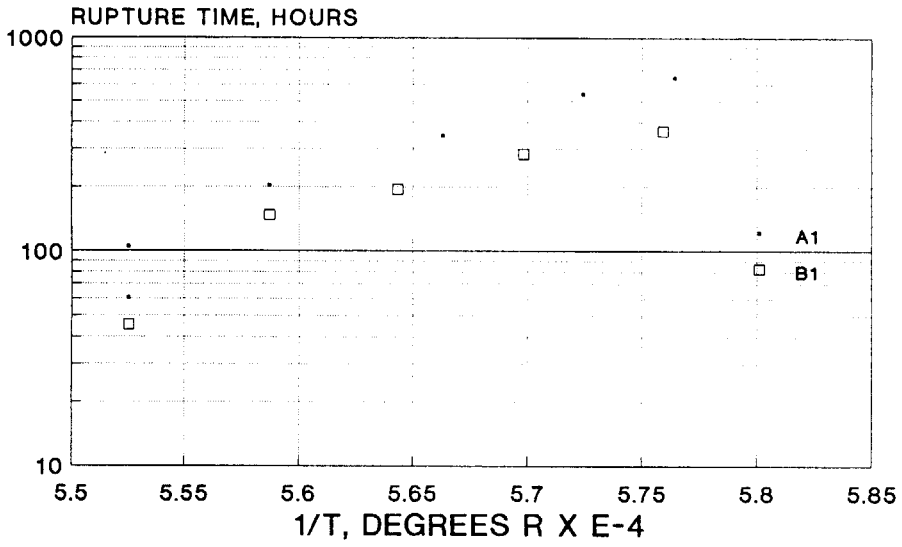

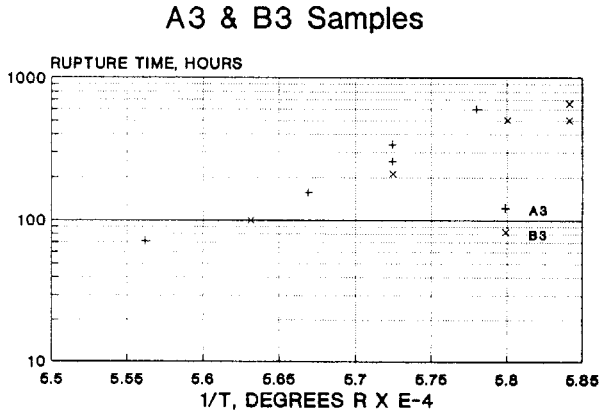

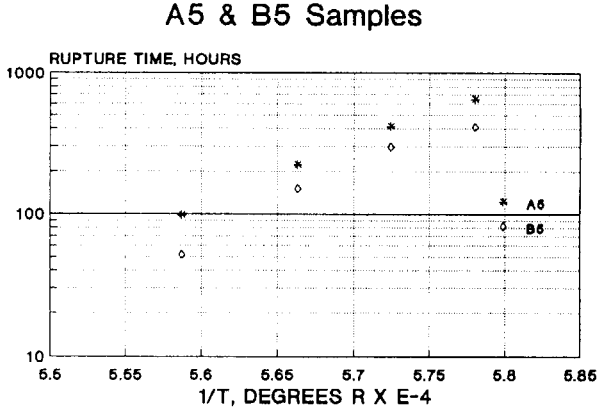

Figure 90 Comparative Rupture Times for A & B Samples

In fact, if one examines the entire spectrum of rupture times determined during this project, from the relatively short term stress-rupture tests to those projected for 1005°F, the greatest variation is a factor of four. Considering the wide range of heat treatments used this is somewhat less than one might expect. As noted earlier, a comparable thermal exposure of 1Cr-0.5Mo led to a tenfold decrease in time to rupture[57].

5.6 Effect of Test Time on the Larson Miller Parameter

If there is a tendency for the Larson Miller parameter to overpredict rupture times it might be visible in a plot of LMP vs time to rupture. As time to rupture increases, the LMP should decrease below the average to that point. This tendency might be exacerbated in the case of the welded samples by a loss of reinforcement effect with increasing time as well.

Figure 91 shows that a decrease in the LMP with increasing time to rupture does not really occur for the A1, A3, and A5 materials. Nor does it occur for the A2 and A4 sample sets. However, the test times are relatively short. Also, the LMP for the A1 series has been shown to match the model from Ref. 56. This implies that the LMP determined from the present test series is consistent with that derived from the longer term tests embedded in the model.

In the case of the weld containing B1 sample, Figure 91 shows that the Larson Miller parameter diminishes with increasing test time. Such an occurrence is also possible in the case of B5, but more data points would be needed to be certain. This behavior is not indicated in the case of B3, where the LMP variation has no trend, and is most likely due to scatter.

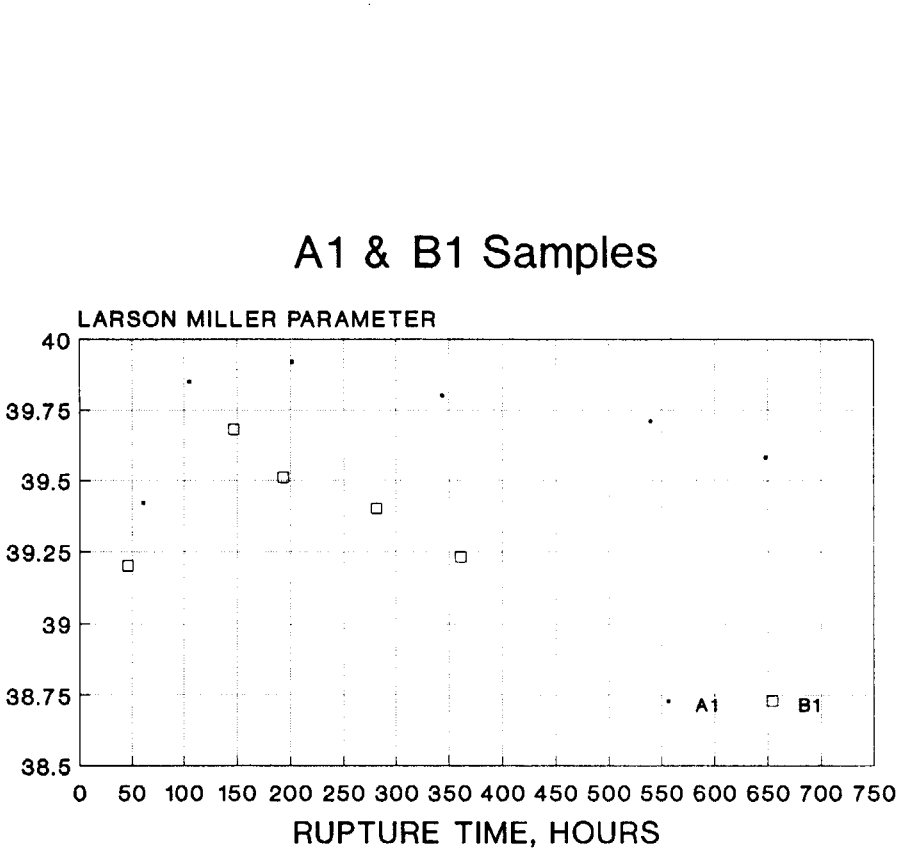

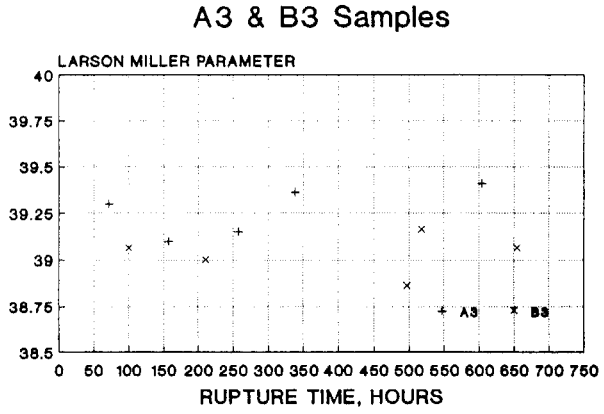

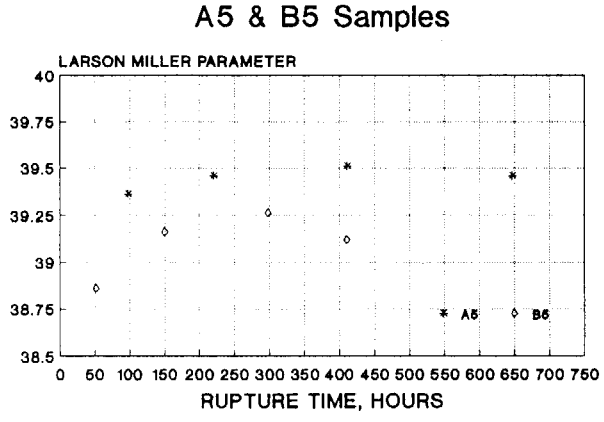

Figure 91 Comparative LMP vs Time Values for A & B Samples

The projected rupture times at 1005°F of the B1 and B5 materials relative to their unwelded A counterparts are essentially equivalent. The B3 material is somewhat better (rupture time ratio of 0.7 vs 0.61 and 0.58), but is absolutely the worst, as is the A3 material in its series.

These results are consistent with the hypothesis that there is a reinforcement effect of the surrounding metal on the coarse grained heat affected zone in the B1 and B5 materials. This effect diminishes with increasing test time because local plasticity and load transfer diminish. The absence of this effect in the case of the B3 material can be ascribed to the greater level of damage inflicted on the base metal as compared to the weld metal. In this picture, the weld heat affected zone becomes less of a liability, and the performances of the welded and unwelded samples are closer.

5.7 Correlations with Field Material

The anomalous surface condition sometimes exhibited by this piping was presented in 5.6 above. Based on the field replicas, this condition appears to have occurred in Field Areas 1 & 2, and Field Area 3C (3 left of weld). The partially decarburized structure has a lower than expected hardness for the recorded thermal exposure. Field Areas 3A & 3B (3 right of weld) have a more normal structure and a slightly higher hardness. Field Area 4 is equivalent to Field Area 3 in terms of location and heat treatment, but has a higher (and more expected) hardness on both sides of the weld.

Field Areas 5 and 6 to the right of the weld are the other end of the pipe section in 3 and 4 left. The hardness here is uniformly higher, and is equivalent to that found for the A3 and A5 samples. The weld hardnesses are the same as for the B3 and B5 plates. This suggests that the heat

treatment did extend through this weld, since the B1 weld hardness was much higher.

What are the possible effects of this anomalous surface condition? It depends on the evaluation method(s) used. In the present case the results of the stress-rupture testing of identically exposed samples adequately quantifies the stress-rupture life of the piping. The field hardness measurements and replication are confirmatory only, and served to point out that in some cases a previously observed anomalous surface condition was present here also.

It would be possible to conduct a Ref. 56 evaluation on the basis of hardness (converted to tensile strength) alone. For a previously uncharacterized 2 1/4Cr-1Mo pipe material with a known service thermal history below Ac_1, an erroneous reduction in measured hardness due to surface decarburization would lead to a low estimate of both the original pipe strength and the original time to rupture. This could lead to early retirement of the pipe, but would be conservative from a safety standpoint.

Material that had seen thermal exposures above Ac_1 followed by an air cool (similar to sample series A2 and A4) could have a higher than expected hardness that would extrapolate back to a higher original strength. This would be translated into an erroneously long rupture life. In the case of material with a history similar to the longer term A2 samples the effect could be substantial.

Both of these errors can be recognized by replication of the area chosen for hardness testing. Material whose surface condition or thermal exposure deviates substantially from that of normally service aged 2 1/4Cr-1Mo is recognizable. Even if the effects of the unusual conditions cannot necessarily be quantitatively assessed, at least the inapplicability of the Ref. 56 evaluation would be clear.

Caution should be used in assessing cavity formation in long service material if the rest of the microstructure is unusual. The effect of a decarburized surface on cavity formation is especially unclear. If cavities tend to nucleate on grain boundary carbides the cavity formation rate in a decarburized volume might be greatly reduced. The normal cavity formation rate for 2 1/4Cr-1Mo is very high relative to iron[23], and probably, to a lesser extent, somewhat higher than carbon steel.

The actual cavity population for a carbon steel near a long term stress-rupture failure was shown in Figures 13 & 14. The same number fraction for 2 1/4Cr-1Mo material would indicate that many years of service remained (Figure 11). However, a much higher population of cavities could be lying just below the decarburized layer in the normal base metal.

It is, therefore, recommended that Ref. 56 life predictions using hardness as a tensile strength surrogate be accompanied by replication metallography to assess the applicability of the model. That is, the microstructure should be roughly typical of that expected for a 2 1/4Cr-1Mo at that stage of life. Substantial deviations should prompt additional evaluation by other means, such as stress-rupture testing of miniature samples.

It should be appreciated that 2 1/4Cr-1Mo is a relatively forgiving material, and has been shown to maintain acceptable stress-rupture properties over a reasonable spectrum of heat treatments. Deviation from the Ref. 56 model only become serious for the A2 series exposures, because of the higher hardnesses produced by these heat treatments. For the A1 material removed from service at 13,000 hours, the model prediction is accurate.

5.8 Directions for Future Research

The model adapted from Ref. 56 does not make accurate predictions for material that has been partially austenitized, or for material that has been subjected to a higher temperature exposure after extended exposure at normal service temperatures. The partitioning of the elements between the matrix and the various carbide phases appears to have something to do with this. In the former case, it causes substantial variations in the Ac_1 temperature, leading to unexpected transformations. In the latter case, the release of carbon and molybdenum back to the matrix probably leads to an increased hardness that is not reflected in proportionally improved stress-rupture properties.

Can the model be altered to accommodate and reflect this behavior? Perhaps, but the model is empirical and apparently accurate when used under the conditions appropriate to its derivation. The addition of equally empirical ad hoc adjustments which complicate the model does not seem worth the effort. Any deviation from the newly defined precursor conditions would again lead to inaccurate predictions.

The model is better used as an indicator of when the thermal exposure seen produces only a simple tempering effect. If a thermal exposure is applied to a 2 1/4Cr-1Mo steel, and the tensile strength change and stress-rupture life change are in conformance with the model, then the predictability of similar exposures for similar material is confirmed.

The primary problem here is that heat treating this material outside of its normal exposure regime is an uncontrolled process, especially if it has been in normal high temperature service for even a relatively short period of time. Many of the thermal exposures, including one of the ones used in the field, degraded the material properties more

than a normal weldment. Yet the weld had to be done in accordance with a properly qualified procedure by a qualified welder. The essential variables were defined for the process, and the results of the procedure were subject to a variety of tests.

A thermal exposure that does not clearly result in the behavior predicted by the model should be qualified before use in the field. The process should be controlled so that qualification in a shop setting will confidently predict the results in the field. Field hardness testing and replication should be used to define the pre and post conditions of the field material for comparison to shop test results. These techniques are adequately developed as they stand, if allowance is made for possibly anomalous surface microstructure.

What are the essential variables for a thermal exposure of this nature? Temperature, time, heating rate, cooling rate, degree of strain, and extent of prior service exposure are all probably important. What variations are allowable before a process must be re-examined? These are the issues that I believe should be the subject of future work.

This investigation could be made using the same basic techniques and tests used in this thesis. It would be a forward looking project without need to specifically test conditions used in a prior field operation. Emphasis could be placed on identifying the essential variables and their sensitivity. Material with no service, short service, and long service should be included in the program if available. Otherwise, material that was thermally aged in the laboratory could be used to check for trends.

6.0 SUMMARY AND CONCLUSIONS

6.1 Two 1450°F heat treatments duplicating field heat treatments used during hot bending of service exposed 2 1/4Cr-1Mo piping, were shown to degrade the stress-rupture properties of the piping. Estimated time to rupture at 1005°F was reduced to half that of the original material in the worst case.

6.2 The intent of selecting 1450°F as the hot bending temperature was apparently to allow a 30°F margin between the bending thermal exposure and the ASME B31.1 Power Piping Code published Ac_1 temperature of 1480°F. This value is wrong. Reliable literature sources and this project indicate that the Ac_1 temperature is between 750 and 780°C (1382 - 1436°F) depending on material chemistry and prior heat treatment.

6.3 The presence of a weld heat affect zone degrades the stress-rupture performance (expressed as estimated rupture time at 1005°F) of 2 1/4Cr-1Mo piping by a factor of 0.6 to 0.7. The actual properties of the weld heat affected zone are probably much worse than this, but the reinforcement effect of adjacent base metal masks this in these relatively short time tests. The presence of the heat affected zone would be expected to be more deleterious in longer tests or in service where the plasticity of the material and resultant load transfer decreases.

6.4 Extended thermal exposures above the Ac_1 temperature (1450°F) degrade the stress-rupture properties of 2 1/4Cr-1Mo material. Exposure followed by air cooling appeared to

saturate after about 25 hours. At this point the performance relative to the as-removed material was reduced to about 0.3 in terms of predicted rupture time at 1005°F.

6.5 Extended exposure just below the Ac_1 temperature (1375°F) also degraded the stress-rupture properties, but to a lesser extent. For an exposure parametrically equivalent to 10 hours at 1450°F the predicted rupture time at 1005°F was reduced to a factor of 0.42 relative to the original material.

6.6 Viswanathan, et al, recently proposed a life prediction model for 2 1/4Cr-1Mo in Ref. 56. This model uses a thermal aging formula to back calculate original tensile strength from current tensile strength, which is estimated from hardness measurements. The calculated original tensile strength is then correlated with original life expectations. The model was extremely accurate for the A1 material, which had been exposed at 1005°F for 13,000 hours. The accuracy decreased for the other heat treatments, being especially poor for the long term above Ac_1 exposures (A2 material).

6.7 The validity of determining life prediction parameters by field characterization has possible pitfalls. These may be avoided by performing a complete characterization consisting of hardness measurements and microstructural replication. The former is needed to develop the predictive data, and the latter is needed to insure that the measured substrate has the expected structure for the nominal thermal exposure.

7.0 REFERENCES

1. Frost, H. J., & Ashby, M. F., Deformation Mechanism Maps, Pergamon Press, 1982.

2. Ashby, M. F., "A First Report on Deformation Mechanism Maps", Acta Met., 20, 1972, 887.

3. Mohamed, F. A., & Langdon, T. G., "Deformation Maps Based on Grain Size", Met Trans., 5, 1974, 2339.

4. Langdon, T. G., & Mohamed, F. A., "A New Type of Deformation Map for High Temperature Creep", Mat. Sci. & Eng., 32, 1978, 103.

5. Luthy, H., White, R. A., & Sherby, O. D., "Grain Boundary Sliding and Deformation Mechanism Maps", Mat. Sci. & Eng., 39, 1979, 211.

6. Ashby, M. F., et al, "Fracture-Mechanism Maps and Their Construction for F. C. C. Metals and Alloys", Acta Met., 27, 1979, 699.

7. Dieter, G. E., Mechanical Metallurgy, 432-470, McGraw-Hill, 1986.

8. Raj, R., & Ashby, M. F., "On Grain Boundary Sliding and Diffusional Creep", Met. Trans., 2, 1971, 1113.

9. Mohamed, F. A., & Ginter, T. J., "On the Nature and Origin of Harper-Dorn Creep", Acta Met., 30, 1982, 1869.

10. Wu, M. Y., & Sherby, Oleg D., "Unification of Harper-Dorn and Power Law Creep Through Consideration of Internal Stress", Acta Met., 32, 1984, 1561.

11. Ahlquist, C. N., Gasca-Neri, R., & Nix, W. D., " A Phenomenological Theory of Steady State Creep Based on Average Internal and Effective Stresses", Acta Met., 18, 1970, 663.

12. Viswanathan, R., Damage Mechanisms and Life Assessment of High Temperature Components, ASM International, 1989.

13. Cane, B. J. & Greenwood, G. W., "The Nucleation and

Growth of Cavities in Iron during Deformation at Elevated Temperatures", Metal Science, 9, 1975, 55.

14. Dyson, B. F., "Constraints on Diffusional Cavity Growth Rates", Metal Science, 10, 1976, 349.

15. Speight, M. V. & Beere, W., "Vacancy Potential and Void Growth on Grain Boundaries", Metal Science, 9, 1975, 190.

16. Needleman, A., & Rice, J. R., "Plastic Creep Flow Effects in the Diffusive Cavitation of Grain Boundaries", Acta Met., 28, 1980, 1315.

17. Raj, R. & Ghosh, A. K., "Stress Rupture", Met. Trans. A, 12A, 1981, 1291.

18. Nix, W. D., "Introduction to the Viewpoint Set on Creep Cavitation", Scripta Met., 17, 1983, 1.

19. Argon, A. S., "Intergranular Cavitation in Creeping Alloys", Scripta Met., 17, 1983, 5.

20. Beere, W., "Models of Creep Cavitation and Their Interrelationships", Scripta Met., 17, 1983, 13.

21. Chen, I., "Mechanism of Cavity Growth in Creep", Scripta Met., 17, 1983, 17.

22. Goods, S. H., "Mechanisms of Intergranular Cavity Nucleation and Growth during Creep", Scripta Met., 17, 1983,

23. Dyson, B. F., "Continuous Cavity Nucleation and Creep Fracture", Scripta Met., 17, 1983, 31.

24. Raj, R., "Correlations Between Cavitation, Creep and Dilation for Multiaxial Loading", Acta Met., 31, 1983, 29.

25. Monkman, F. C., & Grant, N. J., "An Empirical Relationship Between Rupture Life and Minimum Creep Rate", Proceedings ASTM, 56, 1956, 593.

26. Fields, R. J., Weerasooriya, T., & Ashby, M. F., "Fracture Mechanisms in Pure Iron, Two Austenitic Steels, and One Ferritic Steel", Met. Trans. A, 11A, 1980, 333.

27. Baird, J. D., & Jamieson, A., "Creep Strength of Some Synthesized Iron Alloys Containing Manganese, Molybdenum, and Chromium", Journal of the Iron and Steel Institute, 210, 1972, 847.

28. Hopkin, L. M. T., "Influence of Nitrogen on the Creep Resistance of High-Purity Iron and Iron Alloys", Journal of the Iron and Steel Institute, 203, 1965, 583.

29. Baird, J. D., & Jamieson, A., "High-Temperature Tensile Properties of Some Synthesized Iron Alloys Containing Molybdenum and Chromium", Journal of the Iron and Steel Institute, 210, 1972, 841.

30. Baird, J. D., "Precipitation of Nitrides in Iron-Manganese-Nitrogen Alloys", Journal of the Iron and Steel Institute, 204, 1966, 1122.

31. Argent, B. B., et al, "Creep of Ferritic Steels", Journal of the Iron and Steel Institute, 208, 1970, 830.

32. Ridal, K. A., & Quarrell, A. G., "The Molybdenum Carbide Transformation in Ferritic Steels", Journal of the Iron and Steel Institute, 200, 1962, 359.

33. Woodhead, J. H., & Quarrell, A. G., "Role of Carbides in Low Alloy Creep Resisting Steels", Journal of the Iron and Steel Institute., 203, 1965, 605.

34. Godden, M. J., & Beech, J. "The M_2C-M_6C Transformation in Steels Containing Molybdenum", Journal of the Iron and Steel Institute, 208, 1970, 168.

35. Ridal, K. A., & Quarrell, A. G., "Effect of Creep Deformation upon Carbide Transformations in Ferritic Alloy Steels", Journal of the Iron and Steel Institute, 200, 1962, 366.

36. Ridal, K. A., & Quarrell, A. G., "Effect of Creep Deformation at 700°C on the Transformation of Molybdenum Carbides in a Ferritic Steel", Journal of the Iron and Steel Institute, 195, 1960, 307.

37. Baker, R. G., & Nutting, J., "The Tempering of 2 1/4 Cr - 1 Mo Steel after Quenching and Normalizing", Journal of the Iron and Steel Institute, 192, 1959, 257.

38. Abdel-Latif, A. M. et al., "Analysis of Carbides Formed During Accelerated Aging of 2.25Cr-1Mo Steel", Metal Science, 16, 1982, 90.

39. Stevens, R. A., & Lonsdale, D., "Isolation and Quantification by X-Ray Diffraction of Carbide Phases in 2 1/4Cr-1Mo Steel", J. of Mat. Sci., 20, 1985, 3631.

40. Narita, K., et al, "The Isolation and Determination of Carbides in Steel", Trans. Iron and Steel Institute of Japan, 16, 1976, 168.

41. Viswanathan, R., "Effect of Stress and Temperature on the Creep and Rupture Behavior of a 1.25 Pct Chromium - 0.5 Pct Molybdenum Steel", Met. Trans. A, 8A, 1977, 877.

42. Williams, K. R., & Cane, B. J., "Creep Behavior of 1/2Cr1/2Mo1/4V Steel at Engineering Stresses", Mat. Sci. & Eng., 38, 1979, 199.

43. Cane, B. J. & Middleton, C. J., "Intergranular Creep Cavity Formation in Low Alloy Bainitic Steels", Metal Science, 15, 1981, 295.

44. Cane, B. J., "Interrelationship Between Creep Deformation and Creep Rupture in 2 1/4Cr-1Mo Steel", Metal Science, 13, 1979, 287.

45. Viswanathan, R., "Strength and Ductility of 2 1/4Cr-1Mo Steels in Creep at Elevated Temperatures", Metals Technology, 11, 1974, 284.

46. Lonsdale, D. & Flewitt, P. E. J., "Damage Accumulation and Microstructural Changes Occurring During the Creep of a 2 1/4Cr-1Mo Steel", Mat. Sci. & Eng., 39, 1979, 217.

47. Grant, N. J., "Stress Rupture Testing", High Temperature Properties of Metals, ASM, 1951, 41.

48. Grant, N. J., & Bucklin, A. G., "On the Extrapolation of Short Time Stress Rupture Data", Transactions ASM, 42, 1950, 720.

49. Clauss, F. J., "An Examination of High Temperature Stress Rupture Correlating Parameters", Proceedings ASTM, 60, 1960, 905.

50. Manson, S. S., & Ensign, C. R., "A Quarter Century of Progress in the Development of Correlation and Extrapolation Methods for Creep Rupture Data", Journal of Eng. Mat. & Tech., 101, 1979, 317.

51. Manson, S. S., "Time-Temperature Parameters - A Re-evaluation and Some New Approaches", Time-Temperature Parameters for Creep-Rupture Analysis, ASM Publication No. D8-100, ASM, 1968, 1.

52. Goldhoff, R. M., & Hahn, G. J., "Correlation and Extrapolation of Creep-Rupture Data of Several Steels and Superalloys Using Time-Temperature Parameters", Time-Temperature Parameters for Creep-Rupture Analysis, ASM Publication No. D8-100, ASM, 1968, 199.

53. Wilson, D. J., & Freeman, J. W., "Larson-Miller and Manson-Haferd Parametric Extrapolation of Rupture Data for TYpe 304 (18Cr-8Ni), Grade 22 (2 1/4Cr-1Mo), and Grade 11 (1 1/4Cr-1/2Mo-3/4Si) Steels", Time-Temperature Parameters for Creep-Rupture Analysis, ASM Publication No. D8-100, ASM, 1968, 247.

54. Leyda, W. E., & Rowe, J. P., "Application of the Larson-Miller Parameter Method for Evaluation of Data in the Interests of Materials Acceptance", Time-Temperature Parameters for Creep-Rupture Analysis, ASM Publication No. D8-100, ASM, 1968, 311.

55. Williams, W. L., & Ferrara, R. J., "Investigation of the Creep-Rupture Properties of Grades 11, 12 and 22 Cr-Mo Steels", Time-Temperature Parameters for Creep-Rupture Analysis, ASM Publication No. D8-100, ASM, 1968, 331.

56. Viswanathan, R., et al, "Life Assessment of Superheater/Reheater Tubes in Fossil Boilers", ASME J. of Press. Vessel Tech., 116, 1994, 1.

57. Hart, R. V., "Assessment of Remaining Creep Life Using Accelerated Stress Rupture Tests", Metals Technology, 13, 1976, 1.

58. Wada, T. & Eldis, G. T., "Transformation Characteristics of 2 1/4Cr-1Mo Steel", Application of 2 1/4Cr-1Mo Steel for Thick-Wall Pressure Vessels, ASTM STP 755, 1982, p 343.

59. Wada, T., & Biss, V. A., "Restoration of Elevated Temperature Tensile Strength in 2.25Cr-1Mo Steel", Met. Trans. A, 14A, 1983, 845.

60. Cane, B. J., & Williams, J. A., "Remaining Life Prediction of High Temperature Materials", Int. Mat. Reviews, 32, 1987, 241.

61. Bolton, C. J. et al., "Metallographic Methods of Determining Residual Creep Life", Mat. Sci. & Eng., 46, 1980, 231.

62. Cane, B. J., Aplin, P. F., & Brear, J. M., "A Mechanistic Approach to Remnant Creep Life Assessment of Low Alloy Ferritic Components Based on Hardness Measurements", Proceedings of the 1985 Pressure Vessels and Piping Conference, PVP-Vol.98-1, ASME, 1985, 147.

63. Johnson, R. F., & Glen, J., "Some Problems in the Assessment of High-Temperature Properties for Engineering Purposes", Creep Strength in Steel and High-Temperature Alloys, The Metals Society, 1974, 37.

64. Murphy, M. C., & Branch, G. D., "Metallurgical Changes in 2.25CrMo Steels During Creep Rupture Test", Journal of the Iron & Steel Inst., 1971, 546.

65. Klueh, R. L., & Leitnaker, J. M., "An Analysis of the Decarburization and Aging Processes in 2 1/4Cr-1Mo Steel", Metallurgical Transactions A, 6A, 1975, 2089.

66. Andrews, K. W., "Empirical Formulae for the Calculation of Some Transformation Temperatures", Journal of the Iron and Steel Institute, 203, 1965, 721.

67. Kurtz, R. J., et al, "Steam Generator Tube Integrity Program/Steam Generator Group Project, Final Project Summary Report", Prepared for the U. S. Nuclear Regulatory Commission by Pacific Northwest Laboratory, NUREG/CR-5117, PNL-6446, May, 1990, Sections 1.0 & 2.0.

68. Tipler, H. R., & Hopkins, B. E., "The Creep Cavitation of Commercial and High Purity Cr-Mo-V Steels", Metal Science, 10, 1976, 47.

69. Franzoni, U., et al, "Scanning Auger Investigation on Creep Embrittled 2 1/4Cr-1Mo Steel", Scripta Met., 15, 1981, 743.

70. Franzoni, U., et al, "Segregation Effects on Intergranular Creep Cavitation and Fracture Behavior in 2 1/4Cr-1Mo Steel", Scripta Met., 16, 1982, 1127.

71. Stevens, R. A., & Flewitt, P. E. J., "The Effect of Phosphorous on the Microstructure and Creep Properties of 2 1/4Cr-1Mo Steel", Acta Met., 34, 5, 1986, 849.

72. Lewandowski, J. J., " Effects of Impurity Segregation on Sustained Load Cracking of 2 1/4Cr-1Mo Steels-I. Crack Initiation"., Acta Met., 35, 3, 1987, 593.

73. Lewandowski, J. J., " Effects of Impurity Segregation and Test Environment on Sustained Load Cracking of 2 1/4Cr-1Mo Steels-II. Crack Propagation"., Acta Met., 35, 8, 1987, 2081.

74. Mise, S., & Miyoshi, E., "High Temperature Properties of Steel Tubing", A Supplement to the Sumitomo Search, Sumitomo Metal Industries, Ltd., 1973, 64-68.

APPENDIX 1

PRETEST METALLOGRAPHY

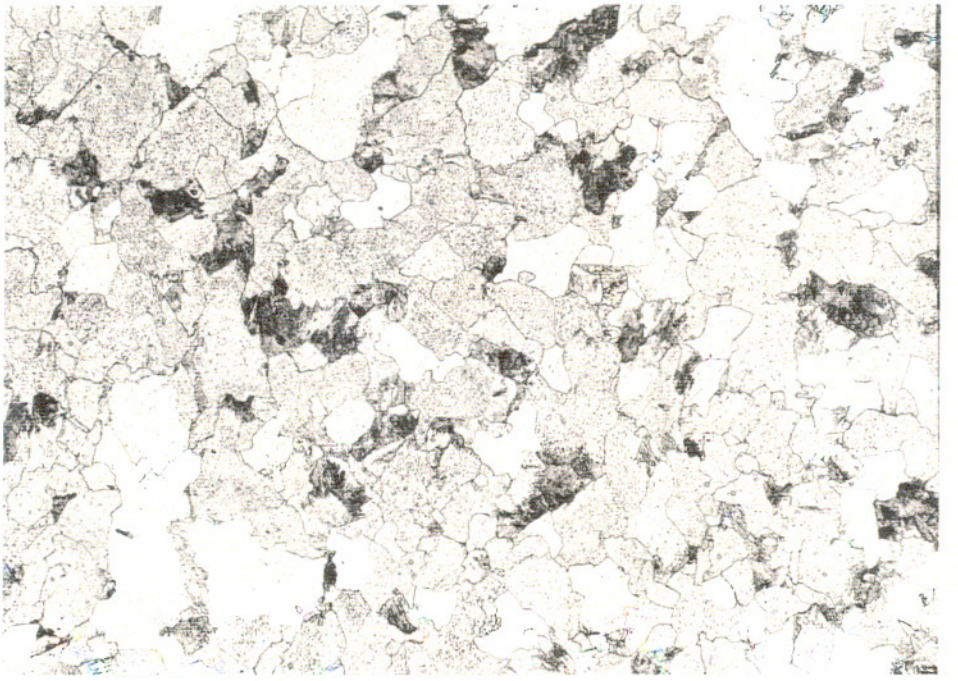

Figure 1-1
Sample A1 (As-removed) 100X Nital

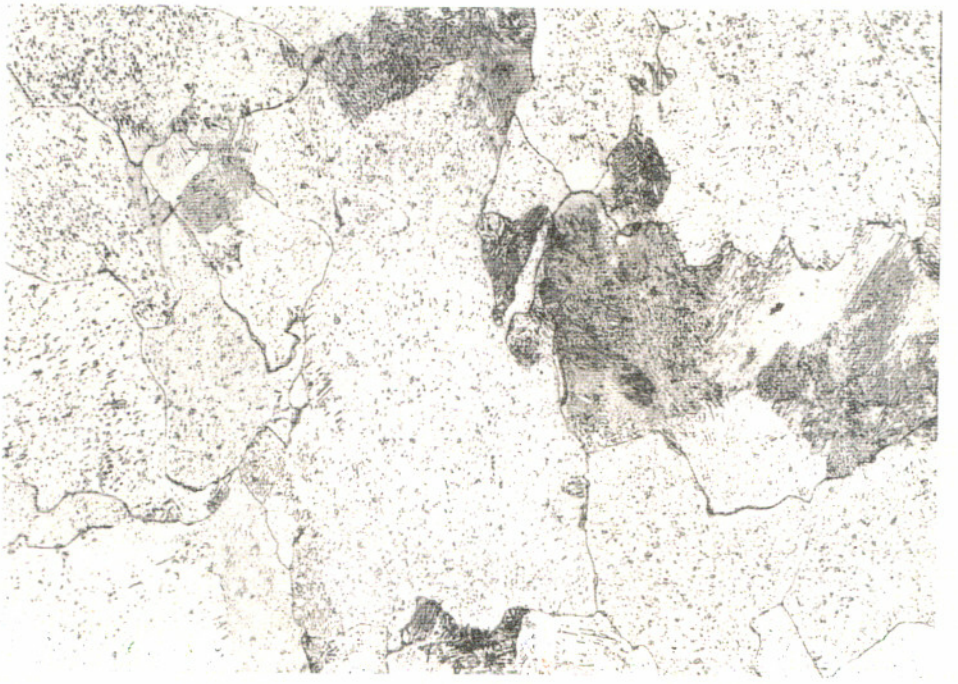

Figure 1-2
Sample A1 (As-removed) 400X Nital

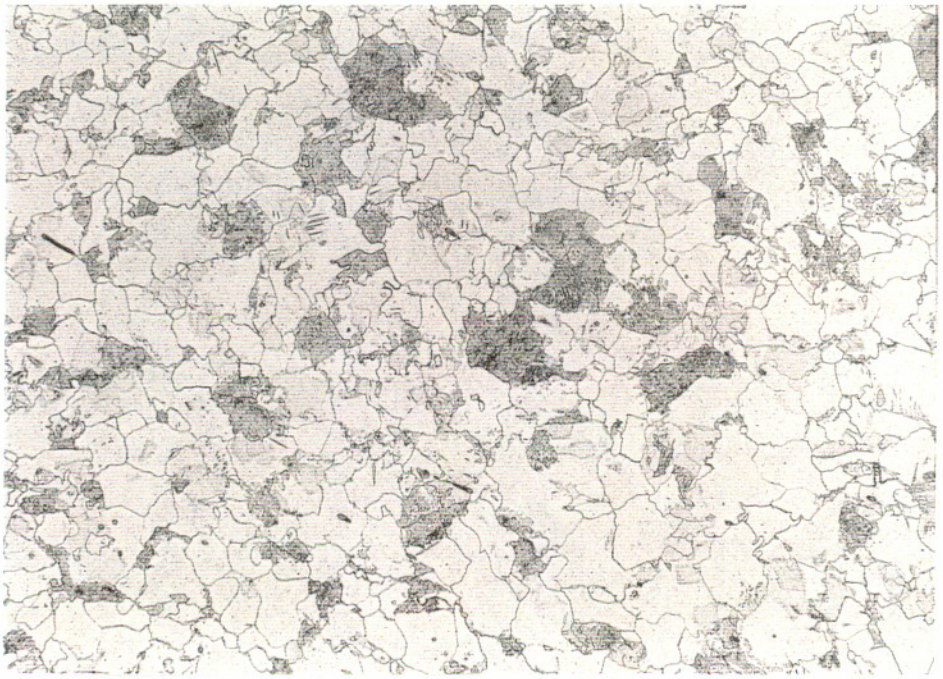

Figure 1-3
Sample A3 (As-removed + 5 hrs 1460°F + Furnace Cool)
100X Nital

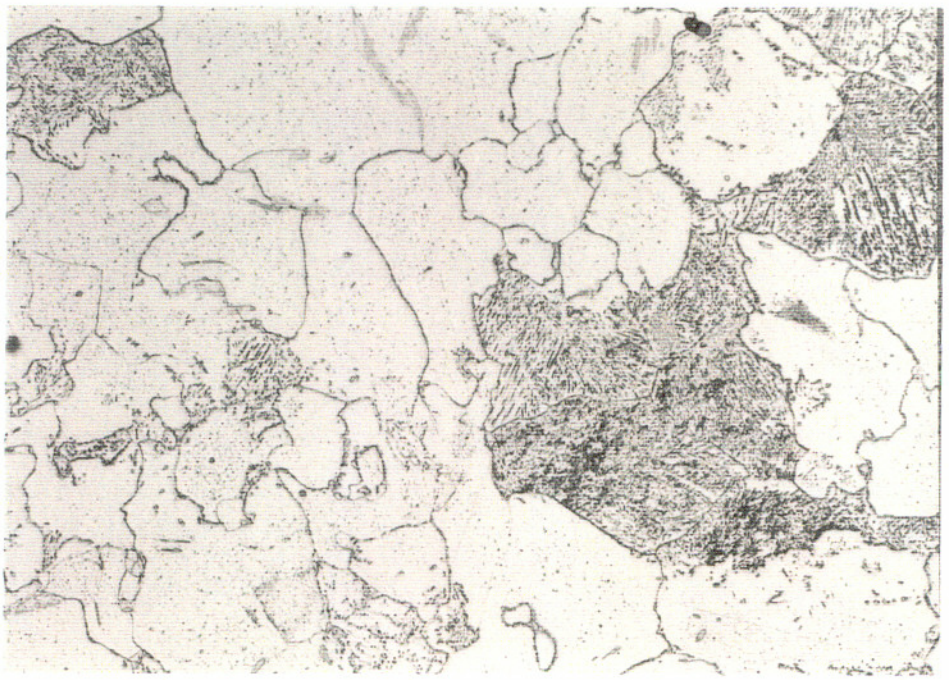

Figure 1-4
Sample A3 (As-removed + 5 hrs 1460°F + Furnace Cool)
400X Nital

Figure 1-5
Sample A5 (As-removed + 10 hrs 1460°F + Furnace Cool)
100X Nital

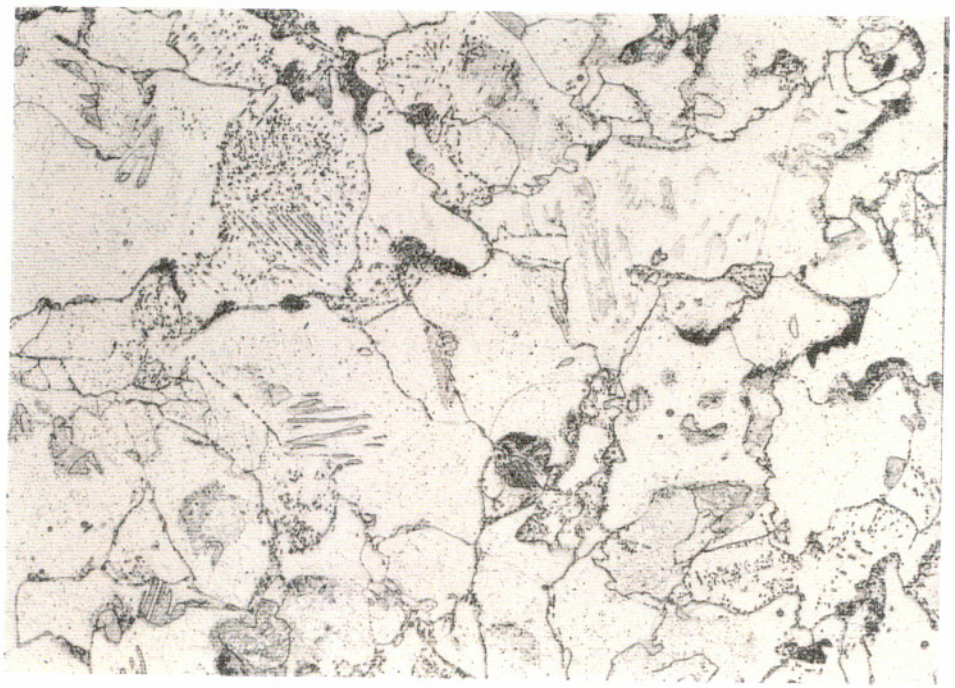

Figure 1-6
Sample A5 (As-removed + 10 hrs 1460°F + Furnace Cool)
400X Nital

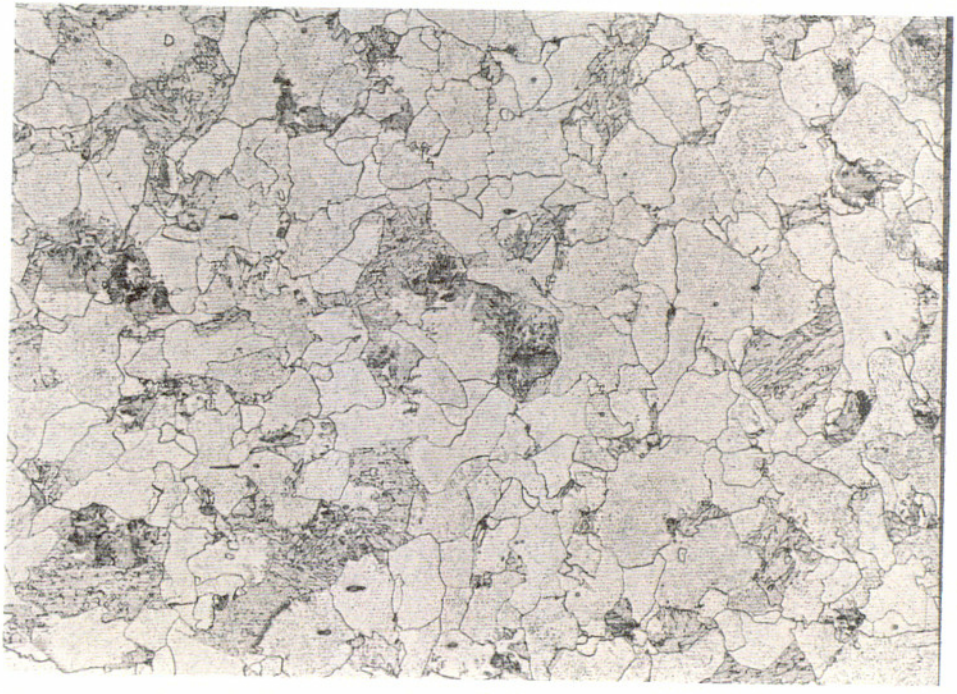

Figure 1-7
Sample A4-8 (As-removed + 8 hrs 1375°F + Air Cool)
100X Nital

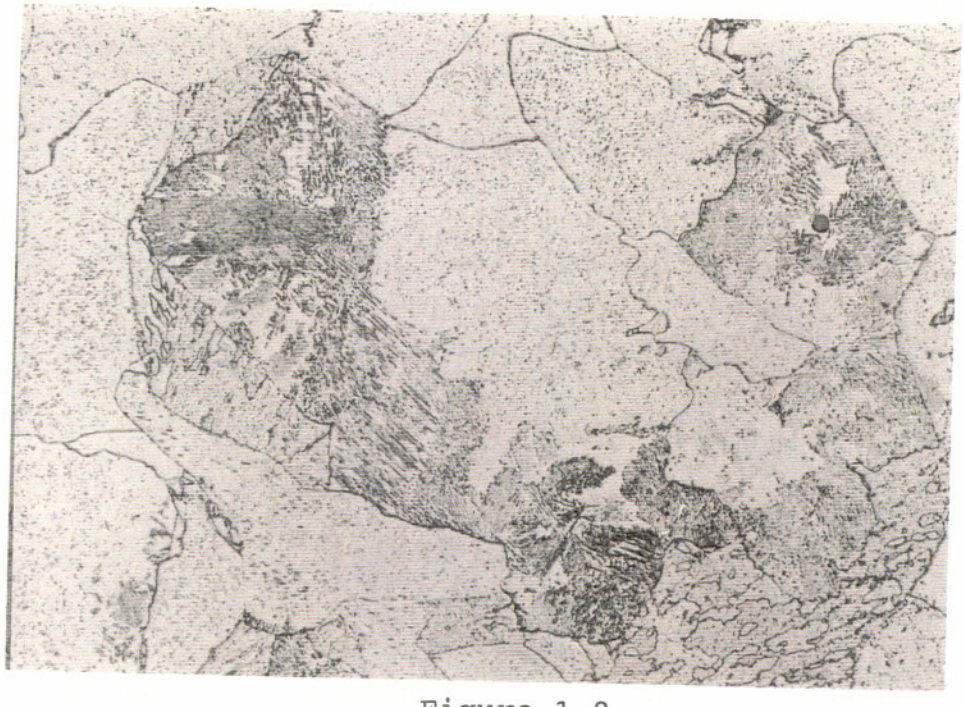

Figure 1-8
Sample A4-8 (As-removed + 8 hrs 1375°F + Air Cool)
400X Nital

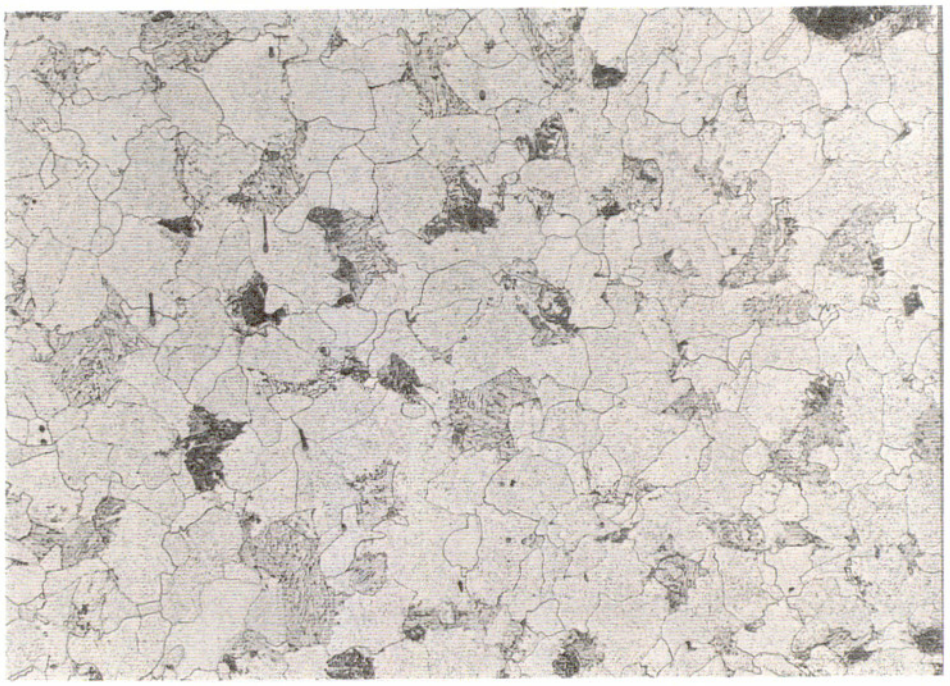

Figure 1-9
Sample A4-13.7 (As-removed + 13.7 hrs 1375°F + Air Cool)
100X Nital

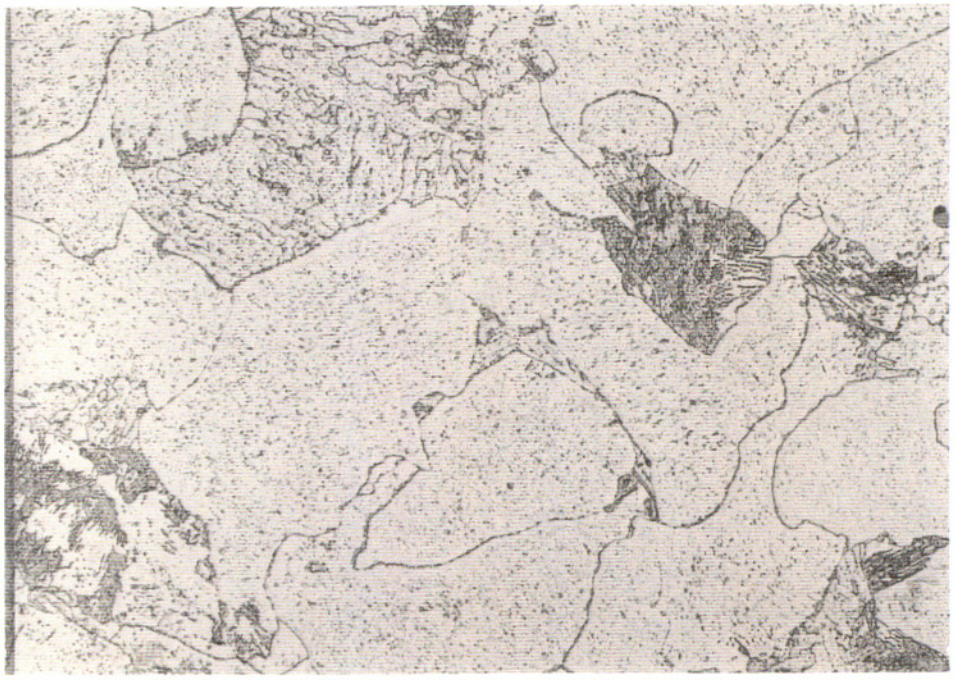

Figure 1-10
Sample A4-13.7 (As-removed + 13.7 hrs 1375°F + Air Cool)
400X Nital

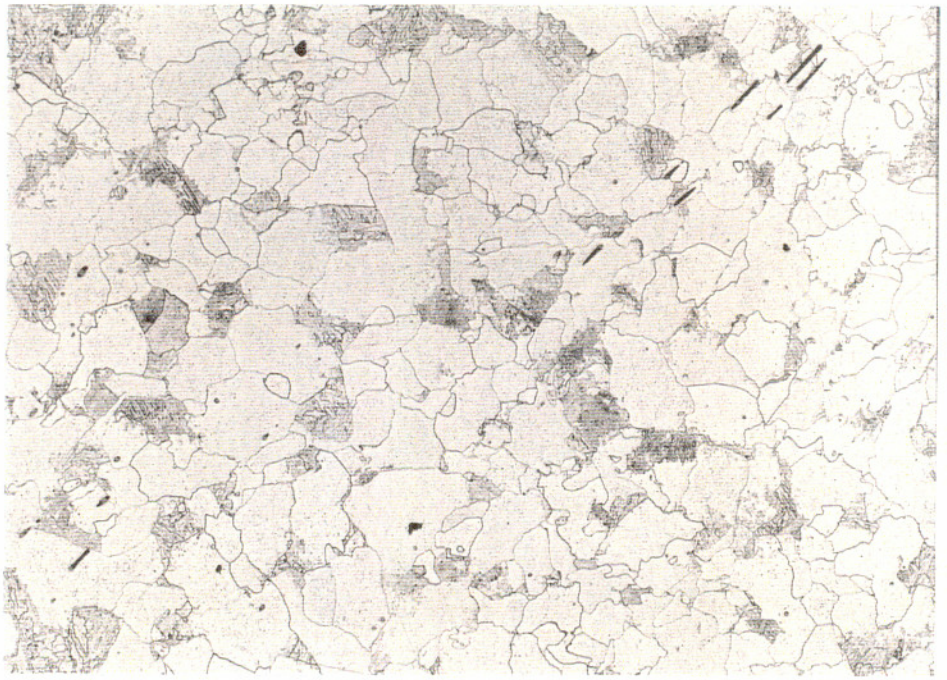

Figure 1-11
Sample A4-28.2 (As-removed + hrs 1375°F + Air Cool)
100X Nital

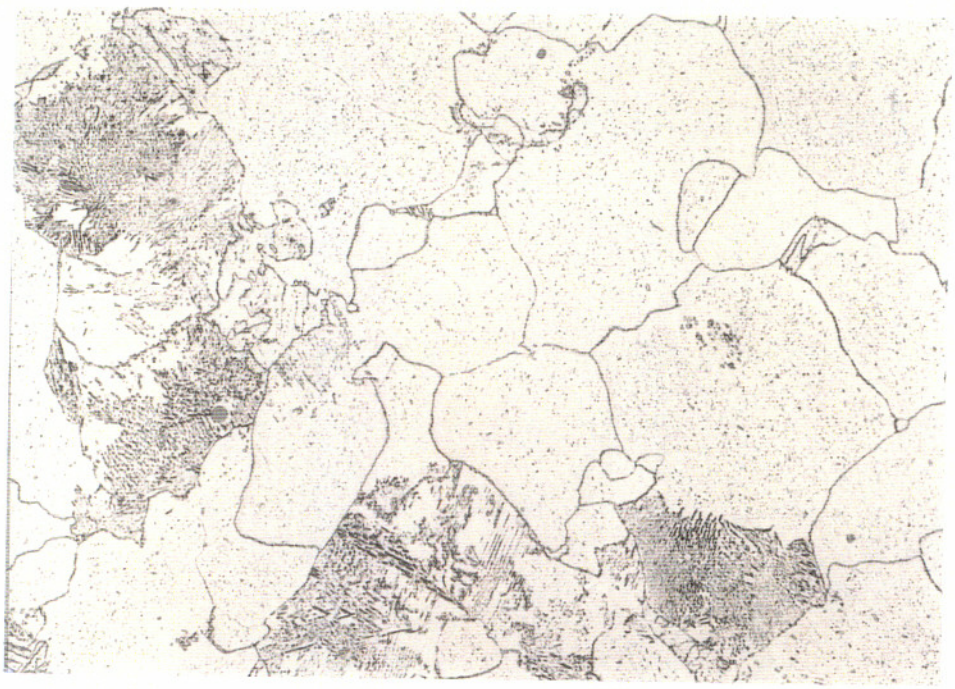

Figure 1-12
Sample A4-28.2 (As-removed + 28.2 hrs 1375°F + Air Cool)
400X Nital

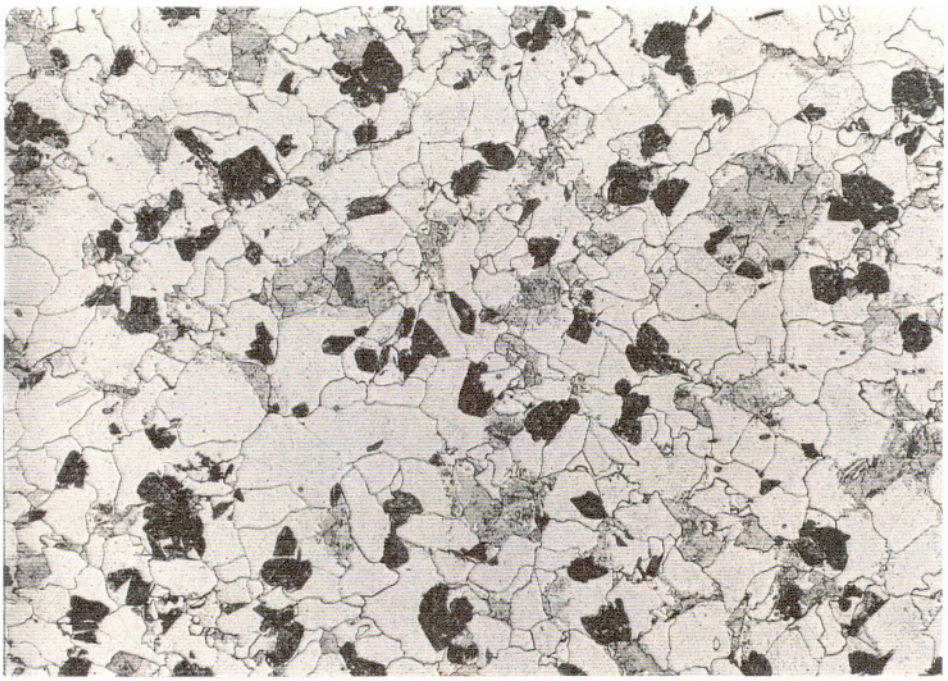

Figure 1-13
Sample A2-2 (As-removed + 2 hrs 1450°F + Air Cool)
100X Nital

Figure 1-14
Sample A2-2 (As-removed + 2 hrs 1450°F + Air Cool)
400X Nital

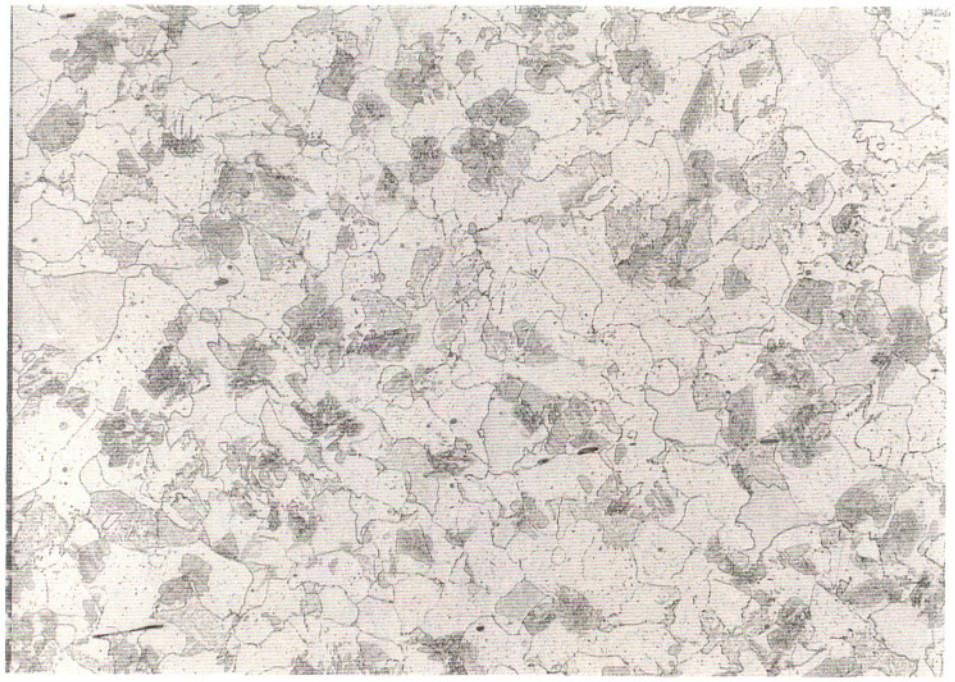

Figure 1-15
Sample A2-25 (As-removed + 25 hrs 1450°F + Air Cool)
100X Nital

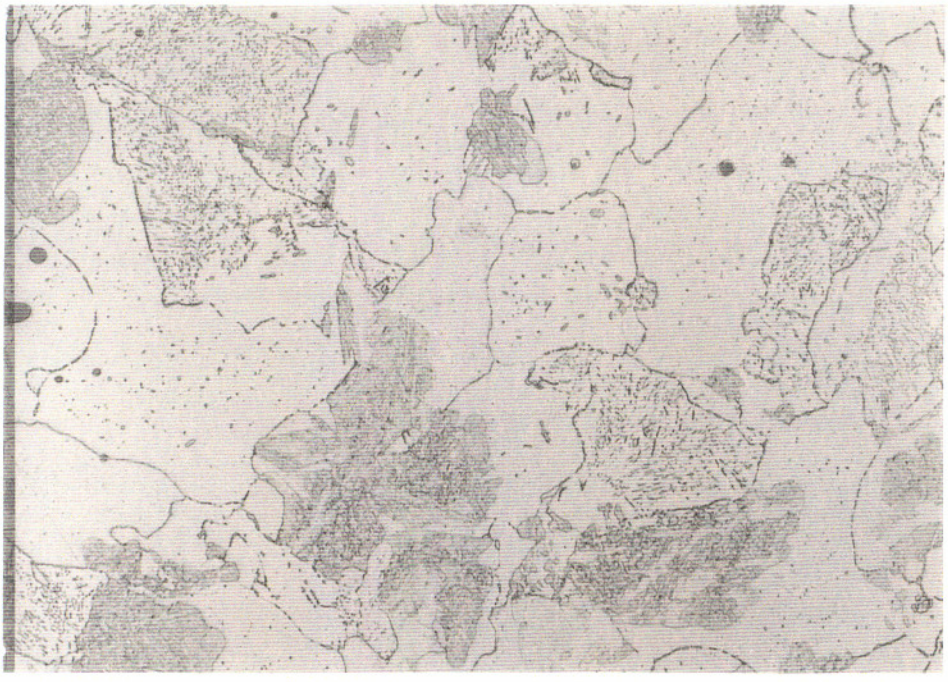

Figure 1-16
Sample A2-25 (As-removed + 25 hrs 1450°F + Air Cool)
400X Nital

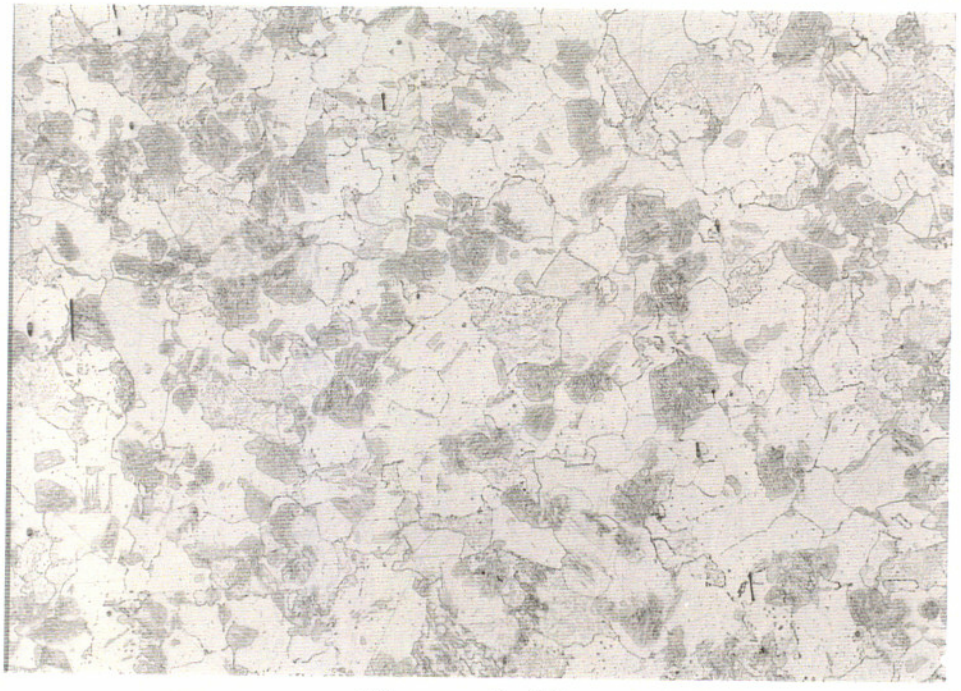

Figure 1-17
Sample A2-50 (As-removed + hrs 1450°F + Air Cool)
100X Nital

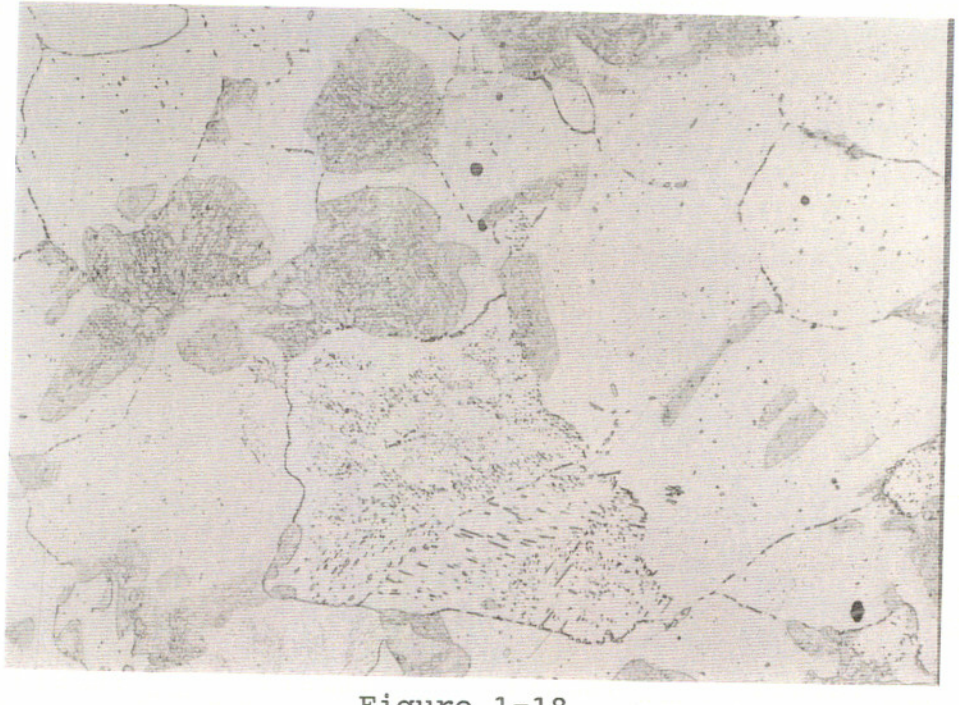

Figure 1-18
Sample A2-50 (As-removed + hrs 1450°F + Air Cool)
400X Nital

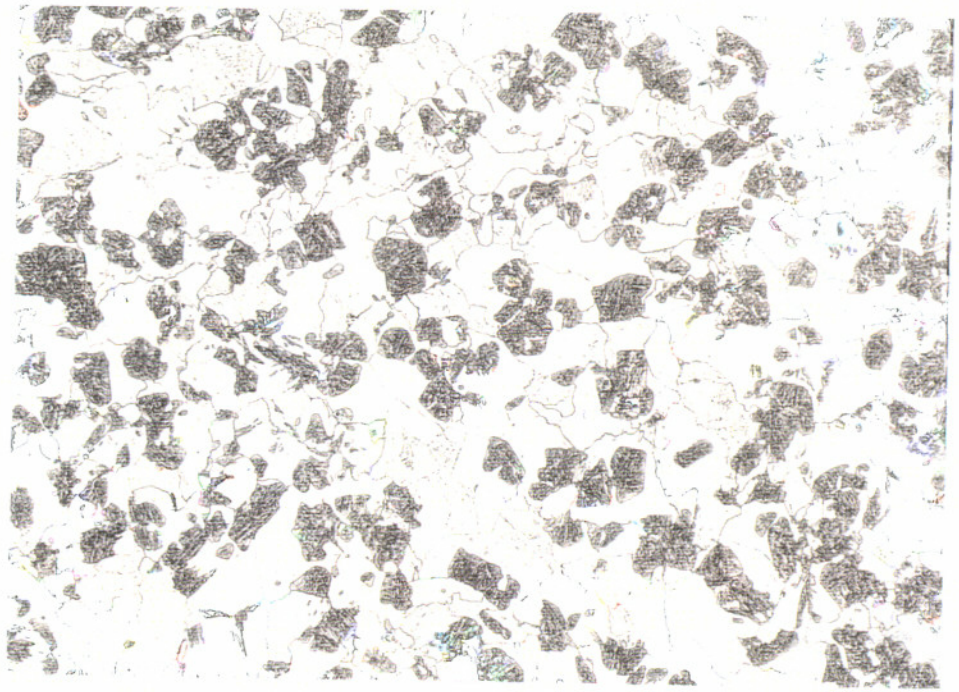

Figure 1-19
Sample A2-100 (As-removed + 100 hrs 1450°F + Air Cool)
100X Nital

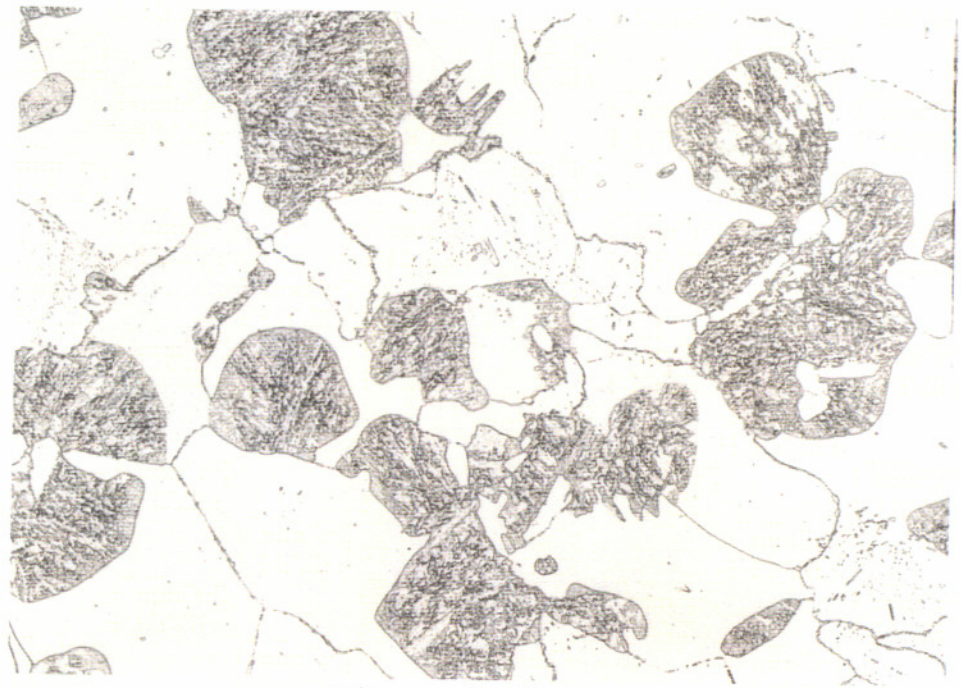

Figure 1-20
Sample A2-100 (As-removed + 100 hrs 1450°F + Air Cool)
400X Nital

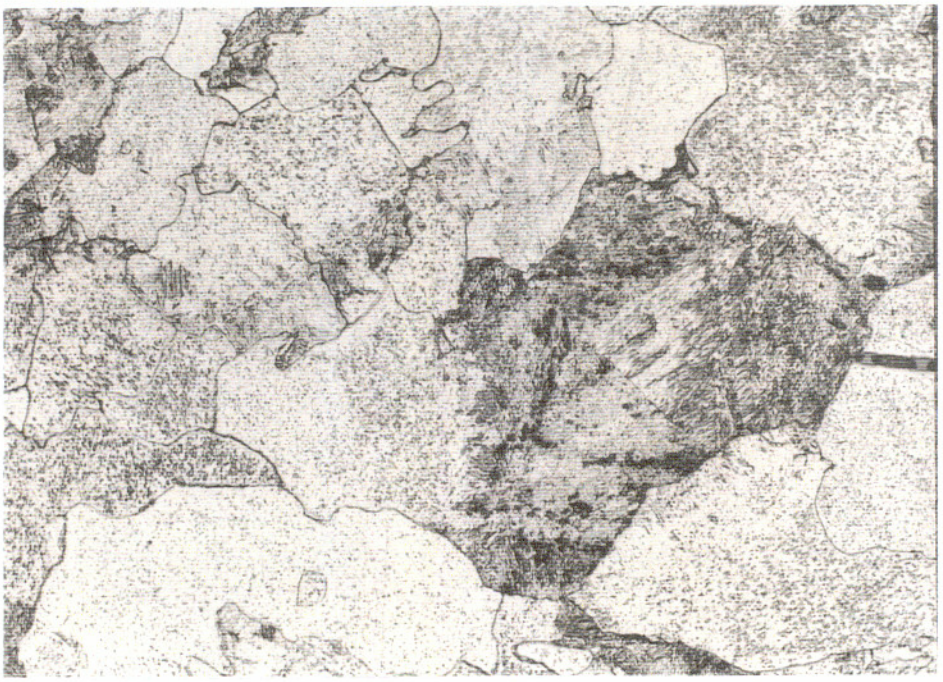

Figure 1-21
Sample B1 (As-removed) Base Metal
400X Nital

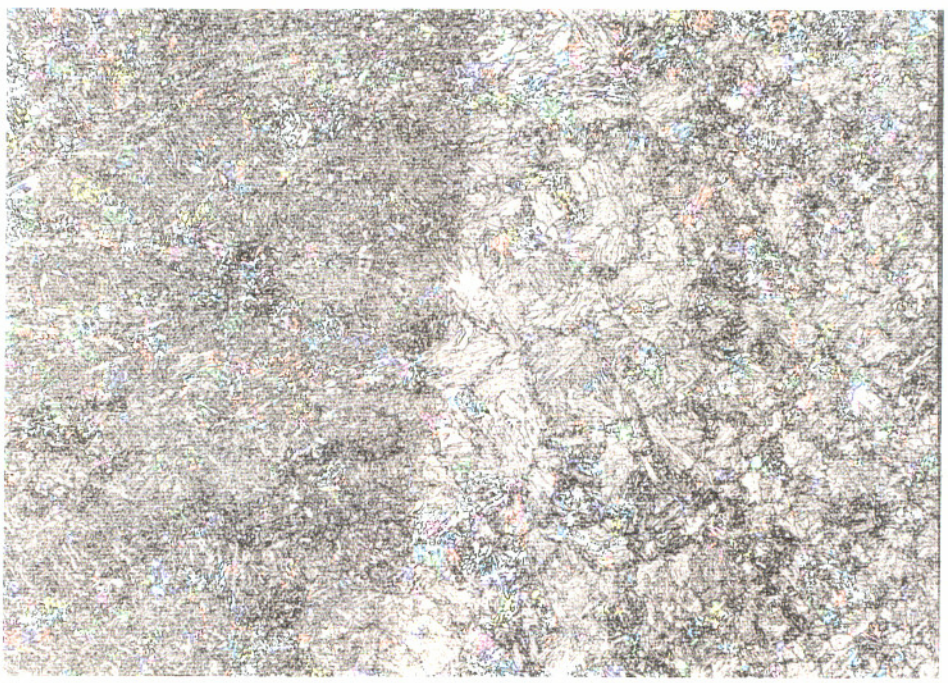

Figure 1-22
Sample B1 (As-removed) Weld HAZ
100X Nital

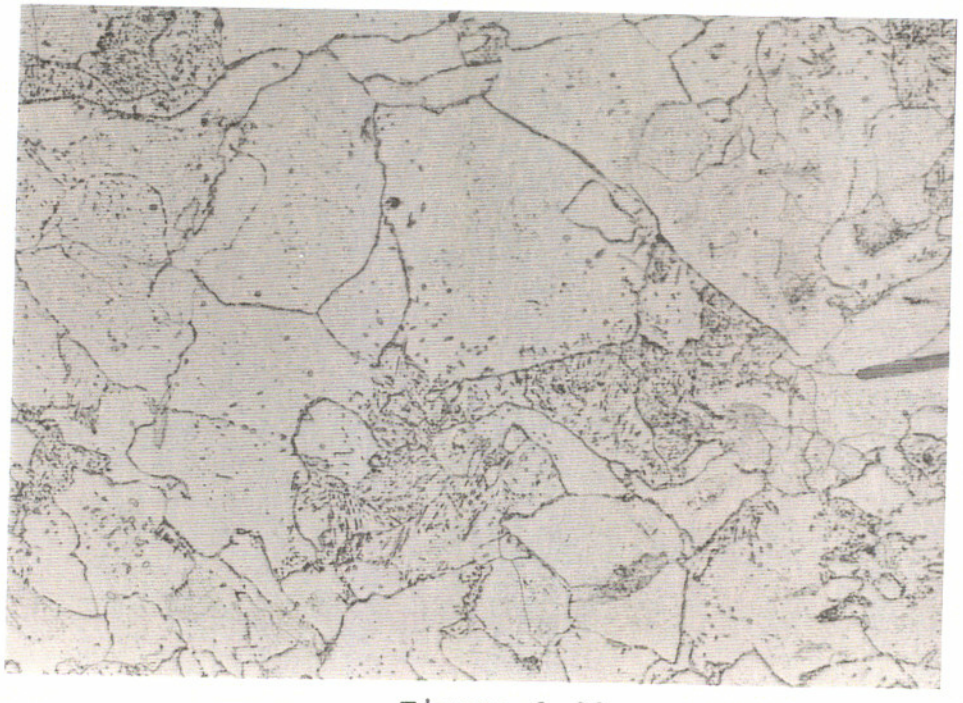

Figure 1-23
Sample B3 (As-removed + 5 hrs 1460°F + Furnace Cool)
Base Metal 400X Nital

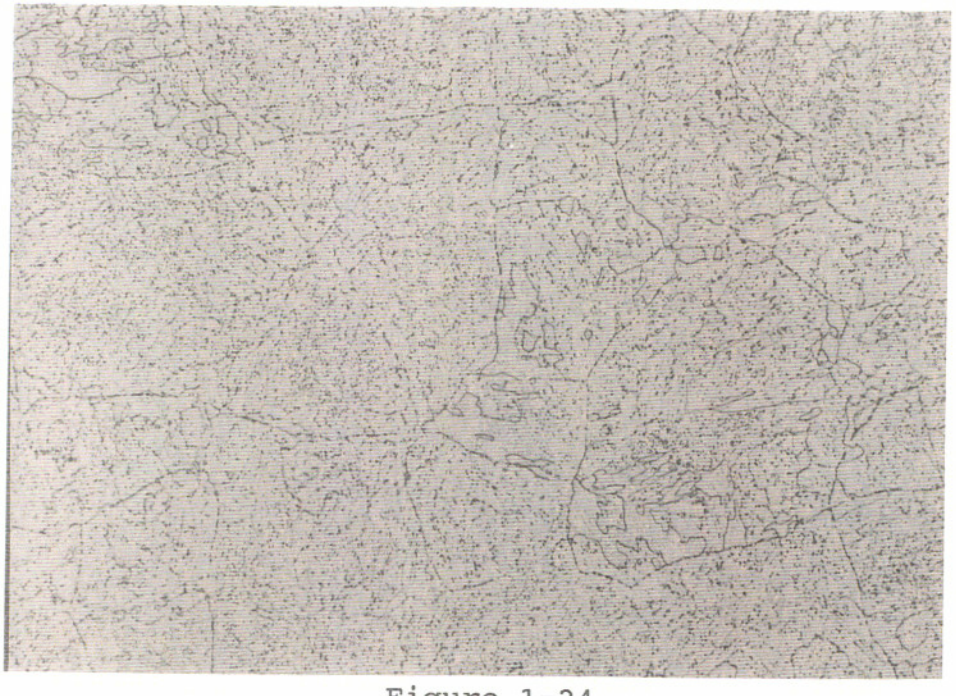

Figure 1-24
Sample B3 (As-removed + 5 hrs 1460°F + Furnace Cool)
Weld HAZ 400X Nital

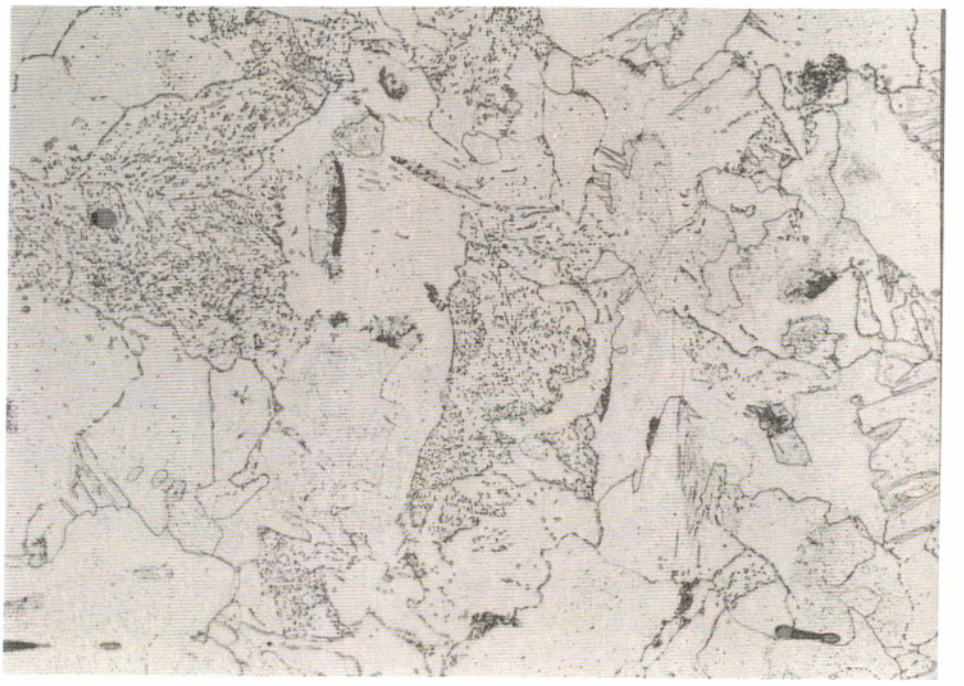

Figure 1-25
Sample B5 (As-removed + 10 hrs 1460°F + Furnace Cool)
Base Metal 400X Nital

Figure 1-26
Sample B5 (As-removed + 10 hrs 1460°F + Furnace Cool)
Weld HAZ 100X Nital

Figure 1-27
Sample B5 (As-removed + 10 hrs 1460°F + Furnace Cool)
Weld HAZ 400X Nital

APPENDIX 2

POST TEST METALLOGRAPHY

Note: Tables III and IV are repeated on the next two pages in order to provide additional context for the sample designations.

Table III
Main Series Stress-Rupture Test Results

	°F	°R	tact, hr.	tcorr, hr.	LMPcorr	
A1	(As-removed)					
	1350	1810	57.2	60.5	39.42	
	1350	1810	97.1	104.5	39.85	
	1306	1766	307.6	342.9	39.80	
	1330	1790	183.6	201.5	39.92	
	1287	1747	475.6	538.8	39.71	
	1275	1735	569.0	647.6	39.58	
					39.71	0.18
A3	(As-removed + 5 hrs 1460°F + Furnace Cool)					
	1287	1747	306.1	338.1	39.36	
	1287	1747	235.7	257.2	39.15	
	1304	1764	145.8	156.9	39.10	
	1338	1798	67.6	71.6	39.30	
	1270	1730	534.1	603.6	39.41	
					39.26	0.13
A5	(As-removed + 5 hrs 1460°F + Furnace Cool)					
	1270	1730	569.2	645.9	39.46	
	1330	1790	91.4	97.5	39.36	
	1287	1747	368.9	411.6	39.51	
	1306	1766	201.6	220.1	39.46	
					39.45	0.06
B1	(As-removed)					
	1279	1739	326.0	360.0	39.23	
	1295	1755	255.5	280.7	39.40	
	1313	1773	177.1	192.7	39.51	
	1330	1790	135.3	146.5	39.68	
	1350	1810	43.2	45.3	39.20	
					39.40	0.20
B3	(As-removed + 5 hrs 1460°F + Furnace Cool)					
	1252	1712	581.2	653.6	39.06	
	1252	1712	448.1	496.6	38.86	
	1316	1776	93.0	98.9	39.06	
	1287	1747	193.8	209.7	39.00	
	1264	1724	463.3	517.5	39.16	
					39.03	0.11
B5	(As-removed + 5 hrs 1460°F + Furnace Cool)					
	1287	1747	270.6	297.1	39.26	
	1270	1730	371.0	410.7	39.12	
	1330	1790	48.8	51.2	38.86	
	1306	1766	139.1	149.6	39.16	
					39.10	0.17
B6	(As-removed + 5 hrs 1460°F + Furnace Cool + Strained 1460°F+ Air Cool)					
	1287	1747	241.7	264.0	39.17	
	1306	1766	144.6	155.7	39.19	
	1325	1785	213.1	235.0	39.93	
	1260	1720	632.4	718.3	39.31	
					39.40	0.36

Table IV
A2 & A4 Stress-Rupture Test Results

T°F	T°R	tact, hr.	tcorr, hr.	LMPcorr	
A2-2 (As-removed + 2 hrs 1450°F + Air Cool)					
1330	1790	126.9	137.0	39.62	
1290	1750	316.6	350.8	39.45	
				39.54	0.12
A2-25 (As-removed + 25 hrs 1450°F + Air Cool)					
1330	1790	45.9	48.1	38.82	
1290	1750	199.2	216.0	39.09	
				38.96	0.19
A2-50 (As-removed + 50 hrs 1450°F + Air Cool)					
1330	1790	49.5	51.9	38.87	
1290	1750	202.4	219.6	39.10	
				38.98	0.16
A2-100 (As-removed + 100 hrs 1450°F + Air Cool)					
1330	1790	52.2	54.8	38.91	
1290	1750	168.1	181.1	38.95	
				38.93	0.03
A4-8 (As-removed + 8 hrs 1375°F + Air Cool)					
1330	1790	82.9	88.2	39.28	
1290	1750	301.0	332.7	39.41	
				39.34	0.09
A4-13.7 (As-removed + 13.8 hrs 1375°F + Air Cool)					
1330	1790	80.8	85.9	39.26	
1290	1750	418.7	471.3	39.68	
				39.47	0.30
A4-28.2 (As-removed + 28.2 hrs 1375°F + Air Cool)					
1330	1790	56.9	59.9	38.98	
1290	1750	272.0	299.1	39.33	
				39.16	0.25

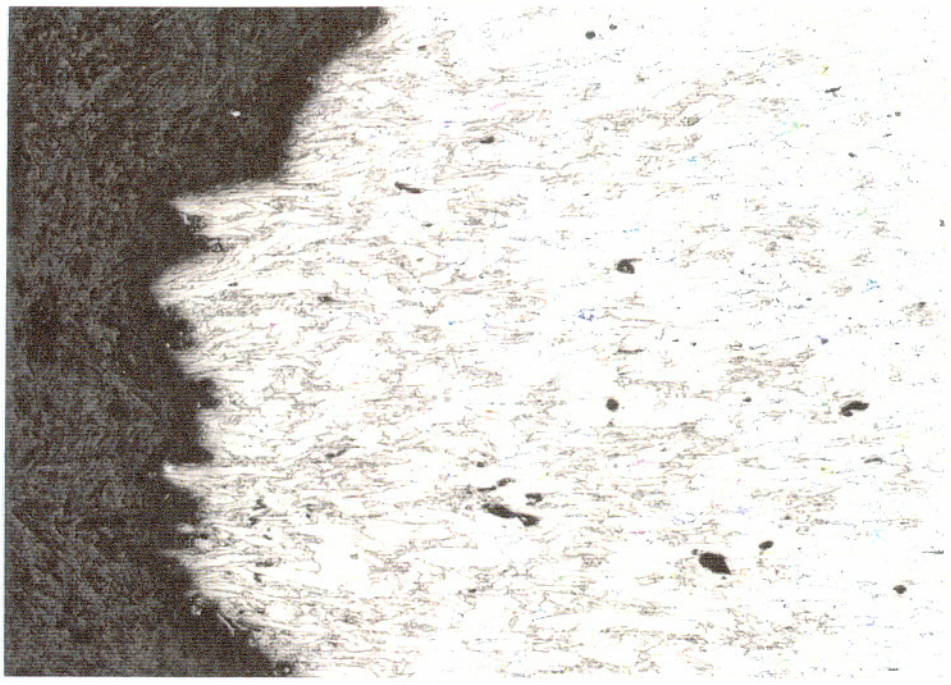

Figure 2-1
Sample A1-4 50X Nital
1287°F 539 hours

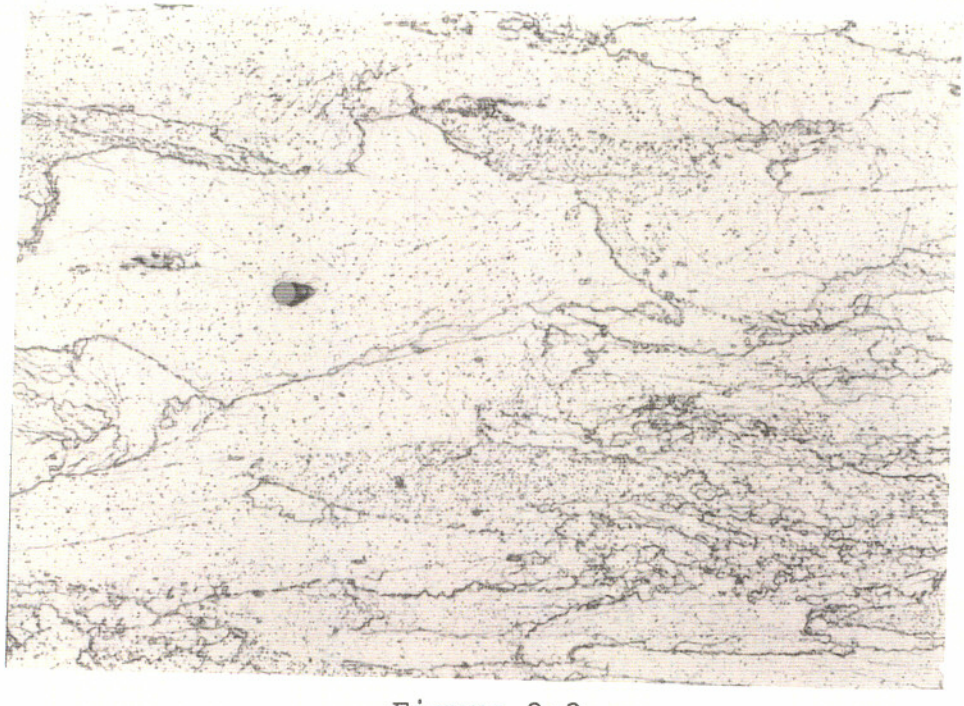

Figure 2-2
Sample A1-4 400X Nital
1287°F 539 hours

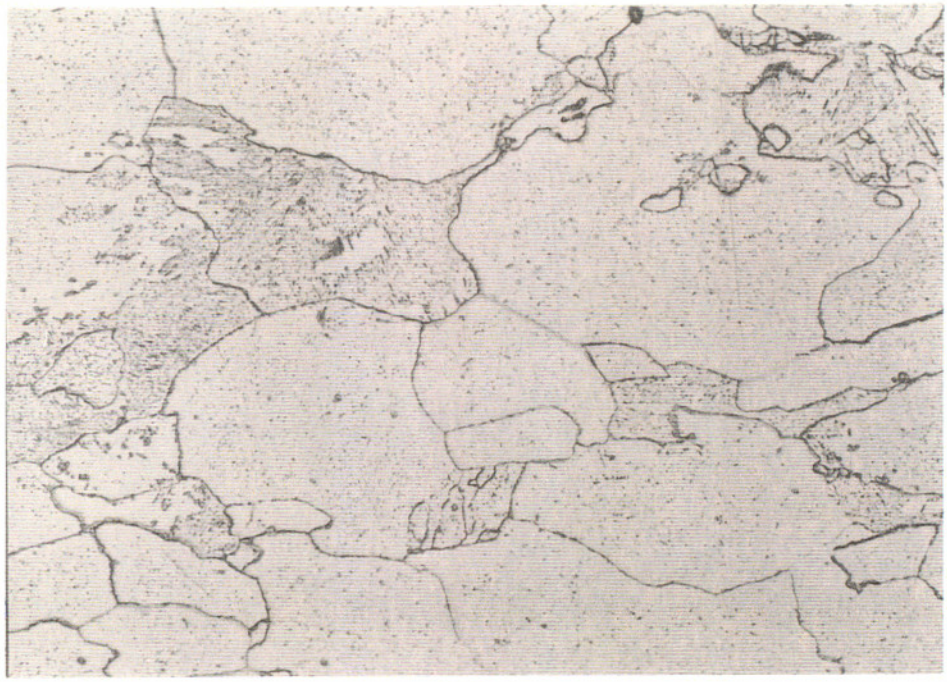

Figure 2-3
Sample A1-4 400X Nital
1287°F 539 hours

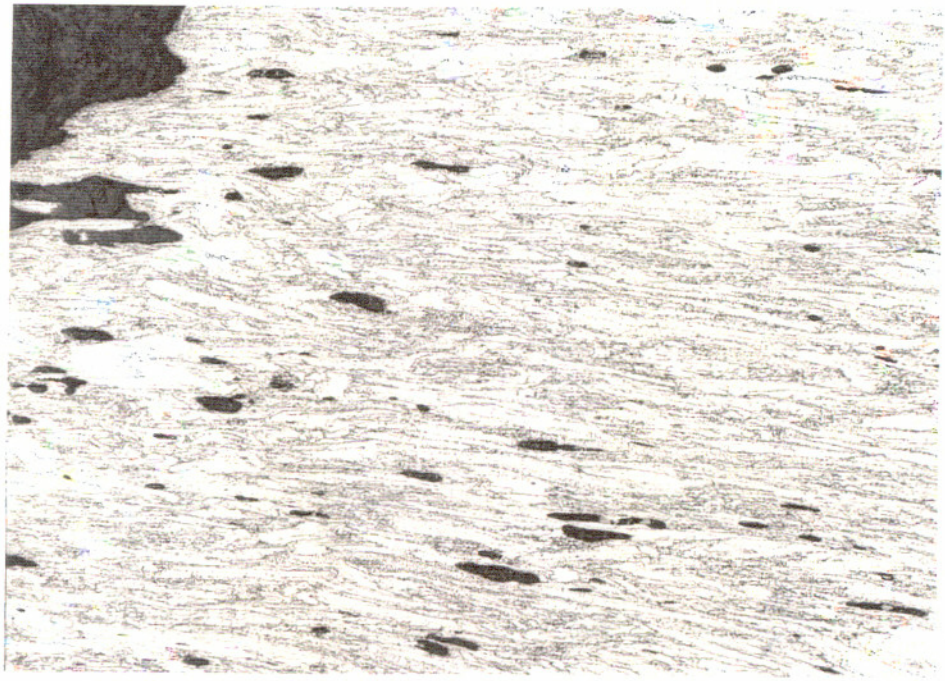

Figure 2-4
Sample A3-2 100X Nital
1270°F 604 hours

Figure 2-5
Sample A3-2 400X Nital
1270°F 604 hours

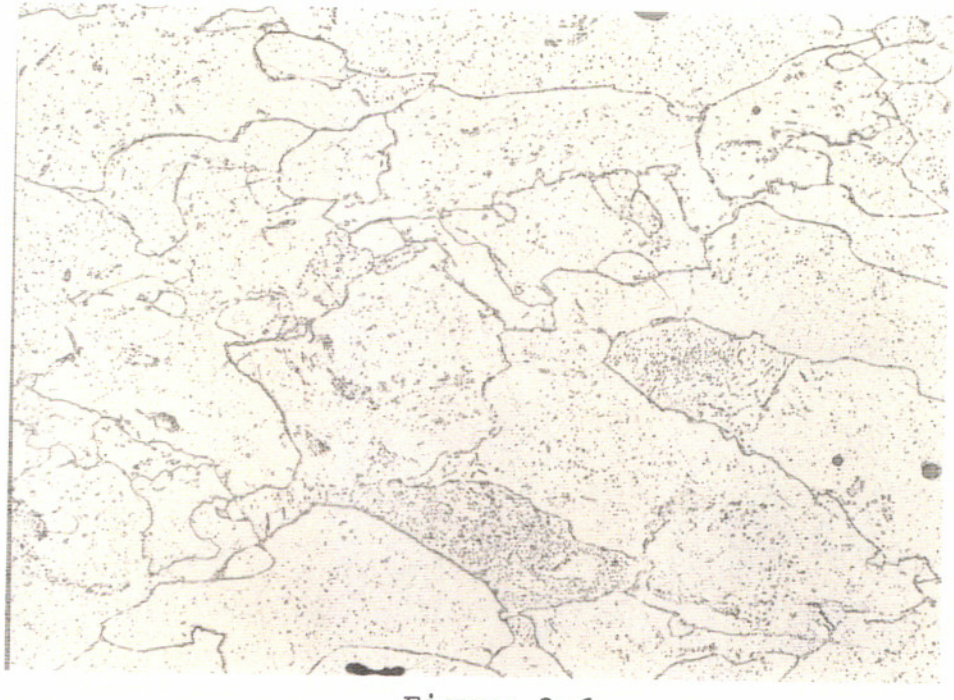

Figure 2-6
Sample A3-2 400X Nital
1270°F 604 hours

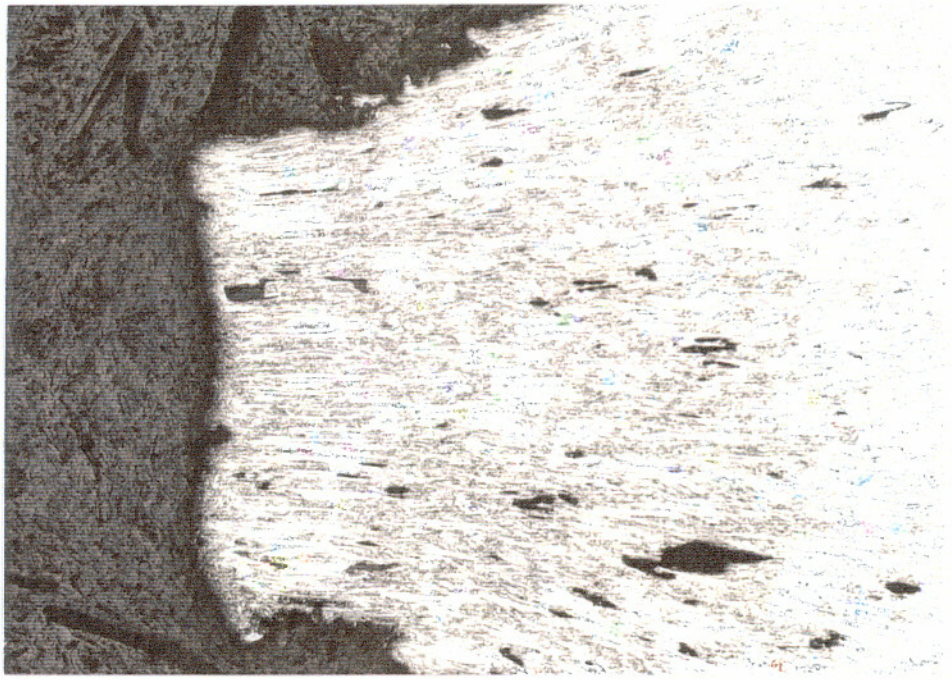

Figure 2-7
Sample A5-4 50X Nital
1330°F 98 hours

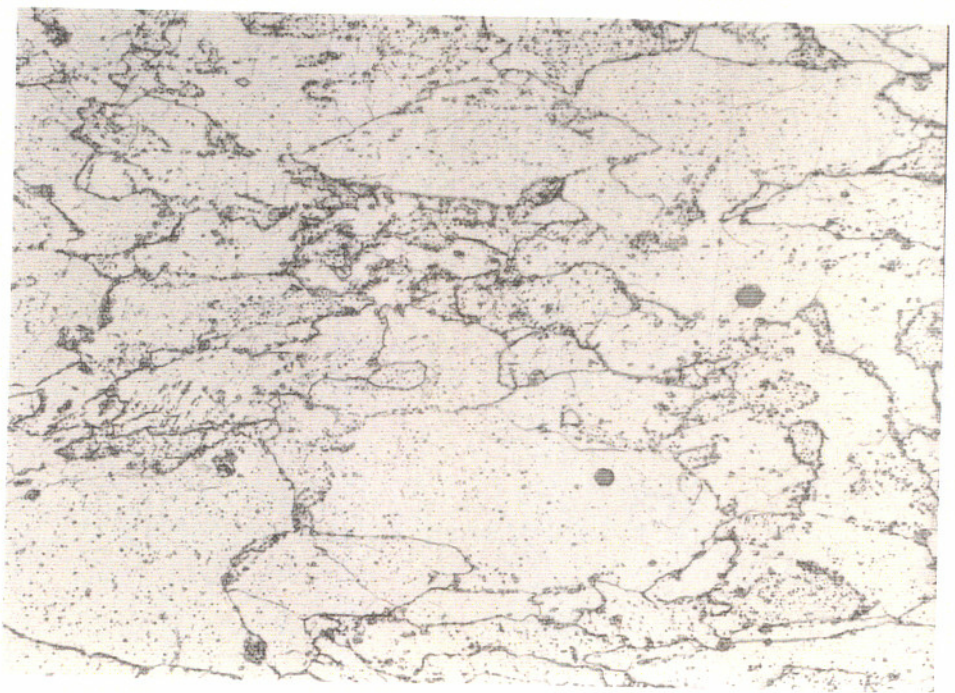

Figure 2-8
Sample A5-4 400X Nital
1330°F 98 hours

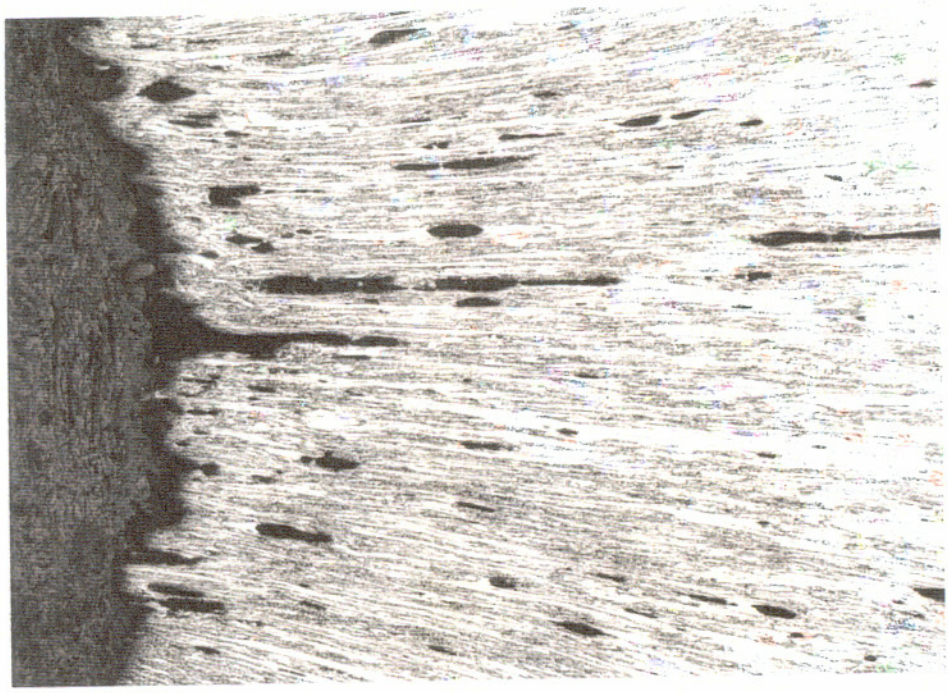

Figure 2-9
Sample A5-2 50X Nital
1270°F 646 hours

Figure 2-10
Sample A5-2 400X Nital
1270°F 646 hours

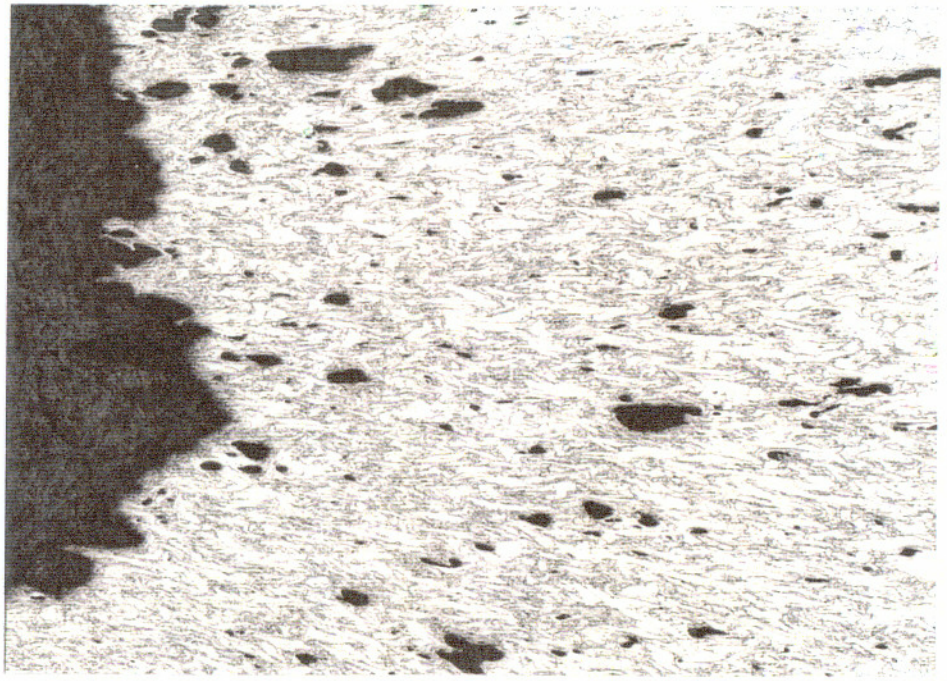

Figure 2-11
Sample A2-25-2 50X Nital
1290°F 216 hours

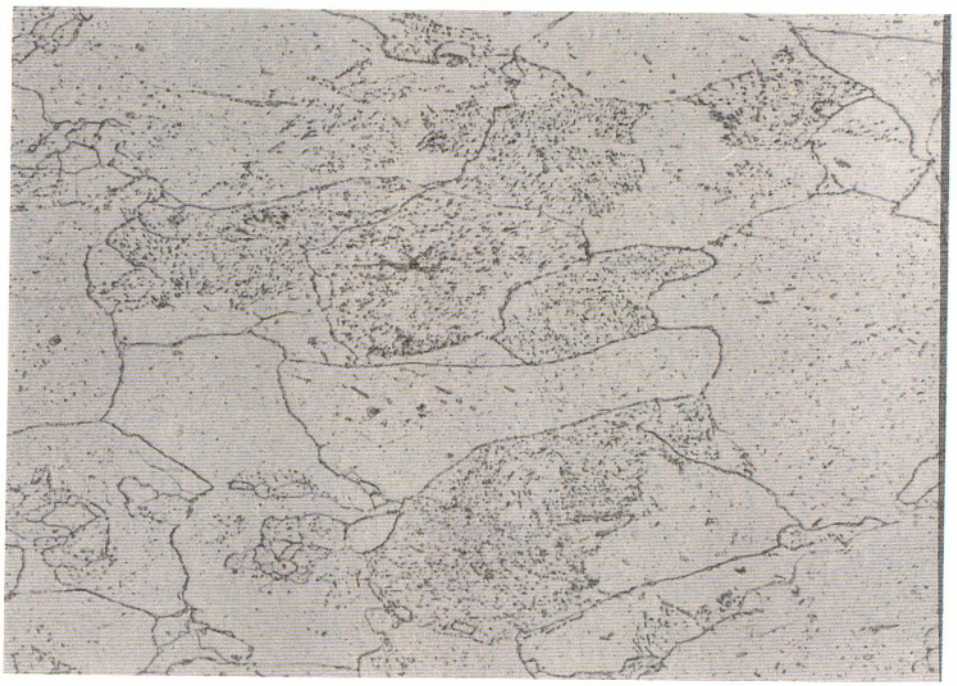

Figure 2-12
Sample A2-25-2 400X Nital
1290°F 216 hours

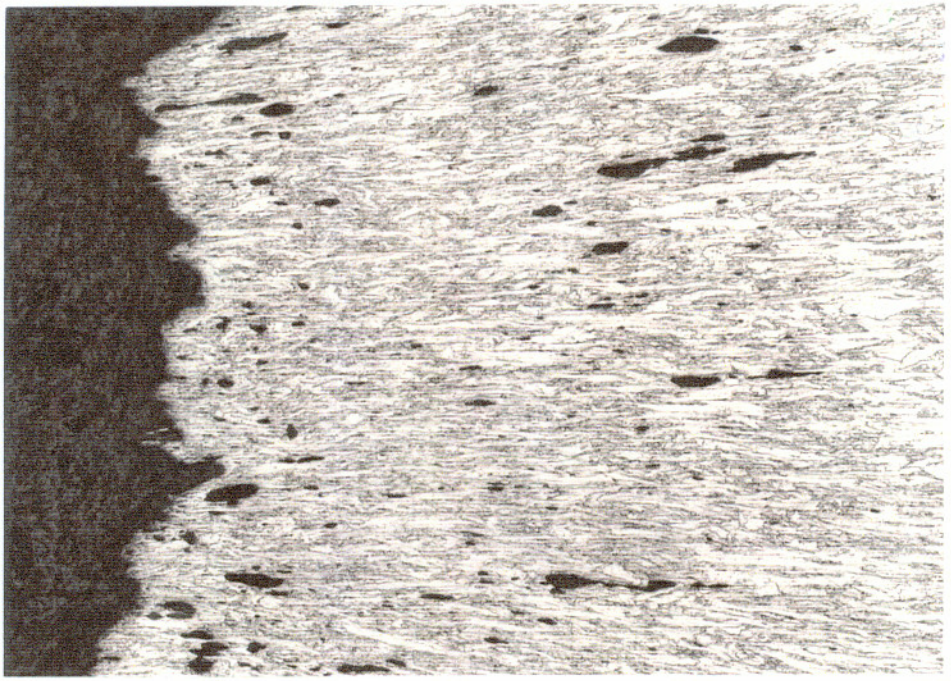

Figure 2-13
Sample A2-100-2 50X Nital
1290°F 294 hours

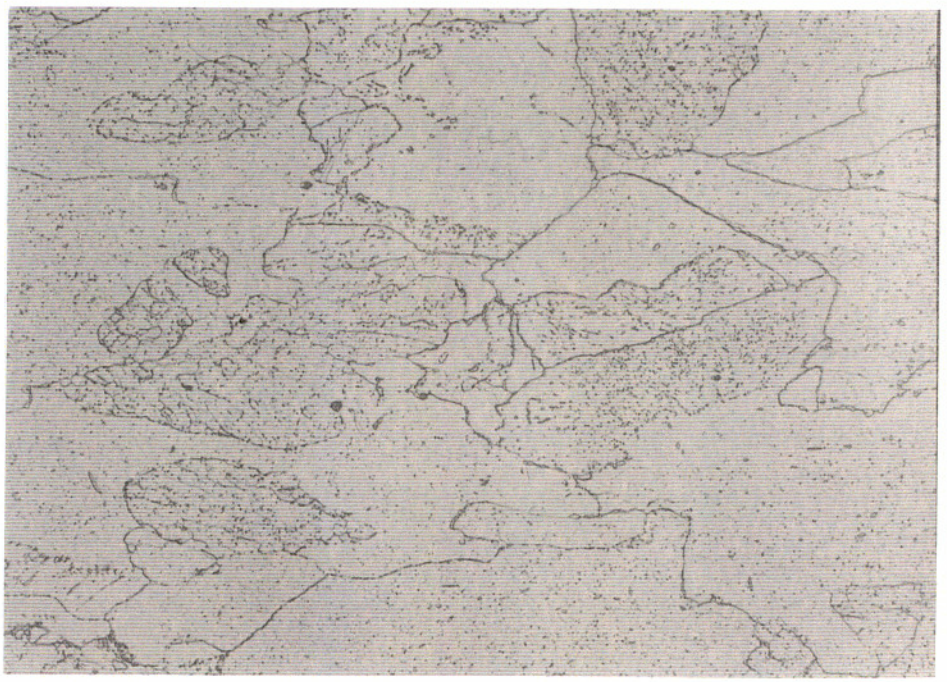

Figure 2-14
Sample A2-100-2 400X Nital
1290°F 299 hours

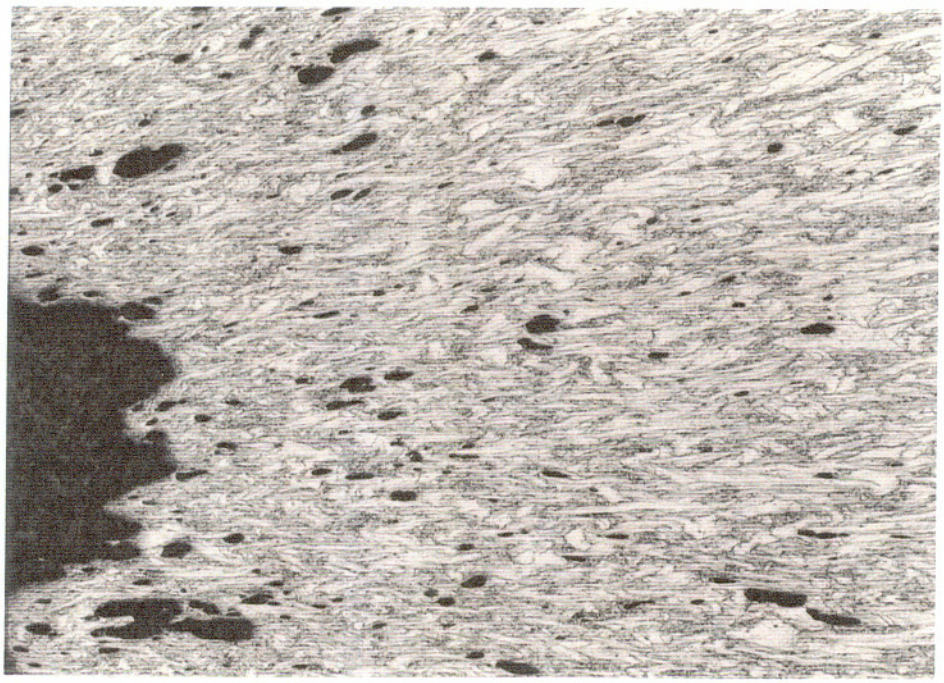

Figure 2-15
Sample A4-8-1 50X Nital
1375°F 88 hours

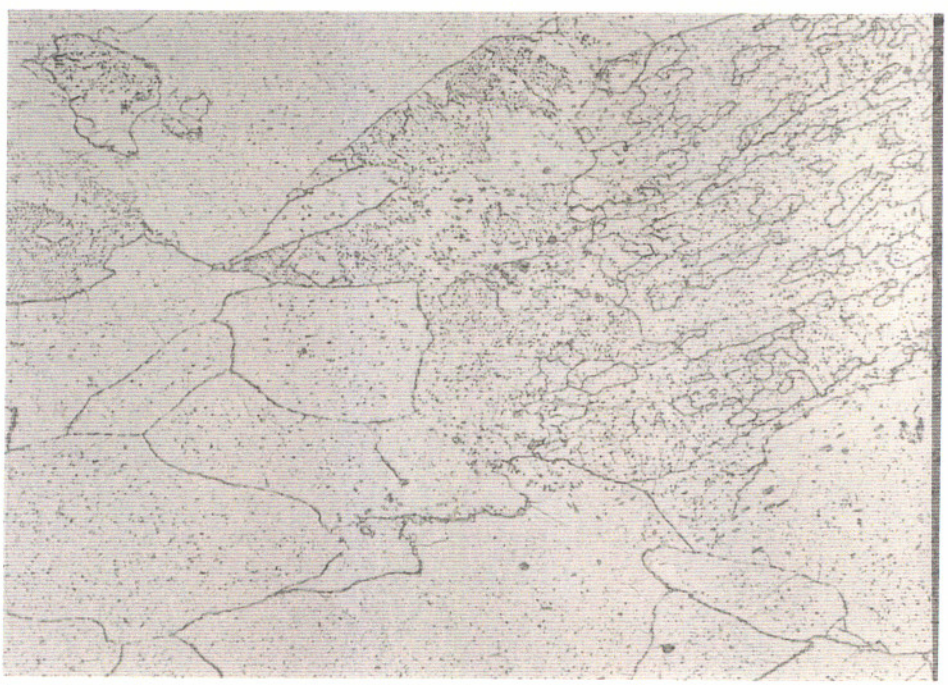

Figure 2-16
Sample A4-8-1 400X Nital
1375°F 88 hours

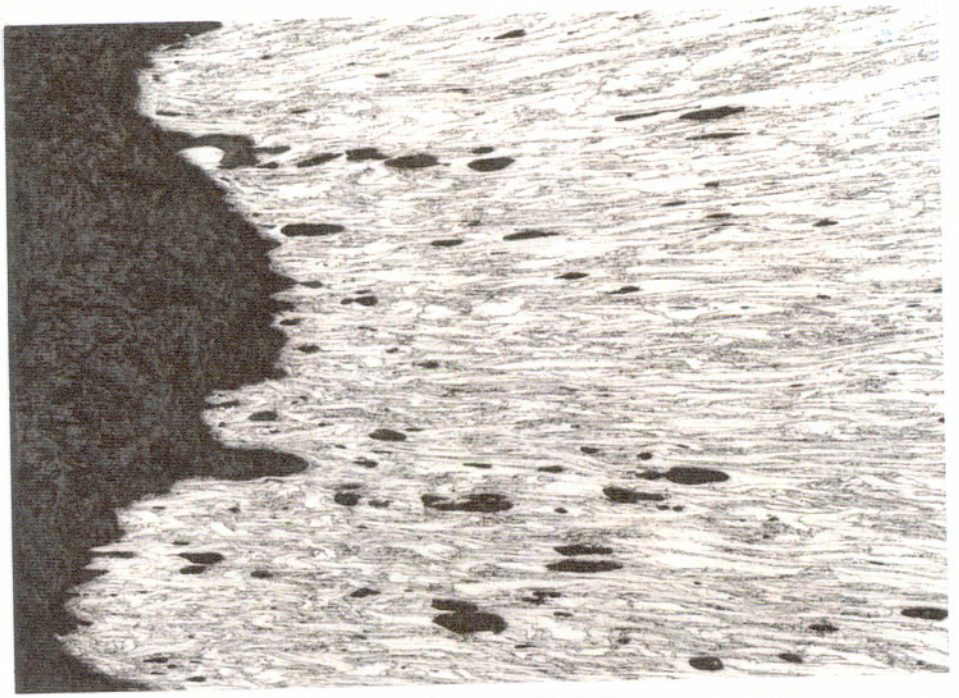

Figure 2-17
Sample A4-13.7-1 50X Nital
1375°F 86 hours

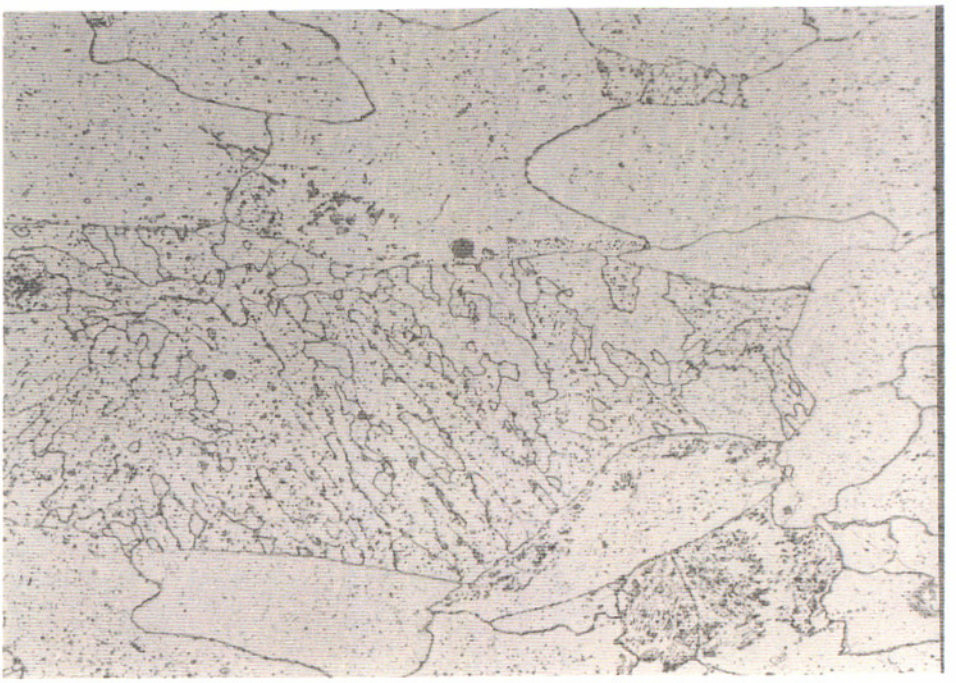

Figure 2-18
Sample A4-13.7-1 400X Nital
1375°F 86 hours

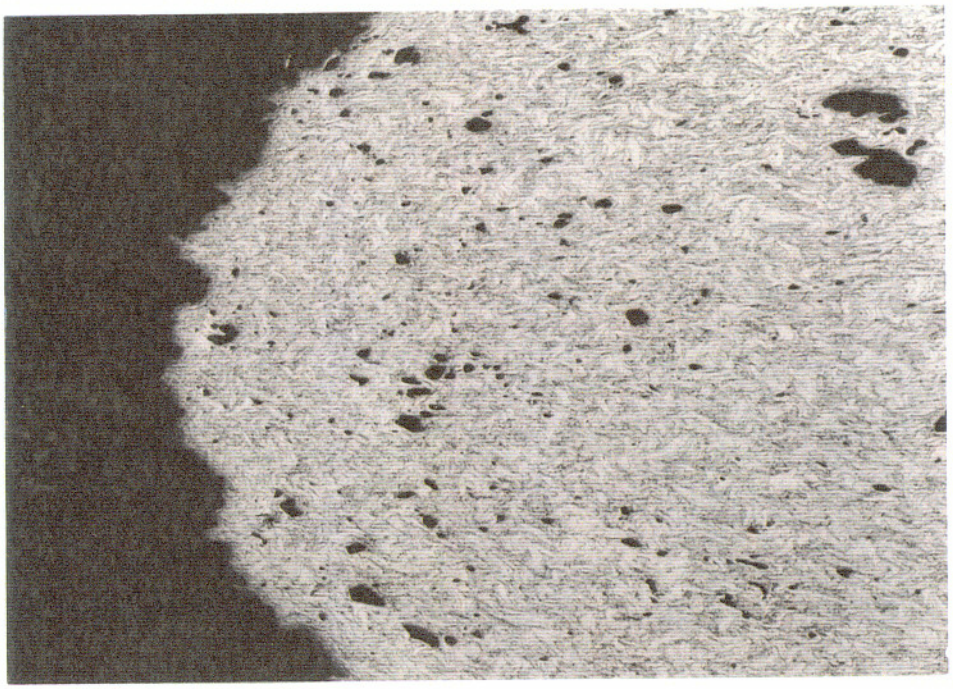

Figure 2-19
Sample A4-28.2-1 50X Nital
1375°F 60 hours

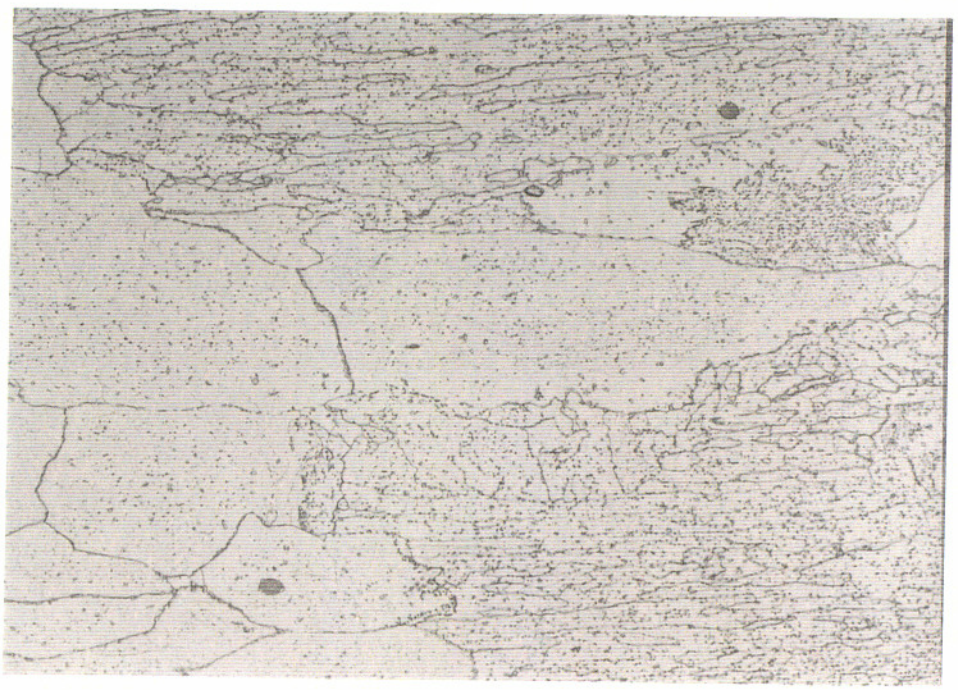

Figure 2-20
Sample A4-28.2-1 400X Nital
1375°F 60 hours

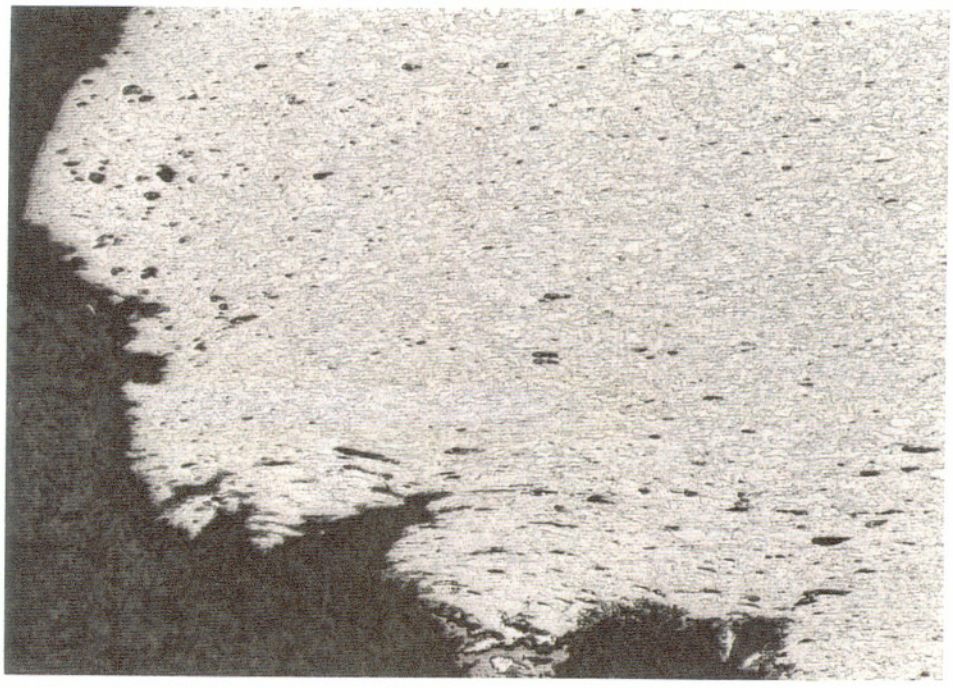

Figure 2-21
Sample B1-2 100X Nital
1279°F 360 hours

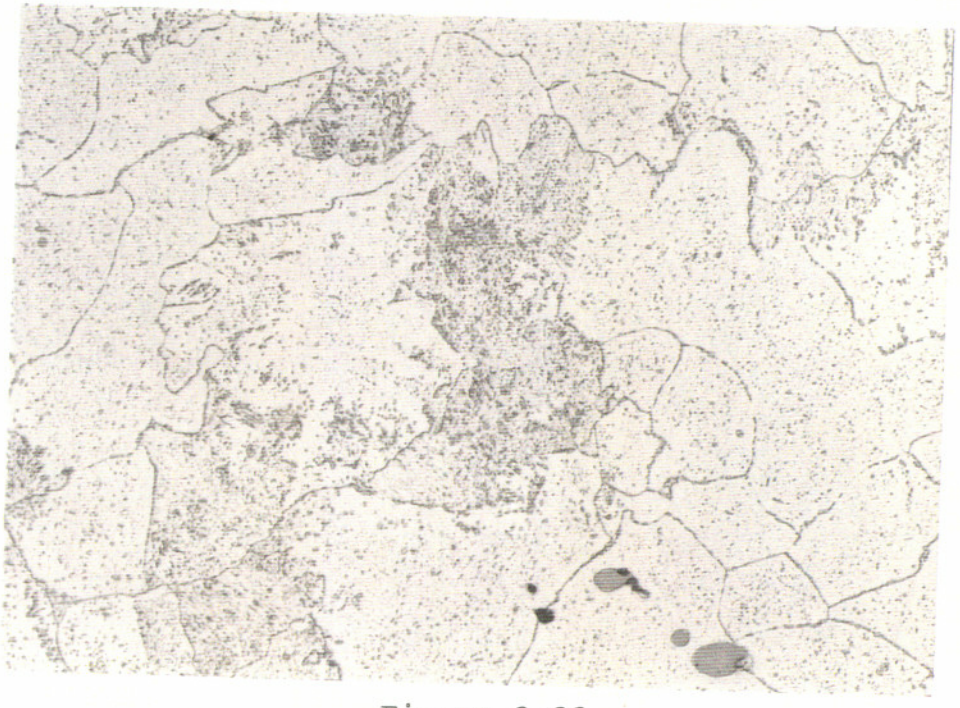

Figure 2-22
Sample B1-2 400X Nital
1279°F 360 hours

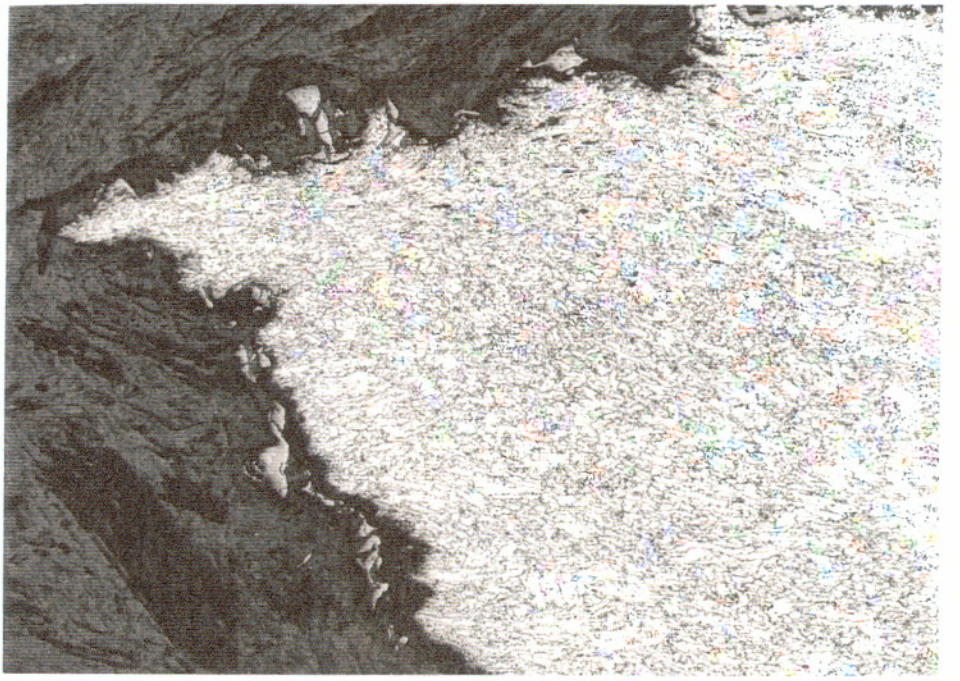

Figure 2-23
Sample B3-5 100X Nital
1252°F 654 hours

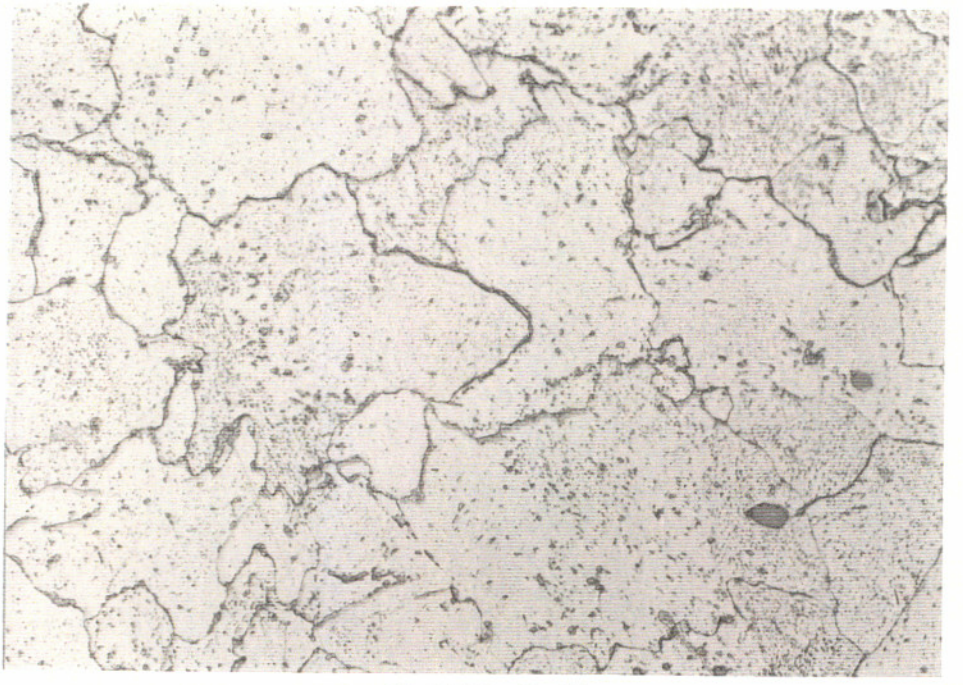

Figure 2-24
Sample B3-5 400X Nital
1252°F 654 hours

Figure 2-25
Sample B5-2 100X Nital
1270°F 411 hours

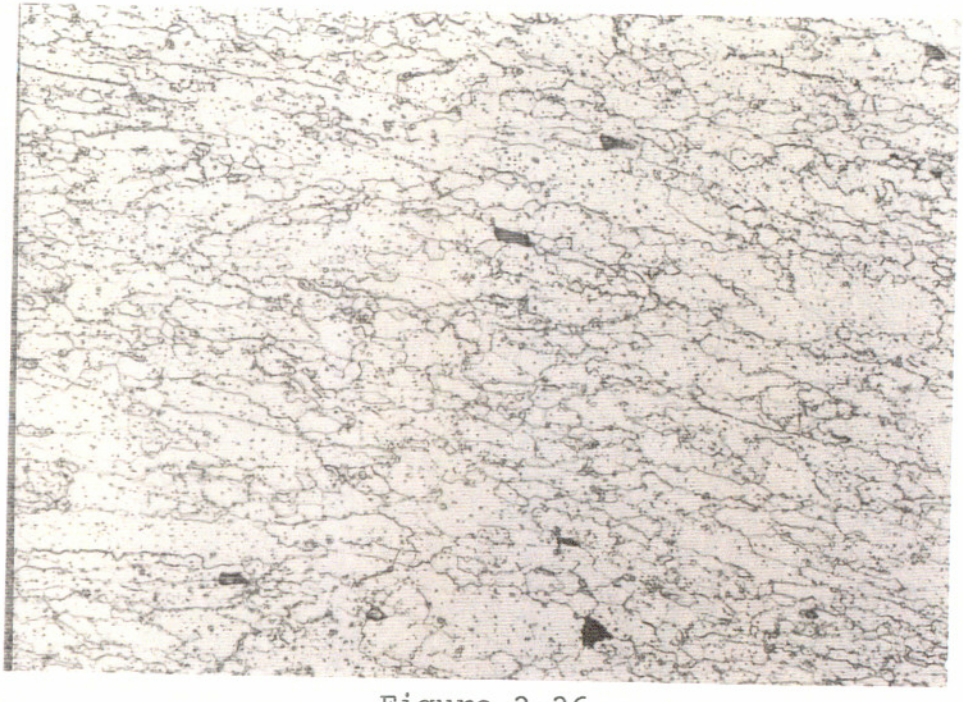

Figure 2-26
Sample B5-2 400X Nital
1270°F 411 hours

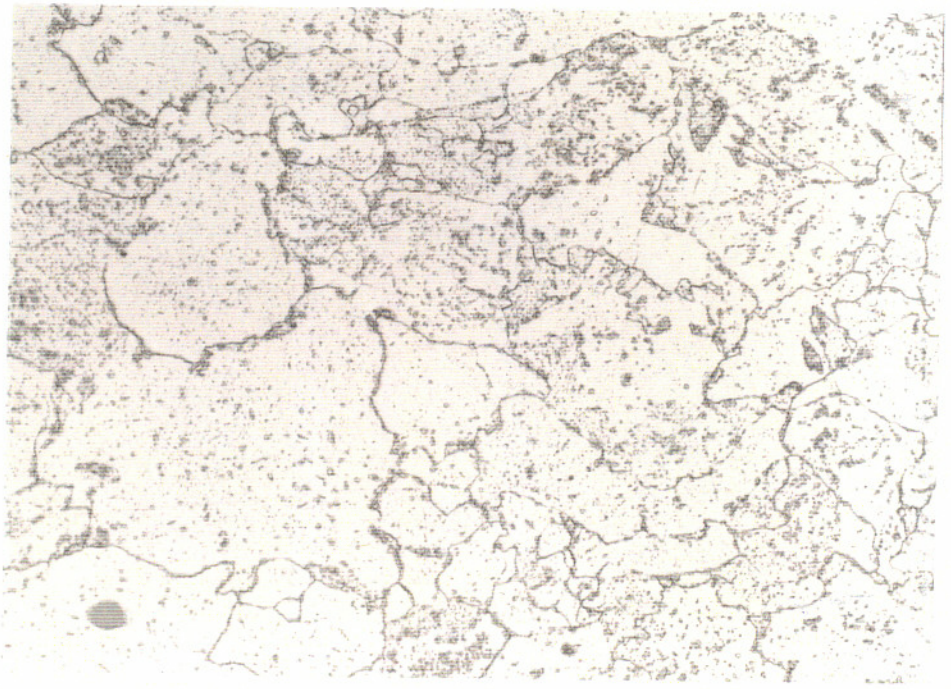

Figure 2-27
Sample B5-2 400X Nital
1270°F 411 hours

Figure 2-28
Sample B6-4 100X Nital
1325°F 235 hours

Figure 2-29
Sample B6-4 400X Nital
1325°F 235 hours

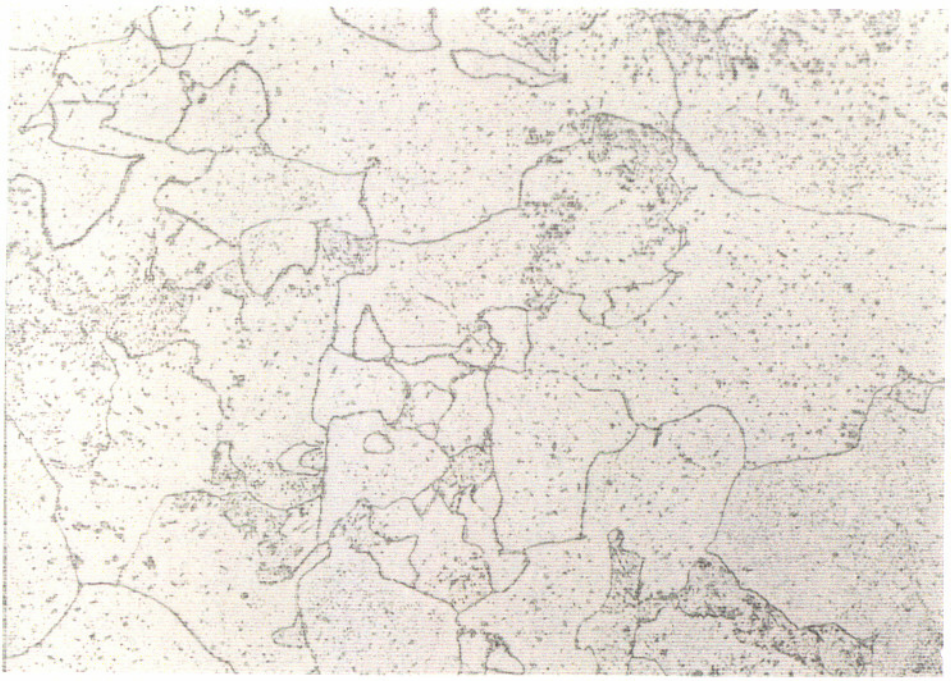

Figure 2-30
Sample B6-4 400X Nital
1325°F 235 hours

VITA

November 21, 1940.....Born - New York, New York

1962.....B.S. Metallurgy
Massachusetts Institute of Technology
Cambridge, Massachusetts

1963.....M.S.E. Materials Engineering
University of Michigan
Ann Arbor, Michigan

1963 - 1966.....Research Engineer
Battelle Northwest Laboratories
Richland, Washington

1966.....Metallurgical Engineer
The Boeing Company
Seattle, Washington

1967 - 1970.....Artillery Officer
U. S. Marine Corps

1970 - 1976.....Principal Development Engineer
Combustion Engineering, Inc.
Nuclear Power Systems
Windsor, Connecticut

1976 - present.....Metallurgist
Portland General Electric Co.
Portland, Oregon

Registered Professional Engineer, Metallurgical Engineering, Oregon

List of Publications

Bodine, G. C., & Carter, J. W., "Relation of Tube Manufacturing Variables to Corrosion and Corrosion Product Release Rates of a Ni-Cr-Fe Alloy in a simulated PWR Primary Water", Materials Performance, Vol. 14, No. ii, 1975.

Williams, J. A. & Carter, J. W., "Creep of Annealed Type 302 Stainless Steel During Irradiation and its Engineering Significance", ASTM STP No. 426, 1967.

Carter, J. W., "The Effects of Irradiation, Cold Work, and Annealing on the Martensite Content of Two Austenitic Stainless Steels", BNWL-238, August 1966.

Carter, J. W., "Creep Resistance of Platinum and Platinum Alloys at 1200°C", HW-4442, 1964.